SLU

Phosphorus chemistry in managed forest soils

Effects of weathering and wood ash fertilization

J.R. Marius Tuyishime
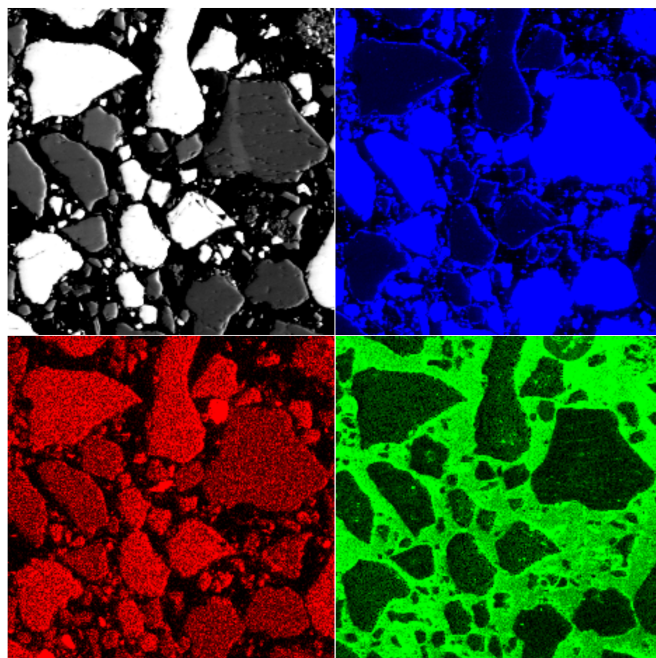
Phosphorus chemistry in managed forest soils

Effects of weathering and wood ash fertilisation

J.R. Marius Tuyishime

Faculty of Natural Resources and Agricultural Sciences
Department of Soil and Environment
Uppsala

SLU

**SWEDISH UNIVERSITY
OF AGRICULTURAL
SCIENCES**

DOCTORAL THESIS

Uppsala 2022

Acta Universitatis Agriculturae Sueciae
2022:75

Cover: micro-X-ray fluorescence images of silicon (upper left), aluminium (upper right), iron (bottom left), and sulfur (bottom right). Prepared by M. Tuyishime using PyMca and ImageJ software.

Phosphorus chemistry in managed forest soils-effects of weathering and wood ash fertilisation

Abstract

Weathering and Podzolisation are key mechanisms that transform primary mineral apatite into a phosphorus (P) pool with low solubility. In addition, intensive forest harvesting removes nutrients from the soil, reducing P availability.

In this thesis, a combination of wet chemical extractions, bulk X-ray absorption near-edge structure (bulk-XANES) spectroscopy, microscopic X-ray fluorescence (μ-XRF) imaging, and μ-XANES was applied to seven Podzolised soils (down to 1 m depth) across Sweden, to study molecular P speciation in the bulk soil and in microsites. Moreover, this thesis examined the fate of wood ash-bound P, when added alone or with repeated nitrogen (N) fertilisation, to the organic layer to return P removed after harvest.

Total P (TP) in the upper 80 cm was $69-379$ g m^{-2}, with 94% of all P residing between $20-80$ cm. More than 50% of all P in B and C horizons was Al-bound P, bound mainly to imogolite-type nanoparticles (ITN), while apatite comprised about 26%. Wood ash increased TP in the organic layer by $6-28$ kg P ha^{-1}, equivalent to $17-39$% of the initial ash-P content. More bioavailable P (Olsen-P) and aboveground biomass P were observed in the ash treatment than in the control, probably due to the dissolution of Ca-bound P from the ash. Wood ash application, especially at a high dose, also increased Al-bound P ($p < 0.001$) by up to 15.6 kg P ha^{-1}.

P speciation across soil profiles was found to be strongly influenced by weathering and Podzolisation, with TP and apatite depletion in the E horizon and mainly Al-bound P and Fe-bound P in the B horizon. Dissolution of Ca-bound P from the ash was almost complete $13-24$ years after ash application, which contributed to increased P availability and P uptake. These novel findings can be useful in improving forest management practices to ensure the long-term sufficiency of P supply to trees. Further work is required to understand the importance of the subsoil for the P supply from the subsoil and to study the fate of wood ash-bound P in the mineral soil.

Keywords: (phosphorus, speciation, bulk soil, microsites, depletion, ash, forestry)

Author's Address: Marius Tuyishime, Swedish University of Agricultural Sciences, Department of Soil and Environment, P.O. Box 7014, 75007, Uppsala, Sweden. Email: marius.tuyishime@slu.se

Fosfors kemi i brukad skogsmark-effekter av vittring och askgödsling

Sammanfattning

Genom vittring och podsolering omvandlas jordens ursprungliga apatit till en fosforpool (P) med en låg löslighet. Dessutom innebär moderna skogsbruksmetoder att näringsämnen tas bort från jorden, vilket ytterligare minskar P-tillgängligheten.

I denna avhandling användes en kombination av våtkemiska extraktioner, röntgenabsorptionsspektroskopi (XANES) på hela prover ("bulk-XANES"), röntgenfluorescens i mikroskala (μ-XRF) och XANES i mikroskala (μ-XANES) för sju podzoliserade jordar (ner till 1 m djup) över Sverige, för att studera P-specieringen. Dessutom undersöktes om och på vilket sätt fosfor bundet i biobränsleaska mobiliserades, när askan tillsattes ensamt eller med upprepad kväve-(N)-gödsling, till humusskiktet i syfte att återföra P som avlägsnats efter skörd.

Den totala fosforhalten (TP) i de översta 80 cm av jordarna var mellan 69 och 379 g m^{-2}. I genomsnitt återfanns 94 % av all P mellan 20 och 80 cm djup. Mer än 50 % av all P i B- och C-horisonter var bunden till Al, huvudsakligen till imogolitnanopartiklar (ITN), medan apatit utgjorde cirka 26 %. Biobränsleaskan ökade TP i humusskiktet med mellan 6 och 28 kg P ha^{-1}, motsvarande mellan 17 och 39 % av askans initiala P-halt. Det fanns mer biotillgängligt P (Olsen-P) och P i ovanjordisk biomassa i askbehandlad jord än i kontrollen, förmodligen på grund av upplösning av Ca-bunden P härrörande från askan. Tillförsel av biobränsleaska, särskilt vid en hög dos, ökade också Al-bundet P ($p < 0,001$) med upp till 15,6 kg P ha^{-1}.

Specieringen av P i markprofilerna visade sig vara starkt påverkad av vittring och podsolisering, med utarmning av TP och apatit i E-horisonten och med huvudsakligen Al-bunden P och Fe-bunden P i B-horisonten. Upplösningen av Ca-bundet P från askan var nästan fullständig, vilket bidrog till ökad P-tillgänglighet och P-upptag. Dessa nya rön kan vara användbara för att förbättra skogsbruksmetoderna i syfte att säkerställa den långsiktiga P-försörjningen. Ytterligare arbete krävs för att förstå hur viktig mineraljordens P är för fosforförsörjningen och för att studera vad som händer i mineraljorden med den P som mobiliserats från biobränsleaskan.

Författarens address: Marius Tuyishime, Sveriges lantibruksuniversitet, Inst.mark och miljö, Box 7014, 75007, Uppsala, Sweden. E-post: marius.tuyishime@slu.se

Dedication

I dedicate this work to my family.

Contents

List of publications

This thesis is based on the work contained in the following papers, referred to by Roman numerals in the text:

I.   Tuyishime, J.R.M.*, Adediran G.A., Olsson B.A., Spohn, M., Hillier, S., Klysubun, W., Gustafsson, J.P. (2022). Phosphorus abundance and speciation in acid forest Podzols – Effect of postglacial weathering. Geoderma, 406, 115500.

II. Adediran G.A.*, Tuyishime, J.R.M., Vantelon, D., Klysubun, W., Gustafsson, J.P. (2020). Phosphorus in 2D: Spatially resolved P speciation in two Swedish forest soils as influenced by apatite weathering and Podzolisation. Geoderma, 376, 114550.

III. Tuyishime, J.R.M.*, Florén, T., Rivard, C., Gustafsson J.P. Microscale heterogeneity of phosphorus bound to secondary Al and Fe precipitates in the B horizons of two Swedish Podzols. Manuscript.

IV. Tuyishime, J.R.M.*, Adediran G.A., Olsson B.A., Zetterberg, T.S., Högbom, L., Spohn, M., Lim, H., Klysubun, W., Borca, C.N., Huthwelker, T., Gustafsson, J.P. (2022). Phosphorus speciation in the organic layer of two Swedish forest soils 13–24 years after wood ash and nitrogen application. Forest Ecology and Management, 521, 120432.

Papers I, II, and IV are reproduced with the permission of the publishers.

The contribution of J.R. Marius Tuyishime to the papers included in this thesis was as follows:

I. Planned the study together with the co-authors. Conducted the fieldwork at Rödålund with support from Olsson, B.A., and Gustafsson, J.P. Performed chemical extractions. Performed bulk-XANES together with Adediran, G.A, and Gustafsson, J.P, with the assistance of Klysubun, W. Did bulk-XANES data analysis and interpretation with the assistance of Gustafsson, J.P. Wrote the manuscript with support and feedback from co-authors.

II. Performed chemical extractions. Collected bulk-XANES data together with Adediran, G.A, and Gustafsson, J.P, with the assistance of Klysubun, W. Performed bulk-XANES data analysis and interpretation with support from Gustafsson, J.P. Together with Adediran, G.A and Gustafsson, J.P, performed µ-XRF and µ-XANES data collection with the assistance of Vantelon.D. Edited the manuscript.

III. Planned the study together with Gustafsson, J.P. Performed µ-XRF and µ-XANES data collection together with Gustafsson, J.P, with the assistance of Rivard, C. Analysed the data. Wrote the manuscript with support and feedback from co-authors.

IV. Planned the study together with the co-authors. Performed fieldwork with support from Olsson, B.A. and Gustafsson, J.P. Did chemical extractions except for P in aboveground biomass. Performed bulk-XANES data with support from Gustafsson, J.P and Klysubun, W and did data analysis. Together with Adediran, G.A, and Gustafsson, J.P, collected µ-XRF, and µ-XANES data with the assistance of Borca, C.N. and Huthwelker, T. Performed statistics. Wrote the manuscript with feedback and support from co-authors.

Abbreviations

AL	Ammonium lactate
ATP	Adenosine triphosphate
Bulk XANES	X-ray absorption near-edge structure spectroscopy of bulk soil
DNA	Deoxyribonucleic acid
DPS	Degree of phosphorus saturation
ITN	imogolite-type nanoparticles
LCF	Linear combination fitting
μ-XANES	Microscale X-ray absorption near-edge structure spectroscopy
OM-C	organometallic complexes
RNA	Ribonucleic acid
WL	White line
WTH	Whole-tree harvesting

1. Introduction

The forests in the Nordic countries cover only 1.6% of the world's forested area, but the region supplies 18%, 15%, and 13% of the world's paper, sawn timber, and pulp, respectively (Nordic Forest Research, 2020). Successful long-term management of forest resources requires healthy trees, which depends on many factors, including soil conditions. The soil medium is crucial as it ensures a supply of essential nutrients for plants, such as nitrogen (N) and phosphorus (P) (Elser *et al*., 2007; Vitousek *et al*., 2010).

Most evidence suggests that temperate and boreal forest growth is primarily N-limited, not P-limited (Binkley & Högberg, 2016). Thus, the P cycle and supply to trees are often not considered critical factors in forest management. However, increasingly P-limiting conditions have been reported in European forests (Jonard *et al*., 2015; Talkner *et al*., 2015), including Nordic boreal regions (Hedwall *et al*., 2017; Yu *et al*., 2018) despite the young age of the soils (<15,000 years).

In the Scandinavian region, prevailing conditions such as cool climate, slowly-decaying evergreen conifer litter, soil acidification, and a parent material consisting of nutrient-poor siliceous glacial till influence the weathering of primary minerals in forest ecosystems (Andersson *et al*., 2014; IUSS Working Group, 2014). These factors lead to Podzolisation as the primary soil-forming process (Lundström *et al*., 2000b). Podzolisation involves the accumulation of large amounts of weathered aluminium (Al) and iron (Fe) mineral phases in the subsoil (B horizon) (Lundström *et al*., 2000a). These chemical compounds can strongly adsorb dissolved P (Parfitt, 1989). Thus, the Podzol (spodic) B horizon stores a relatively large amount of P, but only a minor fraction is bioavailable. Consequently, recycling P (organic P) previously acquired from the mineral soil by plants and deposited mainly in the surface horizon is an important process by which plants

maintain a sufficient P supply (Lang *et al*., 2016; Wood *et al*., 1984). With continued stabilisation of P through binding to Fe and Al in the mineral soil, P availability gradually declines, resulting in 'sink-driven' P limitation (Vitousek *et al*., 2010). However, many details remain unclear, *e.g.* the P forms and their stocks in podzolised soil horizons in boreal regions.

In addition to the build-up of fixed P, there is evidence that logging, particularly whole-tree harvesting (WTH), can lead to a long-term decline in P availability. For example, Yanai (1998) found that WTH in the Hubbard Brook forest ecosystem in New Hampshire, USA, removed 50 kg P ha^{-1} in a single clearcut. The rate of P loss due to WTH is reported to exceed 1 kg P ha^{-1} yr^{-1} (Akselsson *et al*., 2008). In some countries, including Sweden, the application of wood ash, a by-product of wood fuel combustion, is recommended to maintain soil fertility and offset P removal after harvest (Swedish Forest Agency, 2019). The ash contains all nutrients except N (Jacobson *et al*., 2004; Karltun *et al*., 2008; Ring *et al*., 2006).

Many studies have explored the solubility and availability of P after ash application, but the results reported are sometimes contradictory (Augusto *et al*., 2008). Moreover, the mechanisms involved and the fate of ash-bound P product (P speciation) upon addition are largely unknown. Detailed information on the molecular-scale speciation and fate of native and applied P is therefore needed for a fundamental understanding of the reactions that affect P mobility and solubility. To date, this knowledge is lacking for northern boreal soils.

Various chemical extractants are widely used to determine total P and plant-available P (Moody *et al*., 2013; Fixen & Grove, 1990) and assess different P pools with different degrees of solubility (*e.g*. Hedley *et al*., 1982). However, the results provide limited insights into specific P forms, reactivity, interactions, and distribution among P-bearing minerals in soils (van der Bom *et al*., 2022). Furthermore, the soil is heterogeneous (Hesterberg *et al.*, 2017) and contains low-P and highly concentrated micro-sized P spots that also vary greatly in terms of the composition of P species (Adediran *et al*., 2022). For instance, in humid, highly weathered Hawaiian soils affected by dust deposition, Vogel *et al*. (2021) found apatite grains to be present as smaller hotspots with a significantly high P concentration, while Al-bound P was homogeneously distributed at the microscale. Thus, routine chemical extractions may underestimate or overestimate P concentration in soil microsites (microscale spots with unique properties

within the bulk soil) in the subsample used for analysis. Therefore, understanding microscale P speciation is essential to understand better the biogeochemical mechanisms involved, affecting P dynamics and soil fertility (Hesterberg et al., 2011; van der Bom *et al*., 2022).

P *K*-edge XANES spectroscopy is a powerful technique to determine the average P speciation on bulk soil samples (bulk-XANES) (Beauchemin *et al*., 2003, Hesterberg *et al.*, 2017, Prietzel *et al.*, 2016). Moreover, since the soil consists of highly diverse microsites with unique structures and chemical properties (Hesterberg *et al*., 2011), such heterogeneity needs to be addressed to understand P dynamics and biogeochemical mechanisms better. First, μ-XRF is used for mapping spatial co-distribution of P with P-binding minerals such as Al, Fe, and Calcium (Ca) (Hesterberg *et al*., 2017, Rivard *et al*., 2016, Vogel *et al*., 2021, Yamaguchi et al., 2021). Second, the microsites (P spots) of interest should be selected from the map, and then the P *K*-edge μ-XANES is applied to determine local P speciation. This thesis used a combination of wet chemical extractions, bulk XANES, and μ-XRF combined with μ-XANES to evaluate the effects of weathering and wood ash application on solubility, molecular-scale speciation, and the vertical and spatial distribution of P.

2. Aim and objectives

The overall aim of this thesis was to examine how P cycling and speciation are affected by weathering and wood ash fertilisation in managed Podzolised forest soils in Sweden.

The specific objectives of the work were to:

- Assess the molecular speciation and solubility of P in soils under the influence of weathering across soil profiles (Paper I)
- Assess the microscale P distribution and speciation in forest soils as influenced by weathering (Papers II and III)
- Determine the effects of wood ash fertilisation on P speciation and solubility in the organic layer of two managed forests (Paper IV).

3. Background

3.1. Basic chemistry of phosphorus

The unique chemical properties of P are fundamental to understanding its chemical interaction with other elements and minerals. P is the second chemical element in group V of the periodic table. Its atomic number is 15. It has 5 electrons in the outermost shell (its full configuration is $1s^2\ 2s^2\ 2p^6\ 3s^2\ 3p^3$). Compared to its nearest noble-gas neighbours, this is 5 electrons more than for neon and 3 less than for argon. Thus, P can have a range of oxidation states, but in nature, it is found almost exclusively in the maximally oxidized form (+V), as phosphate ions ($H_2PO_4^-$, HPO_4^{2-}, PO_4^{3-}) (Larsen, 1967). Because P is less electronegative than oxygen, the electron distribution and negative charge are partly associated with oxygen (Dixon & Schulze, 2002). This explains why phosphate anions have a strong affinity for, and form surface complexes on, the positively charged surfaces of soil minerals.

3.2. Biological and ecological relevance

Phosphorus is a vital macronutrient for plants and a structural constituent of nucleic acids (DNA and RNA), energy transfer molecules such as ATP, and body parts *e.g.* bones and teeth in humans and animals (Morris & Mohiuddin, 2020). To build their biomass, plants need and take up P in a certain stoichiometric ratio to chemical elements such as N (Elser & Hamilton, 2007). However, to be available for plant uptake, P has to be solubilised and transferred from the solid phase to the soil solution (Pierzynski *et al.*, 2005).

P is often considered a limiting nutrient in forest ecosystems at an advanced stage of pedogenesis (Vitousek *et al*., 2010; Walker & Syers, 1976). From an ecological point of view, P limitation occurs when any addition of P leads to an increase in primary production or ecosystem biomass (Vitousek *et al*., 2010). In contrast, in the young soils in boreal and temperate regions, cyclical glaciations have reset the soil (and primary mineral-containing P), making P limitation less likely (Chadwick *et al*., 1999; Vitousek & Farrington, 1997). Thus N is the limiting nutrient (Binkley & Högberg, 2016). However, recent research has advised signs of P limitation in some forested ecosystems (Almeida *et al*., 2022; Rosenstock *et al*., 2016; Talkner *et al*., 2015; Yu *et al*., 2018). Increased leaching or erosion due to wildfire (Lagerström *et al*., 2009), soil N enrichment, and intensive forestry are also important factors contributing to a decrease in P availability (Akselsson *et al*., 2008).

3.3. Phosphorus forms in soils

In the soil solution, phosphates combine with protons (H^+) to form a number of pH-dependent ionic P compounds (Figure 1). Phosphates ($H_2PO_4^-$, HPO_4^{2-}) are the most abundant ionic P species in the pH range expected for most soils (Kruse *et al*., 2015; Larsen, 1967), and these are the ones that plants and microorganisms can take up from the soil solution (Kruse *et al*., 2015). For simplicity, in this thesis, the term $PO_4^{3-}$is used to designate all phosphate ions when P is expected to occur in inorganic form.

In the Earth's crust, P occurs predominantly as a family of Ca phosphates referred to as apatites ($Ca_5(PO_4)_3(F,Cl, OH)$), which are considered the main source of P in young soils (Walker & Syers, 1976; Newman, 1995; Dixon & Schulze, 2002). Apatite is a common accessory mineral phase in most igneous, metamorphic and sedimentary rocks (Nezat *et al*., 2007). In soils derived from siliceous parent materials, apatite may also be present as inclusions in other minerals (Nezat *et al*., 2007; Syers *et al*., 1967). Unlike discrete apatite grains, apatite inclusions inside weathering-resistant minerals, *e.g.* quartz, in the soil solution are protected against weathering until the host mineral dissolves (Nezat *et al*., 2007; Syers *et al*., 1967).

Two different mechanisms of phosphate retention by Al and Fe mineral compounds have been proposed (*e.g.* Dixon & Schulze, 2002; Parfitt & Atkinson, 1976; Pierzynski *et al*., 2005), e.g.: (i) chemisorption caused by the ligand exchange between P and OH and OH_2 groups at the mineral

surface (inner-sphere complexation). (ii) surface precipitation of P with ionic metals such as Al^{3+} and Fe^{3+} (mainly in acidic soils) and Ca^{2+} (at higher pH) present in the soil solution. The latter process is suggested to increase with increasing concentration (Ler and Stanforth, 2003). The term sorption is often used to designate the overall P removal from the soil solution, regardless of the mechanism.

In soils, the organic P comprises between 20 and 80% of total P (Larsen, 1967) and consists predominantly of inositol phosphates, principally derived from plants (Dalai, 1977; Turner *et al*., 2005). In the mineral soil, myo-inositol hexakisphosphate (IP6, phytic acid) is the major organic P form and is believed to be associated with Al and Fe (hydr)oxides (Turner *et al*., 2007). Phosphodiesters such as DNA and RNA (Spohn, 2020) are the major sources of fresh organic P in the soil (Anderson, 1980). These decompose easily, thus representing a minor organic P species (Turner *et al*., 2005).
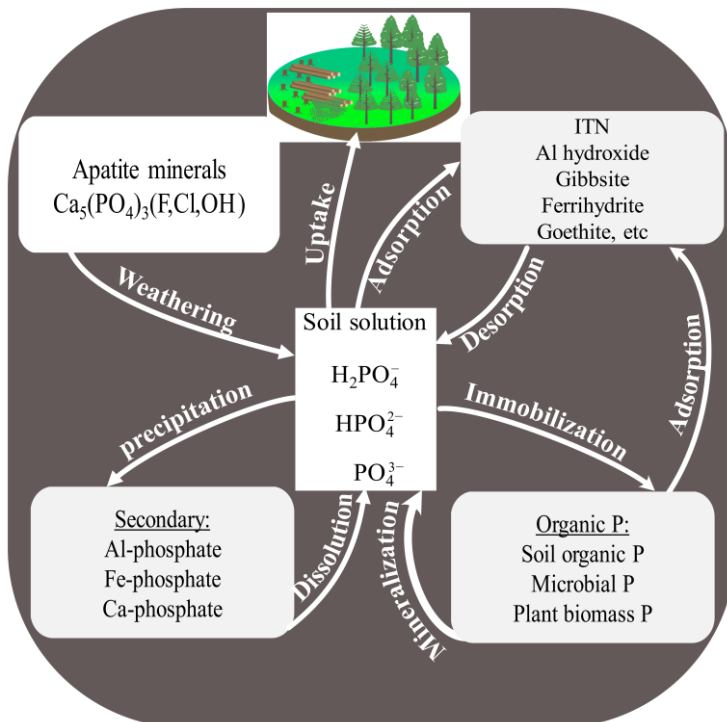
Figure 1: Major phosphorus species and biogeochemical processes in soils. ITN: imogilite-type nanoparticles materials.

3.4. Effects of soil development on phosphorus

3.4.1. Weathering

In unmanaged soils, P enters the biosphere almost exclusively through the geochemical weathering of apatite-bearing rocks, with minimal atmospheric input (Chadwick *et al*., 1999; Walker & Syers, 1976). Walker and Syers (1976) provided a conceptual model of the native P-pedogenic pathway for soils formed from silicate substrates along several chronosequences in New Zealand. Their model posits that total P and lithogenic apatite decline over time due to leaching, while P uptake and sorption of dissolved P increase organic P and Al- and Fe-bound P, respectively (Figure 2). The mineral weathering rate is highest at an early stage of pedogenesis and is mainly controlled by vegetation type, climate, and P content in the parent material (Zhou *et al*., 2018).

At a more advanced stage of soil formation, after up to 10^3-10^5 years, increasing sorption stabilises both organic and inorganic P until the soil reaches a so-called "terminal steady state of profound P limitation" (Vitousek *et al*., 2010; Walker & Syers, 1976). Several studies have confirmed the relevance of Walker-Syers's model for soils from other climates, including studies carried out for young chronosequences in humid temperate climates (Prietzel *et al*., 2013; Turner *et al*., 2007).
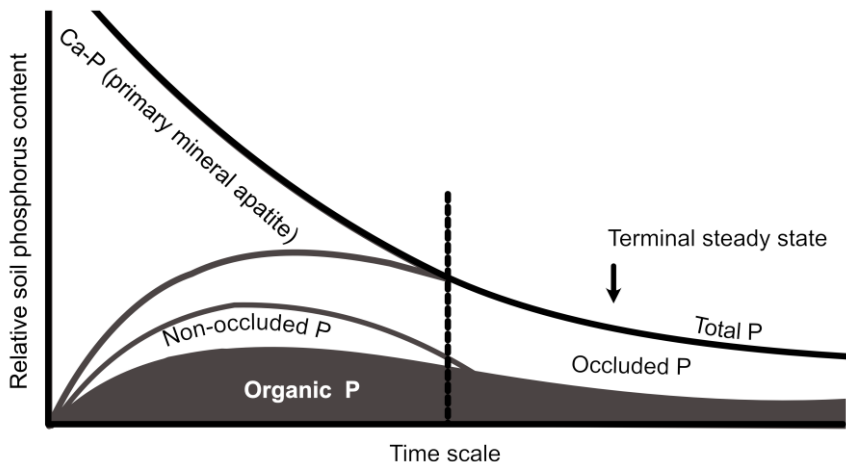
Figure 2: Walker and Syers (1976) conceptual model of changes in forms and amounts of soil phosphorus during long-term ecosystem development. Figure adapted from Walker & Syers (1976).

3.4.2. Podzolisation

The term Podzol, as used in most soil classifications (WRB, 2014), Spodosol (in USA and China), or Podosol (in Australia) (Sauer *et al.*, 2007; Soil Survey Staff, 2014; Wood *et al.*, 1984; WRB, 2014) is derived from the Russian word "*pod*," which means "under," and "*zola*", which means "ash" (Mokma & Buurman, 1987; Sauer *et al.*, 2007). In this thesis, the term Podzol is used. This soil type covers ~5 million km^2 of land world-wide. It is predominant in humid temperate and boreal regions of the northern hemisphere, most commonly in Scandinavia, the north-western Russian Federation, and Canada (IUSS Working Group, 2014; Lundström *et al.*, 2000b). In Sweden, podzolised soils cover more than half of the total forested land area (Gustafsson *et al.*, 1998). These soils are developed from a hard siliceous, nutrient-poor parent material (*e.g.*, glacial or sandy till) (Andersson *et al.*, 2014). Due to their low fertility, Podzols are not suitable for arable production but are productive under forests such as conifers (WRB, 2014).

Several studies have explored the mechanisms of Podzolisation. These include mobilisation, migration, and immobilisation of Al and Fe through the soil profile (Lundström *et al.*, 2000a; Sauer *et al.*, 2007). In this thesis, the current definition of Podzolisation is used (Gustafsson *et al.*, 1998; Lundström *et al.*, 2000b), making it possible to summarise the relevant mechanisms in Scandinavian forest soils, as shown in Figure 3.
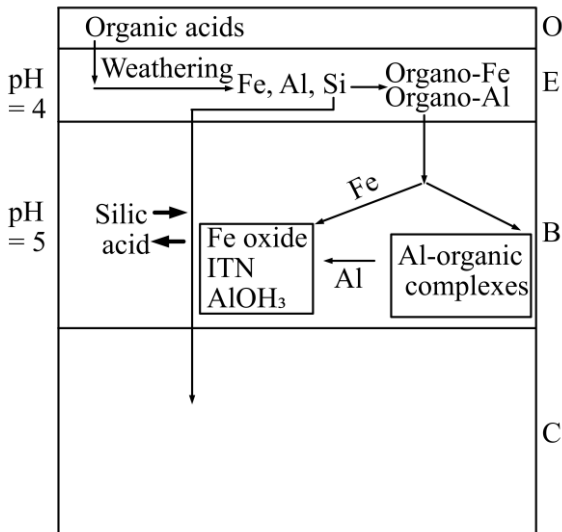
Figure 3: Current view of podzolisation in a soil profile. Figure adapted from Gustafsson et al. (1998). ITN: imogolite-type nanoparticles.

Formation and migration of organometallic complexes (OM-C)

In the surface soil horizon, a large amount of acidity generated by the production of organic acids and exudates from plant roots and mycorrhizal hyphae triggers the weathering of primary silicate minerals (Lundström *et al.*, 2000b). Thus, weatherable minerals, in particular on the surfaces of topsoil minerals, are dissolved and removed. This results in the formation of an eluvial E horizon bleached by organic acids. The E horizon overlies a dark-coloured (reddish black, dark brown, black) illuvial or spodic B horizon rich in Al and Fe.

Organic acids transport the weathered Al and Fe as OM-C from the eluvial E horizon to the B horizon, where they are stopped due to two possible reasons. (i) The OM-C lose their net negative charge and therefore become insoluble; or (ii) the relatively higher pH in the B horizon causes imogolite-type nanoparticles (ITN: proto-imogolite allophane and well-developed imogolite) to form. Once they reach the less acidic spodic horizon, Fe (hydr)oxides are also released from OM-C. Then, the soil solution becomes supersaturated, which results in the precipitation of these minerals (Gustafsson *et al.*, 1998).

Mechanisms of immobilisation and precipitation

Upon arrival in the B horizon, OM-C are microbially degraded, releasing Al^{3+} and Fe^{3+}, which precipitate as Al hydroxides, ITNs, and Fe (hydr)oxides, respectively (Gustafsson *et al.*, 1995; Gustafsson *et al.*, 1998). Together with ferrihydrite, ITNs are, as a rule, the most common surface-active minerals in acidic Podzols (Parfitt, 1989; Parfitt, 1979). Consequently, a large proportion of biogeochemically active P is sorbed onto the positively charged surfaces of Al and Fe surface minerals (Prietzel *et al.*, 2016; Wood *et al.*, 1984), mainly ITNs (Parfitt, 1989). Therefore, the Podzolic B horizon stores a large P pool that may have limited or no availability (Wood *et al.*, 1984).

3.5. Effects of wood ash fertilisation on phosphorus

To increase bioenergy production from the combustion of plant biomass, especially tree tops, branches, and twigs, in order to meet the legally binding climate target of reducing fossil fuel emissions, logging residues are being extracted to a greater extent, *e.g.* through whole-tree harvesting (WTH) (Camia *et al.*, 2021). However, from a forest P nutrition perspective, WTH may be a cause for concern as it leads to accelerated removal of P through harvested biomass compared to convetional way of thinning i.e. stem-only harvesting. This is because P (as well as other nutrients) concentration is higher in leaves, twigs, and branches than in stem wood. According to Yanai (1998), up to 50 kg P ha^{-1} was removed from hardwood forest ecosystems by WTH. Furthermore, a mass balance study carried out for 14,550 Swedish sites showed that at southern sites, forestry results in the loss of more than, on average, 1 kg P ha^{-1} y^{-1} (Akselsson *et al.*, 2019). At the same time, hundreds of thousands of tons of wood ash (estimated 250,000−300,000 tons y^{-1}), a by-product of wood combustion, are produced in Sweden each year (Bjurström *et al.*, 2003; Mellbo *et al.*, 2008). However, only a small fraction of the ash is recycled back into forests to restore nutrient reserves (Swedish Forest Agency, 2019).

Original wood ash (loose ash) contains highly reactive constituents such as metal oxides that can dissolve quickly, resulting in harmful effects on the biota (Karltun *et al.*, 2008). Therefore, stabilising the loose ash by self-hardening or granule formation is recommended to reduce the solubility of chemical compounds in the ash (Steenari & Lindqvist, 1997; Jacobson *et al.*, 2014). Prior to application, the treated ash is crushed (Jacobson *et al.*, 2014).

Wood ash contains all important plant nutrients except N, the proportion of which is very low in ash due to the formation of nitrous oxides during combustion (Karltun *et al.*, 2008). The P content of the stabilised ash varies between 0.17 and 2.2%, depending on the combustion process and the quality of the wood (Augusto *et al.*, 2008; Hannam *et al.*, 2018; Olsson & Westling, 2006; Steenari *et al.*, 1999b). P in the ash is often present as crystalline hydroxyapatite, $Ca_5(PO_4)_3OH$ (Steenari & Lindqvist, 1997). This may explain the long-term effects of ash application on soil P availability. For example, Eriksson (1996) showed, in a column experiment, that 15-20% of the P in the ash dissolved during five months of application to soil.

Wood ash recycling is currently primarily carried out in the Nordic countries and Canada (Augusto *et al.*, 2008; Hannam *et al.*, 2018; Huotari *et*

al., 2015; Pitman, 2006; Reid & Watmough, 2014). Much research on the composition and effects of wood ash application has focused on these regions. P solubility in wood ash-amended soils has also been evaluated in many studies, but with somewhat contradictory results (Augusto *et al*., 2008; Clarholm, 1994; Jacobson *et al*., 2014). Several factors may contribute to the discrepancy in results, including ash application amount, the timescale of the study, rate of dissolution *etc*. (Jacobson, 2003; Jacobson *et al*., 2004; Ohno, 1992) or quality of removed biomass concerning nutrients content. Because of N limitation in soils and the very low content of N in wood ash, N is sometimes added simultaneously with the ash.

4. Materials and methods

4.1. Forest sites

Eight forest sites were selected for the studies in this thesis, to encompass variations in soil geochemistry and climate (Table 1).

Table 1: *Overview of the eight forest sites and soils selected for study in this thesis, organised by location in Sweden (north to south). MAP: mean annual precipitation (mm), MAT: mean annual temperature (°C).*

Forest site	MAP	MAT	Location	Forest type	Parent material	Soil order
Flakaliden (14B)	600	1	64°07′N, 19°27′E	Norway spruce	Glacial till	Albic Podzol
Rödålund (1470)	600	2	64°08′N 19°52′E	Scots pine	Postglacial Sand	Albic Podzol
Tärnsjö	600	5.1	60°08′N 16°55′E	Norway spruce, Scots pine	Postglacial Sandy	Albic Podzol
Kloten	927	4.9	59°54′N 15°25′E	Norway spruce. Scots pine	Glacial till	Albic Podzol
Riddarhyttan (250)	730	3.9	59°48′N, 15°32′E	Scots pine	Sandy	Albic Podzol
Skogaby	1187	7.6	56°33′N 13°13′E	Norway spruce	Glacial till	Albic Podzol
Tönnersjöheden (T103)	1053	6.4	56°40′N 13°05′E	Norway spruce	Postglacial Sandy still	Dystric Arenosol
Asa	800	6.4	57°08′N 14°45′E	Norway spruce	Glacial till	Dystric Arenosol

According to X-ray powder diffraction, the fine-earth mineralogy of the collected soils is dominated by quartz (43−56% w/w), followed by plagioclase and K-feldspar (on average 25% and 17% w/w, respectively). In the B horizon of the selected soils, the poorly crystalline mineral phase of Al varied between 3.3 and 11.1% and those of Fe between 1.0 and 3.2%. Apatite was detectable in the C horizon but never exceeded 0.3% (w/w) (Casetou-Gustafson *et al*., 2019; Simonsson *et al*., 2015 (for Skogaby); supporting data in Paper I). The mineralogy was not analysed for Riddarhyttan.

All eight sites have been used extensively in previous studies for various purposes, including investigation of nutrient supply, tree harvesting effects on forest production *etc*. (Bergh *et al*., 1999; Jacobson *et al*., 2014; Lim *et al*., 2020; Olsson *et al*., 1996).

4.2. Treatments

The effects of wood ash fertilisation on P chemistry were studied at two sites, Rödålund (one of the sites included in the study on P speciation in soil profiles in Paper I) and Riddarhyttan.

Due to the time limitations, not all treatments conducted on these sites were included. Moreover, concerning the effects of fertilisation, the main focus of this thesis was to examine if the wood ash application improves the P status after biomass removal and the mechanism involved. Thus, at Rödålund, treatments 2 and 4 were only selected. The latter treatment was included to assess if there could be an interaction between the wood ash and repeated N fertilisation. At Riddarhyttan, the experiment differs from that of Rödålund. Since the ash was applied at a different dose, the main focus was to assess the effects of changing the amount of wood ash applied. These differences in experimental setups at the two sites (Figure S2, supporting information of paper IV) led us to apply different sampling methods and data analysis (details below).

Rödålund is a managed forest where the effects of different logging methods, wood ash, and N application rates have been studied since 2001. Two types of forest management are compared at the site: (1) stem-only thinning and (2) whole-tree thinning. In 2002, fertilisation with "Skog-Can" N fertiliser, consisting of ammonium nitrate (NH_4NO_3) with the addition of dolomitic lime (5% Ca, 2.4% Mg) and boron (0.2%), was initiated. Different combinations of logging and N fertilisation made the four main treatments,

each assigned to six replicates realised plots (Table 2) with a size of 60×70 m^2, of which 40×50 m^2 is the net plot (Lim *et al*., 2020). Between 2002 and 2019, N fertiliser was added in different doses: control, single N fertilisation with 150 kg ha^{-1}, and repeated fertilisation with 150 kg N ha^{-1} every three years. In this thesis, two treatments (shown in bold in Table 2) were used.

In 2005, each plot was divided into two equal parts, and wood ash (3 Mg ha^{-1}) was added to one of the sub-plots in each main plot. Thus, the Rödålund experiment has a split-plot design, with ash application as the split-plot or sub-plot factor.

Table 2: *Summary of treatments in the Rödålund forest management experiment. Treatments shown in bold were included in studies in this thesis*

Thinning	Nitrogen fertiliser (kg ha^{-1})	Wood ash (Mg ha^{-1})*	Ash-P (%)
1. Stem-only harvesting	0	0	0
2. Whole-tree thinning	**0**	**3**	**1.6**
3. Whole-tree thinning	150 (added once)	3	1.6
4. Whole-tree thinning	**Repeat 150/ three years**	**3**	**1.6**

* Experimental unit for the wood ash is a subplot within plots.

Previous studies conducted at Rödålund showed that whole-tree thinning (WTT) did not affect soil chemical properties, including the carbon (C) stock, compared with stem-only thinning (Lim *et al*., 2020). Hence, in this thesis, WTT was used as a reference when analysing the effects of wood ash application and N fertilisation.

The Riddarhyttan experiment consists of many wood ash treatments at different application rates and N fertilisation levels (Jacobson *et al*., 2014). Since the interest in this thesis was in quantifying the effects of changing the ash dose on P chemistry, only four treatments were selected for study: control (*i.e*. no ash) and application of 3, 6, and 9 Mg wood ash ha^{-1}. The P content in the ash was 0.8%.

The experiment is designed as a randomised block approach, with four different wood ash application doses and three blocks (Jacobson *et al*., 2014). The ash used was self-hardened, crushed ash from a pulp mill in Piteå, northern Sweden, and was applied in 1995. The treatments were assigned to experimental plots (net size 30×30 m^2) surrounded by a buffer strip of about 5 m (Jacobson *et al*., 2014).

4.3. Soil sampling

Soil sampling at all sites was carried out at different times and in different ways, depending on the intended purpose of the samples. In Papers I, II, and III, soil pits (down to 1 m deep) were dug at each site, in the control plots or outside the field experiments. At the Flakaliden and Asa sites, soil samples were taken in October 2013 and March 2014, respectively, and were first used for mineralogical studies. Soils were collected from many pits at each site (Casetou-Gustafson *et al*., 2018). In the current study, we only included soil profiles in control treatments labelled K1 at Asa and 14B at Flakaliden. At Skogaby, the soil samples used were also from the control plot (labelled 24C), one of several soil profiles previously excavated and studied for mineralogical composition (Simonsson *et al*., 2016). Those from Tärnsjö and Kloten were collected in 2017, while the soil pit at Rödålund was excavated in August 2018. At all seven sites, soil samples were taken separately from the organic (O) and eluvial (E) or A horizons to allow the calculation of horizon-specific P stocks. The thickness of the O horizon varied between 5 and 7 cm, while that of the E or A horizon varied between 2 and ~20 cm (Figure 4 and Table S1 in Paper I). From the B horizon down to the C horizon, soil samples were collected at 10-cm intervals. The soil pits at Kloten and Rödålund extended down to only 50 cm and 80 cm, respectively, because of a high content of stones and large boulders (Figure 4).
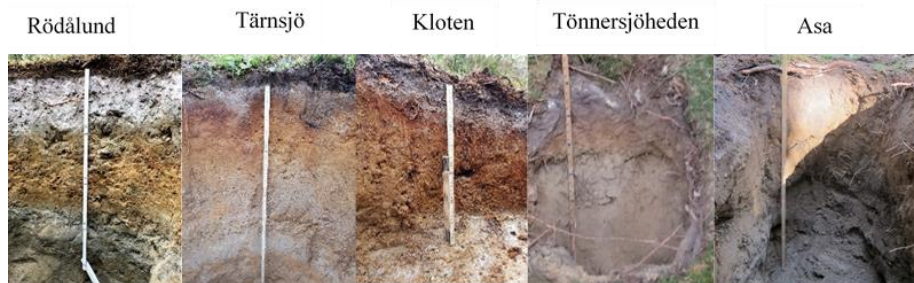
Figure 4: Images of five of the soil profiles studied. Images for Flakaliden and Skogaby are missing. (Photos from Tärnsjö and Kloten: Jon Petter Gustafsson; Tönnersjöheden and Asa: Bengt Olsson and Therese Sahlén Zetterberg).

In Paper IV, only the O horizon at Rödålund and Riddarhyttan was sampled in 2018 and 2019, respectively. At Rödålund, the samples were taken from 10 random locations in each subplot, using a 10 cm diameter soil core. 2 m from each side of the plot was excluded during sampling. All collected

samples were then mixed to make a composite sample. For that study, soil samples were collected from plots where wood ash had been added to the subplots alone or simultaneously with N. In total, 24 samples were collected from 12 plots. At Riddarhyttan, samples were collected as in Rödålund in 2019 from plots treated with 0, 3, 6, and 9 Mg wood ash ha^{-1}. In total, 12 samples were collected, considering three replicates for each treatment dose.

4.4.   Determination of soil properties

Before analysis of soil samples, undecomposed plant litter, roots, and stones were gently removed. Next, fresh samples from the O layer were sieved through an 8 mm stainless steel sieve, while the mineral soil was sieved through a 4 mm sieve of the same type.

The pH (H_2O) of the O horizon was measured on sieved fresh samples in deionzied water (soil: solution ratio 1:10) after shaking the mixture for 24 h (Blakemore, 1987). All soil samples were then air-dried for approximately 7 days at 30 °C and sieved again (<2 mm) before further analyses. For mineral soils, pH (H_2O) was measured in deionized water using a soil:solution ratio of 1:2.5 (van Reeuwijk, 1986).

Total organic C content (orgC) and total nitrogen (TN) were determined after dry combustion of samples (ISO, 1998), using an elemental CN analyzer (TruMac® CN, Leco Corp, St Joseph, MI, USA) for macrosamples. Molar C:P and N:P ratios were calculated based on these C and N fractions and the content of organic P obtained from bulk P-K edge XANES (see below).

The concentration of acid-digestible P (TP) was determined by inductively coupled plasma mass spectrometry (ICP-MS) after HNO_3/H_2O_2 digestion of dried soil, following ISO 11, 466 (ISO, 1995). Oxalate-extractable-Al (Al_{ox}), -Fe (Fe_{ox}), and -silicon (Si_{ox}) were determined using acid-oxalate (see section 4.5). Pyrophosphate-extractable Al and Fe (Al_{py} and Fe_{py}) were quantified using inductively coupled plasma optical emission spectroscopy (ICP-OES) (see Paper I). The degree of P saturation (DPS) on Al and Fe was also calculated, using the molar concentrations of Al- and Fe-bound P as determined by bulk- XANES:

$$DPS = \frac{\text{P bound to Al and Fe}}{0.5 \text{ x (Feox+Alox)}} \qquad (1)$$

with P, Fe_{ox} and Al_{ox} expressed in mmol kg^{-1}.

4.5. Extractable phosphorus

Olsen-P and P-AL, which are $NaHCO_3$-and acid ammonium lactate-extractable P, represent a plant-available P. These were analysed by the AA3 Auto-Analyzer (Seal Analytical, Norderstedt, Germany), using the acid molybdate method as modified by (Wolf and Baker, 1990). P_{ox} represents the acid oxalate-extractable P associated Al_{ox}, Fe_{ox} (see above). They were analysed by inductively coupled plasma optical emission spectroscopy (ICP-OES). Pi_{ox} is the fraction of inorganic P_{ox}, as was analysed by AA3 Auto-Analyzer using the same soil solution. The difference between these two was assigned to organic P (P_{orgox}).

Table 3: *Description of phosphorus (P) extractants and methods used in the studies in this thesis.*

Extractable-P	S:L	Method	Time	Analysis	Reference
Olsen-P	1:20	0.5M $NaHCO_3$ (pH 8.5)	0.5 h	AA3	(Olsen, 1954)
P-AL	1:20	0.1 M NH_4-lactate (pH 3.75)	1.5 h	ICP-OES	(Egnér *et al*., 1960)
P_{ox}	1:100	Acid oxalate (pH 3.0)	4 h	ICP-OES	(van Reeuwijk, 1986)
Pi_{ox}	1:100	Acid oxalate (pH 3.0)	4 h	AA3	(van Reeuwijk, 1986)
TP	-	HNO_3/H_2O_2 digestion	-		ISO 11, 466 (ISO, 1995)

S:L is the soil-to-extractant solution ratio.

4.6. Bulk- and microscale (µ-) soil phosphorus speciation

4.6.1. Phosphorus speciation in bulk soil

To assess P speciation in the bulk soil, P-*K* edge XANES spectra were collected for 108 soil samples (bulk) at beamline 8 (BL 8) (Klysubun *et al*., 2020) of the Synchrotron Light Research Institute (SLRI) in Nakhon Ratchasima, Thailand. These comprised 72 samples from the O, E and A, B, and C horizons (Papers I, II, and III) and 36 samples from the O horizon collected from the fertilisation experiments (Paper IV). The protocol of Eriksson *et al*. (2016) was followed in sample preparation and measurements. Between 4 and 8 scans were made for each sample.

4.6.2. Soil phosphorus speciation in microsites

Microscopic X-ray fluorescence (µ-XRF) imaging was performed to produce elemental distribution maps of P and other relevant elements (Al, Fe, Si) representing the main P-containing phases. Soil samples (0-2, 10-20, and 30-40 cm from Tärnsjö, 40-50 cm from Flakaliden) included in this thesis, were prepared as petrographic thin sections (30 µm thick). The samples were embedded in high-purity epoxy resin and mounted on glass slides at the TS Lab & Geoservices snc, Cascina, Italy.

In this thesis, the P speciation in the soil microsites from the E (0-2 cm) and B horizons of the Tärnsjö soil was studied (Paper II). The µ-XRF maps collected included those of P, Al, and Si, the latter two elements considered as main constituents of the Swedish forest soils.

In Paper III, two-dimensional (2D) tri-colour µ-XRF images of P, Al, and Fe were constructed for the 40-50 cm soil sample from Flakaliden, which is rich in Al_{ox} and Fe_{ox}, to explore in more detail, the extent to which the secondary P phase in the P-rich spodic B horizon can be distinguished as P bound to Al and P bound to Fe.

To obtain high-quality µ-XRF maps for P, the data were recorded immediately above the P K-edge energy (2.6 keV). However, Fe maps were acquired at the L-shell energy because the K-edge is much higher (7.1 eV).

The data in papers II and III were collected at the LUCIA beamline ((Vantelon *et al*., 2016); beam size 2.5×2.5 µm^2, using a Kirkpatrick-Baez (KB) mirror system) at the French national synchrotron research centre SOLEIL in 2019 and 2021, respectively. The µ-XRF images were acquired with a dwell time of 0.3 s and an energy step of 3×3 µm^2. In each µ-XRF map, P K-edge µ-XANES spectroscopy was then applied to up to 20 selected spots (2 and 8 scans per spot).

4.6.3. Analysis of X-ray fluorescence and absorption data

The raw µ-XRF spectra were batch-fitted at each pixel to obtain processed elemental distribution maps using the Python Multichannel Analyzer (PyMCA) software (Solé *et al*., 2007). The ImageJ (Fiji Is Just) software was then used to reconstruct µ-XRF tri-colour maps from elemental distribution images. Moreover, for paper III, a colour picker tool in affinity designer software was used to sample the colour from processed tri-colour µ-XRF maps of P, Al, and Fe. Since some P spots were too small to be clearly seen,

that step was performed to reproduce larger and more visible shapes representing the colour distribution of P spots in the microsites (Figure 8).

Linear combination fitting (LCF) was performed on merged and normalized bulk and µ-XANES spectra according to Eriksson *et al.* (2016). XANES spectra of 14 P standards (Figure 5) used in LCF were also collected at both beamlines. These were chosen to represent P species relevant in podzolised forest soils. The uncertainty associated with the LCF results was further investigated according to Gustafsson *et al.* (2020). Detail on the origin and synthesis of P standards can be found in Gustafsson *et al.* (2020).
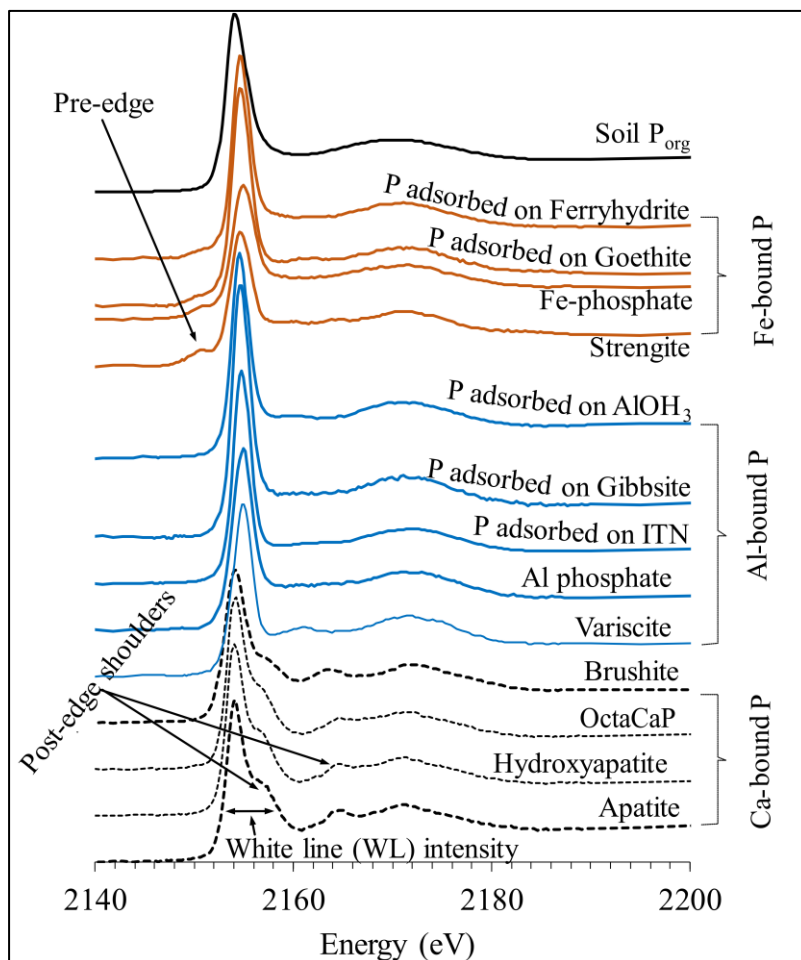
Figure 5: X-ray absorption near-edge spectroscopy spectra of 14 standards representative of relevant phosphorus forms in acid boreal forest soils used in linear combination fitting.

When analysing localised spots for P speciation, the micrometre-sized beam can hit non-homogeneous soil particles or grains. If high-energy elements, such as Fe or Ca, is present in the target microsite, the spectra obtained may become distorted due to the self-absorption effect (Hesterberg, 2010). This may affect the spectral features and make LCF results i.e. the weighted % of P species, less certain. Hence, in paper III, we focused on observing the colour of spots in the μ-XRF images and diagnostic features of μ-XANES spectra (Figure 5). These spectral characteristics are a wider WL with low intensity and a post-edge characteristic of Ca-bound P species, high intensity of the WL and a pre-edge for Fe-adsorbed P, low intensity of the WL and a pre-edge for Fe-phosphates, a higher intensity of the WL characteristic of Al-adsorbed P, low intensity of the WL of the Al-phosphates.

4.7. Phosphorus stocks

4.7.1. Stocks in soil horizons

The TP and P species stocks in each soil horizon were calculated as the amount of TP. First, the concentration of different P species in g per unit area (m^2) was calculated for each sampling depth according to Strand *et al.* (2016):

$$P_{stocks} = BD \times CF_{coarse} \, P \times d \qquad (2)$$

Where CF coarse is a correction factor for stones and boulder content:

$$CFcoarse = 1 - \frac{\text{volume of stones (\%)}}{100} \qquad (3)$$

BD is the bulk density (kg m^{-3}), calculated from the C (% dry weight) content using a pedotransfer function (Nilsson & Lundin, 2006):

$$BD \text{ mineral soil} = 1000. \left(1.5463 \times \left(e^{-0.3130 \times \sqrt{C_{org}}} \right) + 0.207 \times d \right) \qquad (4)$$

$$BD \text{ organic} - \text{rich soil} = 1000. \left(\frac{C_{org}}{-2.1278 + 0.1528 \times C_{org} + 0.2105 \times C_{org}^2} \right) \qquad (5)$$

where C_{org} is organic carbon (% dry weight), P is phosphorus (kg kg^{-1}), and d is sampling depth increment (m). Data on stone content at the study sites were taken from earlier studies as follows: Asa and Flakaliden: Casetou-Gustafson *et al.* (2020); Rödålund: Lim *et al.* (2020); Tärnsjö, Kloten and Skogaby: Stendahl *et al.* (2009); and Tönnersjöheden: Viro (1952).

4.7.2. Phosphorus stocks in the organic layer and above-ground biomass in the fertilisation experiments

The stocks of TP, extractable P, and P species in the wood ash- and N-fertilised O horizon were estimated as a product of P concentrations (mg kg^{-1}) and O layer dry mass (kg m^{-2}). For Rödålund, we used O layer mass data from Lim *et al*. (2020).

P stocks in the above-ground biomass were calculated using the biomass of each tree component (needles+branches+stembark+ Stemwood) collected in 2009 and corresponding P concentrations measured in 2008. We assumed there was no change in the P concentration within one year. More detail can be found in paper IV. This was only calculated for Rödålund because the P concentration in plant biomass from Riddarhyttan was unavailable.

4.8. Statistics

In Paper IV, statistical analysis was performed to determine the effects of wood ash and N application on the P speciation and solubility in the O horizon at Rödålund. Moreover, we applied statistics to quantify the effects of varying amounts of wood ash application on the P speciation and solubility in the O horizon at Riddarhyttan.

As only one soil pit per site was studied in the other papers, *i.e*., there were no replicate pits, it was not relevant to apply statistical methods to analyse differences in P status between sites. Instead, Pearson correlation (or simple regression) analysis was performed in Paper I to investigate the relationships between P and other soil properties. In addition, simple regression analysis was performed to analyse the relationship between oxalate-extractable P (P_{ox}) and P bound to Al and Fe determined from bulk-XANES. The software R (v.4.02) was used for all statistical analyses.

In the Rödålund fertilisation experiment, treatments with repeated N fertiliser at two levels (N and no N addition) were randomly assigned to six replicate experimental plots ($n = 6$). All these plots were divided into two sub-plots each and two wood ash treatments (ash and no ash addition levels) were applied, one to each of the sub-plots in each plot ($n = 12$). The design meant that N was a whole-plot factor, while ash was a sub-plot factor. Therefore, a split-plot analysis of variance (ANOVA) model (Kenward-Roger method) was employed to determine the effects of wood ash and repeated N fertilisation in a two-factor analysis. The model also included the

"Ash $\times$ N" interaction between the two treatment factors, the whole-plot random error, and the regular residual error (sub-plot error). Moreover, the Tukey method (p=0.05) using the least squares means (emmeans) function was used to compare the estimated means of different groups of ash and N treatments. The split-plot model was chosen because it is robust to detect the effects of the subplot factor i.e. wood ash (Gomez and Gomez, 1984).

The Riddarhyttan experiment consisted of a randomized block design. The wood ash (0 (control), 3, 6, and 9 Mg ha^{-1}) was assigned to experimental plots in three blocks ($n = 3$). Linear mixed-effect regression analysis with block and wood ash treatment (as a continuous variable) was chosen to quantitatively determine the effects of ash on P extractability and speciation. The random normality was checked by plotting the final residuals.

5. Results

This chapter begins with a detailed description of solubility, speciation, and vertical distribution of native P in seven soil profiles down to 1 m depth (Paper 1). Next, microscale speciation and spatial distribution of P species in microsites containing Al and Si minerals in the E and B horizons of Tärnsjö are presented (Paper II). Then, results detailing microscale P speciation between secondary Al-bound P and Fe-bound P in the Flakaliden B horizon follow (Paper III). After the results on native P speciation, stocks of P species in different soil horizons are reported (Paper I) before presenting the results of the effects of wood ash and N application (Paper IV).

5.1. Chemical speciation and solubility of native phosphorus

5.1.1. Phosphorus extractability across soil profiles (Papers I and II)

A total of 73 samples were studied across soil profiles. The data are presented as horizon-average P concentrations (Table 4). Based on horizon-average concentrations, the TP range was 18.3−21.6, 1.7− 4.1, 8.3− 11.8, 5.6−24.4, and 7.3−16.7 mmol kg^{-1} in the O, E, A, B, and C horizons, respectively.

Oxalate-extractable P (P_{ox}) was, on average, 77% of TP in the B horizon. In the E/A and C horizons, the proportion of P_{ox} to the TP was 45% and 56%, respectively. The lowest P_{ox} proportion, i.e. P_{ox} to TP ratio, was calculated for Tärnsjö, an Al-and Fe-poor soil profile, especially in the C horizon, with P_{ox} contributing on average 20% in its C horizon. For all soil samples investigated, on average, 66% of P_{ox} was inorganic P (Pi_{ox}). The remaining fraction was assumed to represent organic P (P_{org-ox}) (paper I).

The proportion of P-AL relative to P_{ox} in the O layer was higher than 73%. The proportion ranged between 12 and 56% in the E horizon but never exceeded 5% in the B horizon except at Tärnsjö and Asa, where it was 12%. Olsen-P showed a similar trend but with a lower concentration than P-AL.

Table 4: *Average concentration of extractable P per soil horizon at seven study sites.*

Soil horizon	Depth	TP	P_{ox}	Pi_{ox}	$P_{org\text{-}ox}$	P-AL	Olsen-P
	cm			mmol kg^{-1}			
Flakaliden							
O	>0	18.3	9.1	4.2	4.9	6.6	2.9
E	0-20	2.0	0.9	0.3	0.6	0.5	0.2
B	20-50	24.4	22.6	19.8	2.8	1	0.8
C	50-100	16.7	12.2	10.9	1.3	1.5	0.4
Rödålund							
O	>0	19.2	5.3	2.7	2.6	4.6	1.8
E	0-20	1.7	1.2	0.5	0.7	0.2	0.1
B	20-50	5.6	2.9	2.2	0.7	0.1	0.1
C	50-80	12.1	8.0	7.0	1.0	1.3	0.2
Tärnsjö							
O	>0	18.4	4.3	2.6	1.7	4.4	2.2
E	0-2	2.0	0.5	0.2	0.4	0.2	0.1
B	02-40	15.5	11.6	10.2	1.5	1.3	0.8
C	40-100	14.7	3.0	2.5	0.5	0.6	0.2
Kloten							
O	>0	18.3	4.8	2.5	2.3	5.0	2.2
E	0-7	1.7	0.8	0.1	0.7	0.3	0.1
B	7-40	9.2	6.5	4.1	2.4	0.2	0.1
C	40-50	7.3	5.6	4.4	1.2	0.2	0.1
Skogaby							
O	>0	20.6	7.9	3.6	4.4	6.2	3.8
E	0-10	4.1	3.4	1.0	2.4	1.1	0.6
B	10-60	7.2	6.0	3.6	2.4	0.1	0.1
C	60-100	8.3	3.8	3.0	0.8	0.7	0.1
Tönnersjöheden							
O	>0	21.6	5.5	2.1	3.3	4.8	2.2
A	0-10	8.3	5.6	2.0	3.5	0.8	0.2
B	10-50	16.9	12.5	9.1	3.5	0.6	0.3
C	50-100	14.6	7.6	5.7	1.9	0.9	0.1
Asa							
E	0-10	11.8	7.6	3.3	4.3	0.9	0.3
B	10-50	11.4	7.8	3.2	4.6	0.9	0.2
C	50-100	15.3	9.2	7.2	2.0	1.7	0.1

P_{ox}, Pi_{ox}, and $P_{org\text{-}ox}$ are oxalate-extractable TP, inorganic P, and organic P.

5.1.2. Phosphorus speciation in bulk soil (Paper I)

Concerning the bulk-soil P speciation (Figure 6), P_{org} was the main P fraction of TP in the O layer, accounting for between 73 and 91%. In agreement with the chemical extraction results (Table 4), the concentrations of TP and its fractions were lowest in the E horizon, especially at Flakaliden, Rödålund, Tärnsjö, and Kloten, where the E horizon is well-developed (see Figure 4).

The P speciation in the E horizon was highly variable. For example, in the upper 30 cm, Ca-bound P constituted only between 0 and 29%. On the other hand, Rödålund and Kloten, which are relatively P-poor soils, had a greater proportion of P_{org} in their E horizon (65% and 57% of TP, respectively). The P in the Skogaby E horizon was present mainly as Al-bound P (68% of TP), while the comparable A horizon at Tönnersjöheden and Asa had a high Fe-bound P, accounting for 43% and 39% of TP, respectively.

In the B horizon, P bound to secondary Al and Fe precipitates dominated the P speciation. Al-bound P species, particularly P adsorbed on ITN (detail in Paper I), were most often identified in the best LCF fits, contributing between 42 and 74% of TP. Ferrihydrite-adsorbed P, followed by goethite-adsorbed P, were also important Fe-bound P species detected by bulk-XANES in spodic horizons and throughout the soil profiles. It is important to note that the contribution of P_{org} to TP in the B horizon of the southern sites Kloten and Rödålund was not negligible (10−46% of TP).

For all soil samples analysed, the relevance of Ca-bound P increased with soil depth. However, in the Kloten soil, limited to 50 cm depth by the underlying bedrock, 13% of TP was found as a Ca-bound P fraction and was only detectable in its C horizon. The proportion of this P species was lower than that of other soils' C horizons. Furthermore, this soil showed the highest concentrations of Al_{ox} and Fe_{ox}. By contrast, the sandy Tärnsjö soil, with the lowest levels of Al_{ox} and Fe_{ox}, had the highest Ca-bound P fraction. As for Ca-bound P, Tärnsjö was the richest soil profile, with up to 76% of TP as Ca-bound P in the C horizon.
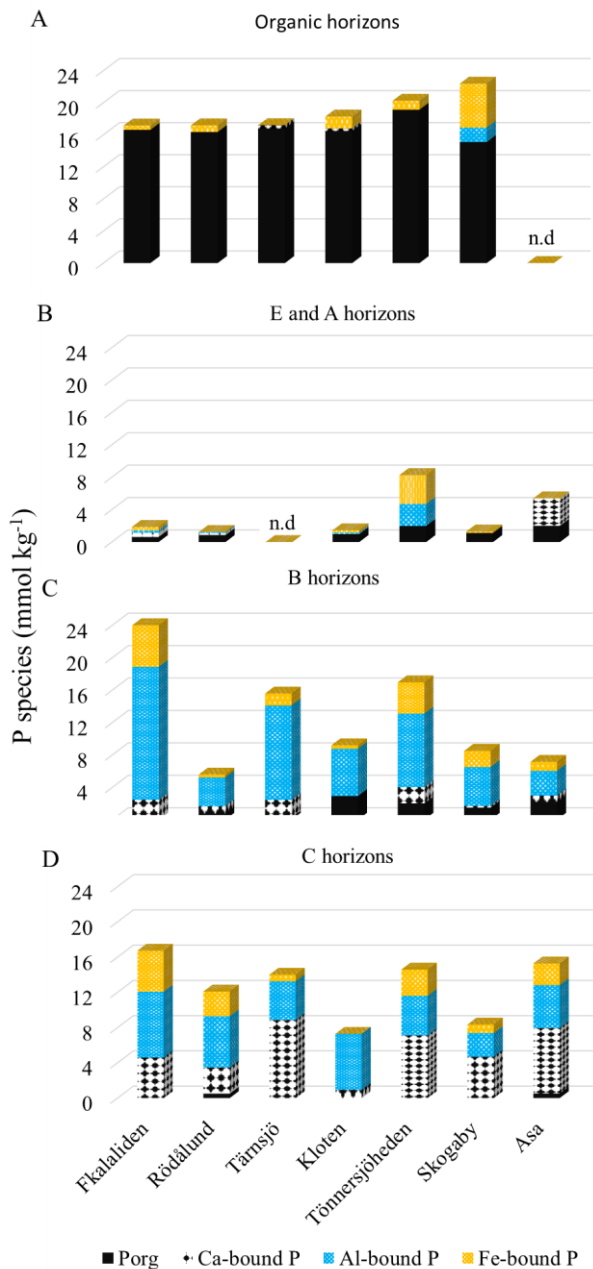
Figure 6: Average phosphorus (P) species (major groups) making up the total P concentration (mmol kg^{-1}) across different soil horizons in seven soil profiles. Soil horizon thickness is reported in Table 4.

5.1.3. Phosphorus speciation in microsites (Papers II and III)

Figure 7 illustrates the μ-scale P distribution in P, Al, and Si co-localisation maps collected from Tärnsjö (Paper II). In Figure 8, a tri-colour μ-XRF image of P, Al, and Fe was collected on the Flakaliden B horizon (40−50 cm) to assess the nature of P associated with pedogenic Al and Fe mineral phases in the B horizons.

E horizons

In Tärnsjö, P spots were few and small in the E horizon (0−2 cm) compared with 10−20 cm and 30−40 cm (Figure 7). Most P spots (tiny green particles) were found on the edges of big Si-containing particles or highly fractured siliceous grains in this very porous and thin horizon (0−2 cm). However, as TP was low (Table 4), μ-XANES (and bulk XANES) spectroscopy were not successful in detecting any P species at Tärnsjö.
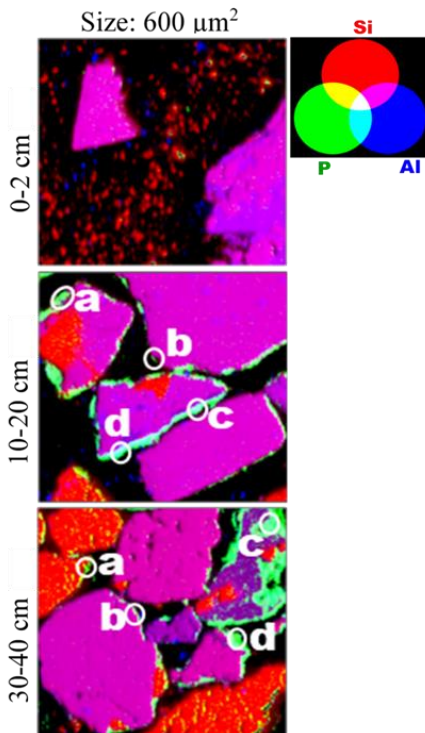
Figure 7: Tri-colour microscopic X-ray fluorescence (μ-XRF) distribution maps of phosphorus (green), aluminium (blue) and silicon (red) obtained for thin soil sections from the 0-2 cm (E horizon), 10-20 cm and 30-40 cm (B horizon) horizons at Tärnsjö.

Regarding the co-localisation of P with Si and Al, µ-XRF maps obtained for 10−20 and 30−40 cm soil depth at Tärnsjö contained relatively large Al and Si particles and large pore spaces (Figure 7). No Ca-bound P was detected by µ-XANES in this horizon.

Visually, in Tärnsjö samples, the P was mainly found at the edges of the Al and Si particles, and P was present predominantly as Al-adsorbed P (29−75% of TP), followed by P adsorbed to Fe (17−49% of TP). For example, at 10−20 cm depth, despite the presence of both Fe-bound and Al-bound P in all spots, Al-bound P was the dominant form in spots (c) and (d), contributing 68% and 83% of TP, respectively. Similarly, the contribution of Al-bound P at 30−40 cm in all spots was at least 57%. Fe-bound P was absent in (d) and was a minor P form in the (a) and (c) spots. In both thin sections, P_{org} was detectable as a minor P species in some locations.

Table 5: *Microscopic X-ray absorption near-edge spectroscopy (µ-XANES) phosphorus (P) speciation in the E and B horizons in the Tärnsjö soil profile, as indicated by linear* combination fitting (LCF). Values *shown are weighted contributions from selected P standards (%). The R-factor is a measure of goodness-of-fit.*

Soil horizon	P spots	P_{org}	Al-bound P		Fe-bound P		Ca-bound P	R-factor
			Al-adsorbed P	Al-P	Fe-adsorbed P	Fe-P		
Tärnsjö								
B 10-20 cm	a	15 ± 2	34 ± 6		51 ± 8			0.004
	b	12 ± 3	39 ± 9		49 ± 12			0.008
	c		68 ± 2		32 ± 2			0.001
	d		68 ± 3	15 ± 2	17 ± 3			0.002
	e	11 ± 2	29 ± 6	22 ± 2	38 ± 8			0.004
B 30-40 cm	a	16 ± 3	61 ± 8		23 ± 8			0.006
	b		57 ± 2	5 ± 1	38 ± 2			0.001
	c	5 ± 2	74 ± 7		23 ± 9			0.004
	d		75 ± 2	25 ± 2				0.002

Al-P: Al phosphate, Fe-P: Fe phosphate.

Flakaliden 40-50 cm is presented as an example in Figure 8 to illustrate the P binding between Al- and Fe-bound P in the B horizons. Most P-containing spots at this soil layer were cyan-coloured, except for spot 2 and especially spot 6, which appeared greener (Figure 8A). In many spots, P co-existed with Al (blue). In agreement with this, most µ-XANES spectra had a strong white-line (WL) intensity (see Figure 5), consistent with the adsorbed P form. A

predominance of Al-bound P was also consistent with LCF results. Al-bound P, mainly adsorbed to ITN, was the most recurrent standard in the best fits and contributed between 54.2 and 99.9% of the total weight (Table 6). However, the µ-XANES spectrum from spot 2 was highly distorted (Figure S8 supporting data of paper III), and the LCF results were uncertain. The fact that spots 2 and 6 appeared, to a large extent, greener than most Al-bound P-dominated spots may indicate the presence of either P_{org} or Ca-bound P.

For instance, in spot 6, P existed predominantly as Ca-bound P (85.6%) (Table 6). Although it also appeared distorted, the µ-XANES spectrum had a wide WL with low intensity and a post-edge characteristic of apatite (Figure S8, supporting data in paper III). In agreement with the µ-XANES features, the µ-XRF map showed this spot as being green. On the other hand, the P in spot 4 was not detectable by XANES, although the cyan colour on the map indicated a predominance of Al-bound P.

The spots where Fe-bound P was present were 3 and 9, contributing 43% and 44.3%, respectively, according to LCF (Table 6). However, the spot's colour did not support this result, as there was no evidence of the yellow colour in the µ-XRF map, which should be expected for spots rich in Fe-bound P. In addition, their spectra did not have a pre-edge, a characteristic of Fe-bound P.
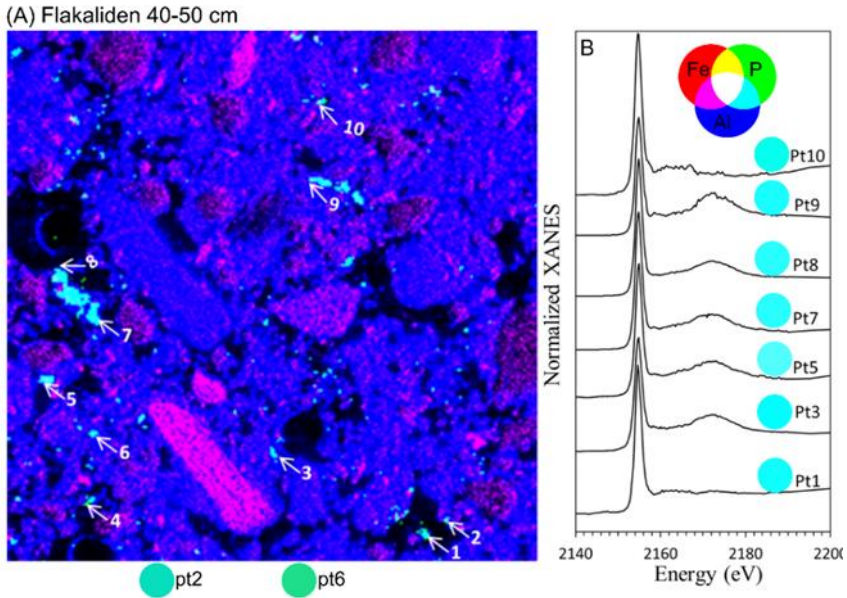
Figure 8: (A) Tri-colour microscopic X-ray fluorescence (μ-XRF) distribution map of phosphorus (green), aluminium (blue) and iron (red) obtained for a 40-50 cm soil sample (thin section) from the Flakaliden soil profile and (B) normalised spot-wise microscopic X-ray absorption near-edge spectroscopy (μ-XANES) spectra obtained from the phosphorus elemental distribution map. The spectra for spots 2 and 6 were distorted and can be found in the supporting information of paper III (Figure S8).

Table 6: *Microscopic X-ray absorption near-edge spectroscopy (μ-XANES) phosphorus (P) speciation in the B horizon (40-50 cm) of the Flakaliden soil profile as indicated by linear combination fitting (LCF). Values shown are weighted contributions from selected P standards (%). The R-factor is a measure of goodness-of-fit.*

Soil horizon	μ- P spots	Porg	Al-bound P		Fe-bound P		Ca-bound P	R-factor
			Al-adsorbed P	Al-P	Fe-adsorbed P	Fe-P		
Flakaliden								
B 40-50 cm	1		100±29					0.03
	2				uncertain			0.3
	3		45±3	12±9		43±1		0.009
	4				n.d			
	5		58±6	16±16		26±12		0.02
	6					13±9	85.6±67	0.2
	7		74±5	6±13		21±2		0.009
	8		65±7	28±18	8±13			0.02
	9		44±9	10±24		46±18		0.05
	10		76±15		76±15			0.03

Al-P: Al phosphate, Fe-P: Fe phosphate. n.d: not detectable.

5.2. Phosphorus species stocks

The amount of P stored in the different soil profiles from the surface layer down to 80 cm depth ranged between 69 and 379 g m^{-2} (Figures 9 and 10). Kloten had the lowest P stocks, partly because that soil is shallow (<50 cm). The total stocks were as follows: Tärnsjö 379 g m^{-2}, Flakaliden 340 g m^{-2}, Tönnersjöheden 310 g m^{-2}, Asa 206 g m^{-2}, Rödålund 184 g m^{-2}, Skogaby 164 g m^{-2} and Kloten 69 g m^{-2}. On average, the TP stock in the O and E/A horizons was 4 g m^{-2} and 9 g m^{-2}, respectively.
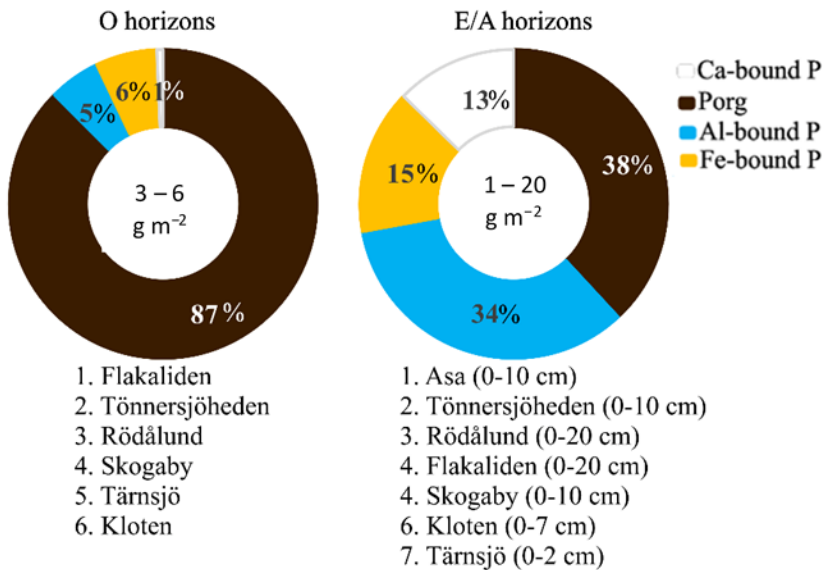
Figure 9: Average composition of the four main phosphorus (P) species groups in the O and E/A horizons of all seven forest soils for which data were available. The percentages indicate the relative contributions of different P species (major groups) to total P as indicated by linear combination fitting (LCF) of P *K*-edge bulk-XANES spectra averaged by the horizon. The range of calculated stocks is presented in the centre of each chart. For each horizon, the sites are ranked from 1 to 7, which is from the highest to the lowest P stocks.

Around 94% of TP was stored in the B and C horizons, partly because these horizons were thicker than the O and E/A horizons. Moreover, P content was substantially higher in the B horizon due to P translocation from the top layer to the B soil horizon by the Podzolisation process. For example, of the TP in the subsoil, mainly in the B horizon, about 60% was adsorbed P (mainly to Al). On average, apatite accounted for 38% of TP in the C horizon. The apatite stocks in the E/A, B and C horizons (down to 80 cm) were, on average, 2%, 20%, and 77% of TP, respectively.
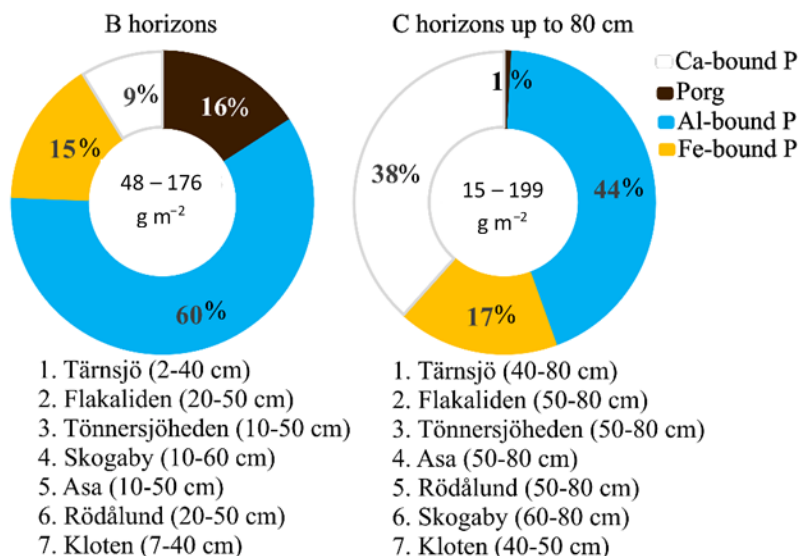
Figure 10: Average composition of the four main phosphorus (P) species groups in the B and C horizons of all seven forest soils for which data were available. Percentages indicate relative contributions of different P species (major groups) to total P as indicated by linear combination fitting (LCF) of P *K*-edge XANES spectra averaged by the horizon. The range of calculated stocks is presented in the centre of each chart. For each horizon, the sites are ranked from 1 to 7, which is from the highest to the lowest P stocks.

5.3. The fate of phosphorus in the organic horizons as influenced by wood ash and N fertilisation (Paper IV)

5.3.1. Extractable phosphorus

As a result of applying wood ash to the Rödålund O horizon, the mean concentrations of both TP and Olsen-P increased by a factor of 1.2, but the change was insignificant (Figure 11). By contrast, Olsen-P in repeated N fertilisation was significantly lower ($p = 0.002$) than in the control treatment. The change in TP was insignificant.
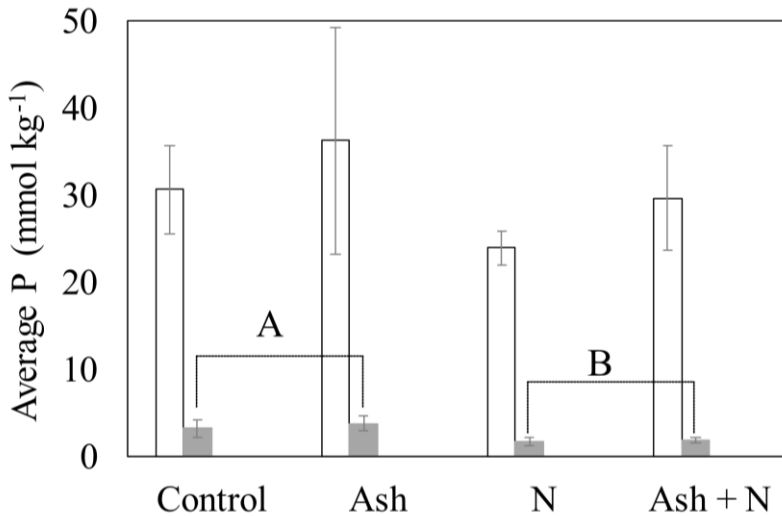
Figure 11: Concentrations of total phosphorus (TP) and Olsen-P (and associated standard deviations) in the O horizon at Rödålund. The data presented are for the treatment groups, but letters (A and B) represent the statistical results of the main treatments. Given that N was a whole-plot factor, different uppercase letters (A, B) indicate a significant difference ($p \leq 0.05$) in the variables between N fertilisation (combined N-only and ash+N treatments) and no N fertilisation (combined control and ash-only treatments) ($n = 6$). Bars without letters indicate no significant difference between the main treatments.

At Riddarhyttan, wood ash application significantly increased TP and Olsen-P content ($p=0.002$ and $p=0.007$, respectively) (Figure 12).
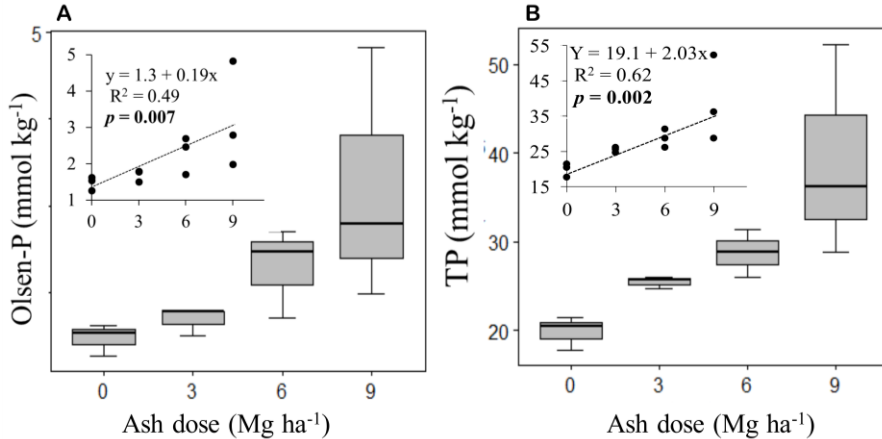
Figure 12: Relationship between amount of wood ash applied and (A) alkaline NaHCO$_3$−extractable phosphorus (Olsen-P) and (B) total P in the O layer at the Riddarhyttan site ($n = 3$). The respective average concentrations per treatment are shown as boxplots.

5.3.2. Phosphorus speciation in bulk soil

Figure 13 shows average P species concentrations (bulk-XANES) per treatment and includes statistics for O horizon samples in long-term fertilisation experiments. The O horizon in the ash treatment with or without simultaneous N addition contained approximately 4.4 mmol kg^{-1} of undissolved Ca-bound P, which was significantly ($p=0.048$) higher than the concentration in the treatment without ash addition (0.4 mmol kg^{-1}). When comparing different treatment groups with wood ash and N, Ca-bound P comprised only 0.5% and 2.7% of TP in the control and N-only treatments, respectively, compared with 6.4% in the ash + N treatment and 18.7% in the treatment with ash only. However, no change in P$_{org}$ (74% of TP) was found. Instead, wood ash with or without N fertiliser significantly ($p=0.009$) increased the concentration of P adsorbed on Al, to 3.1 mmol kg^{-1} compared with 0.9 mmol kg^{-1} in the O horizon in plots without ash application.
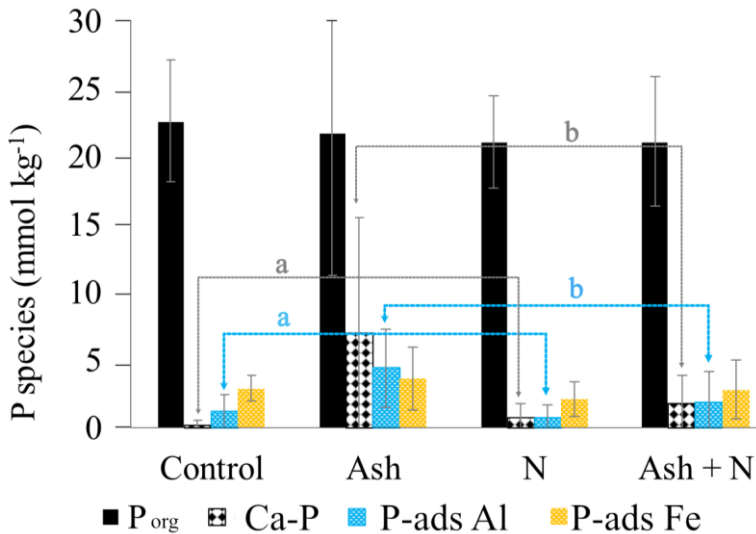
Figure 13: Concentrations of the main phosphorus (P) species groups (and standard deviations) in the O horizon at Rödålund. Values shown are for treatment groups with wood ash addition and nitrogen (N) fertilisation. Different lowercase letters (a, b) indicate a significant difference ($p \leq 0.05$) in the variable between ash treatments ($n = 12$) within N fertilisation treatments (N and no N). Bars without letters indicate no significant difference between or among the treatments.

For the Riddarhyttan site, the effect of different wood ash doses up to 9 Mg ha^{-1} on the P concentration in the O horizon was quantitatively determined (Figure 14). Only 2.3 mmol Ca-bound P kg^{-1} was found in the O horizon in plots treated with the highest ash application rate. Similarly, there was no change in the P_{org} pool (see Paper IV), which comprised, on average, 73% of TP. However, there was a strong relationship between the concentration of P adsorbed on Al ($R^2 = 0.72$, $p < 0.001$) and treatment with wood ash (Figure 14A). The concentration of P adsorbed on Fe also increased significantly ($p = 0.04$), although the slope was weak ($R^2 = 0.35$) (Figure 14B).
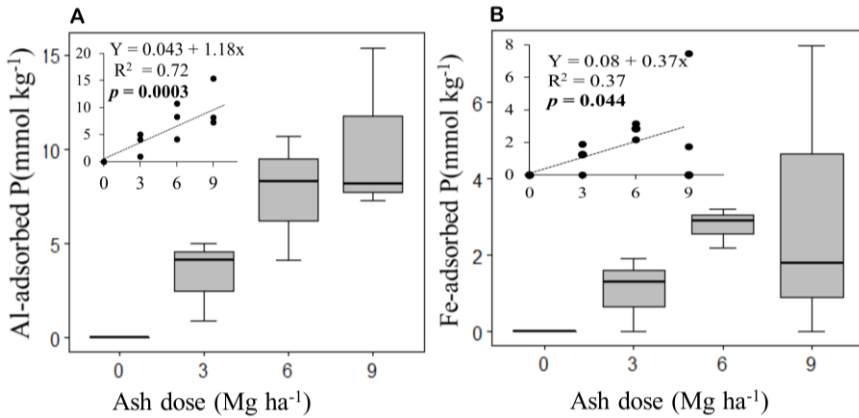
Figure 14: Relationship between amount of wood ash applied and concentration of phosphorus (P) adsorbed to (A) aluminium (Al) and (B) iron (Fe) at the Riddarhyttan site ($n = 4$).

There was a strong relationship between the concentration of Olsen-P and that of bulk-XANES detectable P adsorbed to Al ($R^2 = 0.83$, $p<0.001$), and also between the concentration of Olsen-P and that of bulk-XANES detectable P adsorbed to Fe ($R^2 = 0.74$, $p<0.001$) in the O horizon at Riddarhyttan (Figure 15).
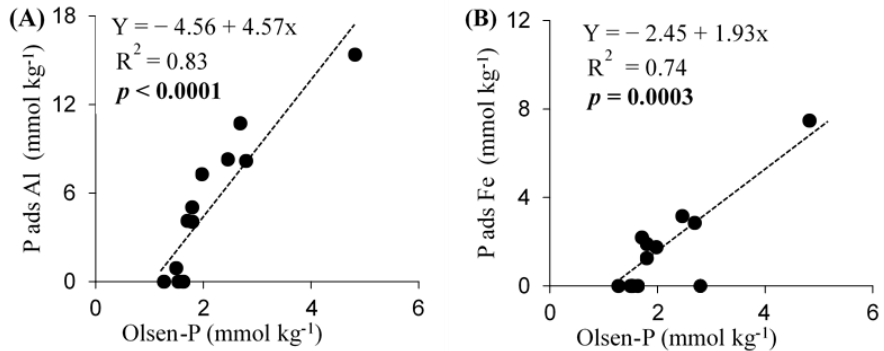
Figure 15: Concentration of phosphorus (P) adsorbed to (A) aluminium (Al) and (B) iron (Fe) as a function of the concentration of Olsen-P across all rates of wood ash addition at Riddarhyttan (n = 3).

6. Discussion

The combination of non-destructive X-ray micro-spectroscopic and conventional chemical extraction methods applied in this thesis enabled detailed exploration, for the first time, of the fate of native and applied wood ash-inherited P and determination of the vertical and spatial distribution of P species in Podzols and Podzol-like soil types.

6.1. Phosphorus speciation across soil profiles

The P speciation results revealed that P_{org} and Al- and Fe-sorbed P were the predominant P species in upper Podzol horizons (O, E, and B). This finding agrees with the conceptual model of soil P transformation, which indicates that as the soil development proceeds, P, initially bound in bedrock as primary minerals (mostly apatite), is transformed into P_{org} and P bound to secondary Al and Fe minerals (Walker & Syers, 1976). The results also align with the P speciation pattern previously observed in non-podzolised forest soils, including those in temperate zones (*e.g.*, Prietzel *et al*., 2013; Prietzel *et al*., 2016b; Prietzel *et al.,* 2022; Hashimoto & Watanabe, 2014). However, in contrast to this thesis, those studies reported a stronger role of Fe-bound P than Al-bound P.

The key features of the P *K*-edge XANES spectra of different Ca-bound P species show similarities (Figure 5) (Ingall *et al*., 2011). Thus, it may not be easy to distinguish between lithogenic primary mineral apatite and secondary Ca phosphates (Hesterberg, 2010, Oxmann, 2014). However, previous studies showed that the formation of secondary Ca phosphates is unlikely under acidic conditions (Eriksson *et al*., 2016; Nezat *et al*., 2008). Therefore, based on acidic conditions of forest soils studied in this thesis, Ca-bound P detectable by XANES is likely apatite, consistent with the

standards of hydroxyapatite and apatite Taiba, which appeared most frequently in the Ca-bound P-dominated samples (Tables S2-S8 in paper I).

Despite the young age of the silicate-derived soils studied in this thesis, they showed low P stocks and the transformation of the primary mineral apatite into adsorbed phosphate and P_{org}. This process appeared to be nearly complete in the E horizon. Much of the apatite dissolution probably occurred early in soil formation, when the rate of weathering was higher (Zhou *et al.*, 2018). Nevertheless, despite intense weathering, a minor apatite fraction was detectable in the upper part of some soil profiles. Part of this apatite was probably present as inclusions in quartz (Syers *et al.*, 1967), a dominant mineral in Swedish acidic forest soils (Casetou-Gustafson *et al.*, 2018; Simonsson *et al.*, 2016).

As expected for a podzolised B horizon, bulk XANES spectroscopy results showed that Al and Fe (hydr)oxide-type minerals, particularly ITN, are the main P host phases. P was present predominantly in inorganic form, but P_{org} was also detectable in the B horizon of most soil profiles studied. The P_{org} in soil inherited from silicate parent materials is often bound onto secondary mineral surfaces (Prietzel et al., 2016). Therefore, in the subsoil enriched with Al and Fe mineral surfaces, P_{org} is probably, to a large extent, adsorbed to these minerals. Our P speciation results are consistent with oxalate-extractable P (mainly inorganic P and some organic P), which peaked in the B horizons.

The predominance of ITN-bound P in the B horizon is not surprising because (i) the concentration of Al is generally higher than that of Fe and (ii) an observed correlation between inorganic Al and oxalate-extractable Si and a consistent Al: Si ratio of 2-3 were found for the B horizon, indicating that inorganic Al was present mainly as ITN (Gustafsson *et al.*, 1995; Lundström *et al.*, 2000b). In addition, (iii) ITN materials have a larger surface area than many other minerals encountered in soils (Kleber *et al.*, 2021; Parfitt, 1989). Nevertheless, Fe-bound P, mainly ferrihydrite-and goethite-adsorbed P, were important P species throughout the soil profile studied in this thesis, as confirmed by the bulk-XANES data. However, despite substantially higher TP concentrations in the B horizons, the ratios of AL- and Olsen-extractable P to the TP were at most 8% and 3%, respectively, providing strong evidence that most P is poorly bioavailable. By contrast, most P_{ox} in the overlying horizons was dissolved in ammonium lactate (AL) and, to some extent, in $NaHCO_3$ (Olsen) solutions.

The Flakaliden and Kloten soils contained the highest concentrations of Al_{ox} and Fe_{ox}. However, these soils differ considerably in P status. Kloten is a P-poor soil with a relatively higher P_{org} fraction in its B horizon. This finding is consistent with the orgC content, which was twice as high as the content in the Flakaliden B horizon. Accumulation of this orgC content has probably led to the formation of P_{org} during mineralisation (Spohn, 2020). However, a low DPS in the Kloten soil (1.8%; Table 2 in paper I) indicates low P availability. Any P made available through P_{org} mineralisation is perhaps almost inevitably re-adsorbed on exposed mineral surfaces. By contrast, the DPS in the Flakaliden B horizon was 4 times greater than in Kloten. These results suggest that the Kloten forest ecosystem mainly strives to recycle the P_{org} previously acquired from the mineral soil to maintain its P demand, with minimal risks of P leaching (Lang *et al*., 2017; Odum, 1969). According to the results in this thesis, Rödålund and Skogaby are also P-poor soils containing P_{org} in their B horizon. By contrast, in the sandy soil at Tärnsjö, DPS was higher than in other soils when comparing their B and C horizons. Like Flakaliden, Tärnsjö is a P-rich soil with low Al_{ox} and Fe_{ox} concentrations as well as a low P_{org}. This was also reflected in the ratios of P-AL and Olsen-P to P_{ox}, which were relatively higher for Tärnsjö.

Weathering in apatite-enriched C horizons could be of great importance for future P supply in these forest ecosystems. For example, acid AL solution (pH = 3.75) dissolved more P in the C horizon than in the more acidic B horizon. This result suggests that continued weathering of apatite can be expected if the subsoil becomes increasingly acidified. However, the dissolution rate will depend on the occurrence of apatite; as discrete grains or inclusions (Nezat *et al*., 2007; Syers *et al*., 1967).

6.2. Phosphorus speciation in microsites

Weathering and Podzolisation mechanisms disassemble rock-bearing minerals into basic molecular units. Through biogeochemical processes, these units combine to form micro/submicron-sized soil particles of unique structures and physical and biogeochemical properties (Hesterberg *et al*., 2017; van der Bom *et al*., 2022). In the soils studied, at several microsites in the B horizon, μ-focused XANES confirmed the predominance of Al-bound P, most likely ITN-bound P.

Unlike for bulk-XANES data collected in the B horizons of Tärnsjö and Flakaliden, P_{org} was detectable in some microsites, although in small

proportions. In contrast, bulk-XANES spectroscopy identified 32% apatite at 30−40 cm but not at 10−20 cm in the Tärnsjö soil, which was not detectable in microsites (see detail below). On the other hand, the apatite fraction in the bulk soil of Flakaliden 40-50 cm comprised 15%. Unlike the Tärnsjö B horizon, in Flakaliden 40-50 cm soil sample, apatite was the predominant fraction detected by µ-XANES in spot 6 (Table 6 and Figure 8). Using some illustrative examples of P-rich soil samples from Tärnsjö and Flakaliden, this thesis showed that P speciation is spatially heterogeneous at the microscale. However, it should be noted that the extent of such heterogeneity depends on the soil substrate and the depth at which the soil sample is collected (Werner *et al*., 2017)

High-resolution maps obtained using a micro-focused beam should reveal greater diversity than bulk-XANES (Hesterberg *et al*., 2017). The finding that µ-XANES did not detect apatite in the Tärnsjö B horizon, unlike bulk-XANES, contradicts the claim that µ-XANES is more sensitive in identifying multiple P species which co-exist in multiple heterogeneous microsites in the soil (Hesterberg *et al*., 2017). In paper II, we hypothesised that the apparent absence of apatite in the Tärnsjö B horizon was because the apatite grains were >600 µm apart, probably not captured within the area mapped. Thus, the apatite spots may not have been present in the 3.6×10^5 µm^2 maps (600×600 µm^2 size).

According to the sample preparation instructions for the bulk-XANES speciation, the area of the soil in contact with the unfocused X-ray beam is 5 x 10^7 µm^2. Moreover, the beam penetrates the soil sample to at most 50 µm (see methods section in Paper I). Interestingly, it should require the collection of about 139 µ-XRF maps of 3.6×10^5 µm^2 each to enable scanning one sample with an unfocused X-ray beam (bulk XANES), considering a thickness of 30 µm used for the µ-XANES P speciation. Therefore, the hypothesis that apatite spots in Tärnsjö soil are highly dispersed (>600 µm apart) (Paper II) probably holds. Recently, Adediran *et al*. (2022) investigated the significance of apatite grains and inclusions more quantitatively, using laser ablation and inductively coupled plasma mass spectrometry (LA-ICP-MS), and confirmed that the apatite spots in the Tärnsjö soil profile were about 1000 µm apart.

It seems like such spatial dispersion of apatite grains observed in the microsites (by µ-XANES) of the Tärnsjö soil profile is somewhat a property of the Flakaliden soil. However, increasing the µ-XRF map resolution at 4.9

$\times 10^5$ μm^2 permitted the identification of apatite in a few microsites of the Flakaliden B horizon (Paper III).

Studies using P K-edge bulk XANES have reported difficulties in distinguishing between Al- and Fe-bound P (Gustafsson *et al*., 2020; Prietzel *et al*., 2016). Moreover, in Paper II, an attempt was made to address this challenge by estimating P speciation in microsites based mainly on the LCF of μ-XANES data. However, a fully satisfactory separation of these two P phases was still not achieved. Including Fe in the μ-XRF mapping and collecting more μ-XANES spectra (paper III), a qualitative analysis of microscale P speciation showed that, compared to the LCF results (Table 6), Fe had less role in the retention of P. Consistent with this, the Al_{ox} content in the Flakaliden B horizon was about three times higher than the Fe_{ox} content (Table 2 in the paper I). Possibly, it could be that the LCF erroneously assigned part of Al-bound P to the Fe-bound P since yellow spots were not present on the map (Figure 8).

Previous studies reported that a pre-edge of the spectrum for ferrihydrite-adsorbed P is less pronounced if the adsorbed P is P_{org} (Prietzel *et al*., 2016a). If this is the case for Flakaliden, one may argue that Fe-bound P is being underestimated. However, in the Flakaliden B horizon, oxalate-extractable P_{orgox} of only 12% of P_{ox} (Table 4) was much lower than oxalate-extractable inorganic P (Pi_{ox}), suggesting that the underestimation of adsorbed P_{org} by the μ-XANES (which includes P_{org} bound to Fe) was unlikely. This agrees with the finding that the absence of yellow-coloured spots and less pronounced pre-edge of spectra suggests that Fe had a less role in binding P. I am not questioning the ability of the LCF to estimate P composition in soil. Rather, in cases when the effectiveness of the LCF is limited due to poor quality of XANES spectra, colour picking from the μ-XRF maps in combination with a more close observation of spectral shapes can yield better results. Therefore, the results obtained for the Flakaliden soil (Paper III) confirmed the predominance of P bound to Al. The predominance of Al-bound P over Fe-bound P is consistent with ITN identified in the Flakaliden 40-50 cm soil sample (see paper III).

As mentioned above, μ-XANES was able to identify P_{org} in some μ-scale spots, while bulk XANES did not suggest the presence of P_{org}. Possibly, P_{org} is locally higher in some μ-scale spots selected for XANES, while the bulk P concentration is low, preventing identification by bulk XANES (Hesterberg *et al*., 2017).

6.3. Distribution of phosphorus stocks in soil horizons

Calculated P stocks in the soil profiles studied (down to 80 cm) were comparable to those reported for East Asian tropical Podzols (Jien *et al.*, 2016) and carbonate-derived soils but lower than P stocks in silicate-derived Cambisols of Central European temperate forest soils (Prietzel *et al.*, 2016b; Prietzel *et al.*, 2022). Moreover, the contribution of the Ah horizons of the temperate ecosystems to TP stocks was 11-56%, which was much higher than the contribution of only 6% from O and E/A horizons combined in the podzolised soils studied in this thesis.

The results obtained in this thesis showed that about 94% of P stocks were contained in the B and C horizons, of which about 60% was present as P-bound to Al, mainly ITN in the B horizon. Despite low stocks in the O and E horizons, the P in those layers was predominantly stored as P_{org} and is most likely bioavailable.

Therefore, recycling of P in the surface soil horizons (O and E), *e.g.*, having a tight coupling between P_{org} decomposition/mineralisation and P uptake (Lang *et al.*, 2017; Wood *et al.*, 1984), could be expected to sustain plant P demand. However, the role of the high subsoil P stock with limited availability is an interesting question yet to be answered by future research.

Based on early research on P cycling conducted on podzolised soils from hardwood forest ecosystems at Hubbard Brook, New Hampshire (Wood *et al.*, 1984), it can be concluded that the vertical distribution of P species and operationally defined Al_{ox} and Fe_{ox} elucidate a stratified regulation of P cycling. In the subsoil, geochemical sorption/desorption, mostly by Al mineral surfaces, control P dynamics. However, in the surface horizons, the dominance of P_{org} reflects the relevance of strict biological (re)cycling of P previously acquired from mineral soil (Lang *et al.*, 2017; Wood *et al.*, 1984).

6.4. Phosphorus speciation in the organic horizons fertilised with wood ash and nitrogen

The results from the Rödålund and Riddarhyttan long-term field experiments showed that the application of wood ash influenced the chemical speciation of P in the O horizon. Enhanced dissolution of Ca-phosphates in the ash due, particularly when the latter had been applied at a higher dose, could be expected to increase the P concentration in the soil solution (Ohno, 1992). When wood ash is added to forest soils, P in the ash interacts with organic acids in the surface horizon, resulting in the enhanced dissolution of Ca-

phosphates (Lundström *et al*., 2000b), the main P species in the wood ash (Steenari *et al*., 1999b). Other factors, such as the amount of ash applied (and associated P), may have resulted in more pronounced P solubility *e.g*., in the case of Riddarhyttan, supporting earlier findings (Jacobson *et al*., 2004).

The observed increase in the concentration of Al-bound P and, to some extent, Fe-bound P, especially at high wood ash application doses, can have two explanations. First, P demand or leaching are possibly not high enough to cause a substantial decrease in soil P. The soil solution will become supersaturated with phosphate ions. Thus, the presence of Al^{3+} and Fe^{3+} ions (see paper IV), probably from the ash, could preferentially retain the ash-dissolved P. Second, alternatively, the pH-raising effects of wood ash likely resulted in the transformation of OM-C to soluble Al and Fe-(hydr) oxide-type compounds. Therefore, in the long term, the chemical equilibrium may shift toward P adsorption (Neubauer *et al.*, 2013). The latter hypothesis is supported by the strong relationship between the amount of ash and Al- and Fe-bound P, and between Olsen-P and Al-bound P (Figure 15).

An unexpected result was the lack of decrease in P_{org} in the ash-amended O horizon since an increasing pH is expected to stimulate OM decomposition (Persson *et al*., 1995). A possible reason is that the formation of P_{org} derived from soil biota in response to an increase in pH contributed to the P_{org} pool (Augusto *et al*., 2008; Persson *et al*., 1995).

While repeated N fertilisation did not affect the P speciation, it showed a marked effect on P solubility, *i.e.* the TP and Olsen-P concentrations decreased. When an ecosystem is N-limited, such as the boreal forests studied in this thesis, an increase in N availability due to N addition stimulates forest growth (Binkley & Högberg, 2016; Lim *et al*., 2020). Consequently, plant P uptake increases, reducing the soil pool of easily available P (Olsen-P). Moreover, microorganisms probably preferentially immobilise any P made available (Heuck *et al*., 2018; Pistocchi *et al*., 2018). Even in the combined N and wood ash treatment, the concentration of Olsen-P was nearly halved compared with the measured concentration in the O layer treated with ash only. This indicates a pronounced effect of N on biological P uptake.

6.5. Implications of the results for forest management

The work performed in this thesis provided novel information on the occurrence of different P forms, their distribution in different soil horizons, and their importance for P solubility and plant availability. Despite the role of recycled P_{org} stored in the O and E horizons in maintaining P availability, the P stock is substantially low compared to the P stock in the subsoil. In addition, the O horizon may be the layer most likely to be affected by forest management, i.e., biomass harvesting, contributing to low P availability. The 60% of P bound in non- or less bioaccessible forms with Al and Fe (III), and to some extent, possible stable P_{org} in the subsoil, raises questions about the long-term P supply and availability in boreal forest ecosystems.

Plants can possibly acquire P from this P pool through naturally evolved strategies such as changes in the root architecture and through the excretion of organic acids by soil microorganisms e.g. mycorrhizal fungi (Doydora *et al*., 2020; Lang *et al*., 2017; Richardson and Simpson, 2011). However, in a mesocosm experiment, it was found that beech was not able to acquire P from goethite (Fe oxides) mineral surfaces (Klotzbücher et al., 2020). P bound onto ferrihydrite surfaces, a more amorphous Fe phase than goethite, is even less desorbable (Doydora *et al*., 2020) than the P adsorbed on goethite and Al hydroxide phases (Doydora *et al*., 2020), particularly if the Fe to Al ratio in the mixture of Fe/Al (hydr) oxides increases (Gypser *et al*., 2018). From the results of this thesis, it can be hypothesised that Al-bound P phases, especially the ITN-adsorbed P, which dominates the P speciation, may be the largest pool of biogeochemically active P in the forest ecosystems studied.

It is also essential to note that the uniqueness of P speciation across microsites in boreal forest soils demonstrated the importance of performing P *K*-edge μ-XANES for describing P species and the biogeochemical processes affecting its mobility. However, the results should be interpreted in light of the limitation that a μ-focused X-ray beam probe only a small area (microscale). Therefore, combining it and the bulk-XANES provided more detailed insights into molecular P speciation, mechanisms, and interaction with other minerals in soils

Erosion and leaching are hydrological processes that affect P dynamics in soils. For most soils, i.e., Kloten with a much lower DPS than the often used threshold (25%) (Beauchemin and Simard, 1999), it is suggested that P leaching from the soil to the surrounding water bodies is negligible due to a strong P fixation on Al and Fe soil particles. However, the low P binding

capacity of the sandy soil from Tärnsjö, which is also apatite-rich in its C horizon, suggests that P is more prone to leaching. Besides soil acidification, a higher rate of apatite dissolution is also expected due to global warming. Published apatite dissolution data (e.g., Guidry and Mackenzie, 2003) indicated that a temperature increase of 2°C will increase the apatite dissolution rate by 10-15 %.

In the context of boreal forests, N deposition and biomass harvest (Akselsson *et al.*, 2008), combined with acidification-driven weathering and Podzolisation, are critical factors contributing to decreased P availability. The detailed chemical description in Paper IV revealed novel aspects of the fate of the ash-applied P in maintaining sufficient P levels in forest soil. The findings on the mechanisms involved can help to explain some of the contradictory results reported in previous studies on the effects of wood ash on P solubility and, perhaps, on tree growth. This thesis identified, in particular, the P pools most likely to be affected by wood ash application and demonstrated how the chemical P speciation in soil upon ash addition influences P solubility.

An increase of between 6 and 28 kg ha^{-1} in TP content (and in the bioavailable P fraction) in the wood ash-amended O layer compared with the control indicated a good potential of the ash to replace nutrients lost with the harvested biomass. The higher P concentrations measured in the ash treatment were partly due to the dissolution Ca-bound P. It is also important to note that residual Ca-bound was detectable 13-24 years after wood ash application, which amounted to between 3.8 and 4.6 kg P ha^{-1} (equivalent to 5.3 and 9.5% of P in the applied ash, respectively). However, the pH-raising effect (by up to 0.22 units compared with the control) should not be ignored, as it can be expected to affect organic matter decomposition and probably cause positive feedback on P solubility in the soil. Moreover, this thesis showed that the application of 9 Mg wood ash ha^{-1} resulted in 15.6 kg Al-bound P ha^{-1}. Hence, the higher dose of wood ash may not be optimal, as it leads to the accumulation of more stable P, possibly because the P supply is higher than the short-term biological demand. Hence, P becomes stabilised.

Tree growth in boreal forests is strongly N-limited, but wood ash application does not result in increased forest growth unless N fertiliser is applied simultaneously with the ash (Binkley & Högberg, 2016; Lim *et al.*, 2020). This thesis showed that repeated N fertilisation can reduce the amount of easily available P because enhanced tree growth in response to high N

availability for plant uptake increases P demand and, thus, P uptake from the soil. Instead, the availability of P (Olsen-P) in the O layer improved slightly due to the ash-P + N compared with the treatment when N was added alone (Figure 16). As a result, this combined fertilisation with ash and N led to a higher P uptake than when N has been added alone (for more detail in paper IV). Overall, these results suggest that long-term P supply can be expected to decline gradually if N deposition prevails, particularly after multiple forest cycles. However, adding a combination of wood ash and N can be considered as a long-term management option.

Control	wood ash (Ca-P)	NH_4NO_3	NH_4NO_3 + ash (Ca-P)	
20 kg P/ha	24 kg P/ha	29 kg P/ha	32 kg P/ha	Biomass P
				uptake
17.0 kg/ha	21.0 kg/ha	14.0 kg/ha	18.0 kg/ha	Total P
2.0 kg/ha	2.2 kg/ha	0.9 kg/ha	1.2 kg/ha	Olsen-P
0.1 kg/ha	4.6 kg/ha	0.4 kg/ha	1.6 kg/ha	Ca-bound P
0.8 kg/ha	2.2 kg/ha	0.3 kg/ha	1.3 kg/ha	Al-bound P

Figure 16: Summarising diagram of stocks of phosphorus (P) in aboveground biomass (above values), total P and Olsen-P (middle), and significantly affected P species (below) in the O layer in boreal forest soil as influenced by wood ash and nitrogen (N) application at Rödålund. The figure adapted from paper IV.

6.6. Conclusions

The overall aim of this thesis was to assess the effects of weathering and wood ash fertilisation on phosphorus speciation, distribution, and solubility in managed forest ecosystems in Sweden. Based on the results obtained in Papers I-IV, the following conclusions were drawn:

- The prevailing mechanisms of acidification-induced weathering and Podzolisation in young coniferous forest ecosystems in the boreal region have resulted in depletion of mineral apatite reserves in the topsoil and B horizon.

- In the B horizon, P speciation results obtained at the macro scale (bulk soil) and the microscopic scale (microsites) all revealed a predominance of P bound to Al, mainly PO_4^{3-} adsorbed to ITN, followed by Fe(hydr)oxides-sorbed P. These P forms were observed to occur mainly at the edges of Al and Si mineral grains or in pore spaces. The importance of apatite increased with soil depth.

- Considering the thickness of the different soil horizons, the bulk density, and the stone content, around 94% of the total soil P stock resides between 20 and 80 cm depth (B and C horizons combined). Of this, around 60% is stored as P bound to secondary Fe and, especially, Al mineral precipitates.

- Up to two decades after wood ash application to the forest O horizons, a small quantity of undissolved Ca-bound P, probably originating from the ash, can be detected in the O horizon.

- Most P bound in applied wood ash dissolves over time, resulting in a high concentration of bioavailable P and P bound to Al and Fe, especially at higher ash application rates.

6.7. Future research

The work presented in this thesis provides a fundamental understanding of P chemistry, (bio)geochemical processes affecting the dynamics of native and wood ash applied P in boreal forest soils. Knowing the chemical P species and in which soil horizon they are predominantly stored can be essential for improving forest management practices and for future research.

For example, the results from this thesis can be useful in predicting the long-term P availability in boreal forests. A model needs to be developed to assess future P supply to the trees based on P speciation and the

biogeochemical processes affecting pools. Moreover, pedogenesis will likely continue to stabilise P in the soil. Therefore, potential opportunities and challenges for plants to access the P stored as P bound to Al and Fe bound P could be explored. For example, these results may be useful to explore what pools mycorrhizal fungi can exploit and to what extent Al-and Fe-bound P are easily accessible to plants and microorganisms.

There is also a need to assess the effects of wood ash application on P dynamics in the mineral soil. This is because some wood ash-bound P is probably leached down to the mineral soil. Moreover, exploring the effects of forest biomass harvesting on P speciation and solubility is recommended.

References

Adediran, G.A., Kielman-Schmitt, M., Kooijman, E. & Gustafsson, J.P. (2022) Significance of phosphorus inclusions and discrete micron-sized grains of apatite in postglacial forest soils. *European Journal of Soil Science*, 73, e13310. https://doi.org/10.1111/ejss.13310

Akselsson, C., Belyazid, S., Stendahl, J., Finlay, R., Olsson, B. A., Erlandsson Lampa, M., Wallander, H., Gustafsson, J. P. & Bishop, K. (2019). Weathering rates in Swedish forest soils. *Biogeosciences,* 16, 4429-4450. https://doi.org/10.5194/bg-16-4429-2019

Akselsson, C., Westling, O., Alveteg, M., Thelin, G., Fransson, A.-M. & Hellsten, S. (2008). The influence of N load and harvest intensity on the risk of P limitation in Swedish forest soils. *Science of the Total Environment,* 404, 284-289. https://doi.org/10.1016/j.scitotenv.2007.11.017

Almeida, J. P., MenichettI, L., Ekblad, A., Rosenstock, N. & Wallander, H. (2022). Phosphorus regulates fungal biomass production in a Norway spruce forest. *Biogeosciences Discussions*, 1-39. https://doi.org/10.5194/bg-2022-165

Andersson, M., Carlsson, M., Ladenberger, A., Morris, G., Sadeghi, M. & Uhlbäck, J. (2014). Geochemical atlas of Sweden. *Geological Survey of Sweden: Uppsala, Sweden*.

Anderson, G. (1980). Assessing organic phosphorus in soils. *The role of phosphorus in agriculture*, 411-431. https://doi.org/10.2134/1980.roleofphosphorus.c16

Arvidsson, H. & Lundkvist, H. (2002). Needle chemistry in young Norway spruce stands after application of crushed wood ash. *Plant and Soil,* 238, 159-174.. https://doi.org/10.1023/A:1014252521538

Augusto, L., Bakker, M. R. & Meredieu, C. (2008). Wood ash applications to temperate forest ecosystems—potential benefits and drawbacks. *Plant and Soil,* 306, 181-198. https://doi.org/10.1007/s11104-008-9570-z

Beauchemin, S., Hesterberg, D., Chou, J., Beauchemin, M., Simard, R. R. & Sayers, D. E. (2003). Speciation of phosphorus in phosphorus-enriched agricultural soils using X-ray absorption near-edge structure spectroscopy and chemical fractionation. *Journal of Environmental Quality,* 32, 1809-1819. https://doi.org/10.2134/jeq2003.1809

Beauchemin, S. & Simard, R. (1999). Soil phosphorus saturation degree: Review of some indices and their suitability for P management in Quebec, Canada. *Canadian Journal of Soil Science,* 79, 615-625. https://doi.org/10.4141/S98-087

Binkley, D. & Högberg, P. (2016). Tamm review: revisiting the influence of nitrogen deposition on Swedish forests. *Forest Ecology and Management,* 368, 222-239. https://doi.org/10.1016/j.foreco.2016.02.035

Bjurström, H., Ilskog, E. & Berg, M. (2003). Askor från biobränslen och blandbränslen–mängder och kvalitet. *Energimyndigheten, ER,* 10, 1-74. (In Swedish).

Blakemore, L. (1987). Soil Bureau Laboratory Methods. A. Methods for chemical analysis of soils. *NZ Soil Bureau Scientific Report,* 80, 44-45.

Borggaard, O., Jdrgensen, S., Moberg, J. & Raben-Lange, B. (1990). Influence of organic matter on phosphate adsorption by aluminium and iron oxides in sandy soils. *Journal of Soil Science,* 41, 443-449. https://doi.org/10.1111/j.1365-2389.1990.tb00078.x

Buurman, P. & van Reeuwijk, L. (1984). Proto-imogolite and the process of podzol formation: a critical note. *Journal of Soil Science,* 35, 447-452. https://doi.org/10.1111/j.1365-2389.1984.tb00301.x

Camia, A., Giuntoli, J., Jonsson, R., Robert, N., Cazzaniga, N. E., Jasinevičius, G., Grassi, G., Barredo, J. I. & Mubareka, S. (2021). *The use of woody biomass for energy production in the EU*, Publications Office of the European Union.

Casetou-Gustafson, S., Akselsson, C., Hillier, S. & Olsson, B. A. (2019). The importance of mineral determinations to PROFILE base cation weathering release rates: a case study. *Biogeosciences,* 16, 1903-1920. https://doi.org/10.5194/bg-16-1903-2019

Casetou-Gustafson, S., Grip, H., Hillier, S., Linder, S., Olsson, B. A., Simonsson, M. & Stendahl, J. (2020). Current, steady-state and historical weathering rates of base cations at two forest sites in northern and southern Sweden: a comparison of three methods. *Biogeosciences,* 17, 281-304. https://doi.org/10.5194/bg-17-281-2020

Casetou-Gustafson, S., Hillier, S., Akselsson, C., Simonsson, M., Stendahl, J. & Olsson, B. A. (2018). Comparison of measured (XRPD) and modeled (A2M) soil mineralogies: A study of some Swedish forest soils in the context of weathering rate predictions. *Geoderma,* 310, 77-88. https://doi.org/10.1016/j.geoderma.2017.09.004

Chadwick, O. A., Derry, L. A., Vitousek, P. M., Huebert, B. J. & Hedin, L. O. (1999). Changing sources of nutrients during four million years of ecosystem development. *Nature,* 397, 491-497. https://doi.org/10.1038/17276

Clarholm, M. (1994). Granulated wood ash and a 'N-free' fertiliser to a forest soil—effects on P availability. *Forest Ecology and Management,* 66, 127-136. https://doi.org/10.1016/0378-1127(94)90152-X

Dalai, R. (1977). Soil organic phosphorus. *Advances in Agronomy,* 29, 83-117. https://doi.org/10.1016/S0065-2113(08)60216-3

Dixon, J. B. & Schulze, D. G. (2002). *Soil mineralogy with environmental applications*, Soil Science Society of America Inc.

Doydora, S., Gatiboni, L., Grieger, K., Hesterberg, D., Jones, J. L., Mclamore, E. S., Peters, R., Sozzani, R., Van Den Broeck, L. & Duckworth, O. W. (2020). Accessing legacy phosphorus in soils. *Soil Systems,* 4, 74. https://doi.org/10.3390/soilsystems4040074

Egnér, H., Riehm, H. & Domingo, W. 1960. Untersuchungen über die chemische Bodenanalyse als Grundlage für die Beurteilung des Nährstoffzustandes der Böden. II. *Chemische Extraktionsmethoden zur Phosphor-und Kaliumbestimmung. Kungliga Lantbrukshögskolans Annaler,* 26, 199-215. In Germany.

Elser, J. J., Bracken, M. E., Cleland, E. E., Gruner, D. S., Harpole, W. S., Hillebrand, H., NgaI, J. T., Seabloom, E. W., Shurin, J. B. & Smith, J. E. (2007). Global analysis of nitrogen and phosphorus limitation of primary producers in freshwater, marine and terrestrial ecosystems. *Ecology Letters,* 10, 1135-1142. https://doi.org/10.1111/j.1461-0248.2007.01113.x

Elser, J. J. & Hamilton, A. (2007). Stoichiometry and the new biology: the future is now. *PLOS biology,* 5, e181. https://doi.org/10.1371/journal.pbio.0050181

Eriksson, A. K., Hillier, S., Hesterberg, D., Klysubun, W., Ulén, B. & Gustafsson, J. P. (2016). Evolution of phosphorus speciation with depth in an agricultural soil profile. *Geoderma,* 280, 29-37. https://doi.org/10.1016/j.geoderma.2016.06.004

Eriksson, J. 1996. Härdade vedaskors upplösning i skogsjord. *En studie i kolonnförsök. Ramprogram askåterföring,* 1996, 50. In Swedish

Fixen, P. & Grove, J. 1990. Testing soils for phosphorus. *Soil testing and plant analysis,* 3, 141-180. https://doi.org/10.2136/sssabookser3.3ed.c7

Gomez, K. A. & Gomez, A. A. (1984). *Statistical procedures for agricultural research*, John wiley & sons.

Guidry, M. W. & Mackenzie, F. T. (2003). Experimental study of igneous and sedimentary apatite dissolution: control of pH, distance from equilibrium, and temperature on dissolution rates. *Geochimica et Cosmochimica Acta,* 67, 2949-2963. https://doi.org/10.1016/S0016-7037(03)00265-5

Gustafsson, J., Bhattacharya, P., Bain, D., Fraser, A. & Mchardy, W. (1995). Podzolisation mechanisms and the synthesis of imogolite in northern Scandinavia. *Geoderma,* 66, 167-184. https://doi.org/10.1016/0016-7061(95)00005-9

Gustafsson, J. P., Braun, S., Tuyishime, J., Adediran, G. A., Warrinnier, R. & Hesterberg, D. (2020). A probabilistic approach to phosphorus speciation of soils using P K-edge XANES spectroscopy with linear combination fitting. *Soil Systems,* 4, 26. https://doi.org/10.3390/soilsystems4020026

Gustafsson, J. P., Karltun, E. & Bhattacharya, P. (1998). Allophane and imogolite in Swedish soils. *Division of Land and Water Resources, Department of Civil and Environmental Engineering, Royal Institute of Technology (KTH), Stockholm.*

Gypser, S., HIrsch, F., Schleicher, A. M. & Freese, D. (2018). Impact of crystalline and amorphous iron-and aluminum hydroxides on mechanisms of

phosphate adsorption and desorption. *Journal of Environmental Sciences,* 70, 175-189. https://doi.org/10.1016/j.jes.2017.12.001

Hannam, K., Venier, L., Allen, D., Deschamps, C., Hope, E., Jull, M., Kwiaton, M., Mckenney, D., Rutherford, P. & Hazlett, P. (2018). Wood ash as a soil amendment in Canadian forests: what are the barriers to utilization? *Canadian Journal of Forest Research,* 48, 442-450. https://doi.org/10.1139/cjfr-2017-0351

Hedwall, P.-O., Bergh, J. & Brunet, J. (2017). Phosphorus and nitrogen co-limitation of forest ground vegetation under elevated anthropogenic nitrogen deposition. *Oecologia,* 185, 317-326. https://doi.org/10.2307/1311067

Hesterberg, D. 2010. Macroscale chemical properties and X-ray absorption spectroscopy of soil phosphorus. *Developments in Soil Science.* Elsevier. https://doi.org/10.1016/S0166-2481(10)34011-6

Hesterberg, D., Duff, M. C., Dixon, J. B. & Vepraskas, M. J. (2011). X-ray microspectroscopy and chemical reactions in soil microsites. *Journal of Environmental Quality,* 40, 667-678. https://doi.org/10.2134/jeq2010.0140

Hesterberg, D., Mcnulty, I. & Thieme, J. (2017). Speciation of soil phosphorus assessed by XANES spectroscopy at different spatial scales. *Journal of Environmental Quality,* 46, 1190-1197. https://doi.org/10.2134/jeq2016.11.0431

Heuck, C., Smolka, G., Whalen, E. D., Frey, S., Gundersen, P., Moldan, F., Fernandez, I. J. & Spohn, M. (2018). Effects of long-term nitrogen addition on phosphorus cycling in organic soil horizons of temperate forests. *Biogeochemistry,* 141, 167-181. https://doi.org/10.2307/1311067

Huotari, N., Tillman-Sutela, E., Moilanen, M. & Laiho, R. (2015). Recycling of ash– For the good of the environment? *Forest Ecology and Management,* 348, 226-240. https://doi.org/10.1016/j.foreco.2015.03.008

Ingall, E. D., Brandes, J. A., Diaz, J. M., DE Jonge, M. D., Paterson, D., Mcnulty, I., Elliott, W. C. & Northrup, P. (2011). Phosphorus K-edge XANES spectroscopy of mineral standards. *Journal of Synchrotron Radiation,* 18, 189-197. https://doi.org/10.1107/S0909049510045322

ISO, D. (1998). 13878. Soil quality-Determination of total nitrogen content by dry combustion (" elemental analysis") (ISO 13878: 1998)," vol., no.

ISO, International Organization for Standardization. (1995). Soil Quality-Extraction of trace elements soluble in aqua regia. ISO 11466, Geneva, Switzerland.

IUSS WORKING GROUP, W. 2014. update (2015). *World Reference Base for Soil Resources. International Soil Classification System for Naming Soils and Creating Legends for Soil Maps. Food and Agriculture Organization of the United Nations, Rome*, 190.

Jacobson, S. (2003). Addition of stabilized wood ashes to Swedish coniferous stands on mineral soils-effects on stem growth and needle nutrient concentrations. *Silva Fennica,* 37, 437-450.

Jien, S.-H., Baillie, I., Hu, C.-C., Chen, T.-H., Iizuka, Y. & Chiu, C.-Y. (2016). Forms and distribution of phosphorus in a placic podzolic toposequence in

a subtropical subalpine forest, Taiwan. *Catena,* 140, 145-154. https://doi.org/10.1016/j.catena.2016.01.024

Jacobson, S., Högbom, L., Ring, E. & Nohrstedt, H.-Ö. (2004). Effects of wood ash dose and formulation on soil chemistry at two coniferous forest sites. *Water, Air, and Soil Pollution,* 158, 113-125. https://doi.org/10.1023/B:WATE.0000044834.18338.a0

Jacobson, S., Lundström, H., Nordlund, S., Sikström, U. & Pettersson, F. (2014). Is tree growth in boreal coniferous stands on mineral soils affected by the addition of wood ash? *Scandinavian Journal of Forest Research,* 29, 675-685. https://doi.org/10.1080/02827581.2014.959995

Jonard, M., Fürst, A., Verstraeten, A., Thimonier, A., Timmermann, V., Potočić, N., Waldner, P., Benham, S., Hansen, K. & Merilä, P. (2015). Tree mineral nutrition is deteriorating in Europe. *Global change biology,* 21, 418-430. https://doi.org/10.1111/gcb.12657

Karltun, E., Saarsalmi, A., Ingerslev, M., Mandre, M., Andersson, S., Gaitnieks, T., Ozolinčius, R. & VArnagiryte-Kabasinskiene, I. (2008). Wood ash recycling–possibilities and risks. *Sustainable Use of Forest Biomass for Energy.* Springer.

Kelly, S., Hesterberg, D. & Ravel, B. (2008). Analysis of soils and minerals using X-ray absorption spectroscopy. *Methods of soil analysis part 5—mineralogical methods,* 5, 387-463. https://doi.org/10.2136/sssabookser5.5.c14

Kleber, M., Bourg, I. C., Coward, E. K., Hansel, C. M., Myneni, S. C. & Nunan, N. (2021). Dynamic interactions at the mineral–organic matter interface. *Nature Reviews Earth & Environment,* 2, 402-421.

Klotzbücher, A., Schunck, F., KLotzbücher, T., Kaiser, K., Glaser, B., Spohn, M., Widdig, M. & Mikutta, R. 2020. Goethite-associated phosphorus is not available to beech (Fagus sylvatica L.). *Frontiers in Forests and Global Change,* 3, 94. https://doi.org/10.3389/ffgc.2020.00094

Kruse, J., Abraham, M., Amelung, W., Baum, C., Bol, R., Kühn, O., Lewandowski, H., Niederberger, J., Oelmann, Y. & Rüger, C. (2015). Innovative methods in soil phosphorus research: A review. *Journal of Plant Nutrition and Soil Science,* 178, 43-88. https://doi.org/10.1002/jpln.201400327

Lagerström, A., Esberg, C., Wardle, D. A. & Giesler, R. 2009. Soil phosphorus and microbial response to a long-term wildfire chronosequence in northern Sweden. *Biogeochemistry,* 95, 199-213. https://doi.org/10.1007/s10533-009-9331-y

Lang, F., Bauhus, J., Frossard, E., George, E., Kaiser, K., Kaupenjohann, M., Krüger, J., Matzner, E., Polle, A. & PrietzeL, J. (2016). Phosphorus in forest ecosystems: new insights from an ecosystem nutrition perspective. *Journal of Plant Nutrition and Soil Science,* 179, 129-135. https://doi.org/10.1002/jpln.201500541

Lang, F., Krüger, J., Amelung, W., Willbold, S., Frossard, E., Bünemann, E. K., Bauhus, J., Nitschke, R., Kandeler, E. & Marhan, S. (2017). Soil

phosphorus supply controls P nutrition strategies of beech forest ecosystems in Central Europe. *Biogeochemistry,* 136, 5-29. https://doi.org/10.1007/s10533-017-0375-0

Larsen, S. 1967. Soil phosphorus. *Advances in Agronomy,* 19, 151-210. https://doi.org/10.1016/S0065-2113(08)60735-X

Larsson, P.-E. & Westling, O. 1998. Leaching of wood ash and lime products: laboratory study. *Scandinavian Journal of Forest Research.*

Ler, A. & Stanforth, R. (2003). Evidence for surface precipitation of phosphate on goethite. *Environmental Science & Technology,* 37, 2694-2700. https://doi.org/10.1021/es020773i

Lim, H., Olsson, B. A., Lundmark, T., DahL, J. & Nordin, A. 2020. Effects of whole-tree harvesting at thinning and subsequent compensatory nutrient additions on carbon sequestration and soil acidification in a boreal forest. *GCB Bioenergy,* 12, 992-1001. https://doi.org/10.1111/gcbb.12737

Lundström, U. S., van Breemen, N. & Bain, D. (2000a). The Podzolisation process. A review. *Geoderma,* 94, 91-107. https://doi.org/10.1016/S0016-7061(99)00036-1

Lundström, U. V., van Breemen, N., Bain, D., van Hees, P., Giesler, R., Gustafsson, J. P., Ilvesniemi, H., Karltun, E., Melkerud, P.-A. & Olsson, M. (2000b). Advances in understanding the Podzolisation process resulting from a multidisciplinary study of three coniferous forest soils in the Nordic Countries. *Geoderma,* 94, 335-353. https://doi.org/10.1016/S0016-7061(99)00077-4

Mellbo, P., Sarenbo, S., Stålnacke, O. & Claesson, T. (2008). Leaching of wood ash products aimed for spreading in forest floors–Influence of method and L/S ratio. *Waste Management,* 28, 2235-2244. https://doi.org/10.1016/j.wasman.2007.09.037

Moody, P. W., Speirs, S. D., Scott, B. J. & Mason, S. D. 2013. Soil phosphorus tests I: What soil phosphorus pools and processes do they measure? *Crop and Pasture Science,* 64, 461-468. https://doi.org/10.1071/CP13112

Mokma, D. & Buurman, P. (1987). Podzols and Podzolisation in temperate regions. *Soil Science,* 144, 79.

Morris, A. L. & Mohiuddin, S. S. (2020). Biochemistry, nutrients.

Neubauer, E., Schenkeveld, W. D., Plathe, K. L., Rentenberger, C., Von Der Kammer, F., Kraemer, S. M. & Hofmann, T. (2013). The influence of pH on iron speciation in podzol extracts: Iron complexes with natural organic matter, and iron mineral nanoparticles. *Science of the Total Environment,* 461, 108-116. https://doi.org/10.1016/j.scitotenv.2013.04.076

Newman, E. (1995). Phosphorus inputs to terrestrial ecosystems. *Journal of Ecology*, 713-726. https://doi.org/10.2307/2261638

Nezat, C. A., Blum, J. D., Yanai, R. D. & Hamburg, S. P. (2007). A sequential extraction to determine the distribution of apatite in granitoid soil mineral pools with application to weathering at the Hubbard Brook Experimental

Forest, NH, USA. *Applied Geochemistry,* 22, 2406-2421. https://doi.org/10.1016/j.apgeochem.2007.06.012

Nilsson, T. & Lundin, L. (2006). Prediction of bulk density in Swedish forest soils from the organic carbon content and soil depth. *Reports in Forest Ecology & Forest Soils,* 91.

Nordic Forest Research. (2020). SNS report: Nordic Forest Statistics 2020-resources, Industry, Trade, Conservation, and Climate.

Odum, E. P. (1969). The Strategy of Ecosystem Development: An understanding of ecological succession provides a basis for resolving man's conflict with nature. *science,* 164, 262-270.

Ohno, T. (1992). Neutralization of soil acidity and release of phosphorus and potassium by wood ash. Wiley Online Library. https://doi.org/10.2134/jeq1992.00472425002100030022x

Olsen, S. R. (1954). *Estimation of available phosphorus in soils by extraction with sodium bicarbonate*, US Department of Agriculture.

Olsson, B. & Westling, O. (2006). *Skogsbränslecykelns näringsbalans*, IVL Svenska Miljöinstitutet. In Swedish.

Oxmann, J. F. (2014). An X-ray absorption method for the identification of calcium phosphate species using peak-height ratios. *Biogeosciences,* 11, 2169-2183. https://doi.org/10.5194/bg-11-2169-2014

Palmqvist, K., Nordin, A. & Giesler, R. (2020). Contrasting Effects of Long-Term Nitrogen Deposition on Plant Phosphorus in a Northern Boreal Forest. *Frontiers in Forests and Global Change,* 3. https://doi.org/10.3389/ffgc.2020.00065

Parfitt, R. (1989). Phosphate reactions with natural allophane, ferrihydrite and goethite. *Journal of Soil Science,* 40, 359-369. https://doi.org/10.1111/j.1365-2389.1989.tb01280.x

Parfitt, R. L. (1979). Anion adsorption by soils and soil materials. *Advances in Agronomy,* 30, 1-50. https://doi.org/10.1016/S0065-2113(08)60702-6

Parfitt, R. L. & Atkinson, R. J. (1976). Phosphate adsorption on goethite (α-FeOOOH). *Nature,* 264, 740-742.

Persson, T., Rudebeck, A. & Wirén, A. (1995). Pools and fluxes of carbon and nitrogen in 40-year-old forest liming experiments in southern Sweden. *Water, Air, and Soil Pollution,* 85, 901-906.

Pierzynski, G. M., McdowelL, R. W. & Thomas Sims, J. (2005). Chemistry, cycling, and potential movement of inorganic phosphorus in soils. *Phosphorus: Agriculture and the Environment,* 46, 51-86.

Pistocchi, C., Mészáros, É., Tamburini, F., Frossard, E. & Bünemann, E. K. 2018. Biological processes dominate phosphorus dynamics under low phosphorus availability in organic horizons of temperate forest soils. *Soil Biology and Biochemistry,* 126, 64-75. https://doi.org/10.1016/j.soilbio.2018.08.013

Pitman, R. M. (2006). Wood ash use in forestry–a review of the environmental impacts. *Forestry: An International Journal of Forest Research,* 79, 563-588. https://doi.org/10.1093/forestry/cpl041

Prietzel, J., Dümig, A., Wu, Y., Zhou, J. & Klysubun, W. (2013). Synchrotron-based P K-edge XANES spectroscopy reveals rapid changes of phosphorus speciation in the topsoil of two glacier foreland chronosequences. *Geochimica et Cosmochimica Acta,* 108, 154-171. https://doi.org/10.1016/j.gca.2013.01.029

Prietzel, J., HArrington, G., Häusler, W., Heister, K., Werner, F. & Klysubun, W. (2016a). Reference spectra of important adsorbed organic and inorganic phosphate binding forms for soil P speciation using synchrotron-based K-edge XANES spectroscopy. *Journal of Synchrotron Radiation,* 23, 532-544. https://doi.org/10.1107/S1600577515023085/hf5306sup1.pdf

Prietzel, J., Klysubun, W. & Werner, F. (2016b). Speciation of phosphorus in temperate zone forest soils as assessed by combined wet-chemical fractionation and XANES spectroscopy. *Journal of Plant Nutrition and Soil Science,* 179, 168-185. https://doi.org/10.1002/jpln.201500472

Prietzel, J., Krüger, J., Kaiser, K., Amelung, W., Bauke, S. L., DIppold, M. A., Kandeler, E., Klysubun, W., Lewandowski, H. & Löppmann, S. (2022). Soil phosphorus status and P nutrition strategies of European beech forests on carbonate compared to silicate parent material. *Biogeochemistry,* 158, 39-72. https://doi.org/10.1007/s10533-021-00884-7

Ravel, B. 2009. ATHENA user's guide. *Athena IFFEFIT*.

Ravel, B. & Newville, M. 2005. ATHENA, ARTEMIS, HEPHAESTUS: data analysis for X-ray absorption spectroscopy using IFEFFIT. *Journal of Synchrotron Radiation,* 12, 537-541. https://doi.org/10.1107/S0909049505012719

Reid, C. & Watmough, S. A. (2014). Evaluating the effects of liming and wood-ash treatment on forest ecosystems through systematic meta-analysis. *Canadian Journal of Forest Research,* 44, 867-885. https://doi.org/10.1139/cjfr-2013-0488

Richardson, A. E. & Simpson, R. J. (2011). Soil microorganisms mediating phosphorus availability update on microbial phosphorus. *Plant Physiology,* 156, 989-996. https://doi.org/10.1104/pp.111.175448

Ring, E., Jacobson, S. & Nohrstedt, H.-Ö. (2006). Soil-solution chemistry in a coniferous stand after adding wood ash and nitrogen. *Canadian Journal of Forest Research,* 36, 153-163. https://doi.org/10.1139/x05-242

Rivard, C., Lanson, B. & Cotte, M. 2016. Phosphorus speciation and micro-scale spatial distribution in North-American temperate agricultural soils from micro X-ray fluorescence and X-ray absorption near-edge spectroscopy. *Plant and Soil,* 401, 7-22. https://doi.org/10.1007/s11104-015-2494-5

Rosenstock, N. P., Berner, C., Smits, M. M., Krám, P. & Wallander, H. 2016. The role of phosphorus, magnesium and potassium availability in soil fungal

exploration of mineral nutrient sources in Norway spruce forests. *New Phytologist,* 211, 542-553. https://doi.org/10.1111/nph.13928

Sauer, D., SponageL, H., Sommer, M., Giani, L., Jahn, R. & Stahr, K. (2007). Podzol: Soil of the year 2007. A review on its genesis, occurrence, and functions. *Journal of Plant Nutrition and Soil Science,* 170, 581-597. https://doi.org/10.1002/jpln.200700135

Simonsson, M., Bergholm, J., Lemarchand, D. & Hillier, S. (2016). Mineralogy and biogeochemistry of potassium in the Skogaby experimental forest, southwest Sweden: pools, fluxes and K/Rb ratios in soil and biomass. *Biogeochemistry,* 131, 77-102. https://doi.org/10.1007/s10533-016-0266-9

Simonsson, M., Bergholm, J., Olsson, B. A., von Brömssen, C. & Öborn, I. (2015). Estimating weathering rates using base cation budgets in a Norway spruce stand on podzolised soil: analysis of fluxes and uncertainties. *Forest Ecology and Management,* 340, 135-152. https://doi.org/10.1016/j.foreco.2014.12.024

Solé, V., Papillon, E., Cotte, M., Walter, P. & Susini, J. (2007). A multiplatform code for the analysis of energy-dispersive X-ray fluorescence spectra. *Spectrochimica Acta Part B: Atomic Spectroscopy,* 62, 63-68. https://doi.org/10.1016/j.sab.2006.12.002

Sparks, D. L., Page, A. L., Helmke, P. A. & Loeppert, R. H. (2020). *Methods of soil analysis, part 3: Chemical methods*, John Wiley & Sons.

Spohn, M. (2020). Increasing the organic carbon stocks in mineral soils sequesters large amounts of phosphorus. *Global Change Biology,* 26, 4169-4177. https://doi.org/10.1111/gcb.15154

Staff, S. 2014. Keys to Soil Taxonomy, 12th Edn Washington. *DC: Natural Resources Conservation Service, United States Department of Agriculture.*

Standardization, I. O. F. (1995). *Soil quality-extraction of trace elements soluble in aqua regia*, ISO.

Steenari, B.-M., Karlsson, L.-G. & Lindqvist, O. (1999a). Evaluation of the leaching characteristics of wood ash and the influence of ash agglomeration. *Biomass and Bioenergy,* 16, 119-136. https://doi.org/10.1016/S0961-9534(98)00070-1

Steenari, B.-M. & Lindqvist, O. 1997. Stabilisation of biofuel ashes for recycling to forest soil. *Biomass and Bioenergy,* 13, 39-50. https://doi.org/10.1016/S0961-9534(97)00024-X

Steenari, B.-M., Schelander, S. & Lindqvist, O. (1999b). Chemical and leaching characteristics of ash from combustion of coal, peat and wood in a 12 MW CFB–a comparative study. *Fuel,* 78, 249-258. https://doi.org/10.1016/S0016-2361(98)00137-9

Stendahl, J., Akselsson, C., Melkerud, P.-A. & Belyazid, S. (2013). Pedon-scale silicate weathering: comparison of the PROFILE model and the depletion method at 16 forest sites in Sweden. *Geoderma,* 211, 65-74. https://doi.org/10.1016/j.geoderma.2013.07.005

Stendahl, J., Lundin, L. & Nilsson, T. (2009). The stone and boulder content of Swedish forest soils. *Catena,* 77, 285-291. https://doi.org/10.1016/j.catena.2009.02.011

Strand, L. T., Callesen, I., Dalsgaard, L. & De Wit, H. A. (2016). Carbon and nitrogen stocks in Norwegian forest soils—the importance of soil formation, climate, and vegetation type for organic matter accumulation. *Canadian Journal of Forest Research,* 46, 1459-1473. https://doi.org/10.1139/cjfr-2015-0467

Swedish Forest Agency 2019. Regler och rekommendationer för skogsbränsleuttag och kompensationsåtgärder (in Swedish). Report 2009/14, Jönköping, Sweden. (In Swedish).

Syers, J., Williams, J., CampbelL, A. & Walker, T. (1967). The significance of apatite inclusions in soil phosphorus studies. *Soil Science Society of America Journal,* 31, 752-756. https://doi.org/10.2136/sssaj1967.03615995003100060016x

Talkner, U., Meiwes, K. J., Potočić, N., Seletković, I., Cools, N., De Vos, B. & Rautio, P. (2015). Phosphorus nutrition of beech (Fagus sylvatica L.) is decreasing in Europe. *Annals of Forest Science,* 72, 919-928. https://doi.org/10.1007/s13595-015-0459-8

Tipping, E., Somerville, C. J. & Luster, J. (2016). The C: N: P: S stoichiometry of soil organic matter. *Biogeochemistry,* 130, 117-131. https://doi.org/10.1007/s10533-016-0247-z

Turner, B. L., Condron, L. M., Richardson, S. J., Peltzer, D. A. & Allison, V. J. (2007). Soil organic phosphorus transformations during pedogenesis. *Ecosystems,* 10, 1166-1181. https://doi.org/10.1007/s10021-007-9086-z

Turner, B. L., Frossard, E. & Baldwin, D. S. (2005). *Organic phosphorus in the environment*, CABI Pub.

van Der Bom, F. J., Kopittke, P. M., Raymond, N. S., Sekine, R., Lombi, E., Mueller, C. W. & Doolette, C. L. (2022). Methods for assessing laterally-resolved distribution, speciation and bioavailability of phosphorus in soils. *Reviews in Environmental Science and Bio/Technology*, 1-22. https://doi.org/10.1007/s11157-021-09602-z

van Hees, P., Lundström, U., Starr, M. & Giesler, R. (2000). Factors influencing aluminium concentrations in soil solution from podzols. *Geoderma,* 94, 289-310. https://doi.org/10.1016/S0016-7061(98)00138-4

van Reeuwijk, L. P. 1986. Procedures for soil analysis.

Vantelon, D., Trcera, N., Roy, D., Moreno, T., Mailly, D., Guilet, S., Metchalkov, E., Delmotte, F., Lassalle, B. & Lagarde, P. (2016). The LUCIA beamline at SOLEIL. *Journal of Synchrotron Radiation,* 23, 635-640. https://doi.org/10.1107/S1600577516000746

Viro, P. J. 1952. Kivisyyden määrittämisestä.

Vitousek, P. M. & Farrington, H. (1997). Nutrient limitation and soil development: experimental test of a biogeochemical theory. *Biogeochemistry,* 37, 63-75. https://doi.org/10.1023/A:1005757218475

Vitousek, P. M., Porder, S., Houlton, B. Z. & Chadwick, O. A. (2010). Terrestrial phosphorus limitation: mechanisms, implications, and nitrogen–phosphorus interactions. *Ecological Applications,* 20, 5-15. https://doi.org/10.1890/08-0127.1

Vogel, C., Helfenstein, J., Massey, M. S., Sekine, R., Kretzschmar, R., Beiping, L., Peter, T., Chadwick, O. A., Tamburini, F. & Rivard, C. (2021). Microspectroscopy reveals dust-derived apatite grains in acidic, highly-weathered Hawaiian soils. *Geoderma,* 381, 114681. https://doi.org/10.1016/j.geoderma.2020.114681

Walker, T. & Syers, J. K. (1976). The fate of phosphorus during pedogenesis. *Geoderma,* 15, 1-19. https://doi.org/10.1016/0016-7061(76)90066-5

Westling, O. & Zetterberg, T. (2007). Recovery of acidified streams in forests treated by total catchment liming. *Acid Rain-Deposition to Recovery.* Springer.

Wolf, A. & Baker, D. (1990). Colourimetric method for phosphorus measurement in ammonium oxalate soil extracts. *Communications in Soil Science and Plant Analysis,* 21, 2257-2263. https://doi.org/10.1080/00103629009368378

Wood, T., Bormann, F. & Voigt, G. (1984). Phosphorus cycling in a northern hardwood forest: biological and chemical control. *Science,* 223, 391-393.

Yamaguchi, N., Ohkura, T., Hikono, A., Hashimoto, Y., Suda, A., Yamamoto, T., Ando, K., Kasuya, M., Northrup, P. & Wang, S.-L. (2021). Microscale heterogeneous distribution and speciation of phosphorus in soils amended with mineral fertiliser and cattle manure compost. *Minerals,* 11, 121. https://doi.org/10.3390/min11020121

Yanai, R. D. (1998). The effect of whole-tree harvest on phosphorus cycling in a northern hardwood forest. *Forest Ecology and Management,* 104, 281-295. https://doi.org/10.1016/S0378-1127(97)00256-9

Yoshinaga, N. & Aomine, S. (1962). Imogolite in some Ando soils. *Soil Science and Plant Nutrition,* 8, 22-29. https://doi.org/10.1080/00380768.1962.10430993

Yu, L., Zanchi, G., Akselsson, C., Wallander, H. & Belyazid, S. (2018). Modeling the forest phosphorus nutrition in a southwestern Swedish forest site. *Ecological Modelling,* 369, 88-100. https://doi.org/10.1016/j.ecolmodel.2017.12.018

Zhou, J., Bing, H., Wu, Y., Sun, H. & Wang, J. (2018). Weathering of primary mineral phosphate in the early stages of ecosystem development in the Hailuogou Glacier foreland chronosequence. *European Journal of Soil Science,* 69, 450-461. https://doi.org/10.1111/ejss.12536

Popular science summary

Forests are the basis for Sweden's welfare. Successful long-term management of forests requires healthy trees, which depend on many factors, including the availability of nutrients, e.g., phosphorus (P). Without knowledge of the form and quantity of P present in the soil, we would not know the potential of the soil to supply the available P for plant uptake. This work aimed to contribute to the sustainability of the forest ecosystem and the forestry sector by answering these questions.

Life on Earth is impossible without P. Not only is P an essential nutrient for plants and crops, but it is also a vital constituent of genetic materials (DNA, RNA), bones, teeth, etc., in all animals and humans.

The P cycle is unique. Unlike nitrogen (N), which is also an essential nutrient that can be biologically fixed from the atmosphere, the source of P is the primary mineral apatite bound in rocks and soils. That means P from this pool is gradually released to supply P to the plants for building their biomass, i.e., the transformation of apatite into an organic P form.

On the other hand, one of the most common challenges, particularly in acid soils such as those in the boreal forest ecosystem, is a strong fixation of P to aluminum (Al) and iron (Fe) minerals. These minerals increasingly stabilise P released from the apatite and organic P pool. Hence, despite a large stock in the soil, P availability decreases over time.

In Sweden, more than 50% of the forest soils are Podzols or podzolised. This soil type consists of three distinctive layers. The organic horizon (O) is on top of the mineral soil, which consists of the E horizon at its surface. The E horizon is relatively acidic due to the accumulation of organic acids from the O horizon, accelerating the transformation of primary minerals. The B horizon is rich in Al and Fe, partly due to their migration from the E horizons. Below is a C horizon in which the parent material is less affected. Therefore,

a large P fraction of the total P in these soils is likely bound to Al and Fe minerals. However, P speciation, i.e., the distribution between different P forms in boreal forest soils, has not been studied. In this thesis, we explored P forms and their vertical and spatial distribution in seven forest soil profiles from northern, central, and southern Sweden.

The main finding from the first three papers was that the total P exists predominantly as organic P on the surface horizons, especially the O horizon. P bound mainly to Al and P bound to Fe are the predominant forms in the B horizon. It was also found that the primary mineral apatite has almost been depleted in the upper 30 cm of soil profiles, but its proportion increased with soil depth. As a result, a large apatite fraction was found in the C horizon.

Even at the micrometre scale resolution, Al-bound P was the main P phase in the B horizon, but the distribution was highly heterogeneous. That means, within the micrometre-size maps of 600 µm × 600 µm or 700 µm × 700 µm, P forms were highly diverse in different spots.

94% of all P resided between 20 and 80 cm depth. In the B horizon about 60% of all P existed as Al-bound P, bound mainly to imogolite-type nanoparticles (ITN). ITN is a type of Al mineral phase typical in the B horizons of Podzols, and they possess a high capacity to fix P. Thus, the subsoil P, mainly P bound to ITN, and apatite dominate the P inventory and probably are of high ecological significance for the long-term P supply and availability.

Moreover, it is recommended to apply wood ash as a potential fertiliser to maintain forest soil fertility after whole-tree harvesting. This is because soil nutrients, including P, contained in the biomass, such as leaves, twigs, and branches, are removed through biomass harvest. Therefore, in the fourth study, the effects of wood ash application were examined, alone or simultaneously with N, on changes in P forms and availability in the O horizon of two coniferous forest soils from Sweden.

This study found that most Ca-bound P expected to be apatite, the main form of P in wood ash, has been consumed almost. Moreover, the ash increased the total and available P in the O horizon and P uptake by plants. On the other hand, while also increasing P in above-ground biomass, nitrogen application reduced easily available P in the O horizon. A combined treatment of wood ash and N further increased P in aboveground biomass.

Populärvetenskaplig sammanfattning

Skogen utgör grunden för Sveriges välfärd. En framgångsrik långsiktig skogsskötsel kräver friska träd och är avhängig många faktorer, däribland näringstillgång, t.ex. vad gäller fosfor (P). Utan kunskap om mängderna fosfor och om vilken form fosforn har, skulle vi inte känna till vilken potential jorden har att förse skogen med tillgänglig fosfor. Det här arbetet syftade till att bidra till uthålligheten av skogsekosystemet och av skogsnäringen genom att besvara dessa frågor.

Livet på jorden är omöjligt utan P. Fosfor är inte bara ett essentiellt näringsämne för växter och grödor, det utgör också en viktig beståndsdel av genetiska material (DNA, RNA), ben, tänder, etc., i alla djur och människor.

Fosforcykeln är unik. I motsats till kväve (N), som också är ett essentiellt näringsämne vilket kan fixeras från atmosfären, är källan till fosfor det primära mineralet apatit i berggrund och jord. Fosforn från detta förråd frigörs gradvis för att förse växterna med P så att de kan öka sin biomassa, d.v.s. apatitens fosfor omvandlas till en organisk fosforform.

Å andra sidan är en av de vanligaste utmaningarna för fosfortillängligheten, särskilt i sura jordar som de i det boreala skogsekosystemet, en stark fixering av P till aluminium (Al) och järn (Fe)-mineral. Dessa mineral stabiliserar det fosfor som frigörs från apatit och från det organiska fosforförrådet. Därför kommer P-tillgängligheten att sakta minska över tid, trots ett stort förråd.

I Sverige klassificeras mer än 50% av jordarna som podsoler eller är podsolerade. Denna jordmån består av tre distinkta horisonter. Den organiska horisonten (O) finns ovanpå mineraljorden som i dess ytliga del består av en E-horisont. E-horisonten är relativt sur pga ackumulation av organiska syror som trängt ner från O-horisonten, vilket i sin tur accelerar omvandlingen (vittringen) av primära mineral. B-horisonten innehåller en stor mängd Al och Fe, delvis pga dessas transport från E-horisonten. Nedanför B-horisonten

finns finns en C-horisonten med ett mer opåverkat modermaterial. En stor andel av den totala mängden P i dessa jordar är sannolikt bunden till Al- och Fe-innehållande mineral. Dock har, tills nu, specieringen av fosfor, dvs fördelningen mellan olika fosforformer, i boreala skogsjordar inte studerats. I denna avhandling har jag utforskat vilka fosforformer som finns, och dess vertikala och rumsliga fördelning, i sju skogsmarksprofiler från de norra, centrala och södra delarna av Sverige.

Det viktigaste resultatet från de tre första artiklarna i avhandlingen var att den dominerande delen av fosforn i O-horisonten utgörs av organiskt P, medan P bundet till Al och Fe var de viktigaste fosforformerna i B-horisonten. Jag fann också att apatiten hade nästan helt försvunnit från de översta 30 cm av jordprofilerna, men att andelen apatit sedan ökade med ökande jorddjup. Som en konsekvens av detta återfanns en stor andel apatit i C-horisonten.

Även i mikrometerskala (600 µm × 600 µm eller 700 µm × 700 µm) var Al-bunden P den viktigaste fosforformen i B-horisonten, men den rumsliga fördelningen var mycket heterogen. Det betyder att fördelningen av fosforformer var mycket olikartad i olika provpunkter.

94% av all fosfor återfanns mellan 20 och 80 cm djup. I B-horisonten utgjordes ca 60 % av fosforn som Al-bundet P, där aluminiumet utgjordes huvudsakligen av imogolitnanopartiklar (ITN). ITN är ett vanligt Al-mineral i podsolers B-horisonter, och de har en stor förmåga att fixera P. Fosfor i mineraljorden, huvudsakligen P bundet till ITN och som apatit, dominerar jordens sammanlagda fosforförråd och är troligen på lång sikt av stor ekologisk betydelse för fosfortillförsel och –tillgänglighet.

Dessutom rekommenderas att tillföra biobränsleaska som näringskälla för att vidmakthålla skogsmarkens bördighet efter helträdsavverkning. Detta beror på att näringsämnen, inklusive P, bortförs genom skörd av biomassa. Därför undersöktes, i den fjärde studien, effekterna av tillförsel av biobränsleaska, ensamt eller i kombination med N, på fosforns former och tillgänglighet i O-horisonten i två svenska barrskogsjordar.

Studien fann att nästan all Ca-bunden P från askan hade lösts upp sedan asktillförseln ägde rum. Dessutom ökades mängderna totalfosfor och tillgängligt P i O-horisonten samt upptaget av P av växter. Tillförsel av kväve ensamt ökade också P i ovanjordisk biomassa, men samtidigt minskade mängden tillgängligt P i O-horisonten. Då en kombinerad behandling av biobränsleaska och N gjordes ökades P ytterligare i den ovanjordiska biomassan.

Acknowledgements

I would like to thank all those who helped me since May 2018, when I started my PhD education.

My main supervisor, Jon Petter Gustafsson, I thank you for trusting my ability to do this work and guiding me throughout my journey as a PhD student. Your hard work inspires me, and thank you for your quick and well-detailed responses when I needed them. I learned a lot from your critical comments and discussion! I also thank you for helping me with scientific development and deep learning about soil chemistry and the state-of-the-art techniques used in soil chemistry research.

Co-supervisors:

Bengt Olsson, thank you for making me love the forests more than before. You helped me learn more about the historical background and management of Swedish forests, which was necessary for this work. I thank you for your guidance, especially in designing and conducting the work for paper IV. Thank you also for teaching me soil sampling methods in forest soils.

Therese Zetterberg, thank you for helping me learn about forest management, for your valuable editing of manuscripts and comments, and for your encouragement. Thank you for the support that you and Bengt provided during the fieldwork.

Marie Spohn: Thank you for your input on biogeochemical processes and the interaction between element cycles. Thank you for your great contribution and critical comments for papers I and IV.

During my PhD time, I had the great opportunity to perform my experiments at three synchrotron facilities. I would like to acknowledge the technical support concerning micro-XRF and micro-XANES provided by our beamline contact persons: Delphine Vantelon and Camille Rivard, at the LUCIA beamline, the French national synchrotron research centre SOLEIL, Camelia N. Borca, and Thomas Huthwelkerg at PHOENIX at the Swiss Light Source (Paul Scherrer Institut, Villigen Switzerland). Moreover, I would like to thank Wantana Klysubun at the BL8 at the Synchrotron Light Research Institute, Thailand, for her great support concerning bulk XANES data collection.

Moreover, I would like to thank all the Soil and Environment department laboratory staff for their support. Mina Spångberg, thank you for your help with phosphorus analysis. I would also like to thank Agnieszka Renman at KTH in Stockholm for providing similar support. Elin L. at our department, thank you for helping with the analysis of carbon and nitrogen.

My research group of soil chemistry, I thank you for (me) being part of this wonderful group of soil chemistry experts and for the different opportunities provided, including teaching on a master's course in environmental geochemistry.

I would like to thank my collaborators:
Adediran G.A., thank you for being a valuable collaborator for my work, helping me learn about synchrotron-X-ray techniques, and for great discussions. Hillier, S., thank you for sharing your expertise in mineralogy, which helped me improve my work. Florén, T, thank you for your collaboration and input in paper III on the identification of imogolite-type minerals. Lim, H., thank you for your collaboration. Högbom, L, thank you for allowing us to include the Riddarhyttan forest in my PhD project, guiding us in sampling, and comments for paper IV.

I would also like to thank you, Carin Sjöstedt, for the excellent discussion and workshops about XRF data analysis, for reading my third manuscript, and amazing comments. Tino Colombi, thank you for the nice discussions, suggestions, and encouragement. I felt more motivated when knocking on my office door to ask how I was feeling during the final stages of writing this thesis.

I have also received valuable support from colleagues and different people. Emma Lannergård. First, I would like to thank you for your kindness and encouragement. I also thank you for your valuable comments and

Phosphorus abundance and speciation in acid forest Podzols – Effect of postglacial weathering

J.R. Marius Tuyishime [a,*], Gbotemi A. Adediran [a], Bengt A. Olsson [b], Marie Spohn [a], Stephen Hillier [a,e], Wantana Klysubun [c], Jon Petter Gustafsson [a,d]

[a] Department of Soil and Environment, Swedish University of Agricultural Sciences, P.O. Box 7014, SE-75007 Uppsala, Sweden
[b] Department of Ecology, Swedish University of Agricultural Sciences, P.O. Box 7044, SE- 75007 Uppsala, Sweden
[c] Synchrotron Light Research Institute (SLRI), 111 Moo 6 University Avenue, Muang District, Nakhon Ratchasima 30000, Thailand
[d] Department of Sustainable Development, Environmental Science and Engineering, KTH Royal Institute of Technology, Teknikringen 10B, 100 44 Stockholm, Sweden
[e] The James Hutton Institute, Craigiebuckler, Aberdeen AB15 8QH, United Kingdom

ARTICLE INFO

ABSTRACT

The molecular speciation of phosphorus (P) in forest soils is of strategic importance for sustainable forest management. However, only limited information exists about soil P speciation in boreal forests. We combined P K-edge XANES spectroscopy, wet chemical P extractions, and X-ray diffraction analysis of soil minerals to investigate the vertical distribution of P species in seven podzolised forest soils differing in soil properties and climatic conditions. The results showed that the total P stock was on average, 4.0 g m^{-2} in the Oe horizon, 9.5 g m^{-2} in the A and E horizons, and substantially higher (117.5 g m^{-2}, and 109.3 g m^{-2}) in the B and C horizons down to 80 cm depth, respectively. Although the Oe horizons contain a minor total P stock, 87% of it was stored as organic P. The composition of P species in the P-depleted A/E horizons was highly variable depending on the site. However, of the P stored in B and C horizons down to 80 cm, 58% was adsorbed P, mostly to Al, while apatite accounted for 25% of P, most of which was found in the C horizons. The apatite stocks in the A/E, B, and C horizons (down to 80 cm) accounted for 2.5%, 20%, and 77.2%, respectively, of the total apatite for all the mineral soils studied. These figures can be explained, first, by the dissolution of primary mineral apatite caused mainly by acidification. Second, P uptake by plants and microorganisms, and the associated formation of the Oe horizons, led to the formation of soil organic P. Further, the formation of organo-metal complexes and podzolization led to the translocation of P to the B horizons, where P accumulated mostly as P adsorbed to imogolite-type materials (e.g. allophane) and ferrihydrite, as shown by P K-edge XANES spectroscopy. In conclusion, this study shows that despite the young age of these soils (<15,000 years), most of the primary mineral apatite in the upper 30 cm has been transformed into organic P, and Fe-, Al-bound PO$_4$. Moreover, the subsoil P, mainly consisting of adsorbed P to Al, and apatite, dominates the P inventory and probably serves as a long-term buffer of P.

1. Introduction

Phosphorus (P) is an essential macronutrient whose availability in soil might constrain forest productivity, succession, and functioning (Elser et al., 2007, Jonard et al., 2015, Lang et al., 2017, Talkner et al., 2015, Vitousek et al., 2010). The total P stock and chemical speciation change with ecosystem development (Walker and Syers, 1976), which affects P availability. Phosphates (PO$_4$), which initially exist within poorly soluble primary minerals, become increasingly retained by newly formed secondary minerals (Walker and Syers, 1976).

Unlike nitrogen (N) that can be biologically fixed from the atmosphere, the atmospheric input of P in soils is small (Chadwick et al., 1999). The vast majority of P in soils is initially bound within primary Ca phosphate minerals (mostly apatite) (Nezat et al., 2007; Nezat et al., 2008; Prietzel et al., 2013). Apatite is progressively weathered, especially early during pedogenesis when the weathering rate is highest (Walker and Syers, 1976; Zhou et al., 2018). Thus, pedogenic apatite declines over geological time scales (Mehmood et al., 2018, Selmants

and Hart, 2010), and the released P becomes biogeochemically active. In boreal and temperate coniferous ecosystems, organic matter-rich surface horizons form where decomposition and plant uptake are closely coupled (Wood et al., 1984). The fate of P in these soils is also affected by podzolization. Most Swedish forest soils were developed from glacially deposited, nutrient-poor parent material (Andersson et al., 2014). In these young boreal systems, the release of organic acids from the surface horizon and plant roots triggers silicate weathering, which leads to the formation of an illuvial E horizon (Lundström et al. 2000; Smits et al. 2014). Then, organic-acid-Al/Fe complexes migrate to the B horizon, where they precipitate mainly as imogolite-type minerals (ITM) (allophane/imogolite), but also as iron(III) (hydr)oxides (ferrihydrite and goethite) (Buurman and van Reeuwijk, 1984; Gustafsson et al., 1995; Gustafsson et al., 1999; Karltun et al., 2000; Lundström et al., 2000). These mineral phases have a very high P sorption capacity (e.g., Hewitt et al., 2021, Takamoto et al., 2021). Consequently, with time a large part of the biogeochemically active P may end up as adsorbed P in the B horizon (Adediran et al., 2020, Prietzel et al., 2016, Wood et al., 1984).

According to the model developed by Walker and Syers (1976), the total P stock decreases with time due to P leaching (Lang et al. 2016; Walker and Syers, 1976) unless tectonic uplift is strong enough to constantly provide substantial input of P from P-bearing minerals to the ecosystems (Buendia et al., 2010; Porder and Hilley, 2011). At a later stage of pedogenesis, the bioavailability of P is decreased, and P occluded within Al and Fe oxides and P associated with organic matter (OM) are the main pools of P (Turner and Condron, 2013; Walker and Syers, 1976). However, it has been argued that some forest soils in central and northern Europe, although at an early stage of soil development, are characterized by a low P nutritional status and P-limited conditions (Ilg et al., 2009; Yu et al., 2018), which may be affected by a low P availability of the P adsorbed to Fe and Al phases in the subsoil. Further, a high N availability due to high atmospheric deposition rates, enhanced forest productivity and intensified use of forest resources may contribute to an increased plant P demand (Akselsson et al., 2008; Heuck et al., 2018; Jonard et al., 2015; Mohren et al., 1986; Yanai, 1998). A mass balance study carried out for 14,550 Swedish sites showed that the annual losses of P from forestry exceeded 1 kg P ha^{-1} in Southern Sweden (Akselsson et al. 2008). Unless these losses are compensated for (i.e. by ash fertilization), the authors claimed that this may lead to a successive transition from N to P limitation.

To address questions relating to the P bioavailability and possible P limitation in the future, it is important to quantify the stocks of the different P species present in the soil. However, with the exception of a few studies on the P chemistry in the uppermost soil horizons (e.g., Giesler et al. 2002; Vincent et al. 2013), there are very few examples of research on P speciation in boreal forest soils detailed enough to provide reliable information on pedogenic P transformations and nutrient limitation. Synchrotron-based X-ray absorption near-edge structure (XANES) spectroscopy at the P *K*-edge is an emerging method, which provides a "fingerprint" for P speciation in soil (Beauchemin et al., 2003; Franke and Hormes, 1995; Hesterberg et al., 1999; Hesterberg, 2010). The spectra of different P species vary in one or more spectral features such as the shape and position of the white-line intensity as well as in post-edge and pre-edge structures (Beauchemin et al., 2003; Werner and Prietzel, 2015). However, P species coexist in a complex geochemical soil matrix, which makes it necessary to use careful and consistent interpretation methods to correctly separate different P species with P *K*-edge XANES spectroscopy (Gustafsson et al., 2020; Hesterberg, 2019). Important sources of uncertainty of XANES include the procedures of energy calibration at the beamline, and the choice of normalization parameters for linear combination fitting (LCF) (Colocho Hurtarte et al., 2019, Werner and Prietzel, 2015). However, as shown by Gustafsson et al. (2020), by careful energy calibration at the beamline, and by applying a probabilistic LCF method, these uncertainties can be minimized.

In this work, we combined bulk P *K*-edge XANES spectroscopy, wet chemical P extractions, and X-ray powder diffraction (XRPD) to investigate the P speciation of seven forest soils representing different soil properties and climatic conditions. The aim was to determine the stocks of the different P species that have developed after 8000–15,000 years of soil formation, particularly addressing the following questions: 1) what are the predominant P species in acid forest soils of Sweden? 2) does P speciation reflect weathering and podzolization in the soils? Our work builds on and extends the work of Adediran et al. (2020), who presented P speciation data for two of the soils of the current study (Tärnsjö and Tönnersjöheden). By analyzing a wider selection of soils, and by calculating the stocks of the different P species, this paper presents a more complete picture of the quantity of different P species and their vertical distribution in boreal forest soils.

2. Materials and methods

2.1. Study forest sites and soils

Soil phosphorus speciation was investigated in seven forest sites across Sweden that are located along a climate gradient ranging from 56 to 64°N (Fig. 1). They also encompass a variation in geochemical conditions and parent materials (Tables 1, 2, and S1). The sites are located on siliceous glacial till and in glaciofluvial or postglacial sandy deposits. The vegetation is dominated by Norway spruce (*Picea abies* L. Karst.) and Scots pine (*Pinus sylvestris* L.), and the soils are well-drained. These forest sites have previously been investigated for different purposes (Albaugh et al., 2009; Bergh et al., 1999; Casetou-Gustafson et al., 2019; Lim et al., 2020; Linder, 1995; Simonsson et al., 2015; Tiberg et al., 2018; Zetterberg et al., 2013). Five of them, Flakaliden 14B, 1470 Rödålund (North), Tärnsjö, Kloten (central) and Skogaby (SW) were classified as Albic
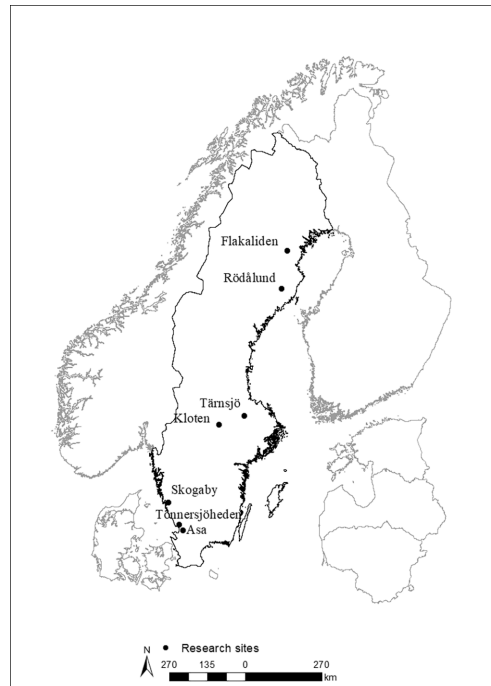
Fig. 1. Location of the study sites.

Table 1

Overview of the studied sites and soils organized by location. MAT is the mean annual temperature, and MAP is the mean annual precipitation.

Study site	Dominant tree species	Location	Parent rock	Soil order[a]	Altitude (m.a.s.l)	MAP mm	MAT °C
Flakaliden 14B	Norway spruce	64°07′N 19°27′E	Glacial till	Albic Podzol	315	600	1
1470 Rödålund	Scots pine	64°08′N 19°52′E	Wave-washed sand	Albic Podzol	250	600	2
Tärnsjö	Norway spruce Scots pine	60°08′N 16°55′E	Wave-washed sand	Albic Podzol	60	600	5.1
Kloten	Norway spruce Scots pine	59°54′N 15°25′E	Glacial till	Albic Podzol	345	927	4.9
Skogaby	Norway spruce	56°33′N 13°13′E	Glacial till	Albic Podzol	110	1187	7.6
Tönnersjöheden T103	Norway spruce	56°40′N 13°05′E	Glacial sandy till	Dystric Arenosol	80	1053	6.4
Asa	Norway spruce	57°08′N 14°45′E	Glacial till	Dystric Arenosol	240	800	6.4

[a] Soil classification according to IUSS Working Group WRB (2014).

Podzols (IUSS Working Group WRB, 2014). The Tönnersjöheden (T103) and Asa soils, both from SW Sweden, classify as Dystric Arenosols (IUSS Working Group WRB, 2014), although the former was very close to being an Entic Podzol. The reason why the Tönnersjöheden soil was not classified as a Podzol was that the A horizon had probably been mixed with large amounts with B horizon material so that the $Al_{ox} + \frac{1}{2}Fe_{ox}$ value (in g kg^{-1}) in the A horizon was slightly more than half of the $Al_{ox} + \frac{1}{2}Fe_{ox}$ value in the upper B horizon (Table S1). Also the Asa soil was very probably subject to podzolization in the past. The historical land use on this site with stone cairns, mechanical soil scarification (Casetou-Gustafson et al., 2020) might have caused soil mixing or overturn of the surface soil horizons.

2.2. Mineralogical characterization by X-ray powder diffraction (XRPD)

For all samples, sieved (<2 mm) samples were micronized in a McCrone mill, and random powders prepared by spray drying the resulting slurries (Hillier, 1999). XRPD patterns were recorded from 4 to 70°2θ using a Bruker D8 diffractometer with Cu K-α radiation and a Lynxeye XE position sensitive detector. Crystalline minerals were identified by aid of patterns from the International Center for Diffraction Data (ICDD) Powder Diffraction File (PDF-4, 2021) and using Bruker DiffracPlus EVA software. Quantitative mineralogical analysis of the diffraction data was performed using a pre-determined full pattern fitting approach as outlined by Omotoso et al. 2006 (participant 18), and more recently by Butler and Hillier (2021). The method does not require the addition of an internal standard but instead includes patterns for amorphous/poorly crystalline phases to enable their direct quantification. The mineralogical composition of bulk soil samples from the Skogaby site was studied previously by Simonsson et al. (2016), while that of the Asa and Flakaliden sites was determined by Casetou-Gustafson et al. (2018). Tönnersjöheden soil mineralogy analysis was carried out at the same time as Flakaliden and Asa but the data has not yet been published. Both previous studies used similar methods, but for the present study the Skogaby soils were rerun on the D8 diffractometer, and the Asa and Flakaliden XRPD data files run previously on the D8 retrieved so that all samples were fitted using precisely the same fitting parameters and full pattern library for the D8 diffractometer. This ensures internal consistency and enables the best comparison of mineralogical analyses from one sample to another.

The results (% by weight) show that the mineralogy of all seven studied soils was dominated by quartz, plagioclase, and potassium feldspar (Table S1). In the B horizon, the highest proportions of amorphous Fe and Al phases, which represent ferrihydrite and allophane were found in the Kloten and Flakaliden soils, which agrees with the wet chemical results, and which is evident also in the P speciation results, see below. In addition, apatite was detected by XRPD mainly in the subsoils except for the Kloten profile where no apatite was detected by XRPD.

2.3. Characterization of chemical soil properties

At each site, a soil pit was excavated and its profile was exposed and prepared for collecting samples (Fig. S3). In total, 73 samples were collected in 10 cm intervals, except for the Oe and E horizons, which were sampled by horizon. The sampling of the Oe and E horizons was adopted to be able to calculate the horizon-specific P stocks in the studied podzolized soils. The Oe horizon thickness ranged between 5 and 7 cm depending on the site. The samples were air-dried, at approximately 30 °C for 7 days and sieved (<2 mm) using a sieve with stainless steel mesh. The soil pH was measured in water using a soil: solution ratio of 1:2.5 (Van Reeuwijk, 1986) for mineral soil samples and a 1:10 ratio for the Oe samples (Blakemore, 1987) after 24 h equilibration time. The amount of organic carbon (C_{org}) and total nitrogen in the soil was determined through dry combustion according to ISO 13878 (1998), using an elemental analyzer for macrosamples (TruMac ® CN, Leco corp, S:t Joseph, MI, USA). Acid-digestible P (TP) was determined by microwave-assisted HNO_3/H_2O_2 digestion of 1 g dry soil according to the method of Church et al. (2017). While this is considered as total P, it should be noted that there may be a small proportion of the P in the soil matrix that is not solubilized by acid digestion procedures (ISO 11074:2015). Surface-reactive Al, Fe, Si and P associated with poorly crystalline Al and Fe minerals (Al_{ox}, Fe_{ox}, Si_{ox} and P_{ox}) were determined using oxalate extraction according to Van Reeuwijk (1986). Briefly, 100 mL acid ammonium oxalate solution (pH = 3.0) was added to 1 g dry soil in 250 mL polyethylene dark bottles covered by aluminium foil. The mixture was equilibrated for 4 h in the dark using an end-over-end shaker. Prior to analysis of Al_{ox}, Fe_{ox}, and Si_{ox} by ICP-OES (inductively coupled plasma optical emission spectroscopy) using a Thermo iCAP 6300 instrument (ThermoFisher Scientific, Waltham MA, USA), the extract was filtered through 0.2 μm single-use filters (Sartorius Minisart®) and diluted five times with ultra-pure H_2O. Further, molybdate-reactive P (Pi_{ox}), representing orthophosphate (Pi_{ox}) in the oxalate extract, was analysed separately using a Seal AA3 AutoAnalyzer (Seal Analytical, Norderstedt, Germany), using the acid molybdate method as modified by Wolf and Baker (1990). The difference between P_{ox} and Pi_{ox} was assigned to oxalate-extractable organic P (P_{org-ox}). Further, the degree of P saturation (DPS) on Al and Fe bound P was calculated using the molar concentrations of Al and Fe bound P as determined by XANES:

$$DPS = \frac{XANES\text{ - }derived\ Al + Fe\text{ - }bound\ P}{0.5 \times (Fe_{ox} + Al_{ox})} \qquad (1)$$

Pyrophosphate-extractable Al (Al_{py}) and Fe (Fe_{py}), representing Al and Fe bound to organic matter, were determined with ICP-OES after 1 g dry soil had been equilibrated in 100 mL of 0.1 M Na pyrophosphate for 16 h (Van Reeuwijk, 1986). Acid ammonium lactate (AL)-extractable P (P-AL), representing short-term geochemically active P, was determined after shaking 3 g of dry soil in 60 mL of AL buffer (adjusted to pH 3.75) for 1.5 h (Egnér et al., 1960) and subsequent analysis by ICP-OES. Plant-available P (P_{Ols}) was determined according to Olsen (1954). Briefly, 2 g soil was equilibrated for 0.5 h with a 40 mL solution containing 0.5 M $NaHCO_3$ (with pH adjusted to 8.5). The suspension was filtered (0.2 μm) before analysis using an AA500 AutoAnalyzer (SEAL analytical). The C_{org}: $P_{org-lcf}$ and N: $P_{org-lcf}$ P ratios were calculated based on mol kg^{-1} concentrations of C_{org} and total nitrogen (N) in the soil OM and XANES-derived organic P ($P_{org-lcf}$). For each soil horizon, the P stocks, i.e. the amount of TP, and P species in g m^{-2} for each soil depth was calculated according to Strand et al. (2016), as follows:

Table 2
Horizon-average properties of the studied soils (mean values).

Horizon	Depth cm	pH	TP mmol kg⁻¹	Al_py	Fe_py	Al_ox	Fe_ox	Si_ox	P_ox	P_lox	P_org-ox	P-AL	P_Ols	DPS %	C g kg⁻¹	N	C:P_org* mol mol⁻¹	N:P_org*	Al:Si
Flakaliden 14B																			
Oe	>0	4.1	18.3	9.9	5.4	18.3	10.8	0.2	9.1	4.2	4.9	6.6	2.9	14.0	208.0	6.0	1040.0	26.0	35.9
E	0–20	4.5	2.0	4.3	1.5	10.7	3.0	0.2	0.9	0.3	0.6	0.5	0.2	12.0	7.7	0.4	951.0	39.5	33.0
B	20–50	4.9	24.4	128.2	33.3	415.5	169.3	108.4	22.6	19.8	2.8	1.0	0.8	8.3	16.4	0.7	n.c	n.c	2.7
C	50–100	5.3	16.7	35.5	2.5	136.3	35.2	44.1	12.2	10.9	1.3	1.5	0.4	15.2	2.9	0.1	n.c	n.c	2.3
1470 Rödålund																			
Oe	>0	4.0	19.2	36.4	4.5	48.2	12.6	0.6	5.3	2.7	2.6	4.6	1.8	9.4	434.0	12.6	2213.0	55.0	18.8
E	0–20	4.5	1.7	12.0	4.8	18.7	12.8	1.2	1.2	0.5	0.7	0.2	0.1	3.6	3.8	0.2	356.0	11.0	7.0
B	20–50	5.4	5.6	57.7	7.3	153.2	25.4	48.6	2.9	2.2	0.7	0.1	0.1	4.3	4.5	0.2	301.0	9.0	1.9
C	50–80	5.4	12.1	35.8	4.1	127.5	25.2	42.2	8.0	7.0	1.0	1.3	0.2	11.9	2.4	0.1	227.0	8.0	2.2
Tärnsjö																			
Oe	>0	4.0	18.4	18.8	2.0	25.3	8.9	0.5	4.3	2.6	1.7	4.4	2.2	11.0	467.0	12.4	2314.0	53.0	13.4
E	0–2	4.3	2.0	4.6	2.5	10.4	4.2	0.4	0.5	0.2	0.4	0.2	0.1	0.0	8.0	0.2	n.c	n.c	13.1
B	2–40	5.0	15.5	46.5	12.5	104.3	39.6	20.9	11.6	10.2	1.5	1.3	0.8	19.8	7.0	<LOD	1665.0	42.5	2.8
C	40–100	6.0	14.7	10.3	2.4	31.3	12.3	13.3	3.0	2.5	0.5	0.6	0.2	24.8	0.7	<LOD	n.c	n.c	1.5
Kloten																			
Oe	>0	3.9	18.3	23.5	5.7	31.4	14.5	0.7	4.8	2.5	2.3	5.0	2.2	7.0	438.0	13.4	2214.0	58.0	10.7
E	0–7	4.1	1.7	13.4	5.2	17.4	5.9	0.5	0.8	0.1	0.7	0.3	0.1	6.0	22.0	0.7	1896.0	50.0	8.4
B	7–40	5.0	9.2	238.9	76.1	576.1	185.1	140.8	6.5	4.1	2.4	0.2	0.1	1.8	29.8	1.1	717.3	23.3	2.4
C	40–50	5.2	7.3	48.4	5.2	176.3	34.7	57.2	5.6	4.4	1.2	0.2	0.1	6.0	4.0	0.2	n.c	n.c	2.2
Skogaby																			
Oe	>0	3.4	20.6	25.9	5.7	33.3	13.9	0.3	7.9	3.6	4.4	6.2	3.8	23.0	424.0	14.7	2340.0	69.0	26.7
E	0–10	3.6	4.1	28.5	39.3	27.0	38.8	1.1	3.4	1.0	2.4	1.1	0.6	9.5	37.1	1.5	2761.5	93.5	–
B	10–60	4.4	7.2	113.3	50.6	207.8	110.0	38.3	6.0	3.6	2.4	0.1	0.1	4.0	16.2	0.7	1084.3	38.5	2.4
C	60–100	4.7	8.3	26.7	3.0	47.6	5.5	12.0	3.8	3.0	0.8	0.7	0.1	14.0	1.6	<LOD	n.c	n.c	1.7
Tönnersjöheden (T103)																			
Oe	>0	3.7	21.6	19.2	7.2	26.2	13.8	0.6	5.5	2.1	3.3	4.8	2.2	15.0	448.0	14.7	1951.0	55.0	11.0
A	0–10	4.2	8.3	96.5	121.2	98.7	131.7	2.7	5.6	2.0	3.5	0.8	0.2	5.0	40.0	1.6	1679.0	59.0	0.9
B	10–50	4.7	16.9	141.9	43.7	260.6	82.5	49.6	12.5	9.1	3.5	0.6	0.3	8.3	18.3	0.9	662.3	27.3	2.4
C	50–100	4.8	14.6	63.8	16.0	90.7	24.8	17.1	7.6	5.7	1.9	0.9	0.1	13.6	6.4	0.2	n.c	n.c	1.5
Åsa																			
A	0–10	4.5	11.8	191.5	74.7	205.1	82.2	22.3	7.6	3.3	4.3	0.9	0.3	4.0	53.6	2.5	2228.0	40.0	0.6
B	10–50	4.5	11.4	203.6	77.9	201.8	85.9	20.1	7.8	3.2	4.6	0.9	0.2	4.8	45.4	2.0	1123.0	19.0	0.3
C	50–100	4.6	15.3	92.0	21.4	92.0	32.9	27.8	9.2	7.2	2.0	1.7	0.1	10.4	9.3	0.4	1.0	n.c	1.8

P_{org}*: organic P as evidenced by XANES ($P_{org-tcl}$). Al:Si calculated as (Al_{ox} - Al_{py})/Si_{ox}. < LOD: below the limit of detection. For more details of all samples, see Table S1. P_{org}* was not calculated because Porg* was not detectable by XANES. n.c: not calculated because Porg* was not detectable by XANES.

$$P_{stock} = BD*CF_{coarse}*P*d \qquad (2)$$

where BD represents bulk density (kg m^{-3}), CF$_{coarse}$ is the correction factor for stones and boulder contents (=1-(stone volume %)/100), P is the P content (kg kg^{-1}), d is the sampling depth increment within the soil horizon (m). The CF$_{coarse}$ was adopted from earlier studies (Asa and Flakaliden, Casetou-Gustafson et al. 2020; Rödålund, Lim et al., 2020; Tärnsjö, Kloten, and Skogaby, Stendahl et al. 2009) in which stoniness had been estimated by the rod penetration method (Stendahl et al., 2013; Viro, 1952), or had been estimated from pit excavations where the volume of stones and gravel was measured (Tönnersjöheden). However, some of the soils are shallow and so the P stocks were not calculated for the whole profile. BD was estimated from the organic C content using the pedotransfer functions developed by Nilsson and Lundin (2006):

$$BD \ mineral \ soil = 1000 \cdot \left(1.5463 \cdot e^{-0.3130 \cdot \sqrt{C_{org}}} + 0.207 \cdot d\right) \qquad (3)$$

$$BD \ humus = 1000 \cdot \left(\frac{C_{org}}{-2.1278 + 0.1528 \cdot C_{org} + 0.2105 \cdot C_{org}^2}\right) \qquad (4)$$

where C is the organic carbon content (% dry weight).

2.4. Phosphorus speciation by X-ray absorption near-edge structure (XANES) spectroscopy

To investigate P speciation at the pedon scale, P K-edge XANES spectroscopy was performed on bulk samples of all Oe, A/E, B and C horizons (Fig. 3 and Table S1) at beamline 8 (BL 8) (Klysubun et al., 2020) of the Synchrotron Light Research Institute (SLRI) in Nakhon Ratchasima, Thailand. The BL8 utilizes synchrotron radiation generated from the SLRI storage ring with an electron beam energy of 1.3 GeV and a beam current ranging from 80 to 150 mA. The X-ray photon energy was scanned by an InSb (1 1 1) double crystal monochromator giving a beam flux of 1.3×10^9 to 3×10^{11} photons s^{-1} (100 mA)$^{-1}$ of 17.7×0.9 mm^2 beam. The soil samples were homogenized, finely ground and sieved (to <50 μm) to optimize X-ray beam penetration in the sample and to minimize the effect of self-absorption. The samples were packed in hollow and stainless steel sample holders (2 mm thick, 1×1.5 cm^2 with a sample window of 0.5×1 cm^2), which were covered with polypropylene X-ray film (Eriksson et al., 2016b). The sample holder was mounted in the sample compartment at 45^0 relative to the incident monochromatic beam. The sample compartment was continuously evacuated with helium (He) gas to lessen the attenuation of X-ray absorption (Kelly et al., 2008). A solid-state 13-element Ge detector measured the fluorescence emitted from the sample in the energy range of 2100–2320 eV. A 2 s dwell time was used per energy step. This energy step was 2 eV between 2100 and 2139 eV, 1 eV between 2139 and 2146 eV, 0.2 eV between 2146 and 2160 eV, 0.3 eV between 2160 and 2190 eV, and 5 eV between 2190 and 2322 eV. The maximum of the first derivative of the spectrum (E$_0$) for the black P was set to 2145.5 eV for energy calibration. A variscite standard (E$_0$ = 2154.05 eV) was frequently measured to check any shift that occurred after every energy re-calibration. Between 4 and 8 scans were collected for each sample.

2.4.1. P K-edge XANES data processing

The computer code Athena, Demeter version 0.9.025 (Ravel and Newville, 2005), was used for all XANES spectral data processing. Before merging multiple scans of a given sample, each scan was examined thoroughly for its quality (e.g. glitches, noise), and, if necessary, corrected for any misalignment of energy, as indicated by the variscite calibration check. The normalization of spectra was carried out as follows: first, correction of the linear baseline by subtracting a linear function from the spectral range below the edge at −30 and −10 eV relative to E$_0$ = 2154.05 eV (the first-derivative maximum of the P K-edge of variscite). Second, the post-edge normalization range was

determined by a linear function between 30 and 45 eV relative to E$_0$ = 2154.05 eV, as a starting point (Eriksson et al., 2016b). Each normalized sample spectrum was thereafter subjected to linear combination fitting (LCF) analysis (Beauchemin et al., 2003). In the current study, 15 standards divided into six species groups were used to provide a good representation of the solid P phase in acid forest soil (Gustafsson et al., 2020):

1. *Soil organic P* (representing generic organic P from a Spodosol Oe horizon).
2. *Phosphate adsorbed to Al*: phosphate adsorbed to allophane, phosphate adsorbed to gibbsite, and phosphate adsorbed to Al(OH)$_3$
3. *Phosphate adsorbed to Fe*: phosphate adsorbed to ferrihydrite, phosphate adsorbed to goethite
4. *Al phosphates*: variscite, amorphous AlPO$_4$
5. *Fe (III) phosphates*: strengite, amorphous FePO$_4$
6. *Ca phosphates*: apatite Taiba, apatite Templeton, hydroxyapatite, octacalcium phosphate (OCP), brushite.

In the LCF, energy shifts were not permitted, the sum of weights (SOW) was not forced to 1, and a maximum of four standards was allowed in the output. The best fit was chosen from all the output fits, as resulted in the lowest R factor (goodness-of-fit parameter of Athena) (Ravel, 2009).

$$R = \frac{\sum (\text{data - fit})^2}{\sum (\text{data})^2} \qquad (6)$$

Moreover, only LC fits having a SOW between 0.95 and 1.05 were accepted. The LC fits were then subject to uncertainty analysis with the AthenaAut software, as detailed by Gustafsson et al. (2020). Briefly, 100 spectral variants for each single LC fit were generated by Latin hypercube sampling. For misalignment in energy calibration and normalization errors, we used Beta (α, β) probability distributions with α = β = 1.5. The maximum energy calibration error, which is equivalent to 0- and 100 percentiles, was set to −0.05 eV and 0.05 eV, respectively. The maximum error in normalization was estimated to be 7% below and at E$_0$, which then decreased linearly to 0 at the lower post-edge normalization limit (set to +30 eV relative to E$_0$ = 2154.05 eV). Each of the 100 spectral variants was then subjected to LCF analysis and the best results for all LCF:s were retrieved. Only models that could describe at least 50% of spectral variants were accepted. To improve statistics for the spectra not covered at 50%, we grouped different species groups into larger groups following the procedure of Gustafsson et al. (2020). For example, all Fe-bound P (phosphate adsorbed to Fe and Fe phosphate) could be grouped into a single group termed "Fe-bound P" if this was necessary to reach 50 %. The concentrations of XANES-derived P species were calculated from the LCF-generated P fractional weights of the TP concentration (in 100%). The fit uncertainty associated with energy calibration and normalization errors was also calculated according to Gustafsson et al. (2020). In this study, the resulting uncertainties of the different fractions were generally in the order of 5 % of TP.

When presenting the results from LCF, we assumed that the sum of all weights corresponded to TP. However, the X-ray beam is not able to penetrate the soil particles more than a few μm at the P K-edge, as was discussed by Eriksson et al. (2016a), while the soil samples had been crushed and sieved to <50 μm. On the other hand, the assumption that acid-digestible P represents TP is similarly uncertain. Hence, the assignment of XANES-derived weights to percentages of TP may not be completely correct, but the weights should be reasonably accurate concerning the relative concentrations of geochemically active (i.e. surface-active) P species in the soil.

3. Results

3.1. Soil characteristics

The characteristics of the studied soils are presented in Table 2 (horizon-averaged data) and Table S1 (data for all individual samples). In all investigated profiles, the pH was low and increased slightly with depth. On average, the pH was 3.9, 4.2, 4.7 and 5.2 in the Oe, A/E, B and C horizons, respectively. The amounts of C_{org} and total N (N) were high in the Oe horizons and decreased substantially with soil depth. When using the XANES-derived organic P from LCF, $P_{org-lcf}$, the element ratios C_{org}: $P_{org-lcf}$ (mol mol^{-1}) ranged between 1040 and 2340 in the Oe horizons. In the mineral soil, these ratios increased generally from the North to the South and decreased with increasing soil depth. In the A/E horizons, the C_{org}: $P_{org-lcf}$ ratios were below 1000 for the two northern sites, Flakaliden and Rödålund, and between 1679 and 2762 for the remaining sites. The N: $P_{org-lcf}$ (mol mol^{-1}) ratio varied between 9 and 93.5 and appeared to be higher for the southern sites, when samples from the same depths are compared.

The concentrations of oxalate-extractable Al (Al_{ox}) and Fe (Fe_{ox}) peaked in the B horizons (the maximum concentrations for all samples were between 166.5 and 821.7 mmol kg^{-1} for Al_{ox}, and between 64.2 and 366.9 mmol kg^{-1} for Fe_{ox}), see Fig. S1. In the C horizons, the concentrations ranged from 25.3 to 188.1 mmol kg^{-1} for Al_{ox} and from 3.9 to 41 mmol kg^{-1} for Fe_{ox}. Minimum concentrations were measured in the E horizons. The concentrations of pyrophosphate-extractable Al (Al_{py}) and Fe (Fe_{py}) were lower than Al_{ox} and Fe_{ox}. Two contrasting soils were those of Kloten and Tärnsjö, which had the greatest and lowest accumulation of both oxalate- and pyrophosphate-extractable Al and Fe, respectively. On a molar basis, the Al_{ox} concentration was always higher than Fe_{ox}, except in the A/E horizons of Tönnersjöheden and Skogaby. The data also revealed that the inorganic Al:Si ratio of the oxalate extract, calculated as $(Al_{ox}-Al_{py})/Si_{ox}$, was consistently between 2 and 3 in the B horizons (Table S1), suggesting ITM (i.e. allophane and imogolite) to be the dominant form of inorganic oxalate-extractable Al (Gustafsson et al., 1999; Gustafsson et al., 1995; Lundström et al., 2000). The DPS ranged between 1 and 34% with the highest and lowest percentages at Tärnsjö and Kloten, respectively. In the B horizons, the former site also showed a higher DPS level, being 2 to 10 times higher than that found in similar horizons at the other studied sites.

3.2. Contents of different extractable P fractions as assessed by wet chemical extractions

The acid-digestible P (TP) concentration ranged from 1.1 to 29.7 mmol kg^{-1} (median = 12.5 mmol kg^{-1}) across all analyzed 73 samples, of which between 13 and 98% could be dissolved in acid ammonium oxalate (Table 2, Table S1). Of the oxalate extractable-P (P_{ox}), on average 66% was Pi_{ox} and the remaining part was assumed to represent organic P (P_{org-ox}) (Table 2). The extracted P increased in the order P_{Ols} < P-AL < P_{ox} < TP. Both TP and P_{ox} were generally low in the A and E horizons.

Most of the P in the B horizons was extracted by oxalate (≥64% of TP); the P_{ox} concentration ranged between 2.7 and 28.9 mmol kg^{-1}. The percentages decreased with soil depth for most of the soils. The lowest relative recovery of P_{ox} was found at Tärnsjö, particularly in the C horizon where P_{ox} formed, on average 20% of TP. By contrast, the DPS was consistently the highest at Tärnsjö, exceeding 25% below 70 cm. The proportion of oxalate-extractable organic P (P_{org-ox}) in relation to P_{ox} was higher in the Oe and A/E horizons and then decreased with increasing soil depth and with decreasing organic C. Unlike P_{ox} and Pi_{ox}, P_{org-ox} was strongly correlated with organic C (r = 0.83, p < 0.001).

3.3. P speciation in soils as evidenced by P K-edge XANES spectroscopy

The contribution of different P fractions varied within and among

soil profiles (Figs. 2 and 3, Tables S2–S8). In the Oe horizons, $P_{org-lcf}$ was the dominant P fraction with a relative contribution between 73 (±3.5) and 91% (±2.4), but there was also a minor contribution from Al- and Fe-, and/or Ca-bound P. In the A/E horizons, the contribution of Al-bound P, $P_{org-lcf}$, Fe-bound P, and Ca-P were 16–68%, 17–57%, 0–43%, and 0–29%, respectively. Although $P_{org-lcf}$ and Ca-P were present in some of the B horizon samples, Al-bound P was the dominant P fraction in the B horizon. The Al-bound P consisted probably mostly of ITM, as evidenced both by the strong relationship between $(Al_{ox}-Al_{py})$ and Si_{ox} (Fig. S2), and by the fact that the "P adsorbed to allophane" standard occurred most frequently in the best fits (Tables S2–S8). Al-bound P contributed to 42–74% of TP followed by Fe-bound P with 5–24%. Of the Fe-bound P (P adsorbed to poorly crystalline Fe oxides + amorphous $FePO_4$), P adsorbed to ferrihydrite and goethite were the most abundant P species throughout the soil profiles, according to the LCF results (Tables S2–S8).

In all soils, Ca-bound P increased with increasing soil depth (Figs. 2 and 3). The Ca-bound P was probably dominated by apatite, which is supported by the fact that apatite occurred most frequently in the best LCF fits (Tables S2–S8). With the exception of the Kloten soil, which was underlain by bedrock at 50 cm, the content of Ca-bound P was 17–63 % in the C horizon down to 80 cm depth (Fig. 3). In the shallow Kloten soil, apatite appeared to have almost completely dissolved. By contrast, Tärnsjö appeared to be the soil with the highest amount of apatite in the C horizon, as Ca-bound P accounted for 63% of the TP between 40 and 80 cm depth (Fig. 2, Table S4). Al- and Fe-bound P were also common P species in the C horizon whereas the contribution of organic P was low, only 0–6%. It is also pertinent to note that there was general consistency between XANES and XRPD in the determination of apatite content within and between soils.

When taking into account bulk densities (Table S1), sample thickness, and stones and boulder content, the P stock in the upper 80 cm of the soils investigated ranged from 69.1 to 379.0 g P m^{-2}. It should be noted that the smallest P stock was calculated for Kloten, simply because its profile was shallower than the others. Unlike the higher P concentration in the surface horizons, the average stock of TP was only 4 g m^{-2} in the O horizons and 9.5 g m^{-2} in the A/E horizons, as compared to 117.5 g m^{-2} and 109.3 g m^{-2} in B and C (down to 80 cm), respectively, which means that 94 % of TP was in the B and C horizons. This substantially larger TP stock in the subsoil was caused in part by higher bulk densities (Table S1), thicker horizons but also by P redistribution. The stocks of separate P species in different horizons followed the same pattern as TP, i.e. high concentrations but low stocks in the O horizons and maximum P species stocks in the subsoil (Fig. 2). Of the TP in the subsoil, 58% was adsorbed P (mainly to Al), while apatite accounted for 25% of the P, most of which was in the C horizons. The apatite stocks in the A/E, B, and C horizons (down to 80 cm) was on average 2.5%, 20%, and 77.2% of the total apatite, respectively. It should be noted that the stocks in the E horizon of the Tärnsjö pedon were not calculated because of its low P concentration, which prevented successful XANES speciation. Moreover, the Asa O horizon was not available and therefore not included in the evaluation.

Possible relationships between XANES-derived P species and extraction results were investigated using correlation analysis. Notably, there was a significant positive correlation between the Ca-bound P, as evidenced by XANES-LCF, and DPS (r = 0.57, p < 0.001) across all 73 soil samples (Table 3), which suggests that a high apatite content led to higher dissolved P and thus to a higher degree of saturation on the Fe oxides and ITM. The $P_{org-lcf}$ was strongly correlated (r = 0.91, p < 0.001) with C_{org} and weakly but significantly correlated also with P_{org-ox} (r = 0.35, p < 0.05). XANES-derived Fe- and Al-bound P was highly significantly correlated with total P_{ox} (r = 0.97, p < 0.001) as well as with Pi_{ox} (r = 0.95, p < 0.001). Moreover, a regression analysis showed that the determination coefficient was (r^2 = 0.95, p < 0.001), (r^2 = 0.92, p < 0.001), and (0.52, p < 0.001) for the pairs [XANES-(Fe + Al)-P; P_{ox}], [XANES-(Fe + Al)-P; Pi_{ox}], and [$P_{org-lcf}$; P_{org-ox}], respectively (Figs. 4
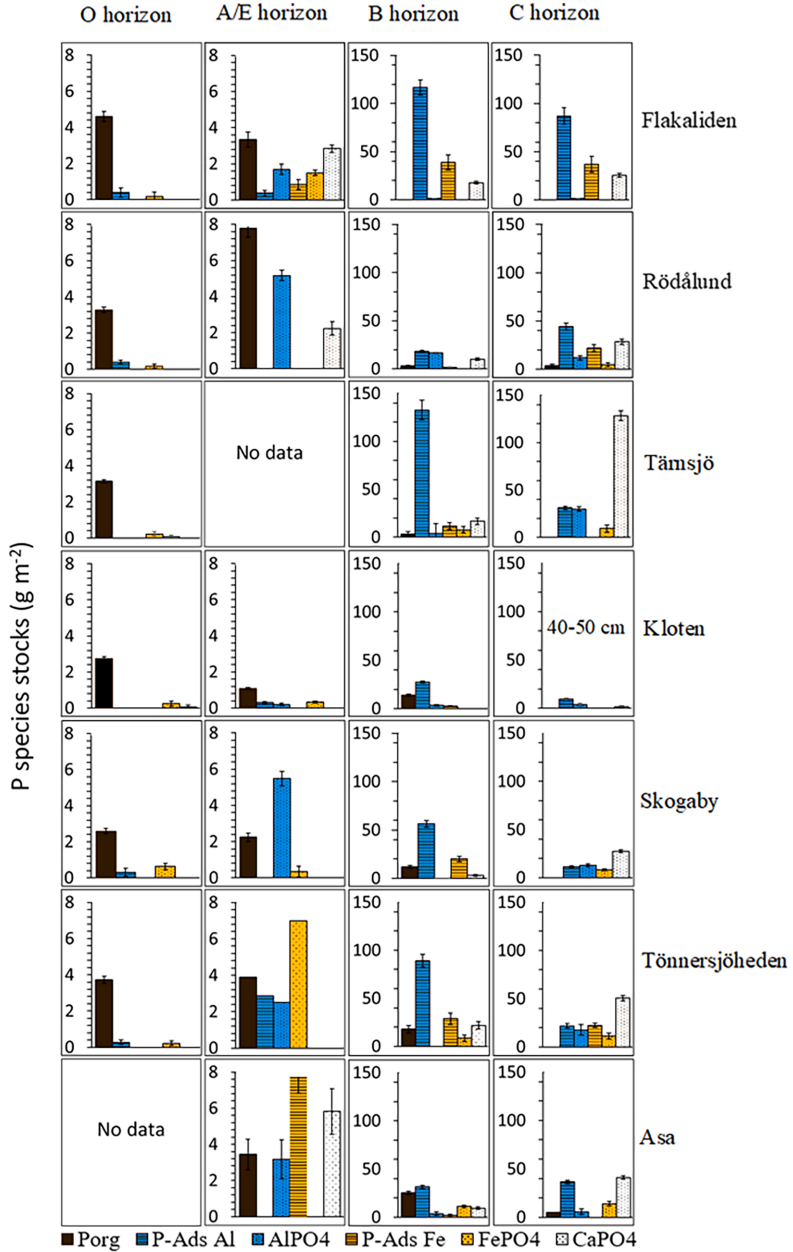
Fig. 2. Stocks of phosphorus (P) species groups in the organic layer, A/E, B, and C horizons (down to 80 cm) in seven forest soils from Sweden. No available data for O horizon for Asa, the E horizon for Tärnsjö, and below 50 cm for Kloten. Error bars indicate the uncertainty associated with the P pools.
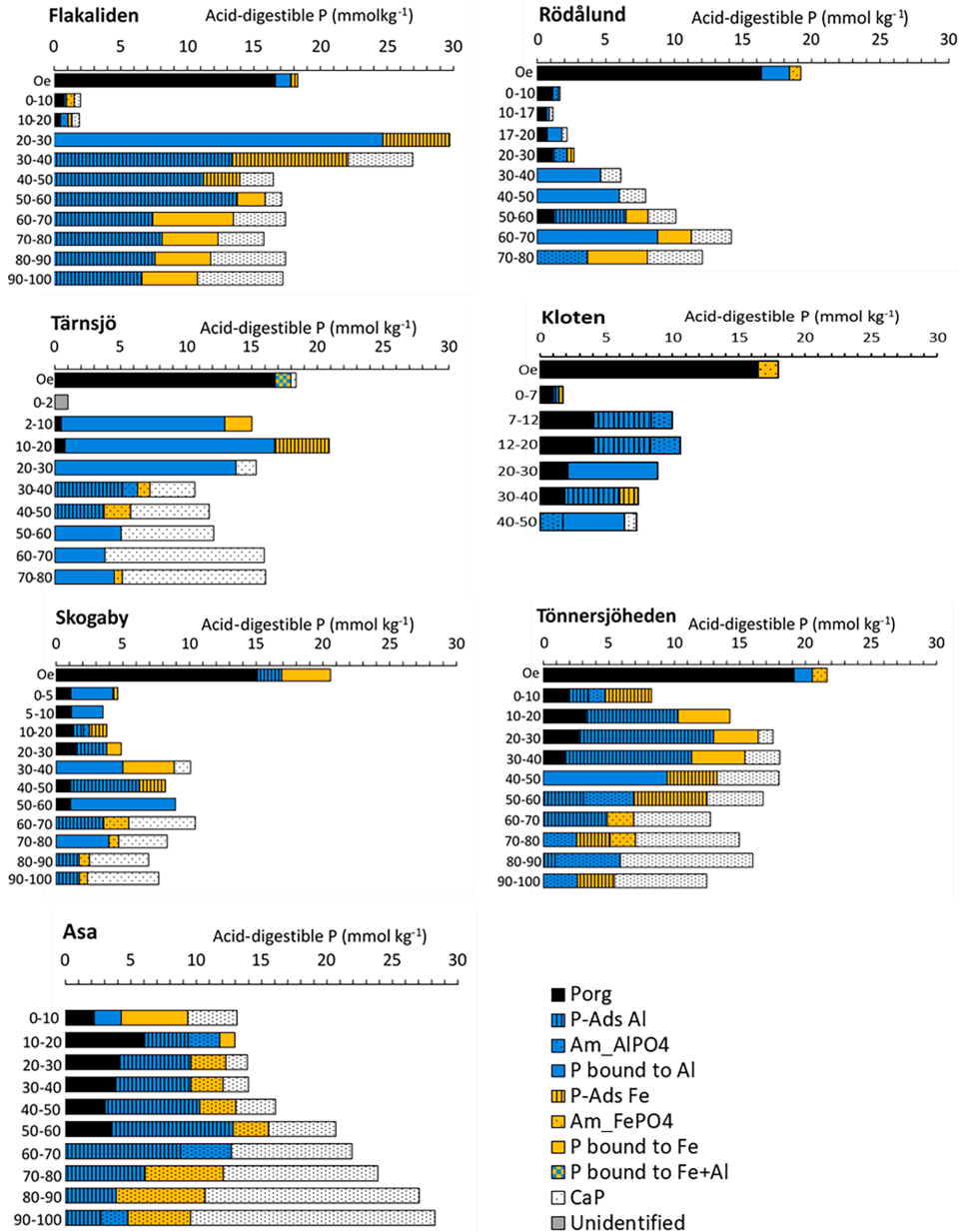
Fig. 3. Relative contributions of different P species to TP in seven forest soils according to P K-edge XANES spectroscopy. Soil depth (cm) is shown on the left. P_{org}: organic P, P bound to Al: the sum of all Al-bound P species, P bound to Fe: the sum of all Fe-bound P species. In the O horizon of Tärnsjö, P bound to Fe + Al represents a case when the probabilistic LCF could not differentiate between P bound to Al from P bound to Fe.

Table 3
Pearson correlation coefficients (r) between extractable P fractions, XANES-derived P species and selected soil properties across all investigated mineral soil horizons.
***: $P < 0.001$, **: $P < 0.01$,*: $P < 0.05$.

	pH	Al_{py}	Fe_{py}	Al_{ox}	Fe_{ox}	Si_{ox}	P_{ox}	Pi_{ox}	P_{org-ox}	C	DPS
TP	0.37**	0.17	0.00	0.28**	0.21	0.28*	0.84***	0.84***	0.26*	−0.07	0.41**
P_{ox}	0.01	0.31*	0.13	0.45***	0.40***	0.42***	−	0.97***	0.46**	0.1	0.08
Pi_{ox}	0.14	0.13	−0.05	0.35**	0.27*	0.39**	0.97***	−	0.23	−0.11	0.21
P_{org-ox}	−0.46***	0.78***	0.72***	0.53***	0.62***	0.25*	0.46***	0.23	−	0.83***	−0.46***
PAL	−0.02	−0.09	−0.05	−0.21	−0.15	−0.25*	0.43***	0.46***	−	−0.03	0.43***
P_{Ols}	−0.14	0.01	0.06	0	0.12	−0.05	0.65***	0.66***	−	0.12	0.30*
$P_{org-lcf}$	−0.24	−0.02	−0.01	−0.02	−0.03	−0.04	0.10	−0.02	0.35*	0.91***	0.3
(Fe + Al)-P	0.16	0.20	0.04	0.36**	0.32**	0.36**	0.97***	0.96***	0.33**	−0.20	0.22
Al-bound P	−0.19	0.17	0.03	0.32*	0.27*	0.31*	0.87***	0.87***	0.25*	−0.05	0.26*
Fe-bound P	0.23	0.25	0.03	0.54***	0.44**	0.54***	0.76***	0.76***	0.2	−0.13	0.04
P-ads Al	0.21	0.05	−0.08	0.24	0.18	0.19	0.87***	0.88***	0.18	−0.11	0.30*
$AlPO_4$	0.46*	−0.04	−0.17	0.02	−0.13	0.12	0.34	0.40*	0.00	−0.16	0.55**
P-ads Fe	0.34	0.37	0.04	0.55***	0.43*	0.51**	0.72***	0.71***	0.31	−0.04	0.17
$FePO_4$	0.05	0.12	0.00	0.25	0.13	0.38	0.80***	0.89***	0.05	−0.15	−0.08
$CaPO_4$	0.37*	−0.21	−0.22	−0.24	−0.22	−0.17	0.04	0.11	−0.22	−0.28	0.57***

and 5). Overall, these results suggest a high level of consistency between the XANES-derived P speciation results and the information gained from wet chemical extractions.

4. Discussion

The P speciation results of this study are consistent with those of Wood et al., who already in 1984 observed that the Podzols they studied were "highly stratified with respect to phosphorus biogeochemistry", with biological control of P in the O and some of the E horizons (as manifested in the predominance of organic P), while in the B horizons P cycling was predominantly "geochemical" and governed by P adsorption/desorption to secondary Al and Fe phases. They are also in general agreement with the Walker and Syers model (Walker and Syers, 1976), i.e., with time, primary mineral apatite is weathered to other P forms such as adsorbed P and organic P. Similar observations were also made by, e. g. Cade-Menun et al. (2000) and SanClements et al. (2010). These and other previous research findings were, however, based on traditional wet-chemistry fractionation methods and in some cases ^{31}P NMR spectroscopy, none of which are well suited to characterize inorganic P phases in subsoils. In the current study, the use of P K-edge XANES spectroscopy combined with traditional wet-chemistry methods permitted a more detailed picture of P speciation. Although similar work
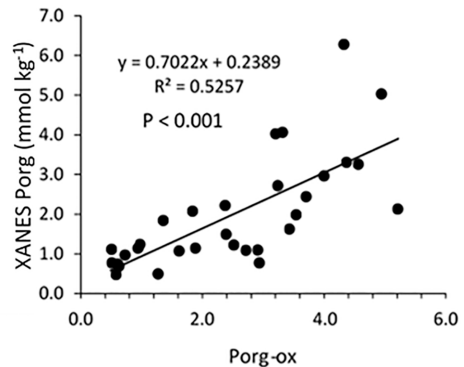
Fig. 5. Relationship between organic P (according to XANES) and organic P determined by oxalate extraction in the mineral soils.
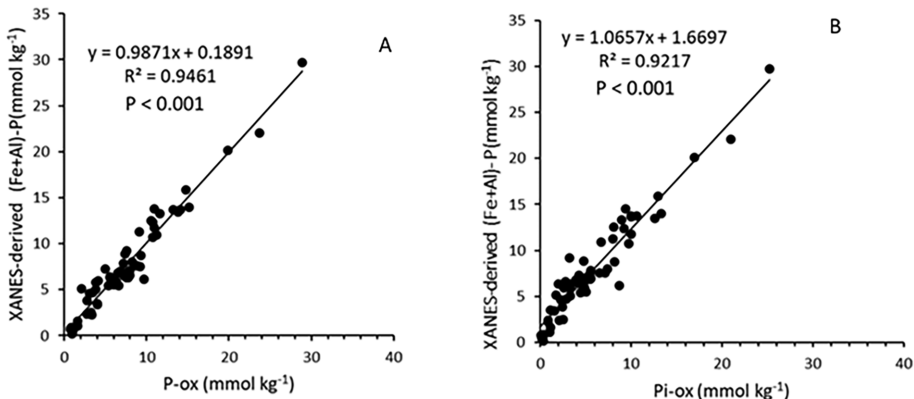
Fig. 4. Relationship of Fe- and Al-bound P (according to XANES) and (A) oxalate-extractable total P and (B) inorganic P, in all the 65 mineral soil samples from seven different forest soils.

was reported recently for other soil profiles from Cambisols and from other non-podzolized soils (Prietzel et al., 2016; Rodionov et al., 2020; Zhang et al., 2021), this study, together with a companion study (Adediran et al., 2020) are the first, to our knowledge, that report detailed XANES-derived P speciation data for Podzols and Podzol-like soils typical of boreal forested environments.

A unique aspect of the current study was the estimation of horizon-specific P stocks associated with different P species, as determined by XANES. These calculations show that in the seven studied profiles only a small part of the P resided in the O and E horizons (6%) while the remaining 94 % was found in the B and C horizons down to 80 cm. In line with this is the finding that, on average, only 6% of the P was organic P, while 58 % was adsorbed to Al and Fe (hydr)oxides (mainly to Al) and 25 % as Ca phosphates in the subsoil horizons. Thus, although the quantitative role of Al and Fe (hydr)oxide-bound P for P uptake has been questioned, it is nevertheless clear that this pool, together with apatite, represents a large reserve of P in the forest ecosystem. The P stocks of this study are in the low to intermediate range when compared to central European forest soils (Cambisols; Prietzel et al., 2016; Lang et al., 2017), and soils from the tropical East Asian region (Jien et al., 2016). The distribution of P species in podzolized soils of temperate regions has been also studied (Werner et al., 2017), although in this case stocks were not calculated.

The investigated forest soils show a marked decline in apatite contents (both in concentrations and stocks) in the topsoils down to about 30–40 cm depth compared to the C horizon after 10,000 to 15,000 years of soil formation. A large part of the TP has been transformed into organic P in the topsoils and to Fe- and Al-bound P in the B horizon. As concerns the B horizons, the XANES data allowed us to clarify the identity of the adsorbed P. Perhaps not surprisingly, P bound to Al and Fe (hydr)oxides and ITM were the major P forms. However, it should be noted that the ITM were of particular importance as a host for adsorbed P: as can be seen in Fig. 3 and Tables S2–S8, P adsorbed to allophane, and other Al-bound P forms, were quantitatively more important than Fe-bound P in all studied soils. There was also a strong increase in the apatite fraction in the mineral soil as a function of soil depth, which is also evident in the mineralogical analysis of soil by XRPD (Table S9). These results extend those of our previous study (Adediran et al., 2020), which used micro-focused X-ray fluorescence and absorption microscopy showing the subsoil apatite to occur both as inclusions in aluminosilicate minerals and as discrete mineral grains. These findings support the ideas of Wood et al. (1984), who found indications that surface horizons rich in roots, bacteria, fungi, and OM are layers of strict biological P retention whereas geochemical processes involving mostly inorganic P pools would predominate in underlying soil horizons. This is probably true for the Oe horizons of the current study, where organic C was about 40 %, and where organic P accounts for a major part of the TP. Previous research has shown that P cycling in forested ecosystems is characterized by tight coupling between the decomposition/mineralization of organic P and uptake in the surface horizon, so that only a minor fraction of the P is taken up from the subsoil (e.g. Klotzbücher et al., 2020; Lang et al., 2017; Wood et al., 1984).

Organic P decreased substantially with increasing soil depth and was a minor P species in the subsoil. The reason for this is likely that plant litter is the main source of P_{org} which is deposited on top of the organic layer (leaf litter) or mostly in the organic layer (root litter). In the mineral soil, organic matter is mainly derived from root litter and mycorrhizal fungi (Buurman and Jongmans, 2005, Richardson and Simpson, 2011) and their density decreases with soil depth, resulting in lower OM input thus low P_{org} (Wood et al., 1984). Alternatively, the occurrence of P_{org} in the subsoil might also be explained by leaching of DOC or colloids through the soil profile (e.g., Werner et al., 2017).

The C_{org}: P_{org} and N: P_{org} ratios in the A/E horizons were most often of a similar magnitude as in the Oe horizon (Table 2, and S1), but then decreased with increasing soil depth and with increasing P concentrations in the mineral soil. This agrees with previous research showing that

high contents of surface Al and Fe minerals result in narrow C_{org}:P_{org} ratios (Werner et al., 2017). In the B horizons, most of the P was associated with Al and Fe phases, which reflects the enrichment of ITM and Fe (hydr)oxides in the B horizon due to podzolization processes (e.g. Lundström et al., 2000). Our results suggest that during pedogenesis, P weathered from apatite in the upper soil horizons has been redistributed, and a major part of this P is now adsorbed in the B horizon. A large part of this redistribution probably occurred early during the Holocene, as the apatite weathering rate was probably higher then (Zhou et al. 2018). The XANES results suggest that ITM was the most important host for adsorbed P in the B horizon. The mineralogical data of the soils studied support this interpretation as they show that allophane (ITM) and ferrihydrite peaked in B horizons (Table S9). The finding that ITM is the most important host for adsorbed P is not surprising given that (i) oxalate-extractable Al was generally much higher than oxalate-extractable Fe in the B horizon (Table 2), and (ii) surfaces with Al-OH groups have a documented high capacity to sorb orthophosphate (e.g. Tiberg et al. 2020). This finding is consistent with that of Takamoto et al. (2021) who found that Al phases exert a stronger control of P than Fe phases in allophanic soils.

The fact that 95% of the variation of the Fe- and Al-bound P could be explained by P_{ox} (which includes also organically bound P), compared to 92% for P_{ox} (Fig. 4), may suggest that organic P should not be ignored as a contributor to the Fe- and Al-bound P pool especially in the podzolized B horizons. As discussed by Gustafsson et al. (2020), adsorbed organic P may contribute to the XANES-derived Fe- and Al-bound P pool, as its XANES spectrum is intermediate to the spectra of adsorbed inorganic P and non-adsorbed organic P. These results are consistent with earlier studies (Borggaard et al., 2004, Yuan and Lavkulich, 1994), reporting that Fe and Al oxy(hydr)oxides are important sorbents for both mineral and organic P, especially in Podzols. To what extent the adsorbed P in the B horizon is available for uptake is a matter of ongoing discussion (Jones and Oburger, 2011; Klotzbücher et al. 2020). Excretion of organic acids from soil microorganisms can mobilize P in acid forest soils with limited P supply (Jones and Oburger, 2011). However, the P uptake by beech was not affected by addition of P-amended goethite in greenhouse experiments (Klotzbücher et al. 2020), which led these authors to put into question the ecological relevance of the large Fe-bound P pool in the subsoil.

In this context, it may be important to consider the fact that ITM and Fe oxide in the B horizon have high P sorption capacities and may serve not only as sources but also as sinks of P. To what extent they can act as sources is probably dependent on the DPS, i.e. to what extent the oxide surfaces are 'saturated' with P. Excretion of organic acids may not lead to increased P uptake if the released P is immediately readsorbed to the Fe and Al phases because of their low DPS. It is of interest to note that the Kloten soil, which was the soil with the lowest DPS in the B horizon, was also the soil with the largest percentage of P as organic P in the B horizon, despite its relatively strong accumulation of ITM and Fe oxide (Fig. 3, Table 2) as shown by extraction (Fig. S1 and S1) and XRPD results (Table S9). Conversely in the Tärnsjö soil, which had the highest DPS in the B horizon, the mineral soil contained very little organic P. This supports the idea that in relatively P-poor Podzols the system would strive for more efficient recycling of organic P, with minimal losses to adsorbed P forms in the subsoil (e.g. Lang et al., 2017; Odum, 2014).

Although the current study confirms the hypothesis of Wood et al. (1984), i.e. that Fe and Al in the subsoil exert a major control of P through geochemical rather than biological cycling, this does not exclude a role of Fe- and Al-bound P for biological uptake, particularly not in P-rich sites. In this respect we hypothesize that ITM and other Al phases such as Al(OH)$_3$, which dominate the P speciation in the B horizon of these boreal Podzols, are more likely sources for geochemically active P than Fe oxides, because of their lower thermodynamic stability under acid conditions (Gustafsson, 2001, Gypser et al., 2021).

In the C horizon, the apatite pool was larger in most of the studied soils, especially in Tärnsjö, Tönnersjöheden, and Flakaliden, which also

have relatively large P stocks. In addition, the DPS in the B and C horizons of these three soils was on average above 8% and 14%, respectively. This suggests that apatite weathering is still going on, which is supported by the fact that the pH is sufficiently low for apatite to be unstable. The result of acid P-AL (pH 3.75) (Table 2, S1) may also indicate that more P is dissolved at low pH in the apatite-dominated C horizon compared with the B horizon, in which Fe and Al are the major P hosts. In the Kloten soil, however, where the DPS was lowest, apatite had been almost completely dissolved from the pedon (Figs. 2 and 3). These trends demonstrate that the long-term effect of apatite weathering on the P availability in these boreal forest soils is substantial, and indicate that apatite-bound P represents a pool that is potentially available via deep root uptake.

5. Conclusions

- In the studied soils, 94% of the TP resides in the mineral soil from about 20 cm to 80 cm depth as adsorbed P and apatite. Although the mobilization of P from secondary Fe and Al compounds has been questioned, this study suggests that these pools could be P resources on which plants can rely in the long term for P uptake, especially since the P stocks in the surface horizons and topsoils are small.
- The combined use of bulk P K-edge XANES spectroscopy and wet-chemical P extractions revealed that organic P dominated the speciation in the organic horizon, whereas PO_4 bound to Fe and Al (hydr)oxides predominated in the B horizon of the studied soils. Al-bound P was higher than Fe-bound P, which may partly reflect the higher content of Al (hydr)oxides including ITM in the B horizon when compared to Fe (hydr)oxides.
- Apatite has been strongly weathered in the topsoils down to about 30–40 cm although the Swedish forest soils are at an early stage of soil development. As a result of podzolization, P from the topsoils (A/E horizons) has been redistributed to the B horizons, most probably as P adsorbed to ITM.
- The degree of P saturation (DPS) varied among the soils and was positively correlated with the content of Ca-bound P, which suggests that apatite weathering remains a determinant of long-term P availability in these soils.

Declaration of Competing Interest

The authors declare that they have no known competing financial interests or personal relationships that could have appeared to influence the work reported in this paper.

Appendix A. Supplementary data

Supplementary data to this article can be found online at https://doi.org/10.1016/j.geoderma.2021.115500.

References

Adediran, G.A., Tuyishime, J.M., Vantelon, D., Klysubun, W., Gustafsson, J.P., 2020. Phosphorus in 2D: spatially resolved P speciation in two Swedish forest soils as influenced by apatite weathering and podzolization. Geoderma 376, 114550.

Akselsson, C., Westling, O., Alveteg, M., Thelin, G., Fransson, A.-M., Hellsten, S., 2008. The influence of N load and harvest intensity on the risk of P limitation in Swedish forest soils. Sci. Total Environ. 404, 284–289.

Albaugh, T.J., Bergh, J., Lundmark, T., Nilsson, U., Stape, J.L., Allen, H.L., Linder, S., 2009. Do biological expansion factors adequately estimate stand-scale aboveground component biomass for Norway spruce? For. Ecol. Manage. 258, 2628–2637.

Andersson, M., Carlsson, M., Ladenberger, A., Morris, G., Sadeghi, M., Uhlbäck, J., 2014. Geochemical atlas of Sweden (Geokemisk atlas över Sverige). Sveriges geologiska undersökning.

Beauchemin, S., Hesterberg, D., Chou, J., Beauchemin, M., Simard, R.R., Sayers, D.E., 2003. Speciation of phosphorus in phosphorus-enriched agricultural soils using X-ray absorption near-edge structure spectroscopy and chemical fractionation. J. Environ. Qual. 32, 1809–1819.

Bergh, J., Linder, S., Lundmark, T., Elfving, B., 1999. The effect of water and nutrient availability on the productivity of Norway spruce in northern and southern Sweden. For. Ecol. Manage. 119, 51–62.

Blakemore, L., 1987. Soil Bureau Laboratory Methods. A. Methods for chemical analysis of soils. NZ Soil Bureau Sci. Rep. 80, 44–45.

Borggaard, O.K., Szilas, C., Gimsing, A.L., Rasmussen, L.H., 2004. Estimation of soil phosphate adsorption capacity by means of a pedotransfer function. Geoderma 118, 55–61.

Buendia, C., Kleidon, A., Porporato, A., 2010. The role of tectonic uplift, climate, and vegetation in the long-term terrestrial phosphorous cycle. Biogeosciences 7, 2025–2038.

Butler, B.M., Hillier, S., 2021. Automated full-pattern summation of X-ray powder diffraction data for high-throughput quantification of clay-bearing mixtures. Clays Clay Miner. 69, 38–51.

Buurman, P., Jongmans, A., 2005. Podzolisation and soil organic matter dynamics. Geoderma 125, 71–83.

Buurman, P., Van Reeuwijk, L., 1984. Proto-imogolite and the process of podzol formation: a critical note. J. Soil Sci. 35, 447–452.

Cade-Menun, B.J., Berch, S.M., Preston, C.M., Lavkulich, L.M., 2000. Phosphorus forms and related chemistry of Podzolic soils on northern Vancouver Island. I. A comparison of two forest types. Can. J. For. Res. 30, 1714–1725.

Casetou-Gustafson, S., Akselsson, C., Hillier, S., Olsson, B.A., 2019. The importance of mineral determinations to PROFILE base cation weathering release rates: a case study. Biogeosciences 16, 1903–1920.

Casetou-Gustafson, S., Grip, H., Hillier, S., Linder, S., Olsson, B.A., Simonsson, M., Stendahl, J., 2020. Current, steady-state and historical weathering rates of base cations at two forest sites in northern and southern Sweden: a comparison of three methods. Biogeosciences 17, 281–304.

Casetou-Gustafson, S., Hillier, S., Akselsson, C., Simonsson, M., Stendahl, J., Olsson, B.A., 2018. Comparison of measured (XRPD) and modeled (A2M) soil mineralogies: a study of some Swedish forest soils in the context of weathering rate predictions. Geoderma 310, 77–88.

Chadwick, O.A., Derry, L.A., Vitousek, P.M., Huebert, B.J., Hedin, L.O., 1999. Changing sources of nutrients during four million years of ecosystem development. Nature 397, 491–497.

Church, C., Spargo, J., Fishel, S., 2017. Strong acid extraction methods for "total phosphorus" in soils: EPA Method 3050B and EPA Method 3051. Agric. Environ. Lett. 2, 160037.

Colocho Hurtarte, L.C., Souza-filho, L.F., Oliveira Santos, W., Vergütz, L., Prietzel, J., Hesterberg, D., 2019. Optimization of data processing minimizes impact of self-absorption on phosphorus speciation results by P K-edge XANES. Soil Syst. 3, 61.

Egnér, H., Riehm, H., Domingo, W., 1960. Untersuchungen über die chemische Bodenanalyse als Grundlage für die Beurteilung des Nährstoffzustandes der Böden. II. Chemische Extraktionsmethoden zur Phosphor-und Kaliumbestimmung. Kungliga Lantbrukshögskolans Annaler 26, 199–215.

Elser, J.J., Bracken, M.E., Cleland, E.E., Gruner, D.S., Harpole, W.S., Hillebrand, H., Ngai, J.T., Seabloom, E.W., Shurin, J.B., Smith, J.E., 2007. Global analysis of nitrogen and phosphorus limitation of primary producers in freshwater, marine and terrestrial ecosystems. Ecol. Lett. 10, 1135–1142.

Eriksson, A.K., Hesterberg, D., Klysubun, W., Gustafsson, J.P., 2016a. Phosphorus dynamics in Swedish agricultural soils as influenced by fertilization and mineralogical properties: Insights gained from batch experiments and XANES spectroscopy. Sci. Total Environ. 566, 1410–1419.

Eriksson, A.K., Hillier, S., Hesterberg, D., Klysubun, W., Ulén, B., Gustafsson, J.P., 2016b. Evolution of phosphorus speciation with depth in an agricultural soil profile. Geoderma 280, 29–37.

Franke, R., Hormes, J., 1995. The P K-near edge absorption spectra of phosphates. Physica B 216, 85–95.

Giesler, R., Petersson, T., Högberg, P., 2002. Phosphorus limitation in boreal forests: effects of aluminum and iron accumulation in the humus layer. Ecosystems 5, 300–314.

Gustafsson, J., Bhattacharya, P., Bain, D., Fraser, A., Mchardy, W., 1995. Podzolisation mechanisms and the synthesis of imogolite in northern Scandinavia. Geoderma 66, 167–184.

Gustafsson, J.P., Bhattacharya, P., Karltun, E., 1999. Mineralogy of poorly crystalline aluminium phases in the B horizon of Podzols in southern Sweden. Appl. Geochem. 14, 707–718.

Gustafsson, J.P., 2001. Modelling competitive anion adsorption on oxide minerals and an allophane-containing soil. Eur. J. Soil Sci. 52, 639–653.

Gustafsson, J.P., Braun, S., Tuyishime, J., Adediran, G.A., Warrinnier, R., Hesterberg, D., 2020. A probabilistic approach to phosphorus speciation of soils using P K-edge XANES spectroscopy with linear combination fitting. Soil Systems 4, 26.

Gypser, S., Schütze, E., Freese, D., 2021. Single and binary Fe-and Al-hydroxides affect potential phosphorus mobilization and transfer from pools of different availability. Soil Systems 5, 33.

Hesterberg, D., 2019. Response to letter to the editor on synchrotron-based identification of reaction products in phosphorus fertilized alkaline soils. Geofis. Int. 337, 150–151.

Hesterberg, D., 2010. Macroscale chemical properties and X-ray absorption spectroscopy of soil phosphorus. Developments in Soil Science. Elsevier.

Hesterberg, D., Zhou, W., Hutchison, K., Beauchemin, S., Sayers, D., 1999. XAFS study of adsorbed and mineral forms of phosphate. J. Synchrotron Radiat. 6, 636–638.

Heuck, C., Smolka, G., Whalen, E.D., Frey, S., Gundersen, P., Moldan, F., Fernandez, I.J., Spohn, M., 2018. Effects of long-term nitrogen addition on phosphorus cycling in organic soil horizons of temperate forests. Biogeochemistry 141, 167–181.

Hewitt, A.E., Balks, M.R., Lowe, D.J., 2021. Allophanic Soils. The Soils of Aotearoa New Zealand. Springer International Publishing, Cham.

Hillier, S., 1999. Use of an air brush to spray dry samples for X-ray powder diffraction. Clay Miner. 34, 127–135.

Ilg, K., Wellbrock, N., Lux, W., 2009. Phosphorus supply and cycling at long-term forest monitoring sites in Germany. Eur. J. Forest Res. 128, 483–492.

Iso, D., 1998. 13878. Soil quality-Determination of total nitrogen content by dry combustion (" elemental analysis")(ISO 13878: 1998)," vol., no.

IUSS Working Group WRB. 2014. World reference base for soil resources 2014. International soil classification system for naming soils and creating legends for soil maps. World Soil Resources Reports No. 106. FAO, Rome.

Jien, S.-H., Baillie, I., Hu, C.-C., Chen, T.-H., Iizuka, Y., Chiu, C.-Y., 2016. Forms and distribution of phosphorus in a placic podzolic toposequence in a subtropical subalpine forest, Taiwan. Catena 140, 145–154.

Jonard, M., Fürst, A., Verstraeten, A., Thimonier, A., Timmermann, V., Potočić, N., Waldner, P., Benham, S., Hansen, K., Merilä, P., 2015. Tree mineral nutrition is deteriorating in Europe. Glob. Change Biol. 21, 418–430.

Jones, D.L., Oburger, E., 2011. Solubilization of phosphorus by soil microorganisms. Phosphorus in Action. Springer.

Karltun, E., Bain, D.C., Gustafsson, J.P., Mannerkoski, H., Murad, E., Wagner, U., Fraser, A.R., Mchardy, W.J., Starr, M., 2000. Surface reactivity of poorly-ordered minerals in podzol B horizons. Geoderma 94, 265–288.

Kelly, S., Hesterberg, D., Ravel, B., 2008. Analysis of soils and minerals using X-ray absorption spectroscopy. Methods Soil Anal. Part 5 5, 387–463.

Klotzbücher, A., Schunck, F., Klotzbücher, T., Kaiser, K., Glaser, B., Spohn, M., Widdig, M., Mikutta, R., 2020. Goethite-associated phosphorus is not available to beech (Fagus sylvatica L.). Front. Forests Global Change 3, 94.

Klysubun, W., Tarawarakarn, P., Thamsanong, N., Amonpattaratkit, P., Cholsuk, C., Lapboonrueng, S., Chaichuay, S., Wongtepa, W., 2020. Upgrade of SLRI BL8 beamline for XAFS spectroscopy in a photon energy range of 1–13 keV. Radiat. Phys. Chem. 175, 108145.

Lang, F., Bauhus, J., Frossard, E., George, E., Kaiser, K., Kaupenjohann, M., Krüger, J., Matzner, E., Polle, A., Prietzel, J., 2016. Phosphorus in forest ecosystems: new insights from an ecosystem nutrition perspective. J. Plant Nutr. Soil Sci. 179, 129–135.

Lang, F., Krüger, J., Amelung, W., Willbold, S., Frossard, E., Bünemann, E.K., Bauhus, J., Nitschke, R., Kandeler, E., Marhan, S., 2017. Soil phosphorus supply controls P nutrition strategies of beech forest ecosystems in Central Europe. Biogeochemistry 136, 5–29.

Lim, H., Olsson, B.A., Lundmark, T., Dahl, J., Nordin, A., 2020. Effects of whole-tree harvesting at thinning and subsequent compensatory nutrient additions on carbon sequestration and soil acidification in a boreal forest. GCB Bioenergy 12, 992–1001.

Linder, S., 1995. Foliar analysis for detecting and correcting nutrient imbalances in Norway spruce. Ecol. Bull. 178–190.

Lundström, U.V., Van Breemen, N., Bain, D., Van Hees, P., Giesler, R., Gustafsson, J.P., Ilvesniemi, H., Karltun, E., Melkerud, P.-A., Olsson, M., 2000. Advances in understanding the podzolization process resulting from a multidisciplinary study of three coniferous forest soils in the Nordic Countries. Geoderma 94, 335–353.

Mehmood, A., Akhtar, M.S., Imran, M., Rukh, S., 2018. Soil apatite loss rate across different parent materials. Geoderma 310, 218–229.

Mohren, G., Van Den Burg, J., Burger, F., 1986. Phosphorus deficiency induced by nitrogen input in Douglas fir in the Netherlands. Plant Soil 95, 191–200.

Nezat, C.A., Blum, J.D., Yanai, R.D., Hamburg, S.P., 2007. A sequential extraction to determine the distribution of apatite in granitoid soil mineral pools with application to weathering at the Hubbard Brook Experimental Forest, NH, USA. Appl. Geochem. 22, 2406–2421.

Nezat, C.A., Blum, J.D., Yanai, R.D., Park, B.B., 2008. Mineral sources of calcium and phosphorus in soils of the northeastern United States. Soil Sci. Soc. Am. J. 72, 1786–1794.

Nilsson, T., Lundin, L., 2006. Prediction of bulk density in Swedish forest soils from the organic carbon content and soil depth. Rep. For. Ecol. For. Soils 91, 41.

Odum, E.P., 2014. The strategy of ecosystem development. The Ecological Design and Planning Reader. Springer.

Olsen, S.R., 1954. Estimation of available phosphorus in soils by extraction with sodium bicarbonate, US Department of Agriculture.

Omotoso, O., McCarty, D.K., Hillier, S., Kleeberg, R., 2006. Some successful approaches to quantitative mineral analysis as revealed by the 3rd Reynolds Cup contest. Clays Clay Miner. 54, 748–760.

Porder, S., Hilley, G.E., 2011. Linking chronosequences with the rest of the world: predicting soil phosphorus content in denuding landscapes. Biogeochemistry 102, 153–166.

Prietzel, J., Dümig, A., Wu, Y., Zhou, J., Klysubun, W., 2013. Synchrotron-based P K-edge XANES spectroscopy reveals rapid changes of phosphorus speciation in the topsoil of two glacier foreland chronosequences. Geochim. Cosmochim. Acta 108, 154–171.

Prietzel, J., Klysubun, W., Werner, F., 2016. Speciation of phosphorus in temperate zone forest soils as assessed by combined wet-chemical fractionation and XANES spectroscopy. J. Plant Nutr. Soil Sci. 179, 168–185.

Ravel, B., 2009. ATHENA user's guide. Athena IFFEFIT.

Ravel, B., Newville, M., 2005. ATHENA, ARTEMIS, HEPHAESTUS: data analysis for X-ray absorption spectroscopy using IFEFFIT. J. Synchrotron Radiat. 12, 537–541.

Richardson, A.E., Simpson, R.J., 2011. Soil microorganisms mediating phosphorus availability update on microbial phosphorus. Plant Physiol. 156, 989–996.

Rodionov, A., Bauke, S.L., von Sperber, C., Hoeschen, C., Kandeler, E., Kruse, J., Lewandowski, H., Marhan, S., Mueller, C.W., Simon, M., Tamburini, F., Uhlig, D., von Blanckenburg, F., Lang, F., Amelung, W., 2020. Biogeochemical cycling of phosphorus in subsoils of temperate forest ecosystems. Biogeochemistry 150, 313–328.

SanClements, M.D., Fernandez, I.J., Norton, S.A., 2010. Phosphorus in soils of temperate forests: linkages to acidity and aluminum. Soil Sci. Soc. Am. J. 74, 2175–2186.

Selmants, P.C., Hart, S.C., 2010. Phosphorus and soil development: does the Walker and Syers model apply to semiarid ecosystems? Ecology 91, 474–484.

Simonsson, M., Bergholm, J., Lemarchand, D., Hillier, S., 2016. Mineralogy and biogeochemistry of potassium in the Skogaby experimental forest, southwest Sweden: pools, fluxes and K/Rb ratios in soil and biomass. Biogeochemistry 131, 77–102.

Simonsson, M., Bergholm, J., Olsson, B.A., Von Brömssen, C., Öborn, I., 2015. Estimating weathering rates using base cation budgets in a Norway spruce stand on podzolised soil: analysis of fluxes and uncertainties. For. Manage. 340, 135–152.

Smits, M.M., Johansson, L., Wallander, H., 2014. Soil fungi appear to have a retarding rather than a stimulating role on soil apatite weathering. Plant Soil 385, 217–228.

Stendahl, J., Akselsson, C., Melkerud, P.-A., Belyazid, S., 2013. Pedon-scale silicate weathering: comparison of the PROFILE model and the depletion method at 16 forest sites in Sweden. Geoderma 211, 65–74.

Stendahl, J., Lundin, L., Nilsson, T., 2009. The stone and boulder content of Swedish forest soils. Catena 77, 285–291.

Strand, L.T., Callesen, I., Dalsgaard, L., De Wit, H.A., 2016. Carbon and nitrogen stocks in Norwegian forest soils—the importance of soil formation, climate, and vegetation type for organic matter accumulation. Can. J. For. Res. 46, 1459–1473.

Takamoto, A., Hashimoto, Y., Asano, M., Noguchi, K., Wagai, R., 2021. Distribution and chemical species of phosphorus across density fractions in Andisols of contrasting mineralogy. Geoderma 395, 115080.

Talkner, U., Meiwes, K.J., Potočić, N., Seletković, I., Cools, N., De Vos, B., Rautio, P., 2015. Phosphorus nutrition of beech (Fagus sylvatica L.) is decreasing in Europe. Ann. Forest Sci. 72, 919–928.

Tiberg, C., Sjöstedt, C., Eriksson, A.K., Klysubun, W., Gustafsson, J.P., 2020. Phosphate competition with arsenate on poorly crystalline iron and aluminum (hydr) oxide mixtures. Chemosphere 255, 126937.

Tiberg, C., Sjöstedt, C., Gustafsson, J.P., 2018. Metal sorption to Spodosol Bs horizons: Organic matter complexes predominate. Chemosphere 196, 556–565.

Turner, B.L., Condron, L.M., 2013. Pedogenesis, Nutrient Dynamics, and Ecosystem Development: The Legacy of TW Walker and JK Syers. Springer.

Walker, T., Syers, J.K., 1976. The fate of phosphorus during pedogenesis. Geoderma 15, 1–19.

Van Reeuwijk, L. P., 1986. Procedures for soil analysis.

Werner, F., De La Haye, T.R., Spielvogel, S., Prietzel, J., 2017. Small-scale spatial distribution of phosphorus in soils from silicate parent material with different degree of podzolization. Geoderma 302, 52–65.

Werner, F., Prietzel, J., 2015. Standard protocol and quality assessment of soil phosphorus speciation by PK-Edge XANES spectroscopy. Environ. Sci. Technol. 49, 10521–10528.

Vincent, A.G., Vestergren, J., Gröbner, G., Persson, P., Schleucher, J., Giesler, R., 2013. Soil organic phosphorus transformations in a boreal forest chronosequence. Plant Soil 367, 149–162.

Viro, P., 1952. Kivisyyden määrittämisestä. On the determination of stoniness. Commun. Instituti Forestalis Fenniae 40, 23.

Vitousek, P.M., Porder, S., Houlton, B.Z., Chadwick, O.A., 2010. Terrestrial phosphorus limitation: mechanisms, implications, and nitrogen–phosphorus interactions. Ecol. Appl. 20, 5–15.

Wolf, A., Baker, D., 1990. Colorimetric method for phosphorus measurement in ammonium oxalate soil extracts. Commun. Soil Sci. Plant Anal. 21, 2257–2263.

Wood, T., Bormann, F., Voigt, G., 1984. Phosphorus cycling in a northern hardwood forest: biological and chemical control. Science 223, 391–393.

Yanai, R.D., 1998. The effect of whole-tree harvest on phosphorus cycling in a northern hardwood forest. For. Manage. 104, 281–295.

Yu, L., Zanchi, G., Akselsson, C., Wallander, H., Belyazid, S., 2018. Modeling the forest phosphorus nutrition in a southwestern Swedish forest site. Ecol. Model. 369, 88–100.

Yuan, G., Lavkulich, L., 1994. Phosphate sorption in relation to extractable iron and aluminum in Spodosols. Soil Sci. Soc. Am. J. 58, 343–346.

Zetterberg, T., Olsson, B.A., Löfgren, S., Von Brömssen, C., Brandtberg, P.-O., 2013. The effect of harvest intensity on long-term calcium dynamics in soil and soil solution at three coniferous sites in Sweden. For. Ecol. Manage. 302, 280–294.

Zhang, Z., Zhao, Z., Liu, C., Chadwick, O.A., Liang, C., Hu, Y., Vaughan, K., Zhu, M., 2021. Vertical patterns of phosphorus concentration and speciation in three forest soil profiles of contrasting climate. Geochim. Cosmochim. Acta 310, 1–18.

Zhou, J., Bing, H., Wu, Y., Sun, H., Wang, J., 2018. Weathering of primary mineral phosphate in the early stages of ecosystem development in the Hailuogou Glacier foreland chronosequence. Eur. J. Soil Sci. 69, 450–461.

Supplementary materials to:

Phosphorus abundance and speciation in acid forest podzols – effect of postglacial weathering

J.R. Marius Tuyishime, Gbotemi A. Adediran, Bengt A. Olsson, Marie Spohn, Stephen Hillier, Wantana Klysubun, Jon Petter Gustafsson

Supplementary figures
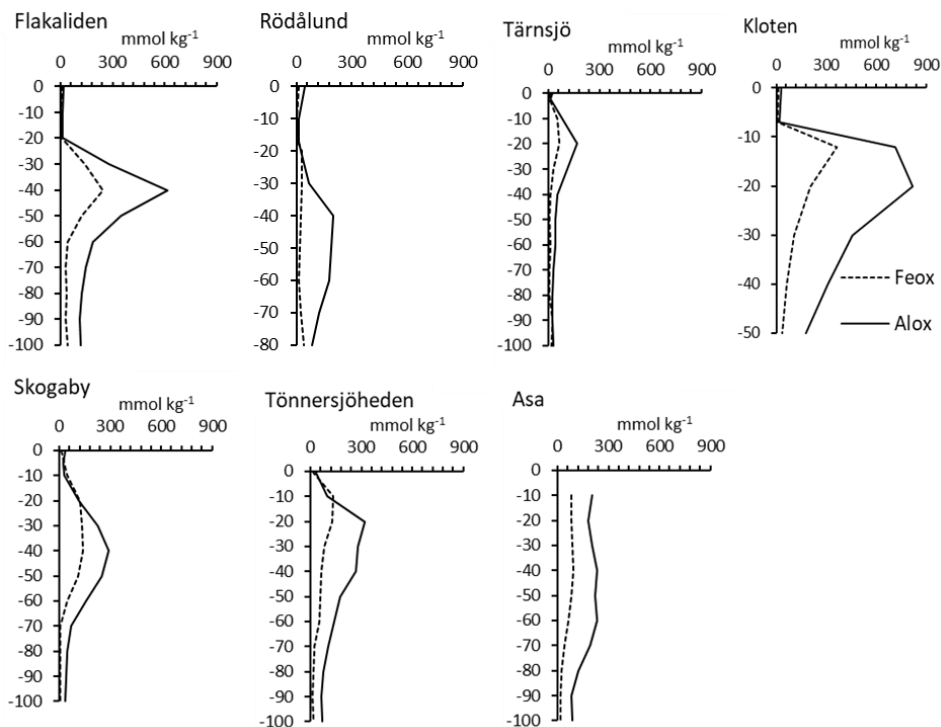
Fig. S1: Distribution of oxalate-extractable Fe (Feox) and Al (Alox) for all seven forest soils
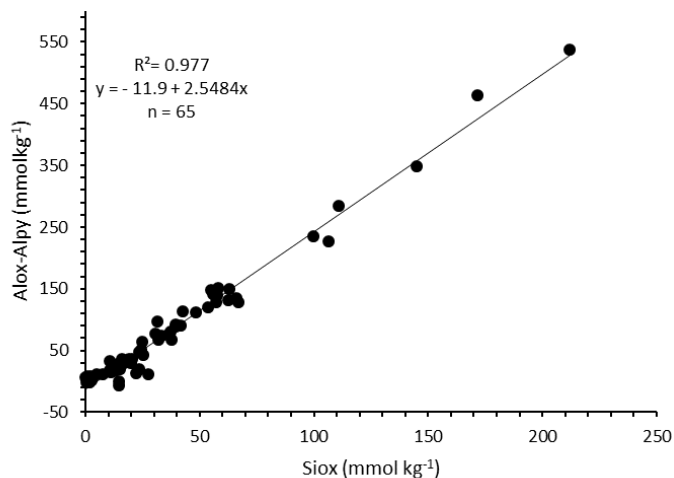
Fig. S2: The relationship between the contents of Si in oxalate extract, and the difference between the contents of oxalate- and pyrophosphate-extractable Al in the mineral soils.
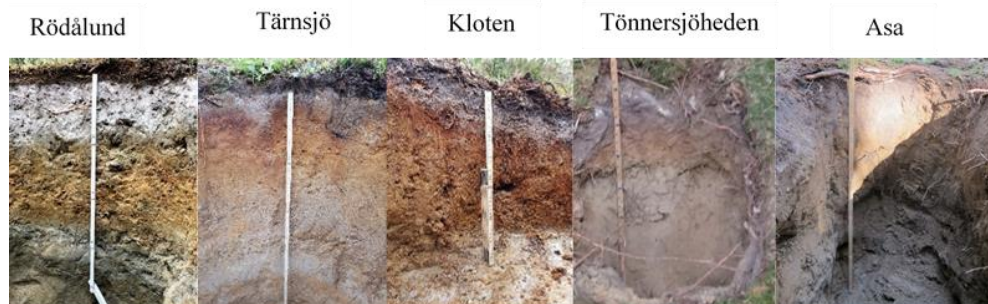
Fig. S3: Pictures of 5 of the soil profiles.

Supplementary tables

Table S1 General soil properties

Horizon	Depth	pH (H₂O)	TP	Al$_{py}$	Fe$_{py}$	Al$_{ox}$	Fe$_{ox}$	Si$_{ox}$	P$_{ox}$	P$_{iox}$	P$_{org\text{-}ox}$	P-AL	P$_{ols}$	DPS	C	N	C:P$_{org}$*	N:P$_{org}$*	BD	Al:Si
	cm		mmol kg^{-1}											%	g kg^{-1}		mol mol^{-1}		kg m^{-3}	
Flakaliden 14B																				
Oe	>0	4.1	18.3	9.9	5.4	18.3	10.8	0.2	9.1	4.2	4.9	6.6	2.9	14	208.0	6.0	1040	26	226.2	35.9
E	0-10	4.3	2.0	2.1	0.7	9.5	2.3	0.2	0.8	0.3	0.5	0.6	0.2	13	11.8	0.5	1272	49	1121.7	43.1
E	10-20	4.6	1.9	6.4	2.3	11.9	3.6	0.2	0.9	0.3	0.6	0.3	0.2	11	3.6	0.2	630	30	1302.3	22.8
B	20-30	4.6	29.7	166.8	60.4	280.1	141.8	42.5	28.9	25.2	3.7	2.6	1.7	14	21.0	0.8	n.c	n.c	1002.9	2.7
	30-40	5.0	26.9	153.9	33.4	618.2	243.0	171.7	23.7	21.0	2.8	0.2	0.4	5	21.1	0.9	n.c	n.c	1002.3	2.7
BC	40-50	5.1	16.5	63.9	6.2	348.2	123.1	111.0	15.2	13.3	1.9	0.1	0.3	6	7.1	0.3	n.c	n.c	1207.7	2.6
	50-60	5.1	17.1	38.1	2.5	188.1	41.0	62.8	14.8	13.0	1.7	0.5	0.5	14	3.9	0.2	n.c	n.c	1292.1	2.4
C	60-70	5.2	17.4	35.7	2.5	147.2	29.6	48.2	13.8	12.6	1.2	1.6	0.5	15	3.2	0.1	n.c	n.c	1314.5	2.3
	70-80	5.3	15.8	34.0	2.5	122.9	32.8	39.4	10.7	9.2	1.5	1.5	0.4	16	2.2	0.1	n.c	n.c	1357.5	2.3
	80-90	5.4	17.4	35.2	2.5	108.8	31.5	33.3	10.9	10.0	0.9	2.3	0.3	17	2.4	0.1	n.c	n.c	1347.2	2.2
	90-100	5.3	16.0	34.3	2.5	114.7	40.9	37.0	10.7	9.7	1.0	1.8	0.3	14	3.0	0.1	n.c	n.c	1322.5	2.2
1470 Rödålund																				
Oe	>0	4.0	19.2	36.4	4.5	48.2	12.6	0.6	5.3	2.7	2.6	4.6	1.8	9.4	434.4	11.3	2213	55	108.1	18.8
E	0-10	4.3	1.7	8.2	1.5	13.4	2.9	0.4	1.1	0.2	0.9	0.4	0.1	5.3	6.7	0.3	485	16	1218.5	11.7
	10-17	4.5	1.1	8.9	2.1	15.8	7.0	1.3	1.0	0.3	0.6	0.2	0.1	1.6	2.4	0.1	291	9	1346.9	5.3
E/B	17-20	4.7	2.2	18.8	10.8	27.0	28.6	2.0	1.6	1.0	0.6	0.1	0.1	3.9	2.6	0.1	292	8	1338.7	4.0
B	20-30	5.1	2.7	45.4	11.2	68.6	28.9	12.6	1.6	1.1	0.5	0.1	0.0	3.2	4.0	0.1	301	9	1287.8	1.8
	30-40	5.6	6.1	73.2	6.8	201.1	27.3	67.1	3.1	2.3	0.8	0.1	0.0	4.1	5.4	0.2	n.c	n.c	1248.8	1.9
BC	40-50	5.4	7.9	54.4	3.9	190.0	20.0	66.2	4.1	3.2	0.6	0.1	0.1	5.7	4.2	0.2	n.c	n.c	1281.9	2.0
	50-60	5.5	10.1	45.2	2.3	177.4	13.9	62.7	6.5	5.5	1.0	0.4	0.1	7.1	3.4	0.1	227	8	1309.7	2.1
C	60-70	5.4	14.2	30.2	3.2	121.6	21.9	39.5	9.1	8.0	1.1	1.3	0.3	15.7	2.1	0.1	n.c	n.c	1358.5	2.3
	70-80	5.4	12.0	32.0	6.8	83.5	39.8	24.4	8.3	7.4	0.9	2.3	0.2	13.0	1.6	0.1	n.c	n.c	1385.7	2.1
Tärnsjö																				
Oe	>0	4.0	18.4	18.8	2.0	25.3	8.9	0.5	4.3	2.6	1.7	4.4	2.2	11	466.6	12.4	2314	53	100.7	13.4
E	0-2	4.3	2.0	4.6	2.5	10.4	4.2	0.4	0.5	0.2	0.4	0.2	0.1	n.c	8.4	0.2	n.c	n.c	1165.0	13.1
B	2-10	4.6	15.0	50.7	21.2	84.2	54.2	10.8	10.7	9.4	1.3	2.1	1.2	21	12.9	0.4	2169	54	1100.2	3.1
	10-20	4.9	20.9	69.0	19.5	166.5	64.2	31.7	19.9	17.0	2.9	1.7	1.0	17	10.8	0.3	1161	31	1138.0	3.1
	20-30	5.2	15.3	48.2	7.4	111.9	29.6	24.7	10.9	10.0	0.9	0.9	0.5	19	3.2	<LOD	n.c	n.c	1316.4	2.6
BC	30-40	5.4	10.7	18.1	1.8	54.5	10.3	16.2	5.0	4.3	0.7	0.4	0.3	22	1.3	<LOD	n.c	n.c	1401.0	2.2
	40-50	5.7	11.8	13.1	0.8	42.0	6.8	16.8	3.8	3.3	0.6	0.4	0.2	24	0.7	<LOD	n.c	n.c	1444.7	1.7
C	50-60	5.9	12.1	11.5	1.3	40.2	9.8	14.3	3.8	3.3	0.6	0.5	0.2	20	0.6	<LOD	n.c	n.c	1457.0	2.0
	60-70	6.1	15.9	9.2	1.1	28.5	7.2	13.2	2.8	2.4	0.4	0.6	0.1	21	0.4	<LOD	n.c	n.c	1470.0	1.5
	70-80	6.2	16.0	8.9	1.8	23.8	6.3	11.1	2.1	1.7	0.4	0.7	0.1	34	0.4	<LOD	n.c	n.c	1470.0	1.3
	80-90	6.0	15.0	8.9	5.2	25.3	25.2	12.1	2.2	1.7	0.5	0.5	0.1	-	0.6	<LOD	n.c	n.c	1442.3	1.3

	90-100	5.8	17.2	10.0	4.1	27.8	18.7	12.5	3.0	2.3	0.7	0.8	0.2	-	0.6	<LOD	n.c	n.c	1454.6	1.4
Kloten																				
Oe	>0	3.9	18.3	23.5	5.7	31.4	14.5	0.7	4.8	2.5	2.3	5.0	2.2	7	438.3	13.4	n.c	58	107.1	10.7
E	0-7	4.1	1.7	13.4	5.2	17.4	5.9	0.5	0.8	0.1	0.7	0.3	0.1	6	22.2	0.7	2214	50	984.6	8.4
B	7-12	4.7	10.0	486.9	230.9	713.6	366.9	106.5	5.8	2.6	3.2	0.5	0.1	1	61.5	2.0	1896	36	721.8	2.1
	12-20	5.0	10.6	283.9	56.6	821.7	203.4	212.0	7.3	3.9	3.3	0.2	0.0	1	38.1	1.6	1271	27	856.2	2.5
	20-30	5.1	8.9	110.6	11.1	459.9	104.7	145.0	6.8	5.0	1.8	0.1	0.1	2	12.5	0.5	779	18	1110.5	2.4
	30-40	5.1	7.4	74.1	5.8	309.3	65.3	99.7	6.0	4.7	1.3	0.1	0.1	3	7.0	0.3	501	12	1210.3	2.4
C	40-50	5.2	7.3	48.4	5.2	176.3	34.7	57.2	5.6	4.4	1.2	0.2	0.1	6	3.7	0.2	n.c	n.c	1298.0	2.2
Skogaby																				
Oe	>0	3.4	20.6	25.9	5.7	33.3	13.9	0.3	7.9	3.6	4.4	6.2	3.8	23	424.3	14.7	2340	69	110.6	26.7
E	0-5	3.5	4.6	23.7	31.7	22.9	31.6	0.3	4.0	1.1	2.9	1.4	0.7	13	42.9	1.8	3250	117	819.0	n.d
E/B	5-10	3.6	3.5	33.3	46.8	31.0	45.9	1.8	2.8	0.9	1.9	0.8	0.5	6	31.2	1.1	2273	70	899.8	n.d
B	10-20	4.1	3.8	102.6	95.3	114.8	121.5	5.0	3.4	0.9	2.5	0.4	0.2	2	27.6	1.1	1877	61	940.2	2.4
	20-30	4.4	4.9	147.6	64.4	225.0	135.1	30.5	4.0	1.6	2.4	0.1	0.1	2	23.2	0.9	1295	43	980.6	2.5
	30-40	4.4	10.1	149.7	50.7	291.5	138.0	55.9	7.4	4.8	2.6	0.1	0.1	4	15.2	0.9	n.c	n.c	1071.6	2.5
	40-50	4.5	8.2	101.3	29.1	252.3	110.0	58.3	8.0	5.3	2.7	0.0	0.1	4	10.2	0.5	782	35	1147.2	2.6
	50-60	4.6	8.9	65.2	13.4	155.4	45.5	41.9	7.2	5.6	1.6	0.1	0.1	8	4.9	0.2	383	15	1261.6	2.2
C	60-70	4.7	10.4	34.2	4.3	69.9	8.6	18.1	5.4	4.4	1.0	0.8	0.2	14	1.9	0.1	n.c	n.c	1370.3	1.9
	70-80	4.7	8.3	27.6	2.5	45.4	4.5	11.5	3.5	2.9	0.6	0.7	0.1	19	1.5	<LOD	n.c	n.c	1392.3	1.5
	80-90	4.7	6.9	24.4	2.8	42.8	4.8	10.6	3.3	2.5	0.8	0.7	0.1	10	1.4	<LOD	n.c	n.c	1396.1	1.7
	90-100	4.7	7.7	20.6	2.4	32.1	3.9	7.7	2.8	2.1	0.7	0.7	-	13	-	<LOD	n.c	n.c		1.5
Tönnersjöheden (T103)																				
Oe	>0	3.7	21.6	19.2	7.2	26.2	13.8	0.6	5.5	2.1	3.3	4.8	2.2	15	448.0	14.7	1951	55	104.8	11.0
A	0-10	4.2	8.3	96.5	121.2	98.7	131.7	2.7	5.6	2.0	3.5	0.8	0.2	5	40.0	1.6	1679	59	847.5	0.9
B	10-20	4.6	14.2	198.1	77.4	318.9	125.4	53.8	11.2	6.7	4.6	0.4	0.2	5	30.3	1.4	774	31	917.3	2.2
	20-30	4.7	17.5	141.6	35.5	280.7	82.9	57.4	13.2	10.0	3.2	0.5	0.2	8	16.6	0.8	508	21	1054.1	2.4
	30-40	4.8	18.0	122.9	27.8	270.3	64.3	55.0	14.1	10.6	3.4	0.7	0.3	8	13.8	0.7	705	30	1091.9	2.7
BC	40-50	4.7	18.0	105.0	33.9	172.4	57.2	32.1	11.6	9.0	2.6	0.7	0.3	12	12.1	0.5	n.c	n.c	1116.3	2.1
	50-60	4.7	16.8	92.9	31.5	139.9	53.8	23.4	10.6	8.1	2.5	0.7	0.2	13	10.0	0.4	n.c	n.c	1151.4	2.0
C	60-70	4.8	12.8	74.9	17.8	104.5	25.0	20.1	7.7	5.6	2.2	0.8	0.1	11	7.9	0.3	n.c	n.c	1192.4	1.5
	70-80	4.8	14.9	56.0	10.5	75.4	14.8	15.1	6.8	5.0	1.8	1.1	0.1	16	5.5	0.2	n.c	n.c	1246.2	1.3
	80-90	5.0	16.0	43.4	7.7	61.4	11.6	13.2	6.3	4.9	1.4	1.2	0.1	16	3.4	0.1	n.c	n.c	1310.1	1.4
	90-100	4.8	12.5	51.6	12.6	72.2	18.7	13.7	6.6	5.0	1.6	0.9	0.1	12	4.7	0.2	n.c	n.c	1268.9	1.5

Asa

A	0-10	4.5	11.8	191.5	74.7	205.1	82.2	22.3	7.6	3.3	4.3	0.9	0.3	4	53.6	2.5	2228	40	770.0	0.6
B	10-20	4.4	12.6	190.1	78.3	183.0	80.2	14.5	8.0	2.8	5.2	1.3	0.3	5	60.9	2.8	875	16	735.1	0.0
BC	20-30	4.5	10.9	203.3	82.6	203.3	90.1	14.5	7.8	2.9	4.9	1.0	0.3	4	48.0	2.2	1225	22	799.7	0.0
	30-40	4.5	11.1	211.4	76.6	211.4	91.0	23.6	7.6	3.2	4.4	0.7	0.1	6	42.7	1.7	1181	18	830.6	0.8
	40-50	4.5	10.9	209.5	74.1	209.5	82.3	27.6	7.8	3.9	4.0	0.6	0.2	4	30.1	1.3	1211	20	919.3	0.4
C	50-60	4.5	12.9	162.8	48.2	162.8	66.0	37.7	9.2	5.5	3.7	0.6	0.1	5	20.4	0.9	1	n.c	1009.7	1.8
	60-70	4.6	13.1	116.1	25.7	116.1	40.6	36.5	8.8	6.5	2.4	0.9	0.1	7	12.2	0.5	n.c	n.c	1115.5	2.1
	70-80	4.6	15.0	80.8	15.2	80.8	23.8	25.4	8.8	7.1	1.8	1.7	0.1	10	6.9	0.3	n.c	n.c	1213.6	1.7
	80-90	4.7	17.3	51.1	8.6	51.1	16.2	18.8	9.3	8.2	1.1	2.7	0.1	18	3.6	0.1	n.c	n.c	1301.5	1.7
	90-100	4.8	18.1	49.1	9.3	49.1	18.0	20.6	9.7	8.7	0.9	2.8	0.2	12	3.3	0.1	n.c	n.c	1311.5	1.7

P_{org}*: organic P as evidenced by XANES ($P_{org-krf}$). Al:Si calculated as (Al_{ox} - Al_{py})/Si_{ox}, BD: bulk density, n.c: not calculated because P_{org}* or Fe-, Al-bound P were not detectable by XANES. <LOD: below the limit of detection.

Table S2: Relative phosphorus speciation (%) in the soil samples from Flakaliden as evidenced by LCF. Standard deviations are shown within parenthesis. For each species group included in the fit, the standard with the highest average weight is shown. The P groups are listed in the materials and method section. The R-factor is the goodness-of-fit parameter reported by Athena.

Flakaliden 14B

Horizon/depth	$P_{org\text{-}lcf}$	Fe-bound P		Al-bound P		Ca-P	R factor
(cm)		$FePO_4$	PO_4-ads Fe	$AlPO_4$	PO_4-ads Al		
Oe	90.8 (3.5)		2.9 (3.2)	6.2 (3.3)			0.0006
	$P_{org\text{-}lcf}$		PO_4-Goeth	PO_4-allo			
E 0-10	38.9 (4.8)	29.8 (3.1)		7.4 (2.9)		24.0 (2.7)	0.0046
	$P_{org\text{-}lcf}$	$FePO_4$		PO_4-allo		Hydroxyapatite	
E 10-20	25.1 (6.0)		15.3 (5.0)	30.4 (5.1)		29.2 (2.7)	0.0046
	$P_{org\text{-}lcf}$		PO_4-Goeth	$AlPO_4$		Hydroxyapatite	
B 20-30			16.9 (8.5)	83.1 (8.5)			0.0013
			PO_4-Goeth	PO_4-allo			
B 30-40			32.5 (5.5)		49.6 (5.6)	18.0 (1.9)	0.0007
			PO_4-Goeth		PO_4-allo	Hydroxyapatite	
BC 40-50			16.6 (9.2)		68.1 (8.3)	15.2 (2.0)	0.0009
			PO_4-Ferri		PO_4-allo	Apatite Taiba	
C 50-60		12.2 (9.2)			80.6 (8.5)	7.2 (2.0)	0.0008
		PO_4-Ferri			PO_4-allo	Hydroxyapatite	
C 60-70		34.9 (11.4)			42.6 (12.2)	22.5 (2.7)	0.0011
		PO_4-Ferri			PO_4-allo	Apatite Taiba	
C 70-80		26.6 (8.2)			51.5 (8.7)	21.9 (2.2)	0.0012
		PO_4-Ferri			PO_4-allo	Apatite Taiba	
C 80-90		24.0 (5.3)			43.6 (5.8)	32.4 (3.0)	0.0012
		$FePO_4$			PO_4-allo	Apatite Taiba	
C 90-100		26.0 (6.6)			41.1 (7.0)	32.9 (2.1)	0.0008
		PO_4-Goeth			PO_4-allo	Apatite Taiba	

PO_4-Ferri: PO_4-adsorbed to ferrihydrite, PO_4-Goeth: PO_4 adsorbed to goethite, PO_4-Allo: PO_4 adsorbed to allophane. Ca-P: Ca-bound P, $P_{org\text{-}lcf}$: soil organic P as determined by XANES. Al-bound P, Al-bound Fe (second row) represent cases when the probabilistic LCF could not distinguish the PO_4 adsorbed to Al from $AlPO_4$, and the PO_4 adsorbed to Fe from $FePO_4$, respectively.

1470 Rödålund

Horizon/depth	$P_{org-lcf}$	Fe-bound P		Al-bound P		Ca-P	R factor
(cm)		$FePO_4$	PO_4-ads Fe	$AlPO_4$	PO_4-ads Al		
Oe	85.1 (3.8)	4.3 (3.1)		10.6 (2.6)			0.0005
	$P_{org-lcf}$	$FePO_4$		PO_4-allo			
E 0-10	68.9 (4.8)			25.2 (3.0)		5.9 (2.0)	0.0097
	$P_{org-lcf}$			$AlPO_4$		Hydroxyapatite	
E 10-17	60.1 (6.0)			17.1 (3.0)		22.8 (3.6)	0.0087
	$P_{org-lcf}$			$AlPO_4$		Hydroxyapatite	
E/B 17-20	34.2 (5.7)			49.1 (3.4)		16.6 (3.0)	0.0036
	$P_{org-lcf}$			$AlPO_4$		Hydroxyapatite	
B 20-30	41.5 (3.7)		19.2 (4.6)	35.1 (6.2)	4.2 (1.5)		0.0025
	$P_{org-lcf}$		PO_4-Goeth	$AlPO_4$	PO_4-Gib		
BC 30-40				76.0 (4.5)		24.0 (4.5)	0.0021
				$AlPO_4$		Hydroxyapatite	
BC 40-50				75.8 (4.6)		24.2 (4.6)	0.0010
				PO_4-allo		Hydroxyapatite	
C 50-60	12.3 (5.8)		15.9 (6.4)		51.8 (5.6)	20.0 (2.8)	0.0008
	$P_{org-lcf}$		$FePO_4$		PO4-allo	Apatite Taiba	
C 60-70			17.3 (5.6)	62.0 (7.1)		20.6 (5.2)	0.0011
			PO_4-Ferri	PO_4-allo		Apatite Taiba	
C 70-80			36.3 (6.4)	30.5 (6.1)		33.2 (3.1)	0.0017
			PO_4-Ferri	$AlPO_4$		Apatite Taiba	

PO_4-Ferri: PO_4-adsorbed to ferrihydrite, PO_4-Goeth: PO_4 adsorbed to goethite, PO_4-Allo: PO_4 adsorbed to allophane. Ca-P: Ca-bound P, $P_{org-lcf}$: soil organic P as determined by XANES. Al-bound P, Al-bound Fe (second row) represent cases when the probabilistic LCF could not distinguish between PO_4 adsorbed to Al from $AlPO_4$, and between PO_4 adsorbed to Fe and $FePO_4$, respectively.

Table S4: Relative phosphorus speciation (%) in the soil samples from Tärnsjö as evidenced by LCF. Standard deviations are shown within parenthesis. For each species group included in the fit, the standard with the highest average weight is shown. The P groups are listed in the materials and method section. The R-factor is the goodness-of-fit parameter reported by Athena.

Tärnsjö

Horizon/depth (cm)	$P_{org\text{-}lcf}$	Fe-bound P		Al-bound P		Ca-P	R factor
		$FePO_4$	PO_4-ads Fe	$AlPO_4$	PO_4-ads Al		
Oe	91.4 (2.4) $P_{org\text{-}lcf}$		6.4 (3.4) PO_4-Goeth*			2.2 (2.2) Brushite	0.0012
E 0-2				n.d			
B 2-10	3.3 (3.6) $P_{org\text{-}lcf}$	13.8 (4.7) $FePO_4$		82.9 (6.1) PO_4-allo			0.0022
B 10-20	3.7 (4.2)		19.9 (6.4) PO_4-Goeth	76.4 (8.5) PO_4-allo			0.0012
B 20-30				90.0 (4.4) PO_4-allo		10.0 (4.4) Hydroxyapatite	0.0012
BC 30-40		8.7 (4.8) $FePO_4$		10.8 (7.3) $AlPO_4$	48.3 (3.3) PO_4-allo	32.1 (3.7) Apatite Templeton	0.0021
C 40-50		17.2 (3.7) $FePO_4$			32.0 (1.6) PO_4-allo	50.8 (3.0) Apatite Templeton	0.0023
C 50-60				41.8 (2.9) PO_4-allo		58.2 (2.9) Apatite Templeton	0.0018
C 60-70				24.0 (1.8) $AlPO_4$		76.0 (1.8) Apatite Templeton	0.0027
C 70-80		3.9 (4.1) $FePO_4$		28.2 (2.1) Variscite		67.9 (2.9) Apatite Templeton	0.0069

PO_4-Goeth: PO_4 adsorbed to goethite, PO_4-Allo: PO_4 adsorbed to allophane. Ca-P: Ca-bound P, $P_{org\text{-}lcf}$: soil organic P. n.d: not detected by XANES. Al-bound P, Al-bound Fe (second row) represent cases when the probabilistic LCF could not separate the PO_4 adsorbed to Al from $AlPO_4$, and the PO_4 adsorbed to Fe from $FePO_4$, respectively. * is the most probable P species when the probabilistic LCF could not separate all P bound to Al and Fe.

Table S5: Relative phosphorus speciation (%) in the soil samples from Kloten as evidenced by LCF. Standard deviations are shown within parenthesis. For each species group included in the fit, the standard with the highest average weight is shown. The P groups are listed in the materials and method section. The R-factor is the goodness-of-fit parameter reported by Athena.

Kloten

Horizon/depth (cm)	$P_{org-lcf}$	Fe-bound P		Al-bound P		Ca-P	R factor
		$FePO_4$	PO_4-ads Fe	$AlPO_4$	PO_4-ads Al		
Oe	90.2(3.5)		8.1 (3.8)			1.7 (3)	0.0012
	$P_{org-lcf}$		Strengite			Brushite	
E 0-7	56.6 (3.2)	16.9 (2.7)		10.7 (3.3)	16.1 (3.0)		0.009
	$P_{org-lcf}$	Strengite		Varscite	PO_4-allo		
B 7-12	40.4 (4.7)			15.9 (6.7)	43.6 (3.0)		0.001
	$P_{org-lcf}$			AlPO4	PO_4-Gib		
B 12-20	38.4 (4.5)			21.3 (5.9)	40.2 (2.5)		0.002
	$P_{org-lcf}$			AlPO4	PO_4-Gib		
B 20-30	23.4 (4.1)				76.6 (4.1)		0.002
	$P_{org-lcf}$				PO_4-allo		
B 30-40	24.9 (3.0)		19 (4.6)		56 (3.7)		0.001
	$P_{org-lcf}$		PO_4-Ferri		PO_4-allo		
BC 40-50				24 (9.5)	63.1 (4.3)	12.8 (5.5)	0.002
				AlPO4	PO_4-allo	OCP	

OCP: octacalcium phosphate, PO_4-Ferri: PO_4-adsorbed to ferrihydrite, PO_4-Allo: PO_4 adsorbed to allophane, PO_4-Gib: PO_4 adsorbed to gibbsite, Ca-P: Ca-bound P, $P_{org-lcf}$: soil organic P as determined by XANES. Al-bound P, Al-bound Fe (second row) represent cases when the probabilistic LCF could not differentiate between PO_4 adsorbed to Al and $AlPO_4$, and between PO_4 adsorbed to Fe and $FePO_4$, respectively.

9

Table S6: Relative phosphorus speciation (%) in the soil samples from Skogaby as evidenced by LCF. Standard deviations are shown within parenthesis. For each species group included in the fit, the standard with the highest average weight is shown. The P groups are listed in the materials and method section. The R-factor is the goodness-of-fit parameter reported by Athena.

Skogaby

| Horizon/depth | $P_{org-lcf}$ | Fe-bound P | | Al-bound P | | Ca-P | R factor |
(cm)		$FePO_4$	PO_4-ads Fe	$AlPO_4$	PO_4-ads Al		
Oe	73.4 (3.5)	17.8 (4.0)			8.8 (5.0)		0.0010
	$P_{org-lcf}$	$FePO_4$			PO_4-allo		
E 0-5	23.8 (3.9)		7.9 (6.9)	68.3 (8.3)			0.0072
	$P_{org-lcf}$		PO_4-Goeth	$AlPO_4$			
EB 5-10	32.5 (4.1)			67.5 (4.1)			0.0046
	$P_{org-lcf}$			$AlPO_4$			
B 10-20	32.1 (4.5)		33.8 (9.8)	12.4 (7.6)	21.6 (5.6)		0.0021
	$P_{org-lcf}$		PO_4-Goeth	$AlPO_4$	PO_4-allo		
B 20-30	30.6 (3.3)	22.0 (7.6)			47.4 (7.5)		0.0017
	$P_{org-lcf}$	PO_4-Goeth			PO_4-allo		
B 30-40		38.1 (8.9)		49.7 (11.5)		12.2 (4.9)	0.0026
		PO_4-Goeth		PO_4-allo		Hydroxyapatite	
BC 40-50	13.3 (3.8)		23.8 (5.1)		62.8 (3.2)		0.0013
	$P_{org-lcf}$		PO_4-Goeth		PO_4-allo		
C 50-60	12.0 (4.6)				88.0 (4.6)		0.0009
	$P_{org-lcf}$				PO_4-allo		
C 60-70		18.1 (4.5)			34.2 (2.5)	47.6 (3.3)	
		$FePO_4$			PO_4-allo	Apatite Taiba	0.0016
C 70-80		8.8 (6.5)		47.6 (5.3)		43.6 (3.6)	
		$FePO_4$		$AlPO_4$		Apatite Taiba	0.0018
C 80-90		11.5 (4.8)			24.7 (1.8)	63.7 (4.0)	
		$FePO_4$			PO_4-Gib	Apatite Taiba	0.0029
C 90-100		7.8 (4.9)			22.8 (1.5)	69.4 (4.8)	
		$FePO_4$			PO_4-Gib	Apatite Taiba	0.0034

PO_4-Gib: PO_4 adsorbed to gibbsite, PO_4-Goeth: PO_4 adsorbed to goethite, PO_4-Allo: PO_4 adsorbed to allophane, Ca-P: Ca-bound P, $P_{org-lcf}$: soil organic P as determined by XANES. Al-bound P, Al-bound Fe (second row) represent cases when the probabilistic LCF could not separate the PO_4 adsorbed to Al and $AlPO_4$, and the PO_4 adsorbed to Fe and $FePO_4$, respectively.

Table S7: Relative phosphorus speciation (%) in the soil samples from Tönnersjöheden T103 as evidenced by LCF. Standard deviations are shown within parenthesis. For each species group included in the fit, the standard with the highest average weight is shown. The P groups are listed in the materials and method section. The R-factor is the goodness-of-fit parameter reported by Athena.

Tönnersjöheden (T103:1)

Horizon/depth	$P_{org\text{-}lcf}$	Fe-bound P		Al-bound P		Ca-P	R factor
(cm)		$FePO_4$	PO_4-ads Fe	$AlPO_4$	PO_4-ads Al		
Oe	88.4 (4.6)	5.2 (3.0)		6.5 (3.1)			0.0004
	$P_{org\text{-}lcf}$	$FePO_4$		$P\text{-}Al(OH)_3$			
A 0-10	24.0 (4.8)		43.0 (6.0)	15.4 (6.8)	17.6 (3.2)		0.0025
	$P_{org\text{-}lcf}$		PO_4-Goeth	$AlPO_4$	PO_4-allo		
B 10-20	22.9 (3.2)		27.8 (7.8)		49.3 (7.7)		0.0008
	$P_{org\text{-}lcf}$		PO_4-Goeth		PO_4-allo		
B 20-30	15.5 (4.8)	19.5 (7.6)			58.6 (8.2)	6.4 (5.0)	0.0007
	$P_{org\text{-}lcf}$	$FePO_4$			PO_4-allo	OCP	
B 30-40	9.0 (6.7)		22.5 (8.9)		53.7 (8.5)	14.8 (3.8)	0.0008
	$P_{org\text{-}lcf}$		PO_4-Goeth		PO_4-allo	OCP	
BC 40-50			21.2 (7.0)	52.6 (7.7)		26.2 (5.6)	0.0008
			PO_4-Goeth	PO_4-Gib		Apatite Taiba	
BC 50-60			33.4 (4.5)	22.9 (10.5)	18.2 (5.0)	25.4 (4.7)	0.0014
			PO_4-Goeth	$AlPO_4$	PO_4-Gib	Apatite Taiba	
C 60-70		15.9 (5.4)			38.3 (2.1)	45.8 (4.0)	0.0015
		$FePO_4$			PO_4-allo	Apatite Taiba	
C 70-80		13.1 (5.5)	17.0 (2.9)	17.0 (6.0)		52.9 (3.4)	0.0017
		$FePO_4$	PO_4-Goeth	$AlPO_4$		Apatite Taiba	
C 80-90				31.2 (3.7)	5.6 (1.8)	63.2 (2.6)	0.0057
				$AlPO_4$	PO_4-allo	Apatite Taiba	
C 90-100			22.6 (3.0)	21.0 (4.9)		56.4 (3.0)	0.0014
			PO_4-Goeth	$AlPO_4$		Apatite Taiba	

PO_4-Gib: PO_4 adsorbed to gibbsite, PO_4-Goeth: PO_4 adsorbed to goethite, PO_4-Allo: PO_4 adsorbed to allophane, Ca-P: Ca-bound P, OCP: Octacalcium phosphate, $P_{org\text{-}lcf}$: soil organic P as determined by XANES. Al-bound P, Al-bound Fe (second row) represent cases when the probabilistic LCF could not distinguish the PO_4 adsorbed to Al from $AlPO_4$, and the PO_4 adsorbed to Fe from $FePO_4$, respectively.

Table S8: Relative phosphorus speciation (%) in the soil samples from Asa as evidenced by LCF. Standard deviations are shown within parenthesis. For each species group included in the fit, the standard with the highest average weight is shown. The P groups are listed in the materials and method section. The R-factor is the goodness-of-fit parameter reported by Athena.

Asa

Horizon/depth (cm)	$P_{org\text{-}lcf}$	Fe-bound P FePO$_4$	PO$_4$-ads Fe	Al-bound P AlPO$_4$	PO$_4$-ads Al	Ca-P	R factor
A 0-10	16.8 (7.1)		38.9(5.3)	15.6(5.3)		28.6(6.2)	0.0007
	$P_{org\text{-}lcf}$		PO$_4$-Ferri	AlPO$_4$		OCP	
B 10-20	46 (4.1)	8.8 (6.8)		18.3 (8.2)	25.3 (6.7)		0.0008
	$P_{org\text{-}lcf}$	PO$_4$-Goeth		AlPO$_4$	PO$_4$-Gib		
BC 20-30	29.8 (5.0)	19.1 (4.0)			39.2 (3.2)	11.8 (2.4)	0.0008
	$P_{org\text{-}lcf}$	FePO$_4$			PO$_4$-llo	OCP	
C 30-40	27.1 (4.8)	17.5 (3.7)			41.5 (3.3)	27.1 (4.8)	0.0008
	$P_{org\text{-}lcf}$	FePO$_4$			PO$_4$-allo	Hydroxyapatite	
C 40-50	18.9 (4.7)	17.1 ((4.1)			45 (3.0)	18.9 (2.1)	0.0009
	$P_{org\text{-}lcf}$	FePO$_4$			PO$_4$-allo	Hydroxyapatite	
C 50-60	17 (4.1)	13.1 (4.1)			44.9 (3.2)	24.8 (1.7)	0.001
	$P_{org\text{-}lcf}$	Strengite			PO$_4$-allo	Apatite Taiba	
C 60-70				17.7 (8.5)	40.1 (4.8)	42.1 (4.1)	0.002
				AlPO$_4$	PO$_4$-allo	Hydroxyapatite	
C 70-80		25.03 (4.46)			25.5 (1.7)	49.4 (3.2)	0.002
		FePO$_4$			PO$_4$-allo	Apatite Taiba	
C 80-90		25.2 (3.1)			14.3 (1.1)	60.4 (3.1)	0.002
		FePO$_4$			PO$_4$-allo	Apatite Taiba	
C 90-100		17 (4.3)		7.3 (3.2)	9.6 (1.4)	66.1 (3.1)	0.002
		FePO$_4$		AlPO$_4$	PO$_4$-Gib	Apatite Taiba	

PO$_4$-Gib: PO$_4$ adsorbed to gibbsite, PO$_4$-Goeth: PO$_4$ adsorbed to goethite, PO$_4$-Allo: PO$_4$ adsorbed to allophane, Ca-P: Ca-bound P, OCP: Octacalcium phosphate, $P_{org\text{-}lcf}$: soil organic P as determined by XANES. Al-bound P, Al-bound Fe (second row) represent cases when the probabilistic LCF could not differentiate between PO$_4$ adsorbed to Al and AlPO$_4$, and between PO$_4$ adsorbed to Fe and FePO$_4$, respectively.

Table S9: XRPD Mineralogical composition (weight %) of the fine-earth (<2mm) fraction of soils from seven forest soils. Di: dioctahedral ; Tri: trioctahedral, Exp: Expandable, amor-Fe, Al, and O are amorphous Fe, Al phases and organic matter. nd = not detected.

Depth	Quartz	Plagioclase	K-feldspar	Amphibole	Epidote	Garnet	Ilmenite	Magnetite	Hematite	Goethite	Rutile	Anatase	Apatite	Gibbsite	Mica (Tri)	Mica/illite (Di)	Chlorite (Tri)	Exp (Tri)	Amor -Fe	Amor -Al	Amor -O
Flakaliden 14B																					
0-10	52.4	22	15.5	1.8	0.7	0.3	0.5	nd	0	nd	0.2	0.1	nd	nd	nd	2.6	0	0.8	nd	0	3
10-20	49.8	22.5	16.9	2.3	1.1	0.5	0.4	nd	0.1	nd	0.2	0.1	0	nd	0.1	3.4	0	1.2	nd	0	1.3
20-30	43.9	21.9	14	3.2	1.3	0.8	0.5	0.2	0.2	nd	0.3	0	0.1	nd	0.1	4.2	0.4	1.4	0.1	3.3	4.1
30-40	38	22.7	12.8	4.1	1.3	1.2	0.3	0.1	0.1	0.3	0.3	nd	0.1	nd	0.3	3.4	1.3	1	1.8	7.7	3.2
40-50	39.2	25.7	13.5	4.2	1.6	1.4	0.4	nd	0.2	nd	0.3	0.1	nd	nd	0.5	3.4	1.5	1.4	1	4.8	0.8
50-60	39.2	27.1	13.9	4.6	1.8	1.3	0.4	nd	0.2	nd	0.3	nd	0.1	nd	0.7	3.8	1.6	1.4	0.1	3.6	nd
60-70	40.1	25.9	13.8	5	1.9	1.5	0.5	nd	0.2	nd	0.3	0	0.2	nd	0.5	3.7	1.7	1.7	nd	2.9	nd
70-80	39.4	26.8	15.4	4.1	1.4	1.2	0.4	0	0.2	nd	0.2	nd	0.1	nd	1.2	3.5	1.7	1.5	nd	2.8	nd
80-90	39.7	27	15.1	4	1.3	1.1	0.3	0.1	0.1	nd	0.2	nd	0.2	nd	1.9	3.5	1.6	1.2	0.1	2.8	nd
90-100	39.8	26.8	14.4	3.8	1.3	1.2	0.4	0.1	0.1	0.6	0.2	nd	0.2	nd	2	3.7	1.5	1.5	0	2.4	nd
Rödålund 1470																					
0-10	50.1	20.6	22.1	0.8	0.6	0.8	0.3	0.1	0.1	nd	0.2	nd	nd	0	nd	3	0.1	0.9	nd	0.5	nd
10-17	46.7	23.4	21.1	1.2	0.6	0.8	0.2	0.2	0.1	nd	0.2	nd	nd	nd	0	3	0.2	1.5	0.1	0.8	nd
17-20	46.5	23.1	20.1	1.5	0.8	1.1	0.2	0.1	0.1	nd	0.2	0	nd	nd	0.1	3.3	0.9	1.2	0.3	0.5	nd
20-30	46.1	23.8	18.7	1.8	1	1.3	0.2	0.2	0.1	nd	0.2	nd	nd	nd	0.1	3.2	0.9	1.1	0	1	0.1
30-40	43.2	24.9	19.7	1.6	0.8	1.3	0.2	0	0.1	nd	0.2	nd	0.1	nd	0.5	3.2	1.2	0.9	0.2	1.8	nd
40-50	43.2	26.3	18.3	1.6	0.8	1.4	0.2	nd	0.1	nd	0.2	nd	0.1	nd	0.6	3.4	1.3	0.7	0.5	1.2	nd
50-60	41.6	26.2	18.9	1.9	1	1.5	0.2	nd	0.1	nd	0.2	nd	0.1	nd	0.3	3.6	1.7	1	nd	1.7	nd
60-70	41.5	25.7	15.9	3	1.3	1.3	0.3	nd	0.2	nd	0.2	nd	0.1	nd	0.3	5.4	1.9	1.4	0.3	1.2	nd
70-80	40.7	25.3	15.3	3	1.2	1.2	0.3	nd	0.2	nd	0.3	nd	0.2	nd	0.6	6.3	2.4	1.5	0.4	1.2	nd
Tärnsjö																					
0-2	46.5	24.9	21.4	1.1	0.7	0.5	0.2	0.2	0.2	nd	0.1	nd	nd	0	nd	2.8	0.1	0.5	nd	0	0.7
2-10	39.9	27.6	21.8	1.3	0.7	0.6	0.2	0.3	0.3	nd	0.2	nd	0.1	nd	nd	3.5	0.8	0.3	nd	1.3	1.2
10-20	40.3	26.9	20	1.7	1.1	0.8	0.2	0.5	0.4	0.5	0.2	nd	nd	0.1	nd	3.7	0.9	0.4	nd	2	0.3

13

	1	2	3	4	5	6	7	8	9	10	11	12	13	14	15	16	17	18	19	20	21
20-30	41	27.3	18.8	2	1.2	0.9	0.3	0.7	0.6	0.2	0.3	nd	nd	nd	nd	3.5	1.8	0.7	nd	0.8	nd
30-40	39.7	29.9	20.3	1.2	0.8	0.6	0.1	0.1	0.2	0.3	0.2	nd	0.1	nd	0.1	3.9	2.1	0.4	nd	0	nd
40-50	39.3	29.6	20.1	1.5	1.1	0.5	0.2	nd	0.1	nd	0.3	nd	0.1	nd	0.1	3.8	2.4	0.3	0.6	0	nd
50-60	40.3	28.4	19.7	1.6	1.1	0.6	0.1	0.3	0.3	0.4	0.2	nd	0.1	nd	0.2	3.6	2.4	0.6	0.1	0	nd
60-70	41.2	26.5	17.7	2.6	1.2	0.8	0.2	1.1	0.5	nd	0.2	nd	0.2	nd	0.5	3.1	2.7	0.6	nd	0.7	nd
70-80	42.9	26.6	17.8	2.4	1.2	0.8	0.2	0.5	0.3	0.2	0.2	0	0.2	nd	0.3	3.6	2.2	0.6	nd	0	nd
80-90	42.4	26.9	18.6	2.2	1	0.6	0.2	0.2	0.2	nd	0.2	0	0.2	nd	0.2	3.4	2.2	0.4	0.7	0.3	nd
90-100	42.2	26.6	18.1	2.5	1.1	0.8	0.2	0.6	0.4	nd	0.2	0	0.3	nd	0.2	3.7	2.2	0.5	0.4	0	nd
Kloten																					
0-7	55.9	17.2	18.3	0.7	0.6	0.2	0.2	0.1	0.2	nd	0.1	0	nd	nd	nd	2	0.1	0.5	nd	0.1	3.8
7-12	43.6	16.4	15.4	1.1	0.7	0.3	0	0.3	0.1	0.6	0.2	nd	nd	nd	0	0.9	0.5	0	3.2	9.2	7.5
12-20	44.8	18.2	16.6	1.3	0.8	0.5	0	0.4	0.1	0.1	0.1	nd	nd	nd	0.1	1.3	0.8	0.1	1.3	11.1	2.4
20-30	47.1	21.1	18.2	1.6	1.1	0.2	0.1	0.3	0.2	nd	0.2	nd	nd	nd	0.1	1.9	1	0.2	0.8	5.6	0.1
30-40	48.1	21.8	18.9	1.5	1.2	0.3	0.2	0.2	0.2	nd	0.2	nd	nd	nd	0	2.2	1.1	0.3	0.4	3.3	nd
40-50	52.1	20.7	18	1.7	1.4	0.3	0.2	0.2	0.2	nd	0.1	nd	nd	nd	0	1.8	1	0.4	0.3	1.5	nd
Skogaby C24																					
0-5	43.7	22.2	17.4	1.1	0.8	0.5	0.3	0.3	0.6	0.2	0.2	0	nd	nd	nd	1.3	0.1	0.2	nd	4.7	6.4
5-10	47.4	21.9	17.4	1.2	0.8	0.5	0.4	0.5	0.6	0.3	0.2	0	nd	nd	nd	1.4	nd	0	nd	4.5	2.7
10-20	46.3	21.5	17.1	1.3	1	0.7	0.4	0.5	0.6	1	0.2	0.1	nd	0	nd	1.3	0.1	0	0.5	5	2.3
20-30	44.7	22.4	17.2	1.5	1	0.6	0.4	0.5	0.6	0.6	0.3	nd	nd	0.1	nd	1.6	0	0.2	0.8	6.7	0.9
30-40	39.6	23.1	17.2	2.7	1.7	0.8	0.3	0.1	0.4	1.6	0.2	0.1	nd	nd	nd	2.8	0.3	0.3	0.9	8	nd
40-50	45.3	23.1	18	1.9	1.1	0.7	0.3	0.5	0.6	0.7	0.2	0.1	nd	0.1	nd	1.9	0.1	0.2	0.6	4.7	nd
50-60	47.5	24.8	17.8	1.8	1	0.7	0.3	0.3	0.5	0.2	0.2	nd	0	nd	0.1	1.2	0.1	0	0.4	3	nd
60-70	48.8	25	18.6	1.7	0.6	0.6	0.2	0.3	0.4	nd	0.2	nd	0.1	nd	0.3	0.8	0.1	0	1	1.6	nd
70-80	48.7	24.8	18	1.7	0.5	0.8	0.2	0.4	0.5	0.3	0.2	nd	0.1	nd	0.3	0.7	0.1	0	nd	2.7	nd
80-90	46	26.2	18.2	1.9	0.8	0.9	0.3	0.5	0.6	0.2	0.2	nd	0.1	nd	0.3	1	0.1	0.1	nd	2.5	nd
90-100	47.6	26	17.7	1.7	0.7	0.6	0.3	0.3	0.4	0.3	0.1	0.1	0.1	nd	0.2	1	0.1	0	nd	2.9	nd
Tönnersjöheden T103:1																					
0-10	39.6	23.1	16.4	2.4	1.0	0.9	0.3	0.4	0.7	1.1	0.3	0.1	nd	nd	nd	1.9	0.2	0.4	0.5	6.3	4.7
10-20	36.8	24.7	15.9	3.3	1.5	1.0	0.3	0.2	0.6	0.9	0.2	0.1	nd	nd	nd	2.1	0.5	0.5	1.6	7.7	2.2

20-30	37.1	25.6	17.1	3.6	1.6	1.2	0.3	0.2	0.6	0.8	0.2	nd	nd	nd	nd	2.4	0.6	0.4	1.3	6.9	nd
30-40	36.4	26.3	16.7	3.9	1.7	1.1	0.3	0.2	0.6	0.7	0.2	0.1	0.1	nd	nd	2.7	0.8	0.6	1.2	6.5	nd
40-50	34.8	27.9	16.1	5.5	1.2	1.7	0.4	0.1	0.6	0.6	0.3	nd	nd	nd	nd	1.7	0.7	1.2	1.5	5.7	nd
50-60	35.5	29.3	16.2	5.0	1.2	1.6	0.5	0.2	0.6	0.1	0.2	nd	nd	nd	nd	1.4	0.7	1.3	1.3	4.9	nd
60-70	37.3	30.2	18.5	3.6	0.7	1.5	0.4	0.5	0.6	nd	0.1	nd	nd	nd	0.1	0.9	0.7	0.1	1.0	3.8	nd
70-80	39.1	30.2	19.1	3.2	0.7	1.3	0.4	0.4	0.5	nd	0.2	nd	nd	nd	nd	0.6	0.6	0.1	1.0	2.5	nd
80-90	38.1	30.8	19.4	3.1	0.7	1.4	0.4	0.5	0.5	nd	0.2	nd	0.0	nd	nd	0.8	0.7	0.3	1.8	1.3	nd
90-100	39.9	30.1	18.8	3.0	0.7	1.3	0.4	0.5	0.6	nd	0.2	nd	0.1	nd	0.1	0.7	0.4	0.1	1.1	2.1	nd
Asa																					
0-10	38.8	22.2	13.5	1.9	2.7	0.4	0.5	0.3	0.6	0.1	0.2	0.1	nd	nd	0.1	3.3	0.7	1	nd	4.8	8.5
10-20	37.9	21.6	13.1	1.8	2.4	0.3	0.5	0.4	0.6	nd	0.2	0.1	0.1	nd	0.1	3.1	0.7	0.8	nd	4	12.1
20-30	39.1	22.2	12.7	1.9	2.9	0.4	0.5	0.3	0.6	0.3	0.2	0.1	0.1	nd	nd	3.2	0.8	0.8	nd	2.9	10.8
30-40	39.6	23.7	15.2	2	2.7	0.4	0.5	0.3	0.6	0.3	0.2	0	0.1	nd	nd	3.5	0.8	1.2	nd	3	5.9
40-50	41.1	23.6	14	2.1	2.9	0.3	0.5	0.4	0.7	0.5	0.2	0	0.1	nd	0	3.7	0.9	0.8	nd	3.2	4.9
50-60	41.2	24.3	14.5	2.1	2.9	0.3	0.6	0.6	0.6	0.3	0.2	nd	0.1	nd	0.1	3.8	1.1	1.2	nd	2.7	3.4
60-70	41.8	25.7	14.5	1.9	3.2	0.5	0.6	0.4	0.6	0.1	0.2	nd	0.1	nd	0.1	3.6	1.4	0.9	nd	3.9	0.4
70-80	42.5	26.8	15	2	3.1	0.5	0.5	0.5	0.6	nd	0.1	nd	0.1	nd	0.2	3.2	1.1	1	nd	1.7	1
80-90	42.4	27.4	15.1	2.2	3.3	0.4	0.5	0.5	0.6	nd	0.1	0.1	0.2	nd	0.3	3.3	1.1	1.1	nd	1.5	nd
90-100	41.6	27.1	15.2	2.3	3.4	0.4	0.5	0.6	0.6	nd	0.2	nd	0.3	nd	0.1	3.4	1.2	0.8	nd	2.4	nd

The Skogaby soils were previously analysed by Simonsson et al. (2016), and Asa and Flakaliden soils by Casetou Gustafson et al. (2018). For the present study the Skogaby samples were rerun on the D8 diffractometer and the Asa, Flakaliden, and Tönnersjöheden XRPD data files run previously on the D8 were retrieved and re-analyzed, so that all soils were analyzed identically.
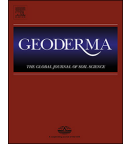
II

Phosphorus in 2D: Spatially resolved P speciation in two Swedish forest soils as influenced by apatite weathering and podzolization

Gbotemi A. Adediran[a], J.R. Marius Tuyishime[a], Delphine Vantelon[b], Wantana Klysubun[c], Jon Petter Gustafsson[a,d,*]

[a] Department of Soil and Environment, Swedish University of Agricultural Sciences, Box 7014, 750 07 Uppsala, Sweden
[b] Synchrotron SOLEIL, L'Orme des Merisiers, Saint Aubin BP 48, 91192 Gif-sur-Yvette Cedex, France
[c] Synchrotron Light Research Institute, 111 Moo 6, Suranaree, Muang, Nakhon Ratchasima, Thailand
[d] Department of Sustainable Development, Environmental Science and Engineering, KTH Royal Institute of Technology, Teknikringen 10B, 100 44 Stockholm, Sweden

ARTICLE INFO

ABSTRACT

The cycling and long-term supply of phosphorus (P) in soils are of global environmental and agricultural concern. To advance the knowledge, a detailed understanding of both the vertical and lateral variation of P chemical speciation and retention mechanism(s) is required, a knowledge that is limited in postglacial forest soils. We combined the use of synchrotron X-ray fluorescence microscopy with multi-elemental co-localisation analysis and P K-edge XANES spectroscopy to reveal critical chemical and structural soil properties. We established a two-dimensional (2D) imagery of P retention and speciation at a microscale spatial resolution in two forest soil profiles formed in glaciofluvial and wave-washed sand. The abundance and speciation of P in the upper 40 cm was found to be influenced by soil weathering and podzolization, leading to spatial variability in P speciation on the microscale ($< 200 \, \mu m$) with P existing predominantly as organic P and as PO_4 adsorbed to allophane and ferrihydrite, according to XANES spectroscopy. These species were mostly retained at sharp edges and in pore spaces within Al and Si-bearing particles. Despite the relatively young age ($< 15,000$ years) of the soils, our results show primary mineral apatite to have weathered from the surface horizons. In the C horizon however, a large fraction of the P was in the form of apatite, which appeared as widely dispersed ($> 600 \, \mu m$) hot spots of inclusions in aluminosilicates or as discrete micro-sized apatite grains. The subsoil apatite represents a pool of P that trees can potentially acquire and thus add to the biogeochemically active P pool in temperate forest soils.

1. Introduction

Phosphorus (P) is a macronutrient needed for the sustenance of all forms of life on Earth. However, the global supply of P is limited (Cordell et al., 2009; Van Vuuren et al., 2010). Temperate and boreal forest ecosystems in northern Europe are associated with soils that were formed after the last glaciation 8000–15,000 years ago. Most of these were developed in glacial till and glaciofluvial or wave-washed sand (Werner et al., 2017a). The primary production of these ecosystems is usually limited by the availability of nitrogen (N), and currently there are few indications of P limitation (Akselsson et al., 2008; Binkley and Högberg, 2016). However, the increased atmospheric N deposition in the last decades have rendered some forest ecosystems more N-enriched, which may increase problems with N leaching (Gundersen et al., 2006), and thereby make P a more critical nutrient (Yu et al., 2018). In addition, today's forest management methods, with harvesting of

biomass, could lead to a successive depletion of bioavailable P in forest soils. This is particularly the case as concerns whole-tree harvesting, but also stem harvesting leads to P losses. A mass balance study carried out for 14,550 Swedish sites revealed that the annual losses of P from forestry exceed 1 kg P ha^{-1} in the southern part of Sweden (Akselsson et al., 2008). This could also contribute to a successive transition from N to P limitation in northern European ecosystems.

The bioavailability of P for plant use depends on its chemical speciation, its relationship with soil particles and proximity to plant roots (Frossard et al., 2000). For P to be bioavailable, it will first need to be weathered from primary minerals, predominantly apatite (Wallander et al., 1997). As many northern European forest soils is of relatively recent origin, they are expected to contain appreciable amounts of apatite in the mineral soil (Walker and Syers, 1976). Apatite weathering has been shown to be strongly dependent on the acidity of the soil; possibly, soil organisms can speed up weathering by excreting organic

* Corresponding author at: Department of Soil and Environment, Swedish University of Agricultural Sciences, Box 7014, 750 07 Uppsala, Sweden.
E-mail addresses: gbotemi.adediran@slu.se (G.A. Adediran), jon-petter.gustafsson@slu.se (J.P. Gustafsson).

acids (Smits et al., 2014; Wallander et al., 1997). Once apatite is dissolved, the released P is potentially bioavailable. However, the released orthophosphate (*o*-phosphate ions) may also be adsorbed by iron (Fe) and aluminium (Al) (hydr)oxides including allophane, which are ubiquitous weathering products in the B horizons of Spodosols (Gustafsson et al., 1999). In addition, some P is also stored in soil organic matter in a variety of P forms (Vincent et al., 2012).

The bulk chemical speciation of P in a soil sample can be estimated by P K-edge XANES spectroscopy with linear combination fitting (Beauchemin et al., 2003). There are many recent examples on the successful use of this technique, also for forest soils (Prietzel et al., 2016). Although the bulk speciation of P is useful to know, it is important to remember that the spectra obtained represent an average of a large number of P phases present in a sample. This can make individual assignments, based on linear combination fitting, uncertain (Gustafsson et al., 2020). In addition, the bulk speciation is not necessarily related to bioavailability, as it does not indicate to what extent the P phases are geochemically active and/or available for plant uptake.

The use of synchrotron-based X-ray fluorescence (μ-XRF) microscopy in combination with spotwise P K-edge X-ray atomic absorption near-edge structure (μ-XANES) spectroscopy can offer valuable additional information on P speciation as it allows multi-elemental mapping as well as solid-state P speciation analysis in-situ (Baumann et al., 2019; Rivard et al., 2016; Werner et al., 2017b). For example, Rivard et al. (2016), studying the effects of fertilization on P species in agricultural soils from Illinois, noticed the presence of some "hot spots" with an enrichment of Ca-bound P, probably apatite. However, their effect on the bulk XANES spectra were insignificant. Werner et al. (2017b), who studied a group of Bavarian Cambisols, found that P-enriched areas coincided with the presence of Al and Fe hydrous oxides, showing that P was bound mainly to Al and Fe of these phases. In microsites, they also found indications of the presence of Al phosphates and also of unusual magnesium (Mg) phases such as $MgHPO_4$, which could not be identified with bulk P-XANES methods. Hesterberg et al. (2017) collected P K-edge XANES spectra from 12 microsites of one Histosol soil sample. In all microsites the P was dominated by organic P and Al-bound P, but the relative proportions of the different species were variable, confirming that μ-XANES was able to provide additional information on the P speciation in localized areas of the samples.

Moreover, bulk soil P-XANES spectroscopy has been used to elucidate weathering-induced apatite dissolution from which the P released can be transformed into other species, such as organic P and P adsorbed on Fe and Al (hydr)oxides, or leached (Eriksson et al., 2016; Prietzel et al., 2016). As a result, the apatite concentration increased with soil depth while the concentrations of organic P and adsorbed P species decreased with depth. This observation is consistent also with previous studies that relied on results from wet extractions (Walker and Syers, 1976; Frossard et al., 1989). However, electron microscopy has been used to show small amounts of apatitic P to be preserved as 'mineral apatite inclusions' (a mineral species present within the matrix of another mineral species) in slowly weathered silicates (Heindel et al., 2018; Syers et al., 1967).

Despite these research efforts, there are many aspects of the two-dimensional (2D) spatial distribution of P that remain unclear, and what this means for our interpretation of soil P cycling and weathering phenomena. Moreover, there is no study to date which has established a 2D-imagery of P distribution and chemical speciation as a function of depth in a soil profile. This visualisation is critical for the accurate conceptualisation of molecular-scale chemical and physical reactions of P in soils and such knowledge is fundamental to the understanding of how P speciation changes over time in response to soil-forming processes (Prietzel et al., 2016; Werner et al., 2017b).

The current study capitalises on recent advances in synchrotron based micro-focused-X-ray fluorescence microscopy and spectroscopy to acquire images of multi-elemental distributions, grain architecture, pore space distributions, and the vertical and lateral distribution of P

chemical species at a very high (< 3 μm) spatial resolution.

The specific aim is to comprehensively study two forest soil profiles in order to: (i) establish the effects of postglacial weathering on the spatial abundance and distribution of primary apatite, (ii) reveal the predominant chemical species of P under the acidic soil conditions that prevail in Podzols, and (iii) elucidate the mechanisms that govern both the vertical and lateral retention of P, at the microscale.

2. Methodology

2.1. Soil sampling and sample preparation

Two soil profiles were excavated in coniferous forests at Tärnsjö and Tönnersjöheden, Sweden, respectively (coordinates: 60.14°N 16.92°E and 56,42°N 13.40°E). The predominant vegetation was *Pinus sylvestris* and *Picea abies* of about 70–120 years of age (Gustafson et al., 2015; Zetterberg et al., 2013). The soils at the two sites were formed under temperate climate. While the soil at Tärnsjö was formed in wave-washed sand and classified as an Albic Podzol (IUSS Working Group WRB, 2014), the soil at Tönnersjöheden was developed in sandy glaciofluvial material. Although podzolized, it did not classify as a Podzol due to significant mixing of the upper horizons and was therefore classified as Dystric Arenosol (Hansson et al., 2011; IUSS Working Group WRB, 2014). At Tärnsjö, an eluvial (E) horizon of about 2 cm thick was found under the organic layer (0–2 cm in depth). This was sampled as well as the uppermost Bs horizon at 2–10 cm. Other mineral soil samples were sampled thereafter at 10 cm intervals to a depth of 100 cm. As there was no E horizon in the profile at Tönnersjöheden, only an A horizon with a gradual transition to the underlying B horizon, the soil samples were collected at 10 cm intervals from the top (A horizon) to a depth of 100 cm. Soils for micro-focused X-ray microscopy and spectroscopy were gently sieved (< 5 mm) to remove stones and debris before air-drying for 72 h. Representative samples from each depth were then embedded in high-purity epoxy resin. Micro-polished petrographic thin sections of 30 μm thick were prepared at TS Lab & Geoservices snc, Cascina, Italy. Soil samples for other analysis were dried at 60 °C for 48 h and subsequently sieved (< 2 mm).

2.2. Measurements of selected soil chemical properties

On sieved (< 2 mm) soil samples, the pH value was measured in a deionised water suspension with a glass electrode (soil: solution ratio 1:2.5). Total P contents (P-t) were determined after microwave-assisted digestion in sealed teflon vessels with a 10:1 mixture of concentrated $HNO_3:H_2O_2$ and subsequent measurement by inductively coupled plasma sector field mass spectrometry (Church et al., 2017). The soils were also subjected to extraction with 0.2 M oxalate buffer at pH 3.0 to quantify non-crystalline and organically-bound metals using the method of van Reeuwijk (1995). The concentrations of P, Al and Fe (designated as P-ox, Al-ox and Fe-ox respectively) in the extract were analyzed by inductively coupled plasma optical emission spectroscopy (ICP-OES) using a Thermo Scientific Icap 6000 instrument (Thermo Fisher Scientific, Waltham, MA, USA). The concentration of inorganic P in the oxalate extract (PO_4-ox) was determined using a Seal AA3 Autoanalyzer (Seal Analytical GmBH, Norderstedt, Germany) employing the acid molybdate method as modified by Wolf and Baker (1990). The concentration of oxalate-extractable organic P (OrgP-ox) was estimated by subtracting PO_4-ox from P-ox. Organic carbon (C) and total nitrogen (N) were analysed by dry combustion (CHN600, LECO).

2.3. P speciation by bulk soil P K-edge XANES analysis

Bulk P K-edge XANES spectra were collected on the soil samples at beam line BL8 of the Synchrotron Light Research Institute (SLRI) in Nakhon Ratchasima, Thailand (Klysubun et al., 2020). Prior to bulk XANES analysis, ~ 4 g of soil samples were milled and sieved

through < 0.05 mm to minimize self-absorption. Powdered samples were then packed into 2 mm thick stainless steel holders (1 × 1.5 cm with a sample window of 0.05 × 1 cm) and covered with polypropylene film (Eriksson et al., 2016). The beamline was equipped with an InSb (1 1 1) crystal monochromator and a solid state 13-element Ge fluorescence detector. The beam size was 12.5 × 0.9 mm and beam flux was 2×10^{11} photons s^{-1} (100 mA)$^{-1}$. To minimize X-ray absorption by air, the sample compartment was filled with helium gas. Spectra of samples and standards were recorded across an energy range from 2100 to 2320 eV. The step size was 2 eV between 2100 and 2132 eV, 1 eV between 2132 and 2144 eV, 0.2 eV between 2144 and 2153 eV, 0.3 eV between 2153 and 2182 eV, and 5 eV between 2182 and 2320 eV. All measurements were recorded using a dwell time of 3 s per energy step.

2.4. Synchrotron micro-focused μ-XRF and μ-XANES

The petrographic soil sections were subjected to both μ-XRF imaging and μ-XANES analysis at the X-ray microscopy beamline LUCIA of the French national synchrotron research facility SOLEIL. The beamline is fitted with a Si(1 1 1) double crystal monochromator. Transmission, fluorescence and total electron yield detection were made simultaneously by means of a silicon pin diode, a silicon drift diode and a measurement of the drain current, respectively (Vantelon et al., 2016). Focusing of the X-ray beam (2.5 × 2.5 μm) was performed with two Kirkpatrick-Baez (K-B) mirrors system. The photon flux was 6×10^{11} photons s^{-1} at 2.6 keV. To minimize X-ray absorption by air, the analysis was performed in a vacuum environment.

Considering the low concentration of P in our thin-sectioned samples and the need to obtain high quality P K-edge μ-XANES spectra, the beamline was optimized for low energy mapping at microscale resolution, and μ-XRF images (600 × 600 μm) of Na, Mg, Al, Si and P were acquired with a dwell time of 0.3 s using a step size of 3 × 3 μm. Although at this low energy we were unable to utilize μ-XRF microscopy to obtain information about the interactions of P with important elements such as Ca and Fe, it was possible to use unique features of the μ-XANES spectra to identify P species associated with Ca and Fe as well as with organic P. For example, calcium phosphates show post-edge shoulders that are unique for different calcium phosphate minerals, Fe bound P shows a distinct pre-edge peak, and organic-P species have a broad white line peak displaced towards lower energy (Hesterberg, 2010; Gustafsson et al. 2020) (see supplementary material Fig. S1).

Spot-wise μ-XANES of P was therefore performed with respect to the spatial distribution of P as revealed by μ-XRF. The P spots were chosen at soil particle surfaces and at pore spaces across the maps to reflect as much as possible the heterogeneity in P distribution that was revealed by μ-XRF. The P K-edge μ-XANES spectra were recorded in fluorescence mode across an energy range from 2100 to 2320 eV. The step size was 2 eV between 2100 and 2139 eV, 1 eV between 2140 and 2146 eV, 0.2 eV between 2146 and 2160 eV, 0.3 eV between 2160 and 2190 and 5 eV between 2195 and 2320 eV. All XANES measurements were recorded using a dwell time of 3 s per energy step. At every selected spot, 4 to 5 high quality μ-XANES scans were acquired and merged to represent a spot.

μ-XRF mapping were also performed on selected P standards and high quality micro-focused P K-edge XANES spectra were obtained at P hot spots. These standards include hydroxyapatite, PO$_4$ adsorbed to ferrihydrite, variscite, PO$_4$ adsorbed to aluminum hydroxide, PO$_4$ adsorbed to allophane and natural soil organic phosphorus from forest mor (SOP). These were complemented with bulk P K-edge spectra of other P compounds such as natural apatite (from Taiba, Sudan), amorphous calcium phosphate, iron(III) phosphate, PO$_4$ adsorbed to goethite, aluminum phosphate and PO$_4$ adsorbed to gibbsite. These standards were collected at BL8 of SLRI and are part of our database of P standards used for routine P speciation analysis in soil. The sources and preparation of the standards are described in Gustafsson et al. (2020). Together, these compounds represent the major P associations

(i.e., Ca-P, Fe-P, Al-P, P adsorbed to Fe and Al, and organic P) that are often encountered in soils.

2.5. Analysis of X-ray fluorescence and X-ray absorption data

The μ-XRF spectra were dead-time corrected and normalized to incoming beam intensities before individual elemental spectra deconvolution. Microscale-resolution elemental maps were obtained after fitting each pixel μ-XRF spectrum using the PyMca X-ray Fluorescence Toolkit (Solé et al., 2007). The ATHENA software package was used to subtract the background and normalize all μ-XANES and bulk soil P XANES spectra (Ravel and Newville, 2005). Solid-phase P speciation was estimated by linear combination fitting (LCF) analysis (Eriksson et al., 2016; Tannazi and Bunker, 2005) using weighted combinations of the reference spectra (Fig. S1). No energy shifts were permitted in the fitting procedure and the fit combinatorics were not forced to sum to 100%. A maximum of 4 out of 15 standard compounds were allowed during the LCF using a least-squares algorithm of the sample XANES spectrum from 2144.05 to 2184.05 eV. The goodness of the fit was estimated by calculating the R factor of the fit; $R = \Sigma_i$ (experimental − fit)$^2/\Sigma_i$ (experimental)^2 (Ravel and Newville, 2005). The sums (Σ) were over 142 data points as flattened mu (E). A lower R factor represents a better match between the standard spectra and the sample spectrum. For the bulk P K-edge XANES results from SLRI, standard deviations of the weights were calculated with a Monte-Carlo approach, in which uncertainties in energy calibration and normalization were considered (for a full account, see Gustafsson et al., 2020). However, for the μ-XANES data, information on these uncertainties were not available, and instead the standard deviations were those given by Athena, which consider only uncertainties of the LCF method itself (Ravel and Newville, 2005).

3. Results

3.1. Soil characteristics

Selected soil chemical properties are presented in Table 1. The soils were predominantly acidic. The lowest pH at both sites was in the organic layer and in the uppermost mineral soils. In Tärnsjö, the pH increased from 4.0 in the organic layer to 6.2 at 80 cm depth before decreasing slightly to between 5.8 and 6.0 at the bottom of the profile. In Tönnersjöheden, the pH increased from 3.7 in the organic layer to 4.6 at 20 cm depth and then remained stable at between pH 4.7 and 4.8 from 30 cm to the bottom of the profile. Total P (P-t) in the mineral soils ranged from 2 to 20 mmol kg^{-1}. In Tärnsjö, the lowest amount of P-t was observed at the E horizon (0–2 cm) while the highest amount was in the illuvial Bs horizon (10–20 cm). A similar pattern was observed in Tönnersjöheden with the lowest amount of P-t at the A horizon (0–10 cm) and the highest at the B horizons (20–50 cm). The distribution of oxalate-extractable elements in the two profiles exhibited similar trends, which were similar to those seen in previous studies on Swedish Podzols (Bain et al., 2003). For example in Tärnsjö, the lowest concentrations of P-ox, Al-ox and Si-ox were in the E horizon, whereas they reached a maximum in the Bs horizon with concentrations of 19, 166 and 31 mmol kg^{-1} respectively before decreasing with depth. The Fe-ox concentrations showed a similar pattern with the lowest concentration in the E horizon and the maximum concentrations of 64 mmol kg^{-1} in the Bs horizon. The Fe-ox concentration also decreased with depth to a concentration of 6.3 mmol kg^{-1} at 70–80 cm but further down it increased again to between 18.7 and 25.2 mmol kg^{-1} at 80–100 cm depth. Similarly, the concentrations of P-ox, Al-ox and Si-ox were lowest in the A horizon of Tönnersjöheden and had maximum concentrations in the Bs horizons (10–30 cm) before decreasing with depth. The amount of Fe-ox in the Tönnersjöheden profile was highest already in the A horizon and then decreased with depth. While most of the P-ox was organic in the uppermost two

Table 1
Soil pH, concentrations (mmol kg^{-1}) of total P (P-t), oxalate (ox) extractable – P (P-ox), phosphate (PO$_4$-ox), organic P (OrgP-ox), Fe (Fe-ox), Al (Al-ox), Si (Si-ox) and percentage organic carbon (Org-C) and total nitrogen (Total-N) in Tärnsjö and Tönnersjöheden soil profile.

Horizon/Depth (cm)	pH	P-t	P-ox	PO$_4$-ox	OrgP-ox	Fe-ox	Al-ox	Si-ox	Org-C	Total-N
					mmol kg^{-1}					(%)
Tärnsjö										
Oe Mor	4.0	18.4	4.3	2.6	1.7	8.9	25.3	0.5	46.66	1.24
E 0–2	4.3	2.0	0.5	0.2	0.3	4.2	10.4	0.4	0.84	0.02
Bs 2–10	4.6	15.0	10.7	9.4	1.3	54.2	84.2	10.8	1.29	0.04
10–20	4.9	20.9	19.9	17.0	2.9	64.2	166.5	31.7	1.08	0.03
20–30	5.2	15.3	10.9	10.0	0.9	29.6	111.9	24.7	0.32	0.01
BC 30–40	5.4	10.7	5.0	4.3	0.7	10.3	54.5	16.2	0.13	< 0.005
C 40–50	5.7	11.8	3.8	3.3	0.5	6.8	42.0	16.8	0.07	< 0.005
50–60	5.9	12.1	3.8	3.3	0.5	9.8	40.2	14.3	0.06	< 0.005
60–70	6.1	15.9	2.8	2.4	0.4	7.2	28.5	13.2	0.04	< 0.005
70–80	6.2	16.0	2.1	1.7	0.4	6.3	23.8	11.1	0.04	< 0.005
80–90	6.0	15.0	2.2	1.7	0.5	25.2	25.3	12.1	0.07	< 0.005
90–100	5.8	17.2	3.0	2.3	0.7	18.7	27.8	12.5	0.06	< 0.005
Tönnersjöheden										
Oe Mor	3.7	21.6	5.5	2.1	3.4	13.8	26.2	0.6	44.80	1.47
A 0–10	4.2	8.3	5.6	2.0	3.6	131.7	98.7	2.7	4.00	0.16
Bs 10–20	4.6	14.2	11.2	6.7	4.5	125.4	318.9	53.8	3.03	0.14
20–30	4.7	17.5	13.2	10.0	3.2	82.9	280.7	57.4	1.66	0.08
30–40	4.8	18	14.1	10.6	3.5	64.3	270.3	55.0	1.38	0.07
40–50	4.7	18	11.6	9.0	2.6	57.2	172.4	32.1	1.21	0.05
50–60	4.7	16.8	10.6	8.1	2.5	53.8	139.9	23.4	1.00	0.04
BC 60–70	4.8	12.8	7.7	5.6	2.1	25.0	104.5	20.1	0.79	0.03
C 70–80	4.8	14.9	6.8	5.0	1.8	14.8	75.4	15.1	0.55	0.02
80–90	4.8	16	6.3	4.9	1.4	11.6	61.4	13.2	0.34	0.01
90–100	4.8	12.5	6.6	5.0	1.6	18.7	72.2	13.7	0.47	0.02

horizons at both sites, P-ox was dominated by inorganic PO$_4$ deeper down in the mineral soil (i.e. throughout the B and C horizons), particularly in the Tärnsjö soil, which had a relatively low organic C content in the B horizon (Table 1).

3.2. P speciation by bulk soil P K-edge XANES

Linear combination fit results of bulk P K-edge XANES spectra are reported in Fig. 1. They showed a predominance of organic P in the O horizon, Al- and Fe-bound P in the A and B horizons, and the presence of primary mineral apatite in the C horizons of the two soil profiles. It is worthy of note that the Ca-bound P was detectable by bulk P K-edge XANES from 20 to 30 cm soil depth, with the abundance appearing to increase with depth at both sites.

3.3. 2D imagery of soil architecture with respect to P retention and speciation

As expected in soils formed on siliceous parent materials, μ-XRF imaging revealed Si and Al as the main constituents of the soil grains (Fig. S2-S3). A morphological analysis of the spatial variation and co-localisation of Si and Al was therefore deemed sufficient to depict particles and pore space distribution in the soil profiles. 2D tri-colour co-localisation of Si (red), Al (blue) and P (green) were therefore used to re-construct the spatial retention of P species with respect to soil particles and pore-spaces distributions across the soil profiles (Fig. 2). The results of this micro-spectroscopic analysis is described below.

(i) P retention and speciation at the E horizon

In agreement with the results of P chemical extractions, synchrotron μ-XRF imaging showed the lowest P abundance in the E horizon (0–2 cm depth) of the Tärnsjö profile (Fig. 2a). The P concentration was too low to yield P K-edge XANES spectra (both by micro and bulk powdered XANES) that could be analysed to deduce the chemical speciation of P. However, morphological examination showed most of the P to be retained at the surface/within the cracks of microscale

(< 20 μm sizes) Si (mostly devoid of Al) containing grains (Fig. S4).

(ii) P retention and speciation at the A and B horizons

A morphological examination of soil grains at the A horizon in Tönnersjöheden (0–10 cm) and the uppermost B horizon in Tärnsjö (2–10 cm) showed that the majority of the soil grains contained both Si and Al (purple colour) (Fig. 2a-b). Phosphorus (P, green) at these depths was mostly retained at the edges and within pore spaces of the soil particles. It is worthy of note that the edges of the non-Al-bearing (mainly silica) particles appeared to contain some P. Moreover, P appeared also to be retained within the cracks that were probably created by soil weathering at the surface of the largest grain in the Tärnsjö 2–10 cm sample. Furthermore, results of spot-wise P speciation analysis by μ-XANES showed significant spatial heterogeneity within the soil grains at the microscale. For example, while P in point (a) of Tärnsjö 2–10 cm existed predominantly as Fe-bound P (e.g. ferrihydrite-bound PO$_4$), there was a different P speciation in point (b), where P was instead present as Al-bound P (e.g. allophane-bound PO$_4$) (Table 2, Fig. S5).

The spatial variation in chemical speciation is easily seen when examining the differences in the pre-edge peaks of the P K-edge XANES spectra (Fig. S5), despite the two spots being < 200 μm apart (Fig. 2). Pronounced pre-edge peaks that occur between 2,149 and 2,152 eV are typical for Fe-associated P, while the pre-edge resonances for Al-bound P are much smaller (Hesterberg et al., 1999). Similar microscale heterogeneity in P speciation was observed in Tönnersjöheden 0–10 cm. For example, while P at point (c) of this depth existed predominantly (56 ± 3% of total P) as Fe-P there was no Fe-P at point (e) which existed predominately (70 ± 6% of total P) as Al-P (Table 3, Fig. S6). The content of organic P as assessed by P K-edge XANES ranged from 9 ± 2 to 19 ± 4% and from 19 ± 1 to 30 ± 3% of total P at Tärnsjö 2–10 cm and Tönnersjöheden 0–10 cm, respectively. In both samples, organic P as assessed by P K-edge XANES was on average < 25 ± 3% of total P, while Al and Fe-bound P were the predominant (up to 75 ± 8%) P species, which were found at the edges and pore spaces of the soil grains.
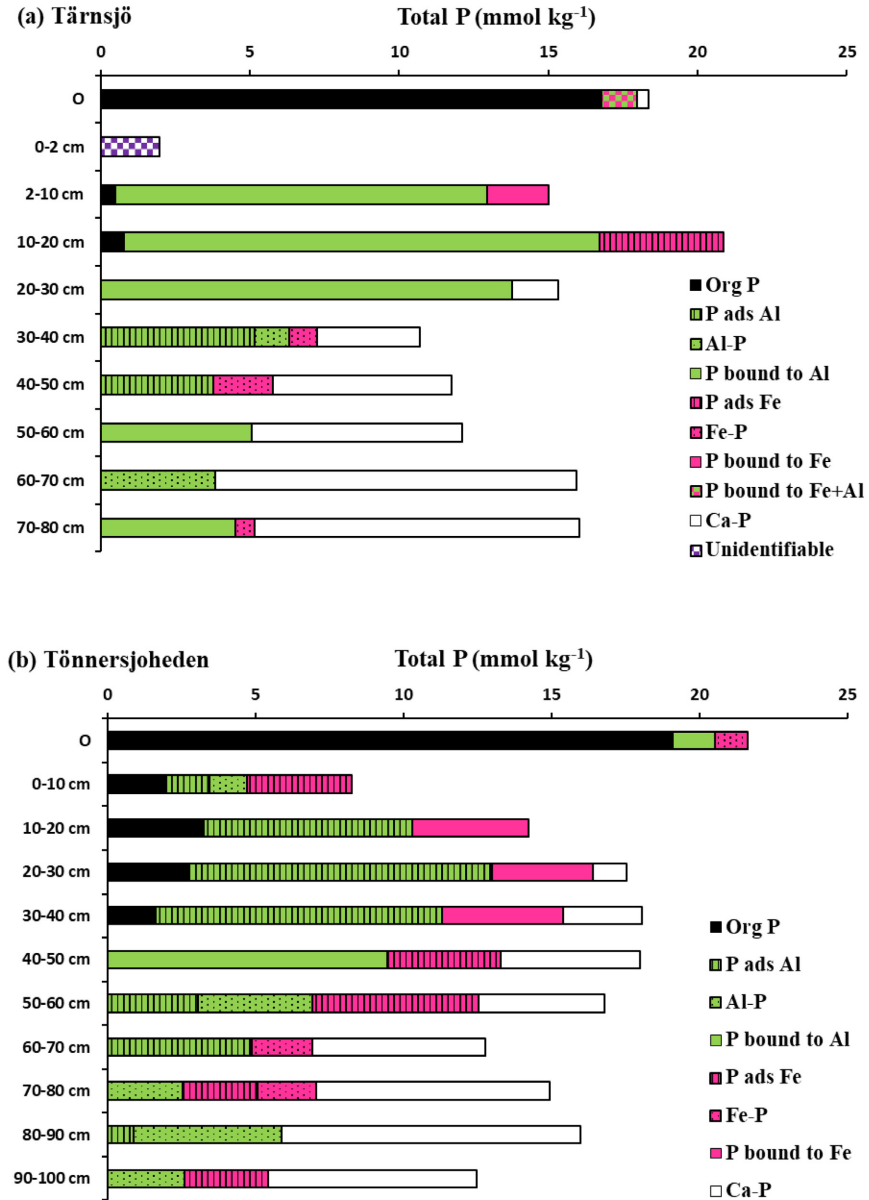
Fig. 1. Phosphorus speciation in the (a) Tärnsjö and (b) Tönnersjöheden soil profiles as evidenced from linear combination fitting (LCF) of bulk soil P K-edge XANES spectra. P ads Al and P ads Fe refer to PO_4 adsorbed to Al and Fe minerals (e.g. PO_4 adsorbed to allophane and PO_4 adsorbed to ferrihydrite), respectively. Al-P and Fe-P refer to $AlPO_4$ and $FePO_4$ mineral phases, respectively. P bound to Al and P bound to Fe represent cases when probabilistic LCF analysis could not differentiate between PO_4 adsorbed to Al from $AlPO_4$ minerals and PO_4 adsorbed to Fe from $FePO_4$ minerals, respectively. In the O horizon of Tärnsjö, P bound to Fe + Al is used as probabilistic LCF could not distinguish between P bound to Al and P bound to Fe.
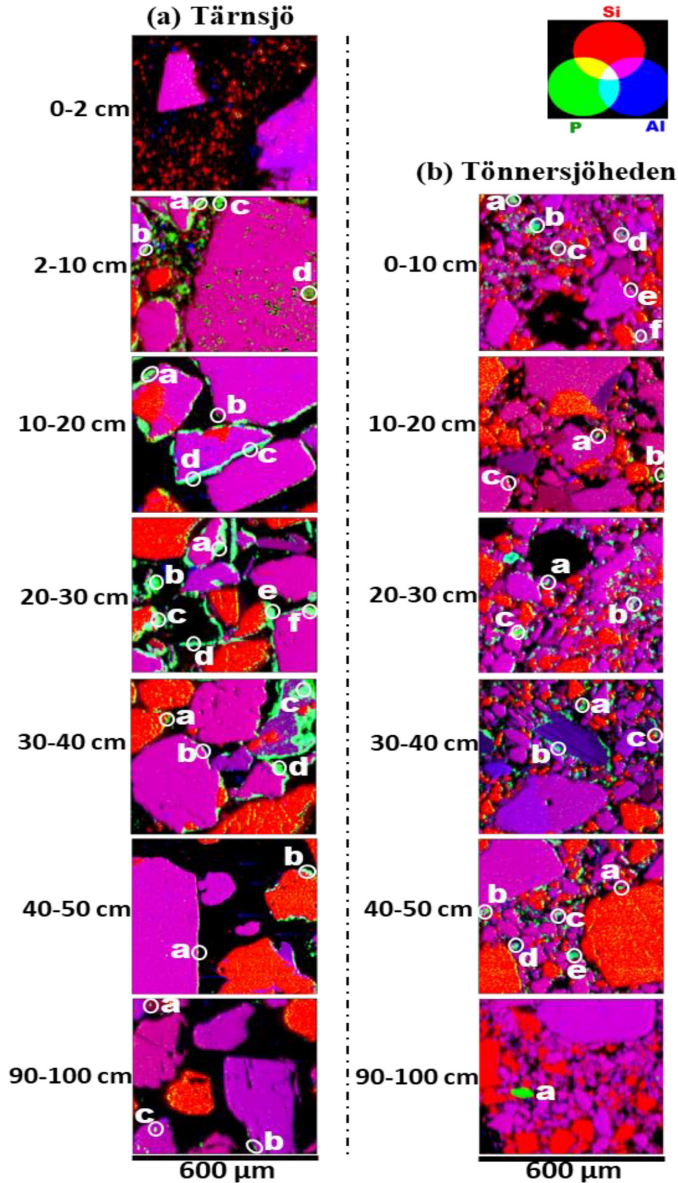
Fig. 2. Spatial variation in P (green) distribution and retention at the edges, surfaces and within pore spaces of Al (blue) and Si (red) bearing soil particles in the (a) Tärnsjö and (b) Tönnersjöheden profiles. The letters a – f on the maps represent spots at which P K-edge μ-XANES data were acquired.

Furthermore, the Tärnsjö 10–20 cm sample contained less of fine (< 20 μm size) particles when compared to the 2–10 cm depth above it. The pore spaces were therefore wider and P was mainly retained at the edges of Si- and Al-bearing particles. The P speciation was also heterogeneous at the microscale. For example, while Fe-bound P was the main form of P at points (a) and (b), P existed predominantly as Al-bound P at points (c) and (d) (Table 2, Fig. S7). The microscale heterogeneity in P speciation was even more pronounced in Tönnersjöheden 10–20 cm (Table 3). For example, while P in point (a) existed predominantly (~90 ± 6%) as inorganic P (as P bound to Fe and Al), in point (b), < 200 μm away, there was a hot spot of organic P (~70 ± 3% of total P at the spot; Fig. S8) according to XANES-LCF.

Table 2

Phosphorus speciation in Tärnsjö soil profile as evidenced from linear combination fitting (LCF) of spot-wise µ-XANES and bulk soil P K-edge XANES spectra. The fits are expressed as percentage contributions from selected P standards. The R-factor is a measure of goodness-of-fit $= \Sigma(\text{data} - \text{fit})^2/\Sigma(\text{data})^2$.

Soil profile	µ-XANES Spots	Organic P	Fe bound P		Al bound P		CaP	R-factor
			FeP	P adsorbed on Fe	AlP	P adsorbed on Al		
2–10 cm	a	9 ± 2		64 ± 9		27 ± 6		0.0043
Bs	b	13 ± 2		24 ± 7		63 ± 6		0.0028
	c	19 ± 4		35 ± 11		46 ± 8		0.0076
	d	16 ± 2		44 ± 8		40 ± 6		0.0034
	Bulk	3 ± 3		14 ± 5[1]		83 ± 6		0.0022
10–20 cm	a	15 ± 2		51 ± 8		34 ± 6		0.004
	b	12 ± 3		49 ± 12		39 ± 9		0.0076
	c			32 ± 2		68 ± 2		0.0009
	d			17 ± 3	15 ± 2	68 ± 3		0.0016
	e	11 ± 2		38 ± 8	22 ± 2	29 ± 6		0.0035
	Bulk	4 ± 4		20 ± 6		76 ± 8[1]		0.0012
20–30 cm	a	5 ± 1		34 ± 5	15 ± 2	46 ± 4		0.0012
	b	5 ± 1		29 ± 4		66 ± 3		0.0007
	c			20 ± 2	12 ± 1	68 ± 2		0.0005
	d	6 ± 2		38 ± 6		56 ± 4		0.0015
	e	12 ± 1			8 ± 2	80 ± 2		0.0029
	f	10 ± 1		29 ± 5		61 ± 4		0.0013
	Bulk					90 ± 4[1]	10 ± 4	0.0012
30–40 cm	a	16 ± 3		23 ± 8		61 ± 8		0.0059
BC	b			38 ± 2	5 ± 1	57 ± 2		0.0011
	c	5 ± 2		23 ± 9		74 ± 7		0.0038
	d				25 ± 2	75 ± 2		0.002
	Bulk		9 ± 5		11 ± 7	48 ± 3	32 ± 4	0.0021
40–50 cm	a				20 ± 1	80 ± 1		0.0009
C	b	9 ± 1			11 ± 3	80 ± 3		0.0046
	Bulk		17 ± 4			32 ± 2	51 ± 3	0.0023
90–100 cm	a	9 ± 2		25 ± 6		66 ± 5		0.0018
	b	14 ± 2		32 ± 8		54 ± 6		0.0029
	c						100	
	Bulk[2]		4 ± 4		28 ± 2[1]		68 ± 3	0.0069

[1] Probabilistic LCF could not differentiate between adsorbed and precipitated species of P bound to Fe or Al.
[2] Bulk soil P K-edge XANES results are shown for the 70–80 cm depth, as results for the 80–100 cm depth were not available. A full data set of bulk soil P K-edge probabilistic LCF is provided under research data.

With increasing depth in the B horizon (down to 40 cm depth), P speciation in the Tärnsjö soil became less heterogeneous as Al- followed by Fe-bound P dominated most of the P microsites (Table 2-3, Fig. S9-S12). The predominance of Al-bound P was in accordance with the greater concentration of oxalate-extractable Al as compared to oxalate-extractable Fe (Table 1).

It cannot be excluded that some of the P that was assigned to fer-rihydrite- and allophane-bound PO_4 was adsorbed organic P species such as phytate rather than PO_4 (Prietzel et al., 2016). In the LCF we did not use any standard for adsorbed phytate, as it was shown that the standard for adsorbed phytate to ferrihydrite and allophane could be well described (with an R factor < 0.001) with about 50% organic P and 50% ferrihydrite or allophane (Gustafsson et al, 2020). Thus, the P K-edge XANES technique used here is not well suited to determine the contribution of adsorbed phytate with any confidence. This constitutes a slight uncertainty for the results obtained in the upper B horizons, where there was both organic P and ferrihydrite- and allophane-bound PO_4 according to our results. Nevertheless, the results from the oxalate extraction show that adsorbed phytate is likely only a very minor part of the adsorbed P in the Tärnsjö soil, as the extracted organic P was only a very small fraction of the extracted total P (Table 1). In the Tön-nersjöheden soil, adsorbed phytate could be slightly more important, but still of smaller significance than adsorbed PO_4, as evidenced by the relationship between inorganic and organic P in the oxalate extract (Table 1).

(iii) P speciation and retention at upper and lower C horizons

The P speciation in the upper C horizon (40–50 cm depth) showed trends similar to the ones observed at the lower B horizons as P was adsorbed at the edges of soil grains or existed as coatings on the flat surfaces of Si-bearing particles at the two sites. At this depth, P existed mainly as inorganic P in both sites. However, while P at all studied spots in Tärnsjö 40–50 cm exhibited little spatial variability and existed mainly as Al-bound P, the P species at Tönnersjöheden 40–50 cm were more diverse, and they consisted mainly of a mix of Al- and Fe-bound P species at the studied spots (Fig. S13-S14).

At the lowest depth of 90–100 cm, there was significant hetero-geneity in P speciation when compared to the upper horizons. In the Tärnsjö 90–100 cm sample, the P in points (a-b) existed predominantly as Al- and Fe-bound P, whereas in point (c) P K-edge µ-XANES detected a hot spot of Ca-bound P, with a XANES spectrum that most resembled apatite (Fig. S15). Detailed morphological examination showed this Ca-bound P spot to be about 10–20 µm in size and to be associated with a larger (> 150 µm) Al and Si-bearing particle, probably a feldspar (Fig. 2a), in which the apatite was present as an inclusion. A similar finding was made at Tönnersjöheden 90–100 cm. Here the Ca-bound P spot appeared as a discrete mineral grain of about 75 µm size (Fig. 2b and Fig. S16). In both cases the P concentration was very high, sug-gesting the presence of apatite or almost pure apatite.

4. Discussion

4.1. Heterogeneity of P chemical species at soil microsites

Soils are developed through a large number of biogeochemical processes that occur at the same time. In the midst of this complexity, a concise analysis of micrometre-scale chemical speciation within a vo-lume of intact soil sample is fundamental to the understanding of mo-lecular-level chemical reactions that govern the long-term cycling of

Table 3
Phosphorus speciation in the Tönnersjöheden soil profile as evidenced from linear combination fitting (LCF) of spot-wise μ-XANES and bulk soil P K-edge XANES spectra. The fits are expressed as percentage contributions from selected P standards. The R-factor is a measure of goodness-of-fit = Σ (data − fit)^2/Σ (data)^2.

Soil profile	μ-XANES Spots	Organic P	Fe bound P		Al bound P		CaP	R-factor
			FeP	P adsorbed on Fe	AlP	P adsorbed on Al		
0–10 cm	a	21 ± 1			22 ± 1	21 ± 3		0.0008
A	b	22 ± 1		37 ± 3	19 ± 1	22 ± 3		0.0007
	c	19 ± 1		56 ± 3	17 ± 1	8 ± 2		0.0006
	d	21 ± 2		29 ± 6	36 ± 2	14 ± 4		0.002
	e	30 ± 3			56 ± 3	14 ± 3		0.0069
	f	19 ± 1		27 ± 2	54 ± 2			0.0032
	Bulk	24 ± 5		43 ± 6	15 ± 7	18 ± 3		0.0025
10–20 cm	a	7 ± 1		41 ± 3	18 ± 1	34 ± 2		0.0003
Bs	b	71 ± 3			29 ± 3			0.0321
	c	6 ± 1		15 ± 4	33 ± 2	46 ± 3		0.0009
	Bulk	23 ± 3	*28 ± 8*[1]			49 ± 8		0.0008
20–30 cm	a	9 ± 1		20 ± 5		71 ± 4		0.0011
	b	5 ± 1		32 ± 6		63 ± 4		0.0014
	c			13 ± 2	5 ± 1	82 ± 2		0.0009
	d	10 ± 2		33 ± 6		57 ± 4		0.0017
	Bulk	16 ± 5	*20 ± 8*[1]		6 ± 2	59 ± 8	6 ± 5	0.0007
30–40 cm	a	19 ± 3		15 ± 10		66 ± 7		0.0047
	b	23 ± 3		25 ± 12		52 ± 9		0.0073
	c			33 ± 3	18 ± 1	49 ± 2		0.0013
	Bulk	9 ± 7	*23 ± 9*[1]			54 ± 9	15 ± 4	0.0008
40–50 cm	a	27 ± 2		32 ± 6		41 ± 6		0.0034
	b			39 ± 6		61 ± 3		0.0018
	c			48 ± 5	32 ± 3	20 ± 4		0.0051
	d			50 ± 2		50 ± 2		0.0009
	e	17 ± 2		16 ± 4	20 ± 1	47 ± 3		0.0009
	Bulk			21 ± 7		*53 ± 8*[1]	26 ± 6	0.0008
90–100 cm	a						100	
C	*Bulk*			23 ± 3	21 ± 5		56 ± 3	0.0014

A full data set of bulk soil P K-edge probabilistic LCF is provided under research data.
[1] Probabilistic LCF could not differentiate between adsorbed and precipitated species of P bound to Fe or Al.

elements. Examination of the variation in P chemical species in spots within 600 × 600 μm of intact soil samples revealed spatial heterogeneity in P chemical compositions. However, the extent of this heterogeneity was different depending both on the species and on the soil horizon. In the C horizon at 90–100 cm depth Ca phosphates, predominantly apatite, were important at both sites. The apatite was very probably inherited from the glaciofluvial parent material, and the μ-XANES results show the apatite to occur as grains or inclusions with a locally very high P concentration causing a patch-wise, highly heterogeneous P distribution in the soil. This is in agreement with earlier research in which apatite was identified in glacial till material with electron microscopy (Nezat et al., 2008). There were, however, also signs of weathering effects in the C horizon, as part of the P were bound to Al and Fe in coatings and in pore spaces. Here, most of the P was present as phosphate adsorbed to allophane, and to a minor extent ferrihydrite.

In the more acidic B horizon, the P speciation in both soils was dominated by Al- and Fe-associated P, mostly present as phosphate adsorbed to allophane and ferrihydrite. This suggests that the originally present apatite had to a large extent been weathered since the soils were formed after the last glaciation. The P speciation appeared to be strongly influenced by podzolization processes, where Al and Fe hydrous oxides, and allophane, are precipitated in the B horizon onto which the o-phosphate ions had been strongly adsorbed. The Al and Fe hydrous precipitates are present as coatings and in the pore spaces, which has been determining for the overall spatial distribution of P in the B horizon. In the Tärnsjö soil, there was a distinct difference as concerns the spatial heterogeneity of the P speciation between the upper 20 cm of the B horizon and the lower part. In the lower part there were smaller differences between individual spots in the relative proportions of the P species; Al-bound P always predominated over Fe-bound P (Table 2). In the uppermost part of the B horizon, however, Al-bound P predominated in some spots, while Fe-bound P predominated in others. A possible interpretation is that a large part of the secondary Al and Fe precipitates in the upper B horizon were formed and precipitated *in situ*, whereas in the deeper part of the B horizon, most of the Al and Fe precipitates were derived from Al and Fe that were mobilized in upper horizons and then translocated to the lower B horizon as organic complexes before being arrested and precipitated. Although a bit speculative, this interpretation is largely consistent with the prevailing ideas of the podzolization process (Lundström et al., 2000). In the Tönnersjöheden soil, however, there was no clear such trend.

A comparison of spot-wise μ-XANES results with those of bulk XANES showed a general consistency with respect to the dominant P species modelled by LCF, especially at the top soils of the two studied profiles. As expected, the higher resolution of P K-edge XANES spectroscopy that was acquired by the use of micro-focused beam shows greater diversity of P species than what was revealed by unfocused bulk soil XANES analysis. This is particularly evident in the better detection of organic P by the spot-wise μ-XANES when compared to that of the bulk XANES. For example, while LCF of bulk soil P XANES detected no organic P at Tärnsjö below 20 cm and at Tönnersjöheden below 40 cm depth, LCF of μ-XANES however estimated the presence of organic P to range from 5 to 16 and from 10 to 27% of total P at some microsites of these depths in Tärnsjö and Tönnersjöheden, respectively (Table 2 and 3). These μ-XANES results are further supported by the estimation of organic P in the ammonium oxalate soil extract, which shows that the proportion of total P in the form of organic P decreases with depth, ranging from 4 to 6% and from 8 to 19% in Tärnsjö 20–100 cm and Tönnersjöheden 40–100 cm, respectively (Fig. S17); at these depths organic P was not detectable by bulk XANES (Fig. 1). A similar loss of sensitivity concerning the detection of organic P species by bulk XANES when compared to spot-wise μ-XANES was previously reported by Hesterberg et al. (2017).

The largest differences between the spot-wise μ-XANES and bulk XANES was in the detection of Ca-bound P. While none of the upper soil horizon (0–50 cm) microsites studied by μ-XANES showed any presence of Ca-bound P, bulk P K-edge XANES showed Ca-bound P to increase with depth from 20 cm at the two sites, ranging from 10 to 50% and from 6 to 26% of total P in the 20–50 cm depths of Tärnsjö and Tönnersjöheden, respectively (Tables 2 and 3). This mismatch is not likely due to the lack of sensitivity in Ca-P detection by the μ-XANES considering the richness in unique futures of the XANES spectra for Ca phosphates when compared to other P species (Hesterberg, 2010) and the higher resolution of μ-XANES when compared to unfocused bulk P K-edge XANES (Hesterberg et al., 2017). Rather, our results suggest that, while Al-P, Fe-P and Org-P were localized at microsites that were < 200 μm apart, the Ca-bound P microsites were highly dispersed, probably > 600 μm apart, and were therefore for the most part not captured within the volume of soil mapped in our experiment. These results conform to the soil micro-chemical reactor concept suggested by Hesterberg et al. (2011), which states that 'each soil microsite represents an independent but interconnected micro-reactor of unique chemical composition'. Our results therefore further emphasize the significance of conceptualizing the soil fabric as networks of localized chemical micro-environments.

4.2. Implications for the influence of soil weathering on P speciation and cycling

Our results of multi-elemental imaging in combination with extraction data, μ-XANES and bulk XANES analysis suggest soil weathering and podzolization as major factors governing the abundance and availability of P in the studied forest soil profiles (Table 1, Fig. 1). Although it is difficult to clearly distinguish the P K-edge XANES spectra of lithogenic primary mineral apatite from those of precipitated or biogenically formed Ca-bound P (Hesterberg, 2010), previous studies of Ca-bound P formation and stability under different pH conditions showed formation of Ca-bound P to be unlikely under acidic soil conditions and the Ca-bound P detected in our study is therefore likely to be primary apatite (Eriksson et al., 2016; Nezat et al., 2008). Results from our study show apatite to occur as dispersed (several hundred μm apart) hot spots in the subsoils as inclusions in aluminosilicates or as discrete apatite grains, whereas the content of the apatite is absent or nearly absent in the upper soil horizons due to weathering. In the subsoil of Tönnersjöheden, appreciable amounts of apatite were identified, despite the relatively low pH (4.7–4.8). In Tärnsjö, such acidic conditions prevailed only in the uppermost horizons, where no apatite was identified. The reason why the Tönnersjöheden apatite has been preserved despite the low pH is not known. Possible reasons include a low surface area of the apatite, and that the pH of the soil at this site may only have been acidified in relatively recent times (Hallbäcken and Tamm, 1986). Our results are consistent with previous observations for soils of many temperate regions in which primary apatite was found to be absent or highly depleted in the upper 40 cm of the soils (Walker and Syers, 1976; Frossard et al., 1989; Werner et al., 2017a).

The primary apatite found in the lower B and C horizons represents a pool of P that trees can potentially acquire and thus add to the biogeochemically active P pool. As noted by Yanai et al. (2005) and Akselsson et al. (2008), this apatite may be important not only for the P nutrition but also for the availability (and leaching) of Ca, due to the very high weathering rate for apatite, particularly under acidic conditions. The μ-XANES data suggest that apatite is present both as inclusions in aluminosilicate minerals and as discrete mineral grains. The relative proportion of these phases is of considerable interest as the weathering rate of the latter is probably much higher, whereas apatite inclusions in feldspar were found to persist even in a strongly acidic E horizon of a Dutch Podzol (van Breemen et al., 2000). However, to quantify the relative importance of these phases, electron microscopy is possibly better suited than μ-XRF, because of the patch-wise

distribution of apatite.

Lang et al. (2017) differentiated between relatively P-rich (often young) forest systems that "acquire" P and P-poor (often older) systems that "recycle" P. Clearly, due to the presence of apatite, it may be argued that our two soils are still acquiring P to some extent, although with time this apatite is likely to dissolve, causing the soils to approach "recycling" systems in the future. Further, Werner et al. (2017a) hypothesized that with increasing podzolisation, forest soils will increasingly recycle organic P whereas secondary Al and Fe precipitates will be dissolved because of the acid conditions and translocated downwards in the profile. According to the model of Werner et al. (2017a) our soils would be in an early stage of podzolisation. However, the B horizons of more northerly located forest ecosystems (such as our two soils) tend to have lower organic matter content at steady state than the systems studied by Werner et al. (2017a), due to lower mean annual temperature and lower N availability (Callesen et al., 2003; Olsson et al., 2009). Thus, the more advanced podzolisation stage, characterized by low pH and high organic matter content in the upper few decimetres of the soil, may therefore never be reached (unless the climate is warmer). Despite this, it seems likely that when all reactive apatite is dissolved from the root zone, the P leaching from these northern Podzols is likely to become very low, due to the presence of non-crystalline Al and Fe precipitates that conserve P within the system and facilitate slow recycling. Therefore from a practical standpoint, such a system can be regarded as a "recycling" system, despite appreciable translocation within the profile and the predominance of inorganic P forms in the soil solid phase.

5. Conclusions

- For the first time, direct micro-spectroscopic data have been provided on spatially resolved chemical speciation of P in two Quaternary forest soil profiles.
- Microscale P heterogeneity in the forest soils was strongly influenced by soil weathering and pedogenesis.
- Due to soil acidity and weathering, lithogenic apatite had been depleted from the top soils, whereas in the C horizon, apatite appeared in hot spots either as inclusions in aluminosilicate minerals or as discrete mineral grains.
- Due to podzolisation, P was most abundant in the B horizons of the soil profiles, existing predominantly as P adsorbed to non-crystalline allophane and ferrihydrite, which were present as coatings on mineral grains and in pore spaces.
- Although the O horizon was dominated by organic P in both soils, the content of organic P was low in the mineral soil, not exceeding 25% of total P on average, although the organic P content was much higher in some microsites.

Declaration of Competing Interest

The authors declare that they have no known competing financial interests or personal relationships that could have appeared to influence the work reported in this paper.

Swedish University of Agricultural Sciences is gratefully acknowledged.

Appendix A. Supplementary data

Supplementary data to this article can be found online at https://doi.org/10.1016/j.geoderma.2020.114550.

References

Akselsson, C., Westling, O., Alveteg, M., Thelin, G., Fransson, A.-M., Hellsten, S., 2008. The influence of N load and harvest intensity on the risk of P limitation in Swedish forest soils. Sci. Total Environ. 404 (2–3), 284–289.

Bain, D., Strand, L.T., Gustafsson, J., Melkerud, P.-A., Fraser, A., 2003. Chemistry, mineralogy and morphology of spodosols at two Swedish sites used to assess methods of counteracting acidification. Water Air Soil Pollut. Focus 3 (4), 29–47.

Baumann, K., Siebers, M., Kruse, J., Eckhardt, K.-U., Hu, Y., Michalik, D., Siebers, N., Kar, G., Karsten, U., Leinweber, P., 2019. Biological soil crusts as key player in biogeochemical P cycling during pedogenesis of sandy substrate. Geoderma 338, 145–158.

Beauchemin, S., Hesterberg, D., Chou, J., Beauchemin, M., Simard, R.R., Sayers, D.E., 2003. Speciation of phosphorus in phosphorus-enriched agricultural soils using X-ray absorption near-edge structure spectroscopy and chemical fractionation. J. Environ. Qual. 32 (5), 1809–1819.

Binkley, D., Högberg, P., 2016. Tamm review: revisiting the influence of nitrogen deposition on Swedish forests. For. Ecol. Manage. 368, 222–239.

Callesen, I., Liski, J., Raulund-Rasmussen, K., Olsson, M., Tau-Strand, L., Vesterdal, L., Westman, C., 2003. Soil carbon stores in Nordic well-drained forest soils—Relationships with climate and texture class. Glob. Change Biol. 9 (3), 358–370.

Church, C., Spargo, J., Fishel, S., 2017. Strong acid extraction methods for "total phosphorus" in soils: EPA Method 3050B and EPA Method 3051. Agric. Environ. Lett. 2 (1), 1–3.

Cordell, D., Drangert, J.-O., White, S., 2009. The story of phosphorus: global food security and food for thought. Global Environ. Change 19 (2), 292–305.

Eriksson, A.K., Hillier, S., Hesterberg, D., Klysubun, W., Ulén, B., Gustafsson, J.P., 2016. Evolution of phosphorus speciation with depth in an agricultural soil profile. Geoderma 280, 29–37.

Frossard, E., Stewart, J.W.B., St., Arnaud, R.J., 1989. Distribution and mobility of phosphorus in grassland and forest soils of Saskatchewan. Can. J. Soil Sci. 69, 401–416.

Frossard, E., Condron, L.M., Oberson, A., Sinaj, S., Fardeau, J., 2000. Processes governing phosphorus availability in temperate soils. J. Environ. Qual. 29 (1), 15–23.

Gundersen, P., Schmidt, I.K., Raulund-Rasmussen, K., 2006. Leaching of nitrate from temperate forests effects of air pollution and forest management. Environ. Rev. 14 (1), 1–57.

Gustafsson, J.P., Braun, S., Tuyishime, J.M.R., Adediran, G., Warrinnier, R., Hesterberg, D., 2020. A probabilistic approach to phosphorus speciation of soils using P K-edge XANES spectroscopy with linear combination fitting. Soil Systems 4 (26).

Gustafsson, J.P., Akram, M., Tiberg, C., 2015. Predicting sulphate adsorption/desorption in forest soils: evaluation of an extended Freundlich equation. Chemosphere 119, 83–89.

Gustafsson, J.P., Bhattacharya, P., Karltun, E., 1999. Mineralogy of poorly crystalline aluminium phases in the B horizon of Podzols in southern Sweden. Appl. Geochem. 14 (6), 707–718.

Hallbäcken, L., Tamm, C.O., 1986. Changes in soil acidity from 1927 to 1982–1984 in a forest area of south-west Sweden. Scand. J. For. Res. 1 (1–4), 219–232.

Hansson, K., Olsson, B.A., Olsson, M., Johansson, U., Kleja, D.B., 2011. Differences in soil properties in adjacent stands of Scots pine, Norway spruce and silver birch in SW Sweden. For. Ecol. Manage. 262 (3), 522–530.

Heindel, R.C., Lyons, W.B., Welch, S.A., Spickard, A.M., Virginia, R.A., 2018. Biogeochemical weathering of soil apatite grains in the McMurdo Dry Valleys, Antarctica. Geoderma 320, 136–145.

Hesterberg, D., 2010. Macroscale chemical properties and X-ray absorption spectroscopy of soil phosphorus, Developments in Soil Science. Elsevier 313–356.

Hesterberg, D., Duff, M.C., Dixon, J.B., Vepraskas, M.J., 2011. X-ray microspectroscopy and chemical reactions in soil microsites. J. Environ. Qual. 40 (3), 667–678.

Hesterberg, D., McNulty, I., Thieme, J., 2017. Speciation of soil phosphorus assessed by XANES spectroscopy at different spatial scales. J. Environ. Qual. 46 (6), 1190–1197.

Hesterberg, D., Zhou, W., Hutchison, K., Beauchemin, S., Sayers, D., 1999. XAFS study of adsorbed and mineral forms of phosphate. J. Synchrotron Radiat. 6 (3), 636–638.

IUSS Working Group WRB, 2014. World reference base for soil resources 2014.

International soil classification system for naming soils and creating legends for soil maps. World Soil Resources Reports No. 106. FAO, Rome.

Klysubun, W., Tarawarakarn, P., Thamsanong, N., Amonpattaratkit, P., Cholsuk, C., Lapboonrueng, S., Chaichuay, S., Wongtepa, W., 2020. Upgrade of SLRI BL8 beamline for XAFS spectroscopy in a photon energy range of 1–13 keV. Radiat. Phys. Chem. 175, 108145.

Lang, F., Krüger, J., Amelung, W., Willbold, S., Frossard, E., Bünemann, E.K., Bauhus, J., Nitschke, R., Kandeler, E., Marhan, S., 2017. Soil phosphorus supply controls P nutrition strategies of beech forest ecosystems in Central Europe. Biogeochemistry 136 (1), 5–29.

Lundström, U.S., van Breemen, N., Bain, D., 2000. The podzolization process. A review. Geoderma 94 (2–4), 91–107.

Nezat, C.A., Blum, J.D., Yanai, R.D., Park, B.B., 2008. Mineral sources of calcium and phosphorus in soils of the northeastern United States. Soil Sci. Soc. Am. J. 72 (6), 1786–1794.

Olsson, M.T., Erlandsson, M., Lundin, L., Nilsson, T., Nilsson, Å., Stendahl, J., 2009. Organic carbon stocks in Swedish Podzol soils in relation to soil hydrology and other site characteristics. Silva Fennica 43 (2), 209–222.

Prietzel, J., Klysubun, W., Werner, F., 2016. Speciation of phosphorus in temperate zone forest soils as assessed by combined wet-chemical fractionation and XANES spectroscopy. J. Plant Nutr. Soil Sci. 179 (2), 168–185.

Ravel, B., Newville, M., 2005. ATHENA, ARTEMIS, HEPHAESTUS: data analysis for X-ray absorption spectroscopy using IFEFFIT. J. Synchrot. Radiation 12 (4), 537–541.

Rivard, C., Lanson, B., Cotte, M., 2016. Phosphorus speciation and micro-scale spatial distribution in North-American temperate agricultural soils from micro X-ray fluorescence and X-ray absorption near-edge spectroscopy. Plant Soil 401 (1–2), 7–22.

Smits, M.M., Johansson, L., Wallander, H., 2014. Soil fungi appear to have a retarding rather than a stimulating role on soil apatite weathering. Plant Soil 385 (1–2), 217–228.

Solé, V., Papillon, E., Cotte, M., Walter, P., Susini, J., 2007. A multiplatform code for the analysis of energy-dispersive X-ray fluorescence spectra. Spectrochim. Acta, Part B 62 (1), 63–68.

Syers, J., Williams, J., Campbell, A., Walker, T., 1967. The significance of apatite inclusions in soil phosphorus studies. Soil Sci. Soc. Am. J. 31 (6), 752–756.

Tannazi, F., Bunker, G., 2005. Determination of chemical speciation by XAFS. Phys. Scr. 2005 (T115), 953.

Van Breemen, N., Finlay, R., Lundström, U., Jongmans, A.G., Giesler, R., Olsson, M., 2000. Mycorrhizal weathering: a true case of mineral plant nutrition? Biogeochemistry 49 (1), 53–67.

Van Reeuwijk, L., 1995. Procedures for soil analyses. International Soil Reference and Information Centre, Wageningen, Netherlands.

Van Vuuren, D.P., Bouwman, A.F., Beusen, A.H., 2010. Phosphorus demand for the 1970–2100 period: a scenario analysis of resource depletion. Global Environ. Change 20 (3), 428–439.

Vantelon, D., Trcera, N., Roy, D., Moreno, T., Mailly, D., Guilet, S., Metchalkov, E., Delmotte, F., Lassalle, B., Lagarde, P., 2016. The LUCIA beamline at SOLEIL. J. Synchrotron Radiat. 23 (2), 635–640.

Vincent, A.G., Schleucher, J., Gröbner, G., Vestergren, J., Persson, P., Jansson, M., Giesler, R., 2012. Changes in organic phosphorus composition in boreal forest humus soils: the role of iron and aluminium. Biogeochemistry 108 (1–3), 485–499.

Walker, T., Syers, J.K., 1976. The fate of phosphorus during pedogenesis. Geoderma 15 (1), 1–19.

Wallander, H., Wickman, T., Jacks, G., 1997. Apatite as a P source in mycorrhizal and non-mycorrhizal Pinus sylvestris seedlings. Plant Soil 196 (1), 123–131.

Werner, F., de la Haye, T.R., Spielvogel, S., Prietzel, J., 2017a. Small-scale spatial distribution of phosphorus fractions in soils from silicate parent material with different degree of podzolization. Geoderma 302, 52–65.

Werner, F., Mueller, C.W., Thieme, J., Gianoncelli, A., Rivard, C., Höschen, C., Prietzel, J., 2017b. Micro-scale heterogeneity of soil phosphorus depends on soil substrate and depth. Sci. Rep. 7 (1), 3203.

Wolf, A., Baker, D., 1990. Colorimetric method for phosphorus measurement in ammonium oxalate soil extracts. Commun. Soil Sci. Plant Anal. 21 (19–20), 2257–2263.

Yanai, R.D., Blum, J.D., Hamburg, S.P., Arthur, M.A., Nezat, C.A., Siccama, T.G., 2005. New insights into calcium depletion in northeastern forests. J. Forest. 103 (1), 14–20.

Yu, L., Zanchi, G., Akselsson, C., Wallander, H., Belyazid, S., 2018. Modeling the forest phosphorus nutrition in a southwestern Swedish forest site. Ecol. Model. 369, 88–100.

Zetterberg, T., Olsson, B.A., Löfgren, S., von Brömssen, C., Brandtberg, P.-O., 2013. The effect of harvest intensity on long-term calcium dynamics in soil and soil solution at three coniferous sites in Sweden. For. Ecol. Manage. 302, 280–294.

Phosphorus in 2D: spatially resolved P speciation in two Swedish forest soils as influenced by apatite weathering and podzolization.

Gbotemi A. Adediran, J.R. Marius Tuyishime, Delphine Vantelon, Wantana Klysubun, Jon Petter Gustafsson.
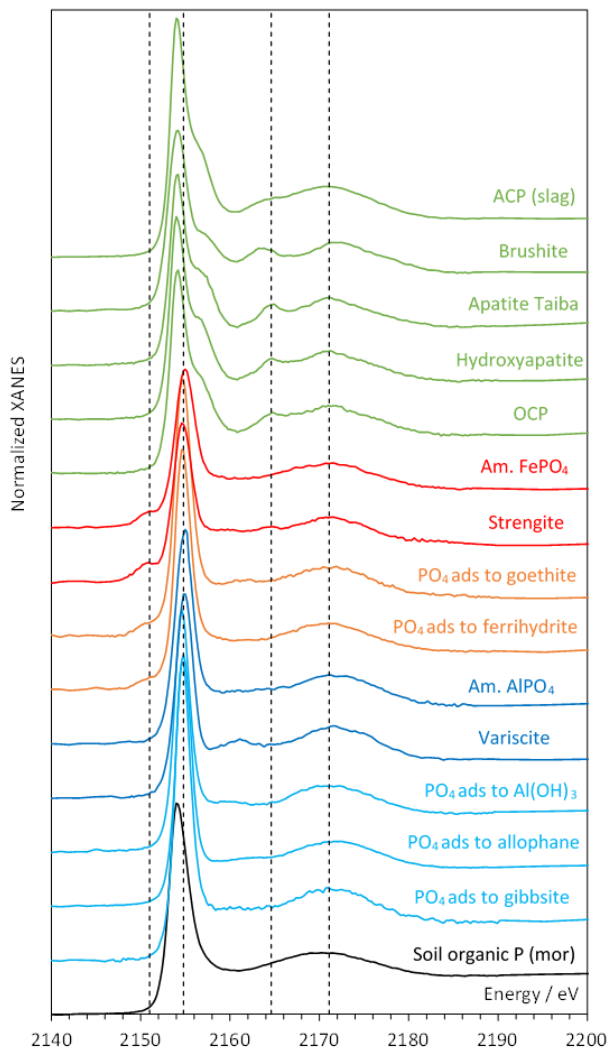
Figure S1. Stacked P K-edge XANES spectra of the 15 references used for bulk P K-edge XANES measurements of soil samples. The dashed lines correspond to the pre-edge of Fe-associated P (2151 eV), the white-line maximum energy of variscite (2154.8 eV), the first post-edge peak of hydroxyapatite (2164.6 eV), and the second post-edge peak of hydroxyapatite (2171.1 eV).
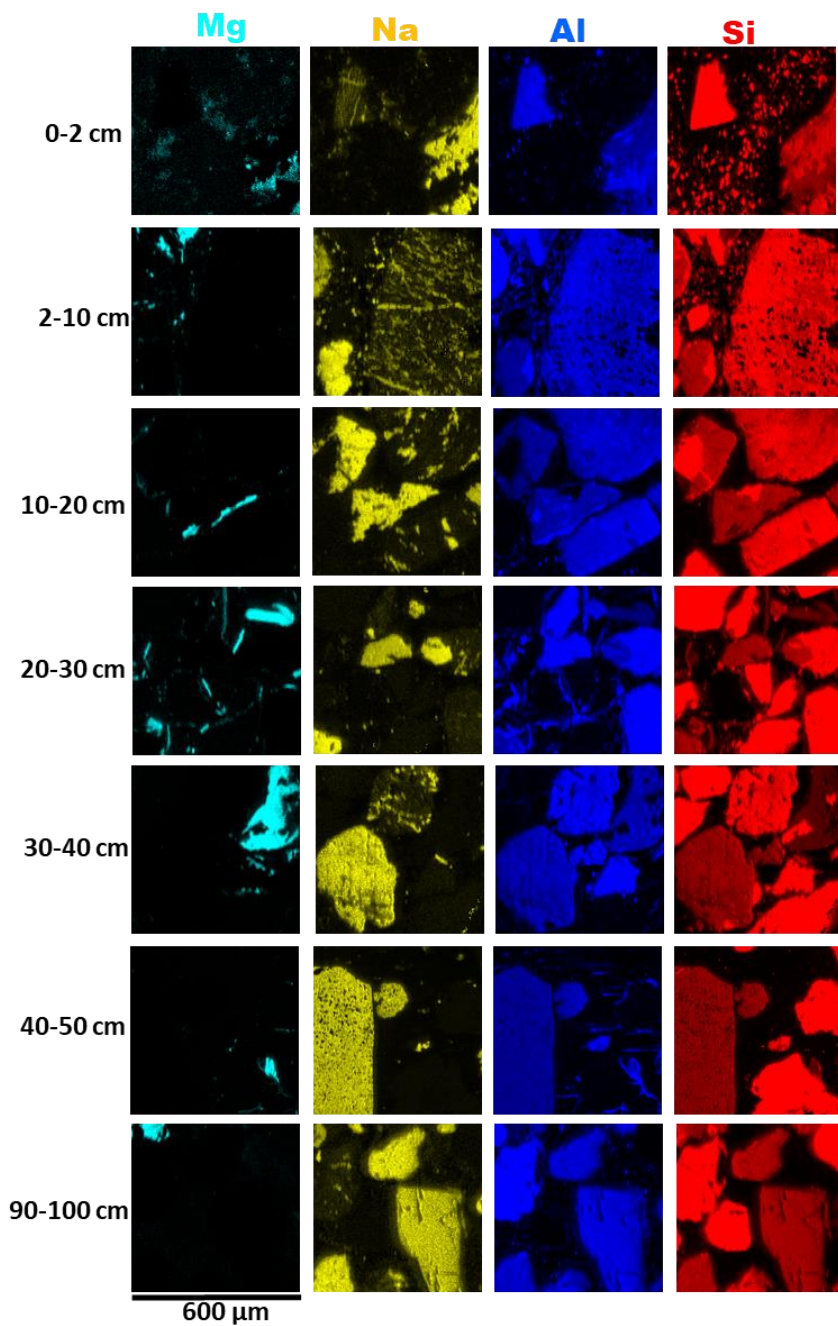
Figure S2: 2D X-ray fluorescence images of Mg, Na, Al and Si in Tärnsjö soil profile.
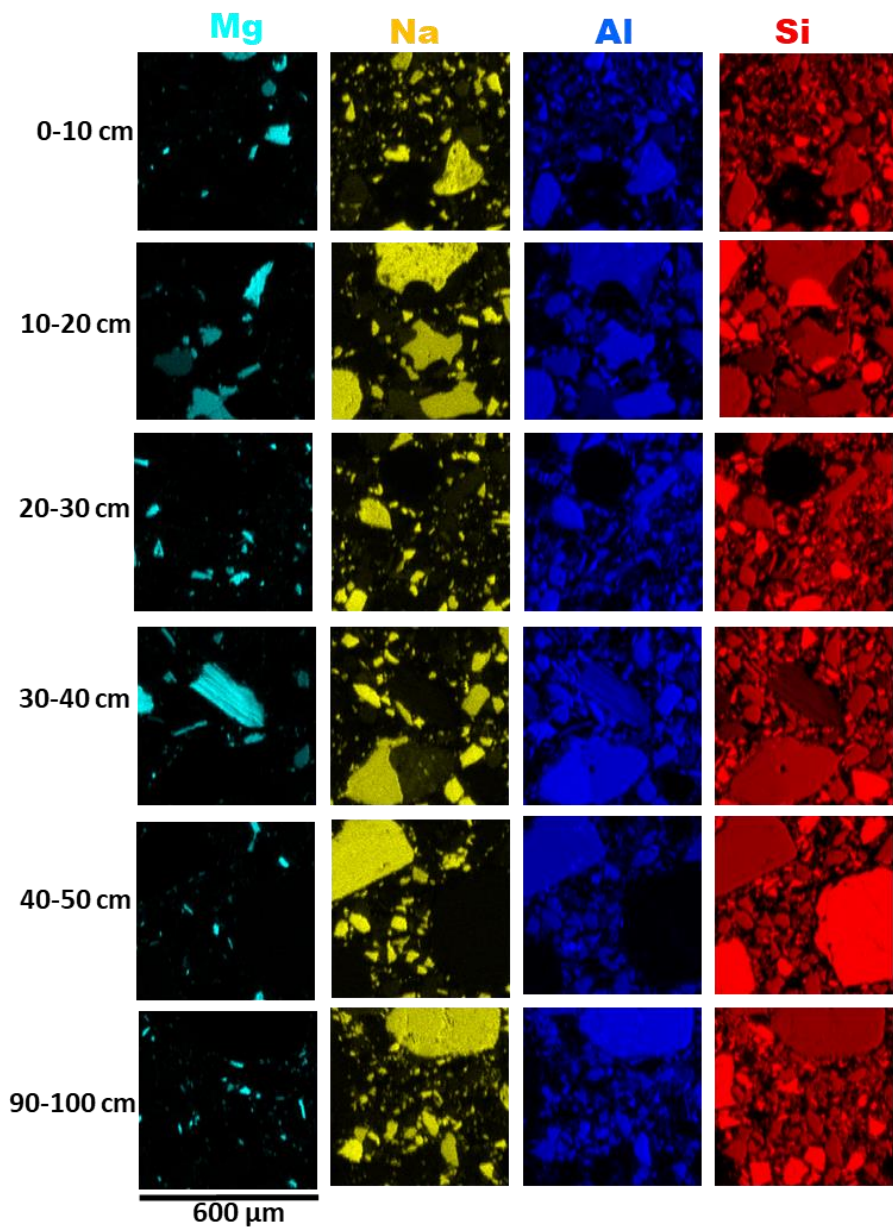
Figure S3: 2D X-ray fluorescence images of Mg, Na, Al and Si in the Tönnersjöheden soil profile.
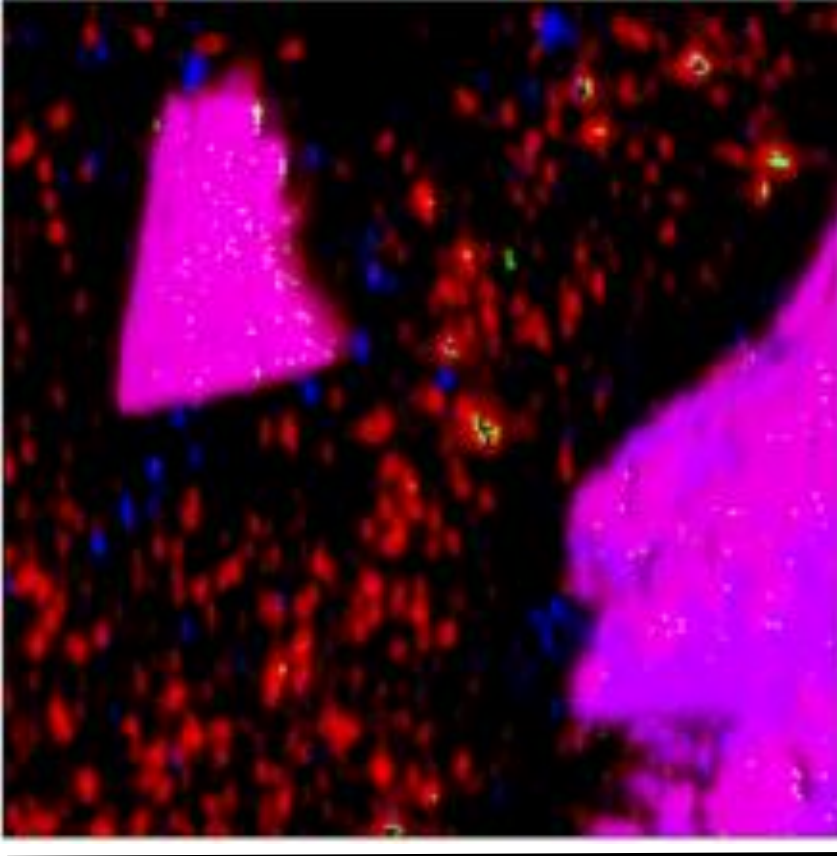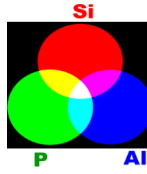
Figure S4: Spatial variation in P (green) distribution and retention at the edges, surfaces and within pore spaces of Al (blue) and Si (red) bearing soil particles in the E horizon (2-10 cm) of Tärnsjö.

Tärnsjö, 2-10 cm
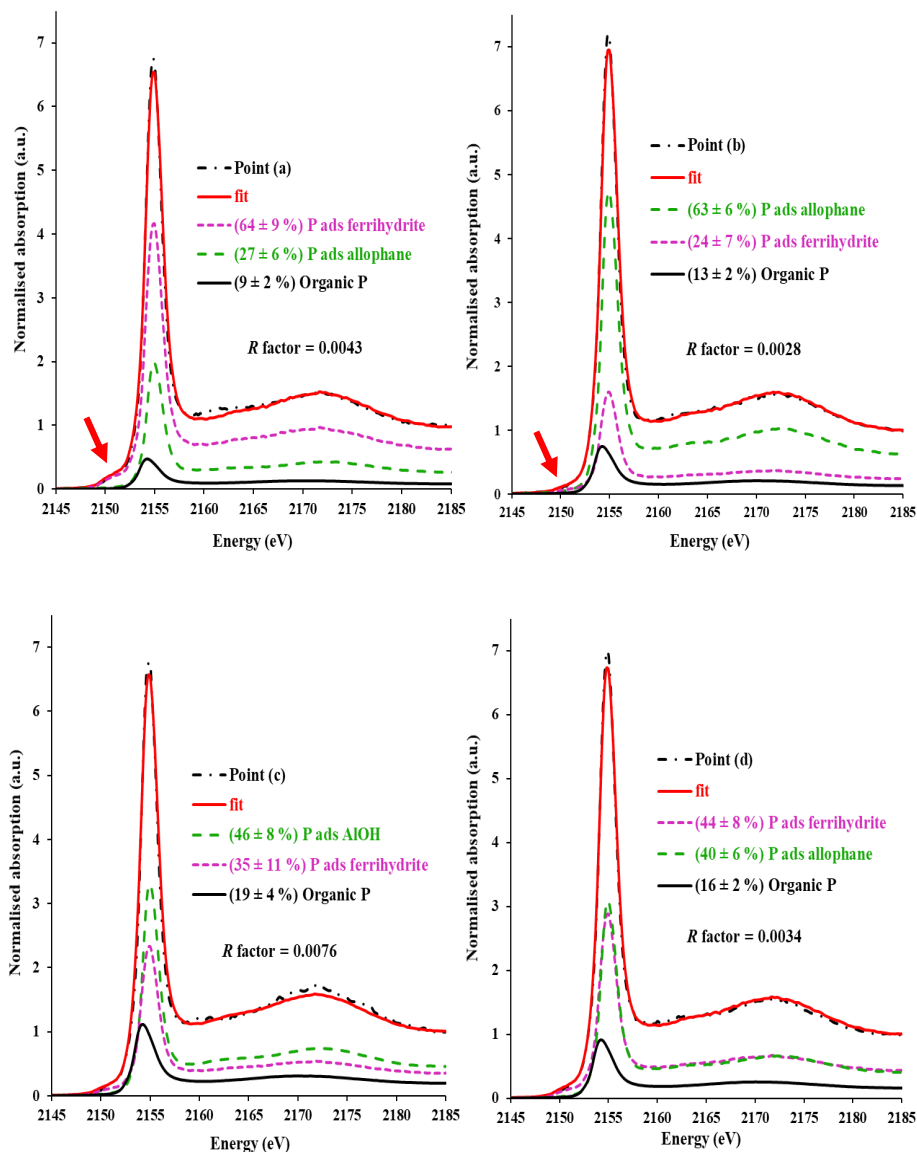
Figure S5: Linear combination fits of micro-focused P K-edge XANES spectra at selected P microsites in Tärnsjö 2-10 cm. The dotted black line shows measured data and the red line is the linear combination fit. The XANES spectra below the fits are P standards with the most significant contributions to the fit. The R factor value is a measure of the goodness-of-fit. The lower the R factor the better the fit.

Tönnersjöheden, 0-10 cm

Point (a), fit, (36 ± 4 %) P ads ferrihydrite, (22 ± 1 %) Variscite, (21 ± 3 %) P ads allophane, (21 ± 1 %) Organic P, *R* factor = 0.0008

Point (b), fit, (37 ± 3 %) P ads ferrihydrite, (22 ± 1 %) OrganicP, (22 ± 3 %) P ads allophane, (19 ± 1 %) Variscite, *R* factor = 0.0007

Point (c), fit, (56 ± 3 %) P ads ferrihydrite, (19 ± 1 %) Organic P, (17 ± 1 %) Variscite, (8 ± 2 %) P ads allophane, *R* factor = 0.0006

Point (d), fit, (36 ± 2 %) Variscite, (29 ± 6 %) P ads ferrihydrite, (21 ± 2 %) Organic P, (14 ± 4 %) P ads allophane, *R* factor = 0.002

Figure S6: Linear combination fits of micro-focused P K-edge XANES spectra at selected P microsites in Tönnersjöheden 0-10 cm. The dotted black line shows measured data and the red line is the linear combination fit. The XANES spectra below the fits are P standards with the most significant contributions to the fit. The R factor value is a measure of the goodness-of-fit. The lower the R factor the better the fit.
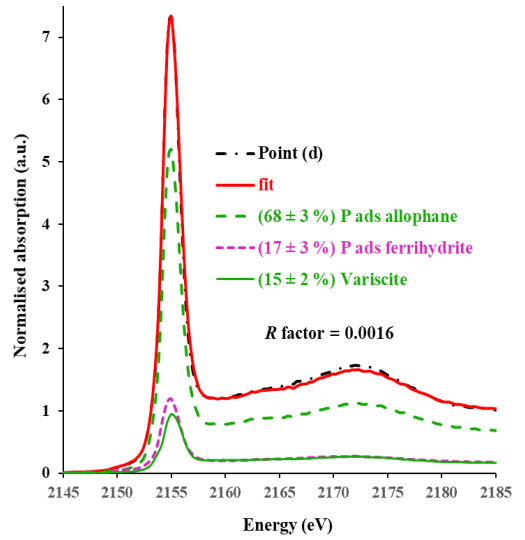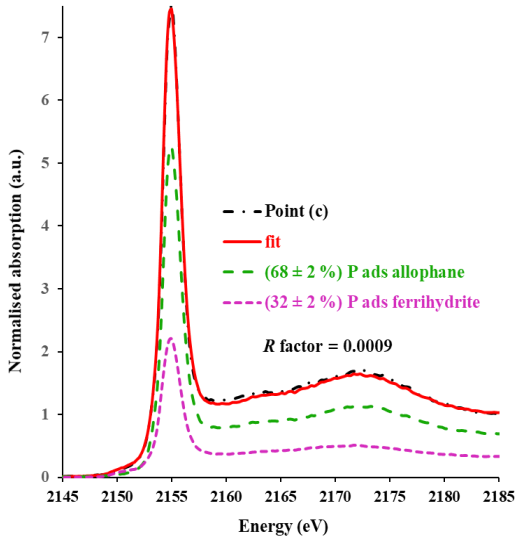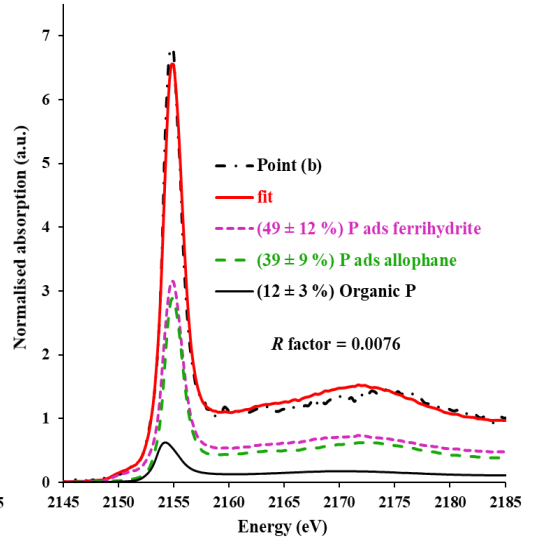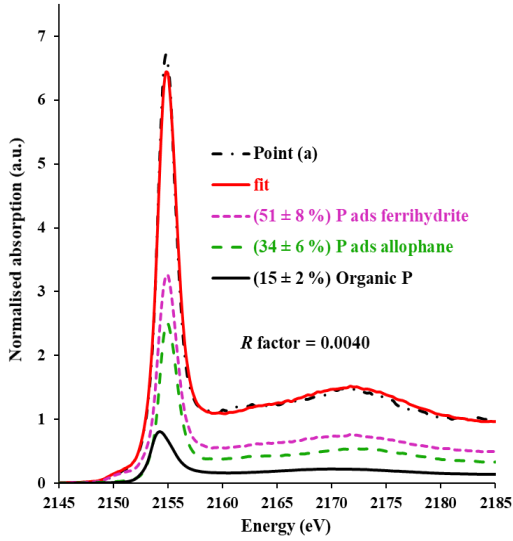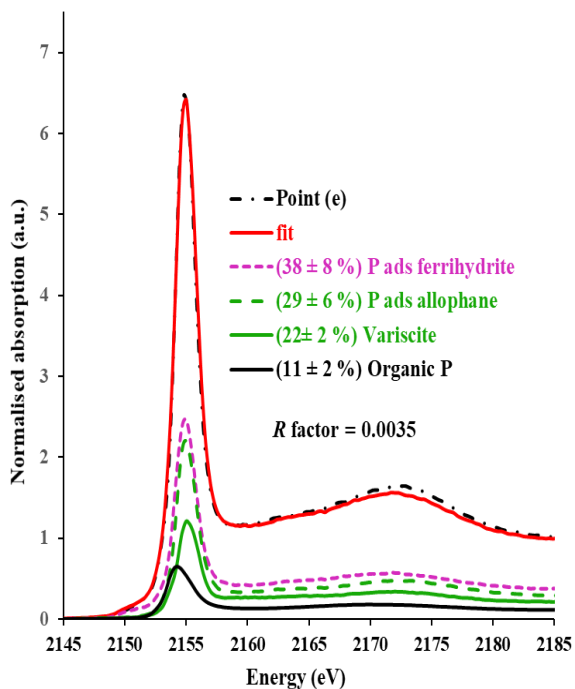
Figure S7: Linear combination fits of micro-focused P K-edge XANES spectra at selected P microsites in Tärnsjö 10-20 cm. The dotted black line shows measured data and the red line is the linear combination fit. The XANES spectra below the fits are P standards with the most significant contributions to the fit. The R factor value is a measure of the goodness-of-fit. The lower the R factor the better the fit.
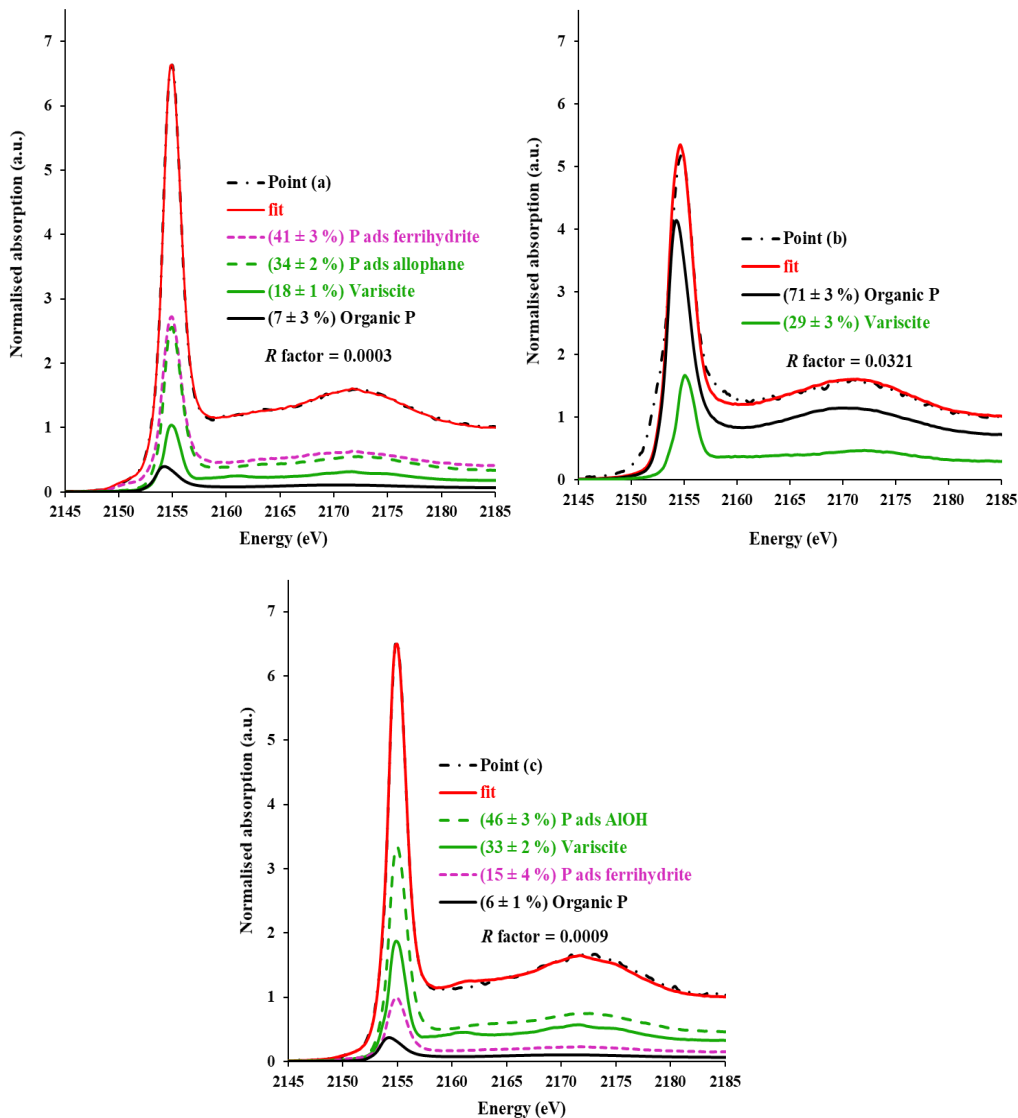
Figure S8: Linear combination fits of micro-focused P K-edge XANES spectra at selected P microsites in Tönnersjöheden 10-20 cm. The dotted black line shows measured data and the red line is the linear combination fit. The XANES spectra below the fits are P standards with the most significant contributions to the fit. The R factor value is a measure of the goodness-of-fit. The lower the R factor the better the fit.

Tärnsjö, 20-30 cm

Figure (a): Point (a), fit, (46 ± 7 %) P ads allophane, (34 ± 5 %) P ads ferrihydrite, (15 ± 2 %) Variscite, (5 ± 1 %) Organic P, *R* factor = 0.0012

Figure (b): Point (b), fit, (66 ± 3 %) P ads allophane, (29 ± 4 %) P ads ferrihydrite, (5 ± 1 %) Organic P, *R* factor = 0.0007

Figure (c): Point (c), fit, (68 ± 2 %) P ads allophane, (20 ± 2 %) P ads ferrihydrite, (12 ± 1 %) Variscite, *R* factor = 0.0005

Figure (d): Point (d), fit, (56 ± 4 %) P ads allophane, (38 ± 6 %) P ads ferrihydrite, (6 ± 2 %) Organic P
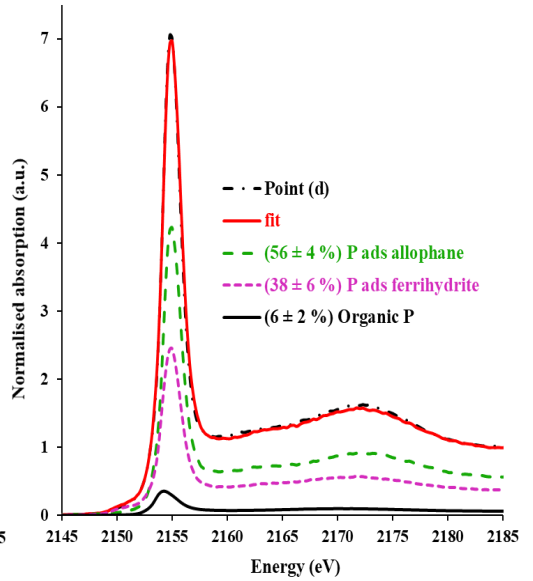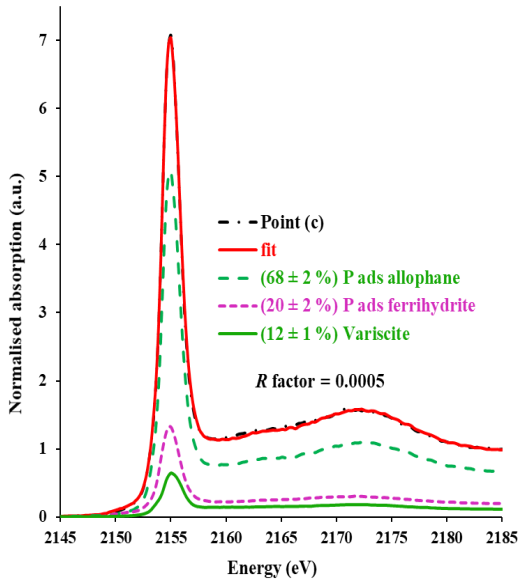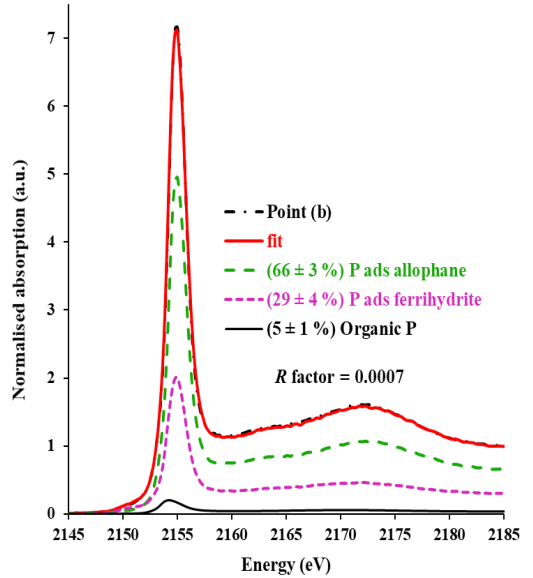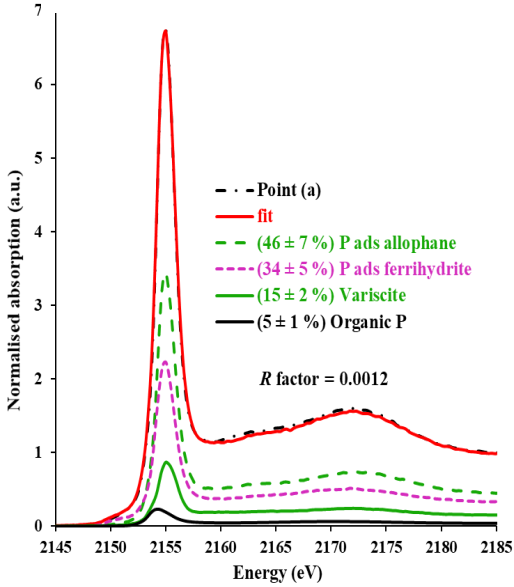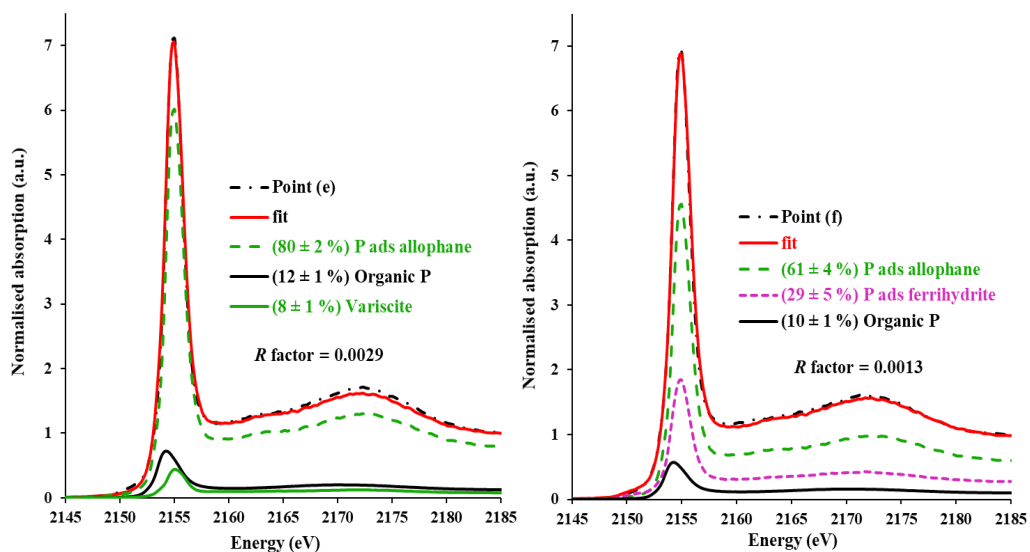
Figure S9: Linear combination fits of micro-focused P K-edge XANES spectra at selected P microsites in Tärnsjö 20-30 cm. The dotted black line shows measured data and the red line is the linear combination fit. The XANES spectra below the fits are P standards with the most significant contributions to the fit. The R factor value is a measure of the goodness-of-fit. The lower the R factor the better the fit.

Tönnersjöheden, 20-30 cm
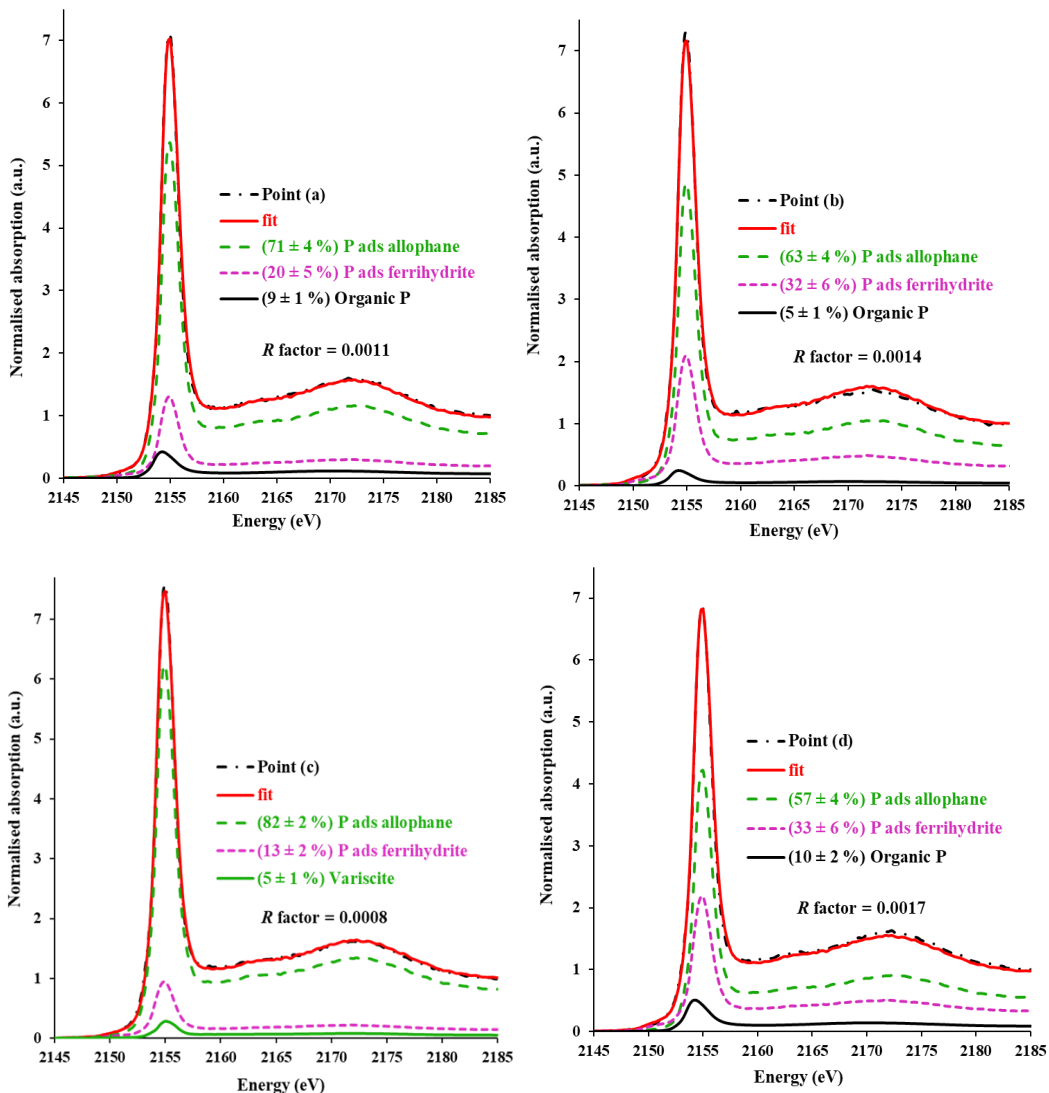
Figure S10: Linear combination fits of micro-focused P K-edge XANES spectra at selected P microsites in Tönnersjöheden 20-30 cm. The dotted black line shows measured data and the red line is the linear combination fit. The XANES spectra below the fits are P standards with the most significant contributions to the fit. The R factor value is a measure of the goodness-of-fit. The lower the R factor the better the fit.

Tärnsjö, 30-40 cm
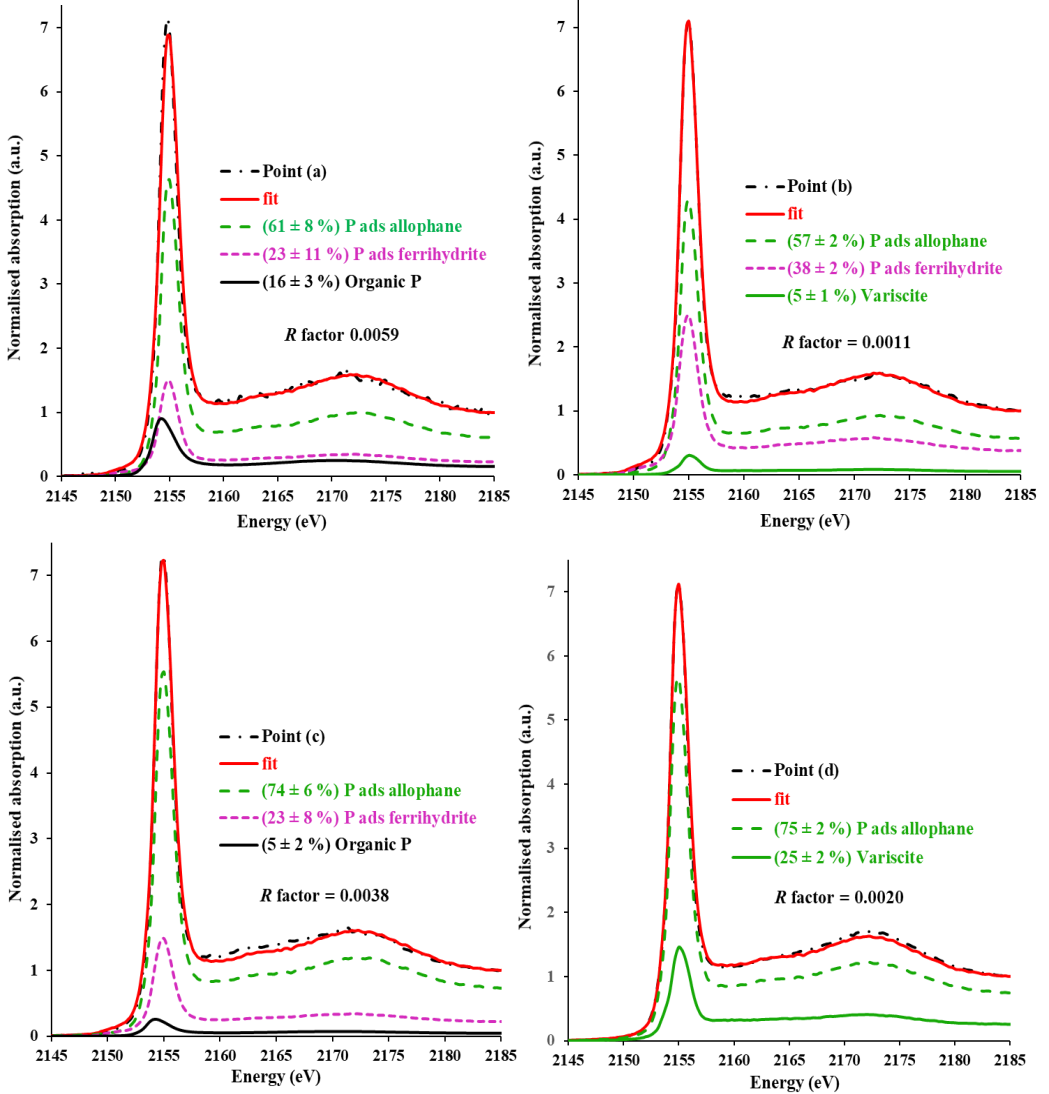
Figure S11: Linear combination fits of micro-focused P K-edge XANES spectra at selected P microsites in Tärnsjö 30-40 cm. The dotted black line shows measured data and the red line is the linear combination fit. The XANES spectra below the fits are P standards with the most significant contributions to the fit. The R factor value is a measure of the goodness-of-fit. The lower the R factor the better the fit.
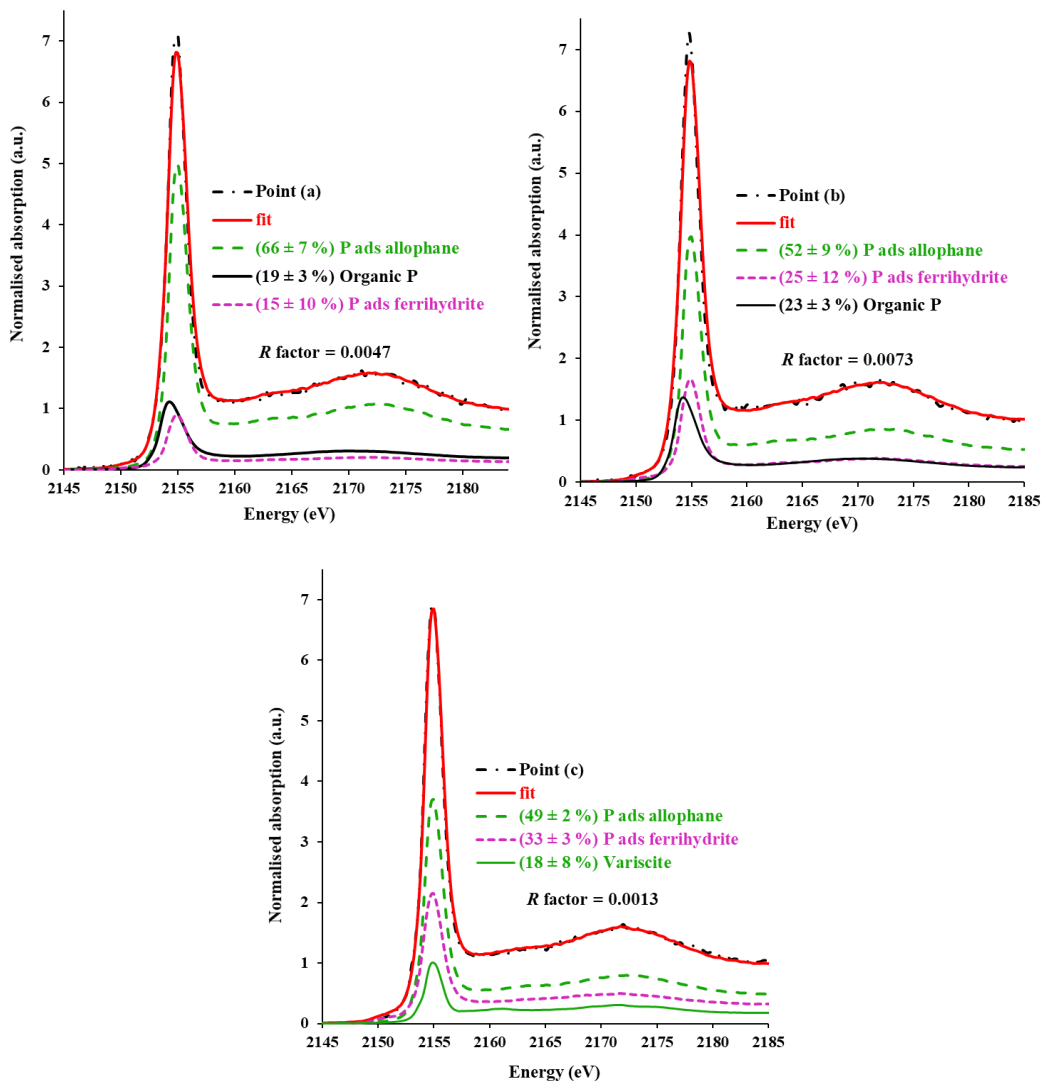
Figure S12: Linear combination fits of micro-focused P K-edge XANES spectra at selected P microsites in Tönnersjöheden 30-40 cm. The dotted black line shows measured data and the red line is the linear combination fit. The XANES spectra below the fits are P standards with the most significant contributions to the fit. The R factor value is a measure of the goodness-of-fit. The lower the R factor the better the fit.

Tärnsjö, 40-50 cm
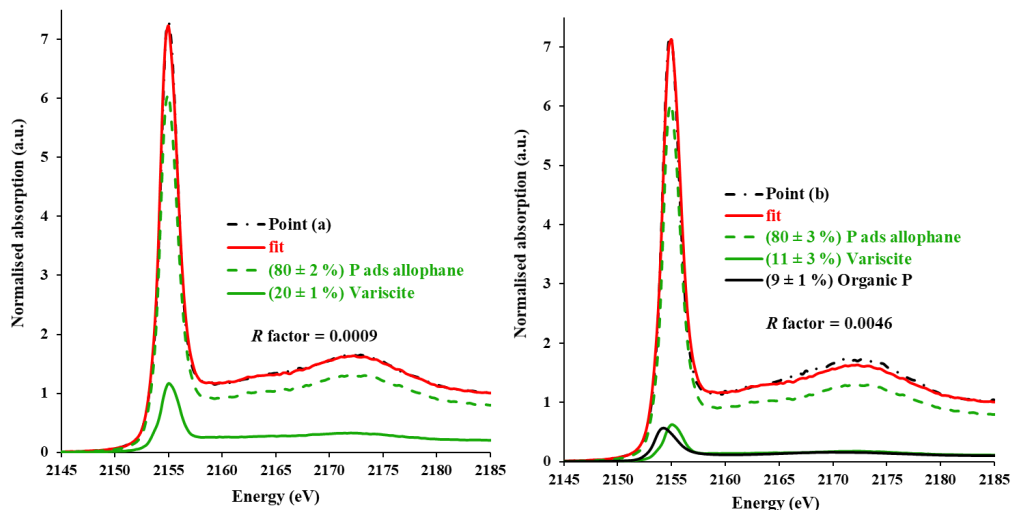
Figure S13: Linear combination fits of micro-focused P K-edge XANES spectra at selected P microsites in Tärnsjö 40-50 cm. The dotted black line shows measured data and the red line is the linear combination fit. The XANES spectra below the fits are P standards with the most significant contributions to the fit. The R factor value is a measure of the goodness-of-fit. The lower the R factor the better the fit.

Tönnersjöheden, 40-50 cm

17
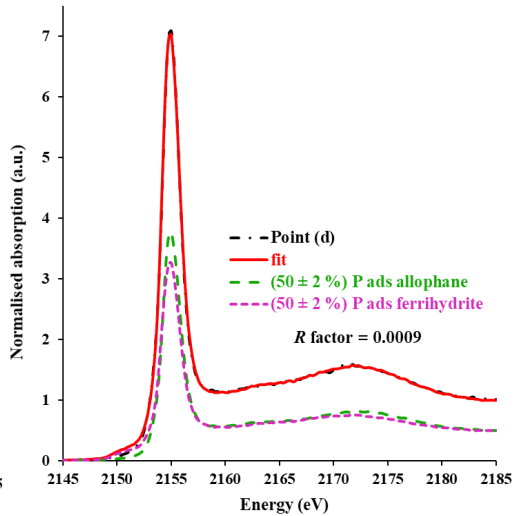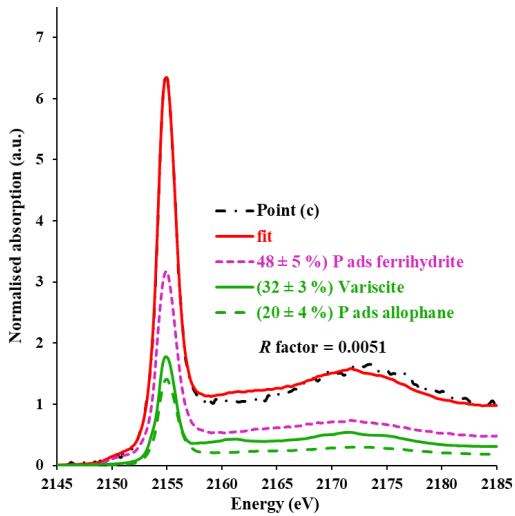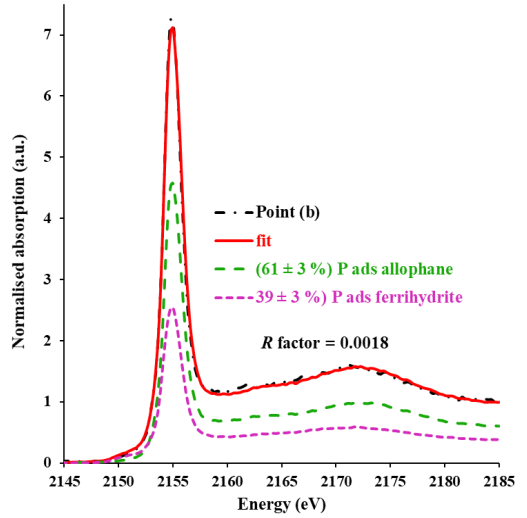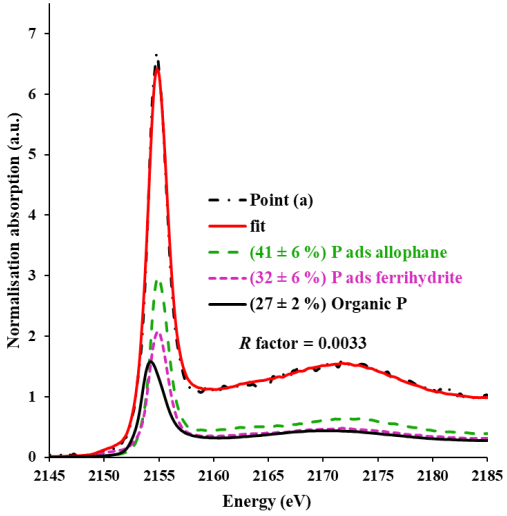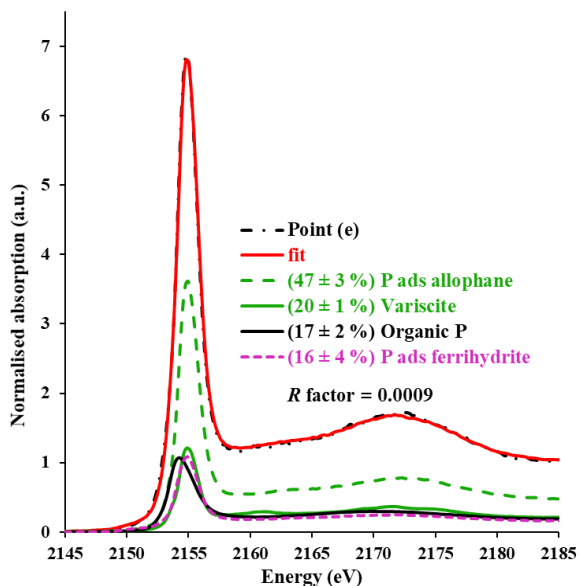
Figure S14: Linear combination fits of micro-focused P K-edge XANES spectra at selected P microsites in Tönnersjöheden 40-50 cm. The dotted black line shows measured data and the red line is the linear combination fit. The XANES spectra below the fits are P standards with the most significant contributions to the fit. The R factor value is a measure of the goodness-of-fit. The lower the R factor the better the fit.
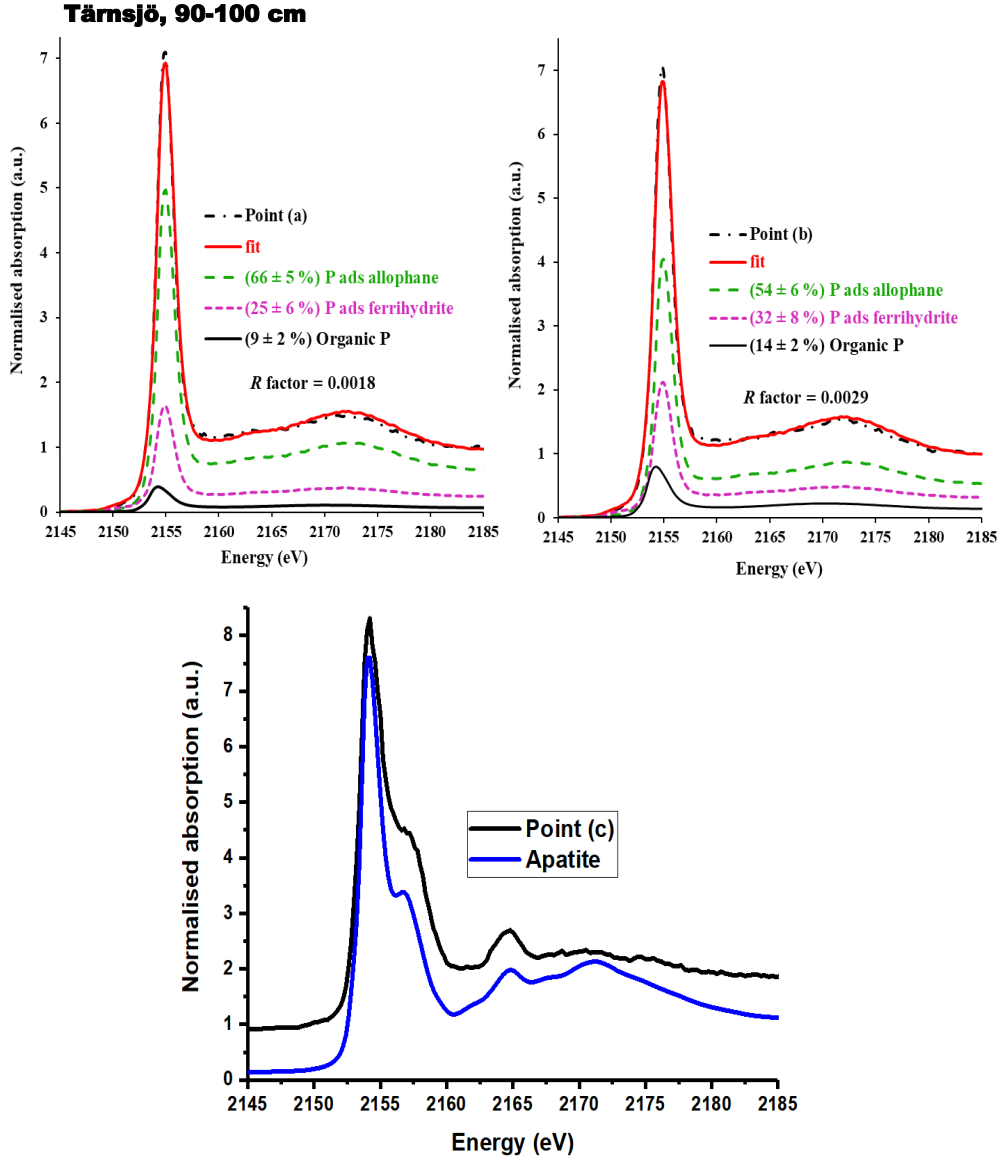
Tärnsjö, 90-100 cm

Figure S15: (a-b) Linear combination fits of micro-focused P K-edge XANES spectra at selected P microsites point a-b in Tärnsjö 50-100 cm. The dotted black line shows measured data and the red line is the linear combination fit. The XANES spectra below the fits are P standards with the most significant contributions to the fit. The R factor value is a measure of the goodness-of-fit. (c) Comparison of micro-focused P K-edge XANES spectra at selected P microsite c in Tärnsjö 50-100 cm with micro-focused P K-edge XANES spectra of mineral apatite.
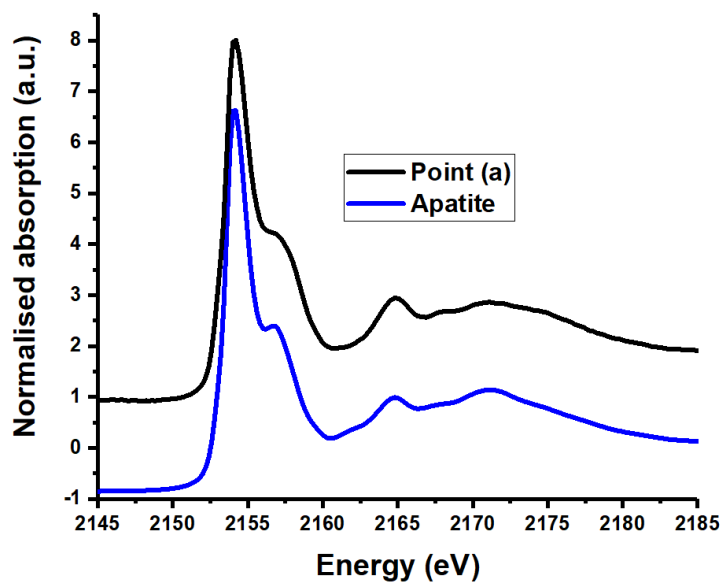
Figure S16: Comparison of micro-focused P K-edge XANES spectra at selected P microsite point a in Tönnersjöheden 90-100 cm with micro-focused P K-edge XANES spectra of mineral apatite.
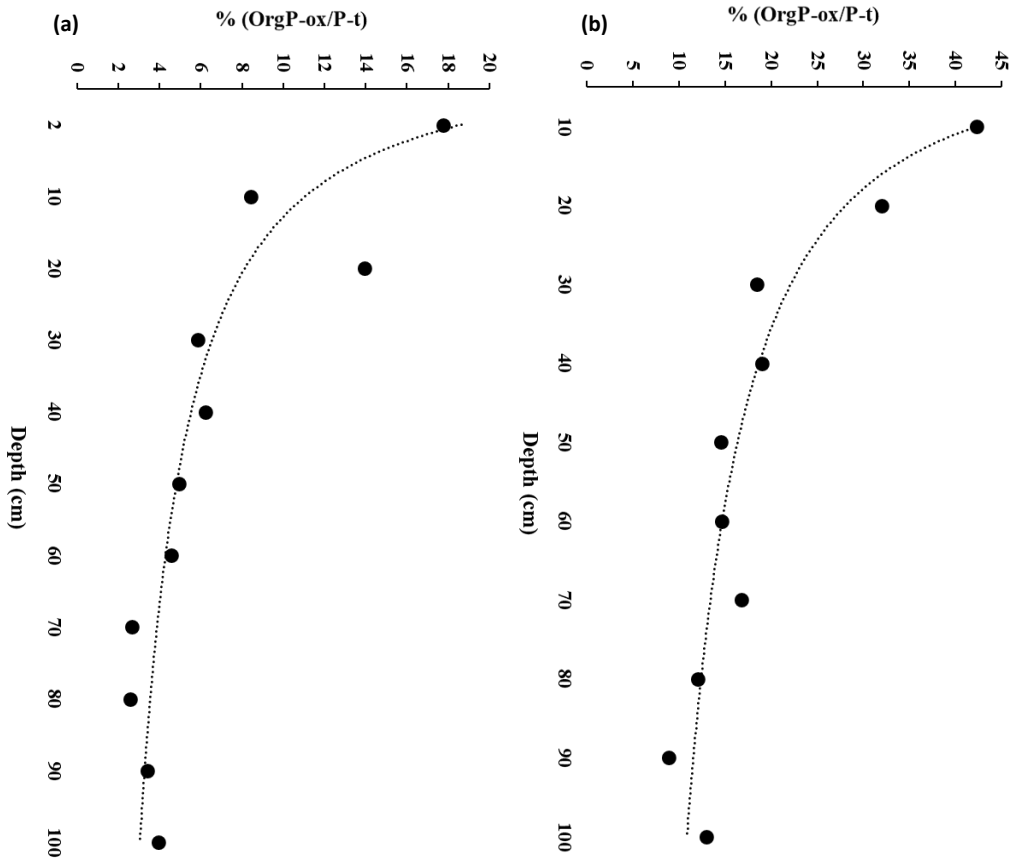
Figure S17: Proportion of total phosphorus (P-t) in the form of organic phosphorus across the soil profile at (a) Tärnsjö and (b) Tönnersjöheden.

IV

Phosphorus speciation in the organic layer of two Swedish forest soils 13–24 years after wood ash and nitrogen application

J.R. Marius Tuyishime [a,*], Gbotemi A. Adediran [a,b], Bengt A. Olsson [c], Therese Sahlén Zetterberg [a], Lars Högbom [d,e], Marie Spohn [a], Hyungwoo Lim [e,h], Wantana Klysubun [f], Camelia N. Borca [g], Thomas Huthwelker [g], Jon Petter Gustafsson [a]

[a] Department of Soil and Environment, Swedish University of Agricultural Sciences, P.O. Box 7014, SE-75007 Uppsala, Sweden
[b] UK Centre for Ecology and Hydrology, Wallingford OX10 8BB, UK
[c] Department of Ecology, Swedish University of Agricultural Sciences, P.O. Box 7044, 750 07 Uppsala, Sweden
[d] The Forestry Research Institute of Sweden – Skogforsk, 751 83 Uppsala, Sweden
[e] Department of Forest Ecology and Management, Swedish University of Agricultural Sciences, 901 83 Umeå, Sweden
[f] Synchrotron Light Research Institute, University Avenue 111, Nakhon Ratchasima 30000, Thailand
[g] Paul Scherrer Institut, Swiss Light Source, 5232 Villigen PSI, Switzerland
[h] Institute of Ecology and Earth Sciences, University of Tartu, 50409 Tartu, Estonia

ARTICLE INFO

ABSTRACT

Application of wood ash to forests can restore pools of phosphorus (P) and other nutrients, which are removed following whole tree harvesting. Yet, the mechanisms that affect the fate of ash-P in the organic layer are less well known. Previous research into the extent to which ash application leads to increased P solubility in the soil is contradictory. We combined synchrotron P K-edge XANES spectroscopy, μ-XRF microscopy, and chemical extractions to examine the speciation and solubility of P. We studied organic horizons of two long-term field experiments, Riddarhyttan (central Sweden), which had received 3, 6, and 9 Mg ash ha^{-1}, and Rödålund (northern Sweden), where 3 Mg ash ha^{-1} had been applied alone or combined with N every-three years since 2003. At the latter site, we also determined P in aboveground tree biomass. Overall, the ash application increased P in the organic layer by between 6 and 28 kg P ha^{-1}, equivalent to 17–39 % of the initial P content in the applied ash. At Rödålund, there was 4.6 kg Ca-bound P ha^{-1} (9.5 %) in the ash treatment compared to 1.6 kg ha^{-1} in the ash + N treatment and < 0.4 kg ha^{-1} in the N treatment and the control. At Riddarhyttan, only the treatment with the highest ash dose had residual Ca-bound P (3.8 kg ha^{-1}). In contrast, the ash application increased Al-bound P (p < 0.001) with up to 15.6 kg P ha^{-1}. Moreover, the ash increased Olsen-P by up to two times. There was a strong relationship between the concentrations of Olsen-P and Al-bound P (R^2 = 0.83, p < 0.001) as well as Fe-bound P (R^2 = 0.74, p = 0.003), suggesting that the ash application resulted in an increased amount of relatively soluble P associated with hydroxy-Al and hydroxy-Fe compounds. Further, there was an 18 % increase in P uptake by trees in the ash treatment. By contrast, repeated N fertilization, with or without ash, reduced Olsen-P. The lower P extractability was concomitant with a 39 % increase in plant P uptake in the N treatment, which indicates elevated P uptake in response to higher N availability. Hence, the application of wood ash increased Al-bound P, easily available P, and P uptake. N fertilization, while also increasing tree P uptake, instead decreased easily available P and did not cause a shift in soil P speciation.

1. Introduction

The forest organic layer acts as a bridge between the vegetation and the mineral soil and is important for the biogeochemical cycling of macronutrients such as phosphorus (P) (e.g. Ladanai et al., 2010; Ponge,

2003; Olsson et al., 1996). In Podzols, much of the P cycling occurs in the organic layer, where there is a tight coupling between uptake/immobilization and biological decomposition (Wood et al., 1984). In the mineral soil, a large amount of phosphate (PO_4) is adsorbed to poorly ordered, surface aluminum (Al) and iron (Fe) mineral phases (Prietzel

---

* Corresponding author.
  E-mail address: marius.tuyishime@slu.se (J.R. Marius Tuyishime).

et al., 2016; Tuyishime et al., 2022), which act as a long-term buffer of the equilibrium P concentration (Wood et al. 1984). Forest harvests remove a large amount of nutrients, which might decrease the long-term availability of P (Akselsson et al., 2008; Yanai, 1998; Yu et al., 2018). Co-limitation of P caused by excessive nitrogen (N) deposition (Hedwall et al., 2017) and increased leaching/erosion due to wildfire (Lagerström et al., 2009) may also contribute to long-term P deficiency.

In the EU, particularly in the Nordic and Baltic countries, logging residues, mainly tree tops, branches, and twigs, are used for energy production. Utilization of the residues has increased over the past decades to meet legally binding targets to reduce fossil greenhouse gas emissions (Camia et al. 2021). This has resulted in the production of hundreds of thousands of tonnes of wood ash each year, as a by-product of wood fuel combustion (Bjurström et al., 2003; Mellbo et al., 2008). In 2001, the Swedish Forest Agency issued non-binding recommendations on wood ash recycling following the harvest of logging residues to maintain long-term sustainable forest management (Swedish Forest Agency, 2019). However, only a small portion of the wood ash is brought back to the forest although the potential is much greater (Swedish Forest Agency, 2019; de Jong et al., 2017). The wood ash contains all nutrients present in the logging residues, except for N, which is lost during combustion. To reduce nutrient losses and mitigate soil acidification the wood ash can be returned back to the forest (Karltun et al., 2008; Larsson and Westling, 1998).

Prior to application, it is recommended to stabilize the loose ash (by self-hardening or formation of granules or pellets), to allow the conversion of highly reactive substances of the ash, e.g. caustic oxides, to more slowly dissolving chemical compounds (Karltun et al., 2008; Steenari and Lindqvist, 1997). To produce hardened and crushed ash, the stabilization is done by moistening the ash and allowing the mixture to harden naturally for one to three months before being crushed (Jacobson et al., 2014). Calcium (Ca), occurring mainly as CaCO$_3$, is the most abundant nutrient element (7–30 % by weight) in the hardened bottom or fly wood ash, whereas the P content is often between 0.17 and 2.2 % of the ash (Olsson and Westling, 2006, Augusto et al., 2008; Hannam et al., 2018, Steenari et al., 1999b). The P in the ash is expected to occur mostly as crystalline hydroxyapatite (Ca$_5$(PO$_4$)$_3$OH) (Steenari and Lindqvist, 1997), and thus, the dissolution of P from the hardened wood ash can be slow over time. In a column experiment, only between 15 and 20 % of the ash-P had dissolved over a period of five months (Eriksson, 1996). The solubilization of the ash-P may therefore be seen as a long-term remedy for the P depletion caused by forest harvest. In Sweden, the recommended dose of wood ash is two or three metric tons per hectare, depending on stand characteristics, with a minimum ash-P content of 7 g kg^{-1} (Swedish Forest Agency, 2019).

The interest in wood ash recycling is greatest in Europe and Canada, particularly in northern Europe (Hannam et al., 2018; Huotari et al., 2015; Pitman, 2006; Reid and Watmough, 2014; Augusto et al., 2008). Previous research has focused on the chemical composition and leaching properties of the ash (Larsson and Westling, 1998; Steenari et al., 1999a; Steenari and Lindqvist, 1997), on the effect of ash application on tree growth and nutrients uptake (e.g. Jacobson et al., 2014; Arvidsson and Lundkvist, 2002), and on the resulting soil and water acid-base status (Westling and Zetterberg, 2007). Yet only a few studies have focused on the chemistry of soil P. Further, the research results into the effect of wood ash application on the solubility of P in forest soils are contradictory (Augusto et al., 2008). For example, Jacobson et al. (2004) found an increase in the stocks of acid ammonium lactate-extractable P (P-AL) in the humus and top mineral soil five years after the application of 6 and 9 Mg ha^{-1} self-hardened, crushed wood ash to two forested sites at Riddarhyttan, central Sweden. Moreover, Nieminen (2009) observed an increase of the water-extractable PO$_4$ − P content in the humus layer following the addition of untreated wood ash (0.5 Mg ha^{-1}) in laboratory microcosms. In contrast, Clarholm (1994) observed no change in 'labile' P, as extracted by 0.5 M NaHCO$_3$ at pH 8.5 ("Olsen P"), 18 months after the application of 4 Mg ha^{-1} of granulated wood ash to a

forest stand in southern Sweden. Similarly, Fransson et al. (1999) did not observe a statistically significant difference in oxalate-extractable P two years after the application of 'slightly hardened' wood ash. Results from Finnish ash fertilization experiments show significant treatment effects on extractable P in some experiments but not in others (Saarsalmi et al., 2004; Saarsalmi et al., 2010). Probably, there are different reasons for these contradictory results. The amount of wood ash (and associated P), the timescale of the study (Jacobson, 2003; Jacobson et al., 2004; Lim et al., 2020), and the dissolution rate of ash-P (Ohno, 1992), which differs between loose and different forms of hardened ash, may all be relevant factors to consider.

Since the N content in wood ash is very low, due to the losses of N during combustion (Karltun et al., 2008), N fertilizers may be applied at the same time as the wood ash (Swedish Forest Agency, 2019). N fertilization is expected to lead to an increased tree growth and to a higher P uptake, thus increasing the P demand (Braun et al., 2010; Flückiger and Braun, 1998; Heuck et al., 2018; Talkner et al., 2015; Weand et al., 2010). It might be hypothesized that the amount of soluble P would be lower in plots treated with ash and N fertilizer compared to those treated with ash only. So far, only a few studies have been carried out that allow us to test this hypothesis. Brais et al. (2015) observed an increase in Mehlich 3-extractable P in the organic layer of a jack pine stand in Canada, which was of the same magnitude in plots treated with both wood ash and N as in those plots where only wood ash was applied, suggesting that N fertilization did not bring about a decrease in P solubility in this case. Similar observations were made in a pot experiment (An and Park, 2021). However, additional evidence is needed as well as an increased understanding of the mechanisms involved.

These dynamics could be better understood if the speciation of P in the soil is known. So far, there are only a few studies that documented changes in P speciation as a result of wood ash fertilization. When the added ash is mixed with the organic layer, e.g. by soil animals (Persson et al., 2021), or leached downward, the P in the ash (mostly apatite; Steenari and Lindqvist, 1997) interacts with organic acids or with soil constituents, e.g. metal–organic complexes (Lundström et al., 2000), causing the wood ash P to dissolve and transform into other species (Alotaibi et al., 2018; Ohno, 1992). Following the dissolution of the ash-P, the amount of P bound to Al and Fe, either as phosphates or as adsorbed surface complexes, may increase (Ohno, 1992). Moreover, the increased pH induced by the ash application stimulates the mineralization of organic matter (OM) and nitrification (Augusto et al., 2008; Cruz-Paredes et al., 2019; Lundström et al., 2003; Persson et al., 1995; Rosenberg et al., 2010). These processes are likely to affect the P speciation of the organic horizons in a complex fashion.

Synchrotron X-ray absorption near-edge structure (XANES) spectroscopy at the P K-edge is one of few available techniques to directly estimate the average composition of P species in soil (Beauchemin et al., 2003; Hesterberg, 2010; Gustafsson et al., 2020). Combining XANES spectroscopy with micro-X-ray fluorescence (μ-XRF) imaging offers complementary insight into the heterogeneous distribution of different P species, as the speciation and co-localization of P with other elements can be resolved on a μm scale (Hesterberg et al., 2017; Werner et al., 2017; Adediran et al., 2020; Vogel et al., 2021). Hence, the objective of the current study was to determine the extractability and speciation of P in the organic layer at two Swedish experimental sites in response to the application of (i) wood ash alone (at Riddarhyttan) and (ii) ash and N application (at Rödålund). In the case of Rödålund, we further relate the P responses to P uptake by trees, as reflected in the accumulation of P in aboveground biomass.

2. Materials and methods

2.1. Study sites

Two experimental sites from managed forests, in which long-term experiments with ash fertilization have been carried out, were chosen

Table 1
Characteristics of study sites.

Characteristic name	1470 Rödålund	250 Riddarhyttan
Latitude	64°08′N	59°48′N
Longitude	19°52′E	15°32′E
Altitude (m a.s.l)	209	135
MAP (mm yr^{-1})	600	730
MAT (°C)	2.3	3.9
Dominant tree species	*Pinus sylvestris*	*Pinus sylvestris*
Stand density (trees ha^{-1})	2040 ± 151	1100
Stand age (years)	52	50
Stem volume (m^3 ha^{-1})	225	150
Parent material	Wave-washed sand	Sandy sediment
Soil order[a]	Albic Podzol	Albic Podzol

[a] Soil classification according to IUSS Working Group (2014). MAP: mean annual precipitation. MAT: mean annual temperature.

Table 2
The amount and composition of wood ash.

Element	Amount and composition of wood ash					
	Rödålund[a]		Riddarhyttan[b]			
	3 Mg ash ha^{-1}			3 Mg ash ha^{-1}	6 Mg ash ha^{-1}	9 Mg ash ha^{-1}
	%	amount (kg ha^{-1})	%	amount (kg ha^{-1})		
Ca	14	420	13.7	411	822	1233
Mg	1.7	51	1.4	42	84	126
Na	0.63	18.9	1.25	37.5	75	112.5
K	6.3	189	6.4	192	384	576
P	1.6	48	0.8	24	48	72
Fe	0.64	19.2	1.1	33.3	66	99
Al	1.4	42	1.9	57	114	171
Si	8.8	264	5.6	168	336	504

[a] From Lim et al. (2020),
[b] From Jacobson et al. (2004) and Ring et al. (2006).

for this study, c.f. Table 1 for site characteristics. Rödålund (64°08′N, 19°52′E) is situated in northern Sweden, near Vindeln, Västerbotten County at 250 m above sea level. The mean annual temperature is 2.3 °C. The mean annual precipitation averaged over the last 30 years is about 600 mm, of which one third falls as snow on frozen ground from mid-October to early May. The site was planted with *Pinus sylvestris* (Scots pine) seedlings in 1996, later *Picea abies* (Norway spruce) (18 %) and *Betula spp.* (8 %) were naturally regenerated (Lim et al., 2020). The ground vegetation is dominated by dwarf shrubs, *Vaccinium myrtillus* and *Vaccinium vitis-idaea*, a ground layer of mosses, *Pleurozium schreberi* and *Hylocomium splendens* and lichens, *Cladonia spp*. The field experiment at this site began in autumn 2001 to study the long-term effects of whole-tree thinning, nutrient compensation on forest production and soil acidification. The soil is an Albic Podzol (IUSS Working Group, 2014) developed on a wave-washed sand deposit (Figure S1A). The organic layer is about 6 cm thick underlain by a strongly weathered E horizon, which is about 17 cm thick. The illuvial B horizon extends to 50 cm depth, below which there is a stony C parent material horizon (Tuyishime et al., 2022).

Riddarhyttan (59° 48′N, 15° 32′E) is located in the county of Västmanland, in the south-central part of Sweden, at 135 m above the sea level. The experiment (250 Riddarhyttan) was established in a 50-year-old pine stand. The mean annual temperature (MAT) and precipitation (MAP) are 3.9 °C and 730 mm, respectively (Table 1). The site is dominated by *P. sylvestris* and the understory vegetation is of *V. myrtillus* type (Jacobson et al., 2004). The site is a permanent recharge area for groundwater. The soil profile (Figure S1B) is classified as an Albic Podzol (IUSS Working Group, 2014) developed on sandy sediment. The organic layer is approximately 5 cm thick above a 2 cm-thick E horizon. The oxalate-extractable P, Al and Fe concentrations in this horizon are 0.03 g kg^{-1}, 0.46 g kg^{-1} and 0.54 g kg^{-1}, respectively, compared to 0.25 g kg^{-1}, 4.9 g kg^{-1} and 2.8 g kg^{-1} in the upper B horizon (unpublished data).

2.2. Field experiments and sampling

The Rödålund experiment was designed using the split-plot approach, which consists of six replicated plots (60 × 70 m^2, of which 40 × 50 m^2 is the net plot), to which each of the following four treatments was assigned: stem-only thinning, whole-tree thinning, whole-tree thinning with compensatory fertilization (150 kg N ha^{-1}), and whole-tree thinning with repeated fertilization (150 kg N ha^{-1} every third year). The total dose of N applied with repeated fertilization 2005–2019 was 750 kg ha^{-1}. The N fertilizer 'Skog-Can' was composed of ammonium-nitrate with additions of dolomite lime (5 % Ca, 2.4 % Mg) and boron (0.2 %). Each plot was split into two halves, and the wood ash (3 Mg ha^{-1}) was added to one of the subplots within plots once in 2005. When compared to stem-only thinning, whole-tree thinning did not affect soil chemical properties or the carbon stock (Lim et al., 2020). Therefore, in the present study, we used whole-tree thinning as a

reference, and whole-tree thinning with repeated fertilization as a N fertilization treatment, focusing on the interactive effect between wood ash and the repeated N fertilization (Figure S2). The self-hardened and crushed wood ash applied at this site originated from a fly ash produced at the Falun district heating plant in 2003–2004 using a boiler with a bubbling fluidizing bed and flue gas condensation (Lim et al., 2020).

The Riddarhyttan experiment was designed according to a randomized block design. The wood ash was applied in September 1995 to experimental plots (net size 30 × 30 m^2) surrounded by a buffer strip of about 5 m (Jacobson et al., 2014). The treatments of different doses from 3, 6, and 9 Mg ash ha^{-1} (3D, 6D, and 9D) (Table 2), including the control, were assigned to experimental plots arranged in three blocks (*n* = 4, c.f. Figure S2). The blocking was done based on stand parameters, the number of stems per plot, basal area, and site characteristics (e.g. soil moisture, ground vegetation, site index). For further information about the experiment, see Jacobson et al. (2004). The ash applied to this site was self-hardened, crushed wood ash, which originated from a pulp mill in Piteå, northern Sweden.

At Rödålund, sampling was done in August 2018. Ten soil cores (10 mm diameter) were collected from the organic horizon at random locations inside each subplot, excluding 2 m from the edge of the net subplot, then mixed to make a composite sample. In total, 24 composite samples from 12 plots were collected. At Riddarhyttan, samples from the organic horizons were taken in a similar way in 2019 from plots treated with wood ash and from control plots.

2.3. General chemical properties and P solubility

Undecomposed plant litter and roots were gently removed from fresh samples and sieved through an 8-mm steel mesh. The samples were then air-dried at 30 °C for seven days and sieved again (<2 mm). The pH of fresh samples was measured in deionized water using a soil: solution ratio of 1:10 (Blakemore et al., 1987). Total organic carbon (TOC) and total N (TN) contents were determined after dry combustion according to ISO 13,878 (ISO, 1998), using an elemental CN analyzer (TruMac® CN, Leco corp, S:t Joseph, MI, USA). The concentrations of oxalate-extractable Al (Alox), Fe (Feox), and P (Pox) were determined at pH 3.0 according to van Reeuwijk (1995), where Al, Fe and P were quantified with ICP-OES using a Thermo ICAP 6300 instrument. Olsen-P was determined according to Olsen (1954). Briefly, 2 g dry sample was equilibrated for 30 min with a 40 mL solution containing 0.5 M NaHCO$_3$ (with pH adjusted to 8.5). The suspension was centrifuged at 3000 rpm for 10 min and filtered before P analysis by the molybdate-blue colorimetric method using an AA500 AutoAnalyzer (SEAL analytical). Acid-digestible P or total P (TP) was determined after HNO$_3$/H$_2$O$_2$ digestion of 1 g dry material, and subsequent quantification with ICP-MS following ISO 11,466 (ISO, 1995).

2.3.1. Phosphorus stocks in the aboveground biomass and organic layer

P and N stocks in aboveground biomass at Rödålund in 2009 were estimated based on each component of tree biomass (stemwood, stem-bark, branches, and needles) and the corresponding TP concentration in tree biomass sampled in 2008, assuming that the P concentration in 2009 were the same as in 2008. The biomass of each component (stemwood, bark, branches, and foliage) was estimated using a combination of a derived site-specific allometric function for each component and repeated measurements of tree dimensions of all trees (diameter at 1.3 m, tree height, and length of live crown; Lim et al., 2020). Milled samples of each tree fraction from 2008 were analyzed for P using HNO_3/H_2O_2 digestion as above. Total N was analyzed after dry combustion as above. For Riddarhyttan, data on P stocks in biomass are not available.

For the organic horizons, the stocks of P and other elements were calculated by multiplying the element concentration ($mg\ kg^{-1}$ dry mass) with the organic layer stock ($kg\ m^{-2}$) (Table S3 and S4). For the site Rödålund, data on the organic layer stock were taken from Lim et al. (2020), while for Riddarhyttan they are presented here for the first time (Table S4).

2.4. Assessment of phosphorus speciation

2.4.1. Bulk P K-edge XANES spectroscopy

Phosphorus K-edge XANES spectroscopy was performed on bulk samples at beamline 8 (BL8) (Klysubun et al., 2020) of the Synchrotron Light Research Institute (SLRI) in Nakhon Ratchasima, Thailand. BL8 utilized synchrotron radiation generated from the SLRI storage ring with an electron beam energy of 1.4 GeV and beam flux was 3×10^{11} photons s^{-1} $(100\ mA)^{-1}$. The X-ray photon energy was scanned by an InSb (1 1 1) double crystal monochromator giving a beam flux of 1.3×10^9 to 3×10^{11} photons s^{-1} $(100\ mA)^{-1}$. The scanning was done on finely milled samples ($<50\ \mu m$) mounted in hollow and stainless-steel sample holders (2 mm thick, $1 \times 1.5\ cm^2$ with a sample window of $0.5 \times 1\ cm^2$), and covered with P-free polypropylene X-ray film (Eriksson et al., 2016). The sample spectra were recorded in the fluorescence-yield mode in the energy range of 2100–2320 eV using a solid-state 13-element Ge detector. The step size was 2 eV between 2100 and 2139 eV, 1 eV between 2139 and 2146 eV, 0.2 eV between 2146 and 2160 eV, 0.3 eV between 2160 and 2190 eV, and 5 eV between 2190 and 2322 eV. A two-second dwell time was used per energy step. Between 4 and 8 scans were collected for each sample. Collected P K-edge XANES spectra of samples were analyzed using linear combination fitting (LCF) (Ravel, 2009) using the Athena software (version 0.9.25). The LC fits were subsequently processed for uncertainty analysis using the AthenaAut software according to Gustafsson et al. (2020). Ten standards divided into six species groups were used to provide a good representation of the solid P phase in the surface horizons of acid forest soil (Gustafsson et al. 2020): 1) soil organic P (representing generic organic P from a Spodosol organic horizon), PO_4 adsorbed to Al (PO_4 adsorbed to allophane, PO_4 adsorbed to gibbsite, and PO_4-adsorbed to $Al(OH)_3$)), 3) PO_4 adsorbed to Fe (PO_4 adsorbed to ferrihydrite, PO_4 adsorbed to goethite), 4) amorphous $AlPO_4$, 5) amorphous $FePO_4$, and 6) CaP (apatite Taiba and hydroxyapatite).

To some extent, these assignments are only indicative. As previously shown, organic P species, when adsorbed to Fe and Al (hydr)oxides, result in spectra intermediate between those of soil organic P and those of PO_4 adsorbed to Al or Fe (Gustafsson et al., 2020). During LCF, energy shifts were not permitted, the sum of weights (SOW) was not forced to 1, and a maximum of four standards was allowed in the output. When presenting the results from LCF, we assumed that the sum of all weights corresponded to TP.

2.4.2. Micro-focused X-ray fluorescence spectroscopy

To provide additional support for bulk P K-edge XANES analysis, a replicate from each of the experimental treatments at Rödålund (Plot 1a:

Control - no fertilization, Plot 1b: ash fertilized, Plot 24a: N fertilized, Plot 24b: N and ash fertilized) was selected and subjected to micro-focused X-ray fluorescence imaging of multiple elements (e.g., Al, P, S and Ca), and X-ray atomic absorption near-edge structure (μ-XANES) spectroscopy at the P and S K-edges. For this analysis, representative samples from each treatment were embedded in high-purity epoxy resin. Micro-polished petrographic thin sections of 30 μm thick were prepared at TS Lab & Geoservices snc, Cascina, Italy. μ-XRF and μ-XANES spectra were collected on petrographic thin sections at the PHOENIX (Photons for the Exploration of Nature by Imaging and XAFS) beamline at the Swiss Light Source (Paul Scherrer Institut, Villigen, Switzerland), using the PHOENIX I (X07MB) branch, which used a double crystal mono-chromator (Bruker, AXS GmbH) and covers energies from 0.8 to 8 keV. For the measurements, a Si (1 1 1) crystal was employed. Focusing of the X-ray beam was performed with two Kirkpatrick-Baez (K-B) mirrors. The intensity of the incoming beam was measured as a total electron yield (TEY) signal on a Ni coated polyester foil, located *c.* 1 m upstream of the sample, at *c.* 5×10^{-7} mbar of pressure. Fluorescence signals were collected using an energy dispersive detector with four elements of silicon drift diodes (Vortex, Hitachi, California 91311, USA). To minimize X-ray absorption by air, the analysis was performed in a vacuum environment. μ-XRF images ($400 \times 400\ \mu m^2$) were acquired with a dwell time of 0.4 s per point using a step size of $3 \times 3\ \mu m^2$ at an excitation energy of 2500 eV. For each pixel, the full fluorescence spectrum was recorded, which contains the signature of all excited elements including P and some major elements known to influence its speciation (e.g. Al, Ca and S)). Here the S image serves as a proxy for OM (carbon) interactions with P (Adediran et al., 2021). Although the S imaged by μ-XRF could be both inorganic and organic, the proportion of the S that is bound by organic carbon can be resolved by S K-edge XANES analysis (Adediran et al., 2021). Further, spot-wise μ-XANES data on P and S were collected at spots with varying concentrations according to elemental imaging. P and S K-edge μ-XANES spectra were recorded in fluorescence mode over the 2.10–2.22 and 2.45–2.55 keV energy ranges for P and S respectively, with 0.2 eV steps. For each sample, up to 8 high-quality μ-XANES scans from different P spots were merged to one spectrum.

The μ-XRF spectra were dead-time-corrected and normalized to incoming beam intensities before individual elemental spectrum deconvolution. Microscale-resolution elemental maps were obtained after fitting each pixel μ-XRF spectrum using the PyMca X-ray Fluorescence Toolkit (Solé et al., 2007). The P μ-XANES spectra were subjected to probabilistic LCF analysis as described above in section 2.4.1. The S K-edge μ-XANES spectrum consists of distinct resonance peaks, whose energy positions are linearly correlated to the oxidation state of the S species (Vairavamurthy, 1998). These peaks were decomposed by Gaussian curve fitting as described in Prietzel et al. (2011), using the software package PeakFit (version 4.12, Systat Software, Inc.). The areas of the best-fitting peaks were calculated and multiplied by a weighting factor (Prietzel et al., 2011), which accounts for the variation in the absorption cross-section per unit mass with the S oxidation state (Veronesi et al., 2013; Prietzel et al., 2011).

2.5. Statistical analyses

For Rödålund, a two-factor analysis of variance was used to determine the effects of wood ash and repeated N fertilization on P speciation and solubility. A split-plot ANOVA model (Kenward-Roger's method) was applied, which consists of N as whole-plot factor and ash as sub-plot factor. Thus, the wood ash and N were added in a factorial way such that the levels of N factor (corresponding to N and no N addition) are ordered in six replicates ($n = 6$) randomly assigned to experimental plots, whereas the ash factor levels (for ash and no ash addition; $n = 12$) are randomly arranged *within* the *N*-factor in the sub-plots. The model also includes the "Ash × N" interaction between the two treatment factors, the whole-plot random error, and the regular residual error (sub-plot error). With the split-plot design, the precision of the measurement of
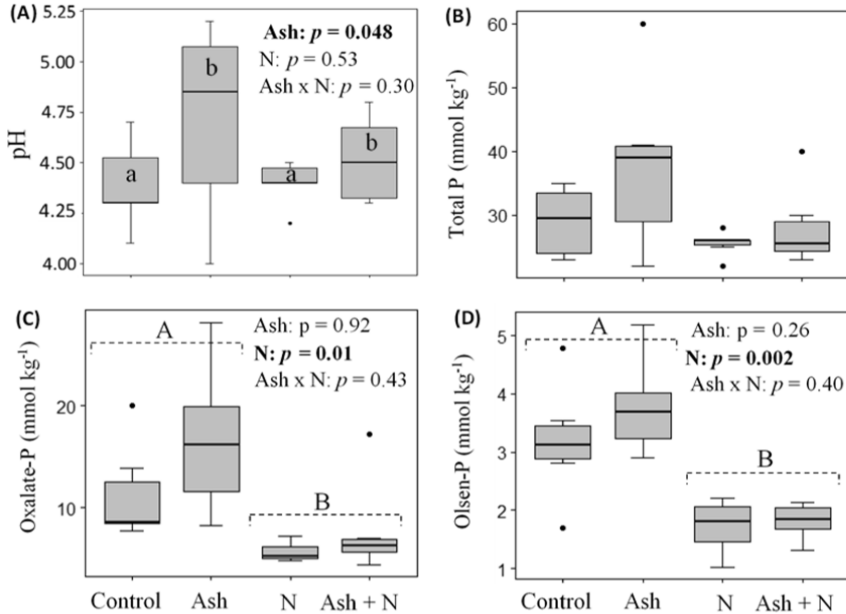
Fig. 1. pH (A), total P (B), acid oxalate-extractable P (Pox) (C), and alkaline NaHCO₃-extractable P (Olsen-P) (D) at Rödålund. The data are presented based on the interactive treatments of wood ash and N. Dissimilar upper case letters (A and B) indicate a significant difference (at $p \leq 0.05$) in the variables between repeated *N*-fertilized and control ($n = 6$). Dissimilar lower case letters (a and b) indicate a significant difference (at $p \leq 0.05$) in the variable among ash treatments ($n = 12$) within N fertilization treatment (N and no N). Boxplots without letters indicate no significant difference between or among the treatments.

Table 3
General chemical properties (mean values) of the investigated organic horizons.

Study site	Treatment	pH	Alox	Feox	TOC	N	C:Porg	N:Porg
			mmol kg^{-1}		g kg^{-1}		mol mol^{-1}	
Rödålund	Control	4.38 ± 0.1	44.1 ± 14.3	14.2 ± 4.5	332 ± 21.7	9.67 ± 0.4	1247.9 ± 94	31.5 ± 2
	Ash	4.72 ± 0.2	40.1 ± 17.7	17.8 ± 4.6	337 ± 27.6	9.50 ± 0.7	2192 ± 1045	50.7 ± 22
	N	4.4 ± 0.0	42.0 ± 14.4	14.2 ± 3.1	404 ± 14.9	14.5 ± 0.4	1621 ± 106	49.8 ± 2
	Ash + N	4.52 ± 0.1	51.4 ± 16.5	16.5 ± 4.9	399 ± 17.8	14.7 ± 0.9	1627.1 ± 136	50.7 ± 4
Riddarhyttan	0 Ash	3.93 ± 0.1	42.7 ± 11.6	18.9 ± 6.7	430 ± 9.6	11.0 ± 0.1	1835.3 ± 145	40.1 ± 2
	3 Ash	3.93 ± 0.0	50.7 ± 11.6	26.5 ± 6.7	387 ± 4.8	10.8 ± 0.3	1541.9 ± 111	36.6 ± 2
	6 Ash	4.13 ± 0.0	46.7 ± 11.6	22.0 ± 6.7	372 ± 13.8	10.5 ± 0.7	1703.9 ± 80.5	41.2 ± 1
	9 Ash	4.97 ± 0.2	64.8 ± 11.6	29 ± 6.7	284 ± 7.6	8.3 ± 0.5	1035.1 ± 121	25.9 ± 3

the sub-plot factor is increased (there are more observations) at the expense of the whole-plot factor (Gomez and Gomez, 1984). Therefore, this model fits well with the data from Rödålund as it is robust for testing the effects of wood ash. Moreover, the Tukey method (with $p = 0.05$)

using Least Squares Means (emmeans) function was used to compare estimated means of different groups of ash and N treatments.

For Riddarhyttan, a linear mixed-effect regression analysis with block and wood ash treatment (as a continuous variable) was used to

Table 4
Analysis of variance for the main effects of wood ash and N treatments and their interaction (ash × N) on soil chemical properties in organic layer at the site Rödålund. Quantitative relationship between wood ash treatment levels and soil chemical properties in the organic layer at Riddarhyttan. All effects were statistically analysed at the 0.05 significance level.

Study site	Treatment	Alox	Feox	TOC	TN	C:Porg	N:Porp
Rödålund	Ash	$p = 0.85$	$p = 0.45$	$p = 0.98$	p = 0.91	$p = 0.38$	$p = 0.40$
	N	$p = 0.77$	$p = 0.88$	**$p = 0.039$**	**p = 0.0005**	$p = 0.86$	$p = 0.46$
	Ash × N	$p = 0.64$	$p = 0.85$	$p = 0.82$	p = 0.80	$p = 0.38$	$p = 0.44$
Riddarhyttan	R²	0.14	0.08	0.86	0.55	0.36	0.38
	p value	**0.041**	0.37	**< 0.001**	**0.006**	**0.038**	**0.033**

Alox and Feox: acid oxalate-extractable Al and Fe (mmol kg^{-1}). TOC and TN: total organic carbon and nitrogen (g kg^{-1}).C: Porg and N: Porg: molar C to organic P ratio (mol/mol). N: Porg: molar N to organic P ratio (mol/mol).
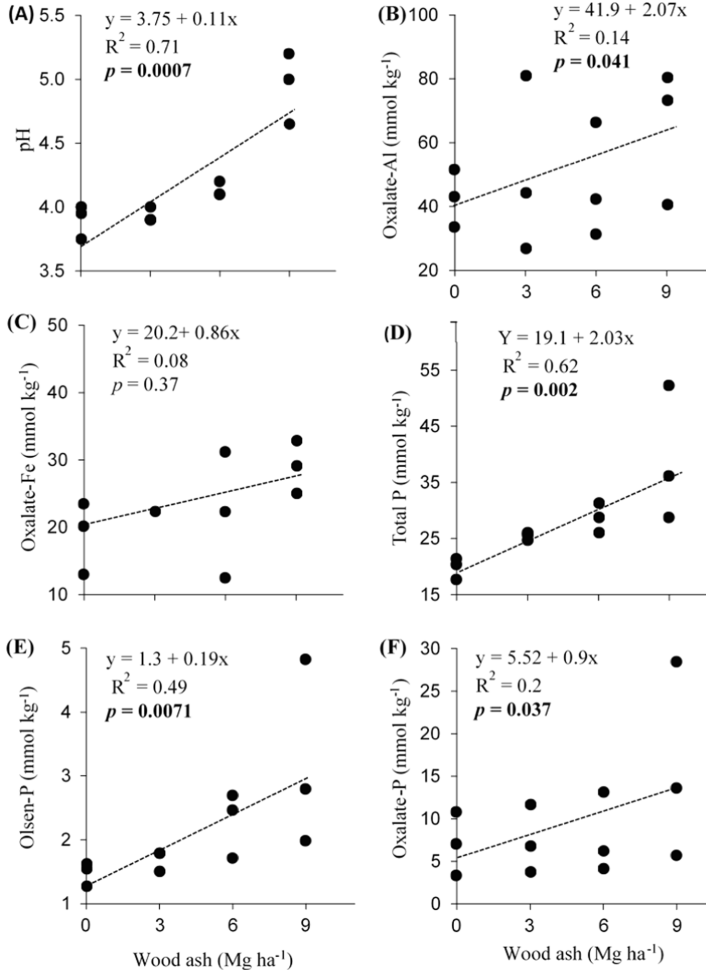
Fig. 2. Relationships between the amount of wood ash added and pH (A), acid oxalate-extractable Al (Alox) (B) and Fe (Feox) (C), total P (D), alkaline NaHCO₃-extractable P (Olsen-P) (E), and acid oxalate-extractable P (Pox) (F), in the organic layer of the Riddarhyttan site, ($n = 4$).

determine the effects of ash on extractable P and the P speciation in the organic horizon. The regression model was chosen because the ash treatments are different treatment levels of a numeric variable, i.e. the levels describe a measurable quantity of the ash. The random normality was checked by plotting the final residuals. All statistical analyses were performed using R (v.4.02).

3. Results

3.1. Soil chemical properties and P extractability as affected by treatment

At Rödålund, the application of 3 Mg ash ha^{-1} to the organic horizon increased the pH by 0.22 units compared to the control ($p = 0.048$) (Fig. 1A). Other main properties, e.g. TOC, TN, Alox, Feox, and the molar N:Porg and C:Porg ratios were not significantly affected by the ash

application (Table 3 and Table 4). The same was true for Pox and for Olsen-P, although the averages were higher in the ash treatment by a factor of approximately 1.5 and 1.2, respectively (Fig. 1). In contrast, the N fertilization of the organic horizon increased the concentrations of TOC ($p = 0.039$) and TN ($p < 0.001$) significantly (Table 3 and Table 4), but the effect on the molar N:Porg and C:Porg ratios were not significant. The concentrations of Pox and Olsen-P decreased significantly in response to N addition (Fig. 1C and 1D; $p = 0.016$ and $p = 0.002$, respectively). When considering interactive treatment groups, the Pox concentration increased from 5.6 mmol kg^{-1} in the N-only treatment to 7.8, 11.2, and 16.6 mmol kg^{-1} in the ash + N, control, and ash-only treatments, respectively (Table S2). Likewise, Olsen-P increased from 1.72 mmol kg^{-1} in the N-only treatment to 1.81, 3.18, and 3.78 mmol kg^{-1} in the ash + N, control, and ash-only treatments.

At Riddarhyttan, the pH of the organic horizon increased as a

6
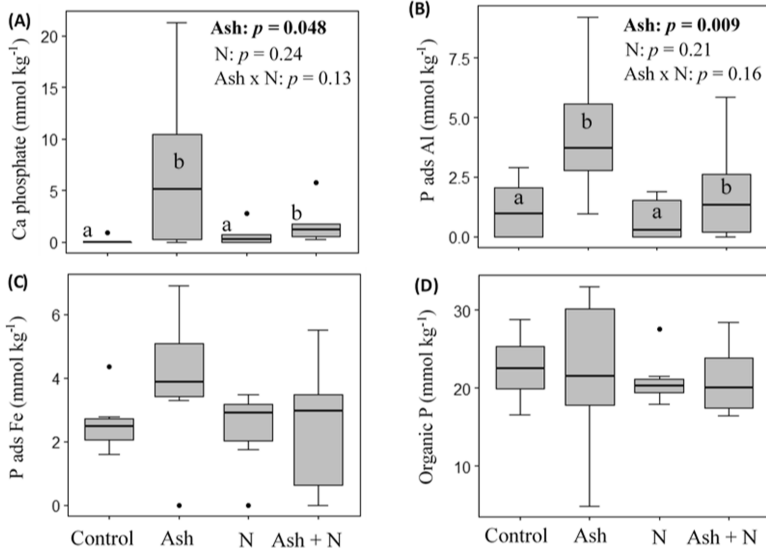
Fig. 3. Ca-bound P (A), P adsorbed on Al (B), P adsorbed on Fe (III) (C), and organic P (C) at the Rödålund site (organic layer). The data are presented based on the interactive treatments of wood ash addition and N fertilization. Dissimilar lowercase letters (a and b) indicate a significant difference (at $p \leq 0.05$) in the variable among ash treatments ($n = 12$) within N fertilization treatments (N and no N). Boxplots without letters indicate no significant difference between or among the treatments.

function of the ash dose ($R^2 = 0.71$, $p < 0.001$; Fig. 2A), whereas the concentrations of TOC and TN decreased ($p < 0.001$ and $p = 0.006$, respectively) (Table 3 and Table 4). Similarly, the molar C:Porg and N: Porg decreased significantly with increasing ash dose, but the effect was not strong; $R^2 = 0.36$ and 0.38 (Table 4). The concentrations of TP, Olsen-P, and Pox increased with increasing wood ash application rate ($p = 0.002$, $p = 0.007$, and $p = 0.037$, respectively; Fig. 2D, 2E, and 2F). The increase of the concentration of Pox was concomitant with that of Alox ($p = 0.047$ (Fig. 2B).

3.2. Bulk P K-edge XANES speciation

At the Rödålund site, the concentration of Ca-bound P (probably apatite) was found to be 4.4 mmol kg^{-1} in the wood ash treatment, which is statistically ($p = 0.048$) higher than the 0.4 mmol kg^{-1} found in the organic layers without ash (Fig. 3A). The highest Ca-bound P concentration was measured in the ash-only treatment, 7.1 mmol kg^{-1}, which was 18.7 % of the TP. In the other treatment, Ca-bound P was much lower, i.e. 1.8 mmol kg^{-1} (6.4 % of TP), 0.68 mmol kg^{-1} (2.7 % of TP), and 0.15 mmol kg^{-1} (0.5 % of TP) in the ash + N, N-only, and control treatments, respectively. It should be noted that the N fertilizer used at Rödålund contained some Ca and other base cations. The LCF of the bulk XANES spectra also showed the relative contribution of total P associated with Al and Fe not to exceed, on average, 20 % of the TP for all organic horizons from Rödålund (Fig. S3). The wood ash treatment significantly ($p = 0.009$) increased the concentration of P adsorbed on Al (P ads Al) in the ash-fertilized subplots (Fig. 3B). Considering different interactive treatment groups, the concentration of this P species decreased from 4.4 mmol kg^{-1} in the ash-only treatment to 1.9, 1.2, and 0.7 mmol kg^{-1} in the ash + N, control, and N-only treatment, respectively (Table S2). No significant difference was found for the P adsorbed on Fe (P ads Fe) concentration (Fig. 3C). Organic P (Porg) species accounted for, on average, 73.4 % of the TP concentration, thus, being the main P fraction (Fig. S3). However, there was no change in this P form caused by either treatment (Fig. 3D).

At Riddarhyttan, fertilization with wood ash did not change the contribution of Porg, which accounted for an average of 73 % of the TP

of the organic horizon (Fig. 4A and Table S4). Bulk XANES results showed that on average, 2.3 mmol kg^{-1} of Ca-bound P, which represents only 4 % of the TP, was found in the O horizons treated with 9 Mg ha^{-1}, while no Ca–bound P was measured in the remaining samples (Table S2). However, a strong quantitative relationship ($R^2 = 0.72$, $p < 0.001$) between the amount of wood ash and the concentration of P ads Al was found (Fig. 4B). Similarly, the concentration P ads Fe in the organic layer increased significantly ($p = 0.044$) with increasing ash dose although the slope was not strong ($R^2 = 0.35$) (Fig. 4C). Furthermore, there was a strong relationship between the concentration of Olsen-P and that of P ads Al ($R^2 = 0.83$, $p < 0.001$) as well as with the concentration of P-ads Fe ($R^2 = 0.74$, $p < 0.001$) (Fig. 5) in the organic layers of Riddarhyttan.

3.3. Microscale distribution and speciation of P at Rödålund

In the control (un-fertilized treatment), P was mainly co-localized with S (cyan color in Fig. 6a). Analysis of the S K-edge μ-XANES showed S to be predominantly organic-S (Fig. S5). This was further supported by P K-edge μ-XANES showing P in this treatment to be mainly organic-P (Fig. 6b). Apart from the P and S co-localizations, there was evidence of the presence of some Ca-bearing P particles in the N fertilized treatment. These micro-sized P particles were more prominent in the treatments fertilized with only ash and under combined ash and N fertilization. μ-XRF imaging of multiple elements in these treatments shows P at these particles to be co-localized with Al and Ca. Again, this observation was further supported by P K-edge μ-XANES results. The ash and ash + N fertilization treatments influenced P speciation in the organic layer by increasing the proportion of inorganic P species (mainly as Al and to a lesser extent Ca bound P) from ~ 3 % in control (unfertilized) and N fertilized treatments, to ~ 51 % and 13 % in treatments fertilized with only ash, and ash + N, respectively. Although only one replicate from the experimental treatments at Rödålund was subjected to these detailed μ-XRF and μ-XANES analyses, the result is in general agreement with the results of P speciation by bulk P K-edge analysis across all the plots at the two sites.
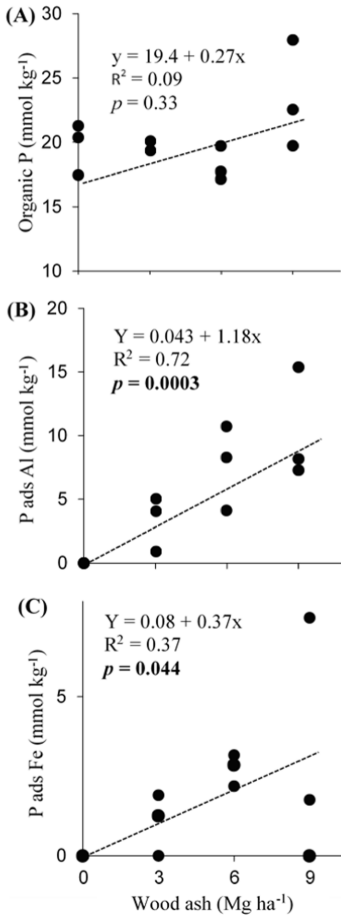
Fig. 4. Relationships between amount of added wood ash and organic P (A), P adsorbed to Al (B), and P adsorbed to Fe (C) at the Riddarhyttan site ($n = 4$).
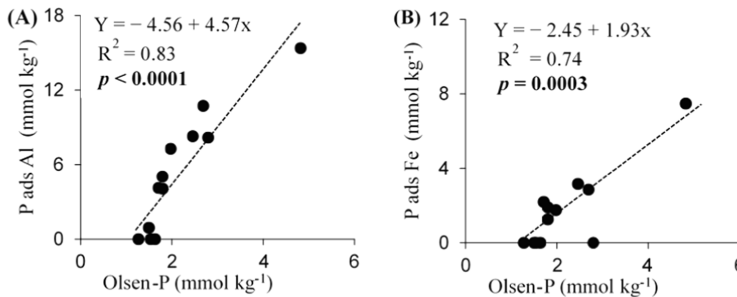
3.4. Phosphorus stocks in aboveground biomass

The results on above ground biomass at Rödålund are reported in Fig. 7. Repeated N fertilization resulted in a significant ($p = 0.012$), 39 % higher P stock in the aboveground tree biomass in 2009 compared to the control (30.4 compared to 21.9 kg P ha^{-1}). The response was due both to an increased P concentration ($p = 0.004$) in biomass and to an increased tree biomass stocks ($p = 0.015$). The P stock following ash treatment was 16 % higher than that in the control (28.0 compared to 24.2 kg P ha^{-1}, $p = 0.032$). The ash application did not affect tree biomass. There was no significant interaction between N fertilization and ash treatment ($p = 0.77$). The P-to-N ratio (by mass) of the total needle biomass was significantly increased by the P-containing ash treatment ($p = 0.002$) compared to the control under unfertilized conditions, from 10.2 % to 12.5 % (Fig. 7B). The interaction between N fertilization and ash treatment was also significant ($p = 0.01$). However, repeated N fertilization had no effect on the P-to-N ratio ($p = 0.349$; 11.6 % in N treatment, 11.1 % in control) contrary to the expected decrease in the P-to-N ratio.

4. Discussion

Application of wood ash influenced P speciation and resulted in increased P concentrations in the organic horizon. By contrast, repeated N fertilization resulted in the opposite effect on extractable P concentrations, although no effect on P speciation was found. To our knowledge, this is the first study describing the long-term effects of wood ash application on the soil P speciation at the micro- and molecular scales. Essentially, our results reinforced previous research on soil solution P chemistry, which showed that wood ash increased the P concentrations in soil solution, resulting in increased sorption of P (Ohno, 1992). Our study focused on the effects on the organic layers, as they are the most likely to be affected by forest management. A combination of μ-XRF/μ-XANES and P K-edge bulk-XANES spectroscopy revealed distinct changes in P speciation after ash application, as Al-bound P accumulated, while most of the ash-P dissolved, except for some residual Ca-bound P at high ash loads. P associated with Al and Ca was more prominent in the ash treatments, especially when ash was added alone. The presence of residual Ca-bound P is also evident from the normalized P K-edge XANES spectra of the ash treatment, which appeared to have broader white-line features and post-edge characteristics typical of Ca-bound P (Fig. S3).

The increased soil P concentrations after ash application at Riddarhyttan might have resulted from the added P in the ash. The addition of 6 and 9 Mg ash ha^{-1} (6D and 9D) corresponded to 48 and 72 kg P ha^{-1}. This led to an increase in TP in the organic layer of 10 and 28 kg P ha^{-1}, respectively (Table 5), which is equivalent to 21 and 39 % of the P content in the applied ash. At Rödålund, the application of 3 Mg ha^{-1} corresponded to 48 kg P ha^{-1}, while the organic horizon P increased

Fig. 5. Concentration of P adsorbed to Al (A) and Fe (B) as a function of the concentration of Olsen-P at Riddarhyttan across all rates of wood ash addition ($n = 4$).
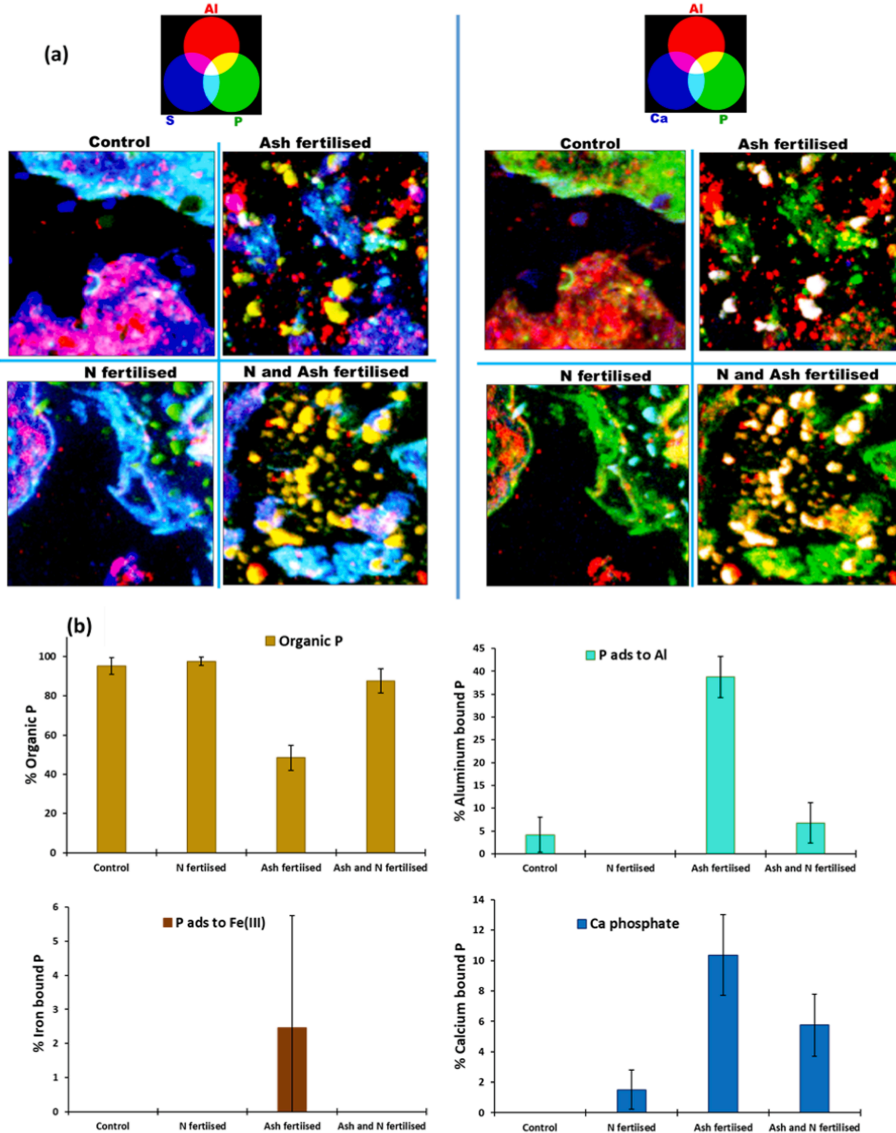
Fig. 6. (a) Synchrotron μ-XRF imaging of P (green) co-localisation with Al (red), S and Ca (blue), and **(b)** molecular speciation of P as found by linear combination fitting of P *K*-edge μ-XANES in selected experimental plots at Rödålund. The % on y-axis indicate the contribution of P species to the total P weight according to the LCF of spectra.

with 8 kg P ha^{-1}, equivalent to 17 % of the P in the applied ash. Although these percentages were similar at the two sites, XANES spectroscopy showed that the ash dissolution patterns differed at the two sites. At Rödålund, the presence of 4.6 kg P ha^{-1} as Ca-bound P in the ash-treated plots (compared to 0.1 kg P ha^{-1} in the control plots), together with the above-mentioned evidence from μ-XRF/μ-XANES, showed that the increased P concentration of the organic horizon was

partly due to the presence of undissolved ash particles in the ash-treated Rödålund plots. By contrast, Ca-bound P was absent from the plots treated with 6 Mg ash ha^{-1} at Riddarhyttan and only 3.8 kg P ha^{-1} in those treated with the highest dose, showing that the Ca-bound P of the ash had dissolved more completely at this site, perhaps due to different characteristics of the ash that was used (Table 2), and/or the longer time that had passed since ash application (24 years in Rödålund vs 13 years
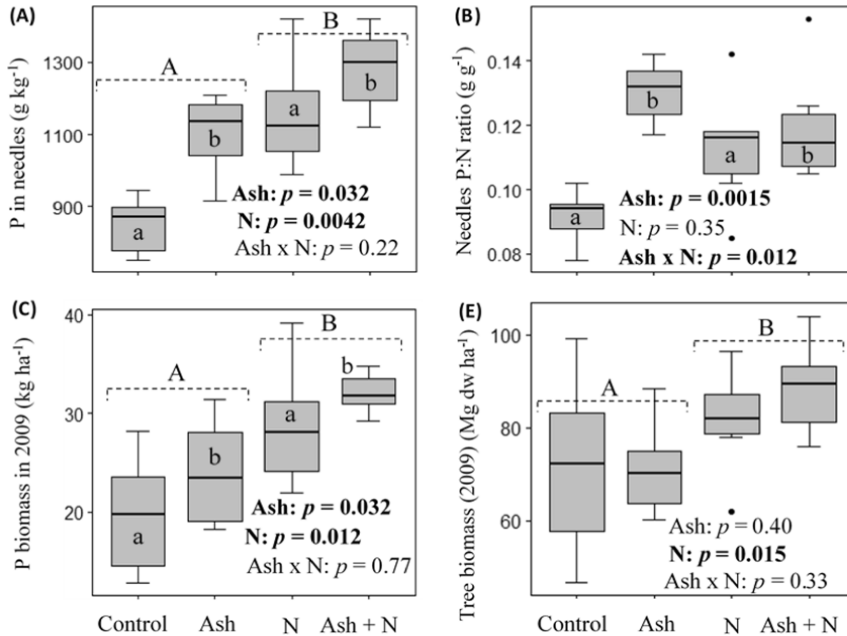
Fig. 7. The concentrations of TP in needles (A), needle P:N ratio (B), P stock in biomass in 2009 (C), and tree biomass in 2009 (D), at the site Rödålund. Dissimilar upper case letters (A and B) indicate a significant difference ($p \leq 0.05$) in the variables among the N and no N treatment ($n = 6$). Dissimilar lowercase letters (a and b) indicate a significant difference in the variable among ash treatments ($n = 12$) within N fertilization treatment (N and no N). Boxplots without letters indicate no significant difference between or among the treatments.

Table 5
Phosphorus stocks of the investigated organic horizons.

Study site	Treatment	TP	Olsen-P	Pox	Porg	P ads Al	P ads Fe	AlPO$_4$	FePO$_4$	CaP
		kg ha^{-1}								
Rödålund	Control	16.8 ± 2.2	1.97 ± 0.4	6.5 ± 1.1	13.2 ± 1.9	0.8 ± 0.4	1.5 ± 0.2	0.7 ± 0.7	0.4 ± 0.4	0.1 ± 0.1
	Ash	20.5 ± 2.7	2.2 ± 0.4	9.6 ± 2.1	10.6 ± 1.3	2.1 ± 0.5	2.9 ± 1.3	0.0 ± 0.0	0.3 ± 0.3	4.6 ± 2.2
	N	14.3 ± 0.7	0.95 ± 0.1	3.2 ± 0.3	11.8 ± 0.8	0.3 ± 0.2	1.3 ± 0.3	0.1 ± 0.1	0.2 ± 0.2	0.4 ± 0.3
	Ash + N	17.9 ± 1.6	1.17 ± 0.1	4.97 ± 1.2	13.5 ± 1.1	1.3 ± 0.6	1.6 ± 0.6	0.0 ± 0.0	0.3 ± 0.4	1.6 ± 0.5
Riddarhyttan	Control	30.2 ± 3.0	2.3 ± 0.2	10.1 ± 2.3	30.0 ± 2.9	0.0 ± 0.0	0.0 ± 1.9	n.d	n.d	0.0 ± 0.0
	3 Ash	36.1 ± 7.0	2.4 ± 0.5	11.6 ± 5.3	29.1 ± 4.2	5.1 ± 2.1	1.73 ± 1.0	n.d	n.d	0.0 ± 0.0
	6 Ash	40.2 ± 5.7	3.3 ± 0.7	11.2 ± 4.2	25.1 ± 1.6	11.2 ± 3.5	3.9 ± 1.9	n.d	n.d	0.0 ± 0.0
	9 Ash	58.8 ± 14.1	4.8 ± 1.6	24.5 ± 11.7	34.3 ± 2.5	15.6 ± 4.9	5.0 ± 3.8	n.d	n.d	3.8 ± 3.8

n.d: not detectable by the bulk P K-edge XANES.

in Riddarhyttan). Instead at Riddarhyttan, the concentration of P bound to Al and to Fe increased, with 15.6 and 5.0 kg P ha^{-1} respectively, in the highest ash dose treatment. Increased dissolved P concentrations and a higher pH, allowing hydrolysis of organically complexed Al and Fe, could have shifted the chemical equilibrium towards P adsorption, as shown by a strong relationship between Olsen-P and P ads Al/Fe. Although Al- and Fe-bound P increased also at Rödålund after ash treatment, the increase was much smaller (Table 5). Apart from the difference in ash quality, the variations of P responses between the two sites may also be explained by the higher content of oxalate-extractable Fe and Al in the Riddarhyttan organic horizons, in combination with the higher Fe and Al content of the applied ash. This may have provided a larger number of adsorption sites for P. Taken together, our results show that the wood ash application increased the P levels in the organic

horizons and that the increase was mainly due to labile P bound to Al and Fe phases, which may be a source of plant-available P (Amadou et al., 2022).

We observed a decrease in TOC, TN as well as molar N:Porg and C: Porg ratios in response to ash application at the site Riddarhyttan. A reason for this might be increased OM decomposition by the pH-raising effect of the ash (Persson et al., 2021; Rosenberg et al., 2010). By contrast, Porg was unaffected by ash application, at both sites. There could be different reasons for this. It might be that the ash application increased decomposition, but that the turnover time of phosphorylated organic compounds is longer than that of non-phosphorylated organic compounds, and hence no effect on Porg is visible yet. Second, and more likely, it could be that the formation of Porg increased in response to ash application as the soil biota formed Porg from ash-derived P stimulated

by the pH in the ash-amended organic horizons (Augusto et al., 2008; Persson et al., 2021; Persson et al., 1995). It may also be that apatite dissolution from the ash resulted in increased fungal biomass (Forsmark et al., 2021; Mahmood et al., 2003), which likely contributed to Porg, and thus kept this pool unaffected. The lack of an effect of N application on Porg can also be explained by an increased demand for P by biota in response to N addition, which favors P immobilization by ectomycorrhizal fungi (Forsmark et al., 2021; Heuck et al., 2018). This is consistent with the molar N:Porg and C:Porg (based on organic P fraction), which were unaffected by the long-term, repeated N fertilization (c.f. Table 3 and Table 4).

The TP, Pox, and Olsen-P stocks all declined in response to repeated N fertilization, which confirms previous studies about the effect of N addition on organic horizons in temperate regions, including Scandinavian coniferous forests (Heuck et al., 2018). The increased N availability due to N addition is expected to enhance P uptake by plants and potentially microorganisms, which reduces easily available P. Hence, any available P from organic sources is likely efficiently immobilized by microorganisms (Heuck et al., 2018; Pistocchi et al., 2018). The combination of ash and N fertilizers also nearly halved the easily available P stock (Olsen-P) compared to the organic horizons that only received ash (Table 5), despite the additional input of P from the ash. This emphasizes the effect of N fertilizer on plant P uptake.

The results concerning P stocks in aboveground biomass demonstrated that both N fertilization and ash addition increased tree P uptake (based on the 2009 data). The ash treatment also increased the foliage P/N ratio in contrast to the N treatment, where this ratio remained unaffected. The ratio increased from 9.2 % in the control to 13 % in ash treatment. In both cases, the P concentration was near or above the optimum level (Knecht and Göransson, 2004). The effect of the ash treatment was expected owing to the high P content of the ash. Despite the increase in P uptake, the ash treatment had no effect on tree growth (Fig. 7D), regardless of N fertilization. This suggests, first, that the increased P stocks in biomass of this treatment reflected a higher P availability, not a higher demand, and second, that the tree growth was not limited by P at the site. On the other hand, the significantly higher P uptake and tree growth following N fertilization likely explain the reduced concentrations of available P. The maintained P/N ratio of foliar biomass in N treatment indicates a strong capacity of the Rödålund stand to increase P acquisition in parallel with increased N uptake. This finding deviates to some extent from the results of other long-term fertilization experiments in Nordic forests, including sites that are very close to Rödålund (Palmqvist et al., 2020; Tamm et al., 1999; Binkley and Högberg, 2016). According to the latter findings, the N addition increased tree growth and P uptake (as in Rödålund) but resulted in lowered P/N ratios in needles, and hence complementary additions of P and other elements were needed for sustained production. From a forest production perspective, the addition of P from the wood ash in Rödålund showed no additive effect. However, wood ash treatment in combination with N resulted in higher P uptake (+12.4 kg ha^{-1} increase) than in N-only treatment (+9 kg ha^{-1}), indicating that adding hardened wood ash can ameliorate N-induced P deficiency while maintaining tree growth, more so after multiple forest cycles. Hence, one important result of this study is that wood ash did increase plant-available P forms in the soil and increased P uptake in trees regardless of the N fertilization treatment. This result is probably general to a wide group of soil and forest conditions.

5. Conclusion

This study provides in-depth insights into the fate of added P from self-hardened wood ash to the forest organic horizon and how this influences soil P, organic carbon, and nitrogen as well as P uptake by trees. Decades after wood ash applications, there were still undissolved Ca phosphates, albeit in small quantities, which very likely were derived from the ash. As the ash dissolved, the P solubility and P bound to Al and

Fe increased, while the organic P pool remained unchanged. The high solubility of P in the ash-fertilized plots increased the P uptake by plants, as reflected by the higher P stock in aboveground biomass. The ash application may also have resulted in a P availability that was higher than required by the trees. Long-term, repeated N fertilization significantly increased P uptake by trees and decreased levels of available P in the organic horizon. In summary, the application of wood ash increased Al-bound P and increased the levels of easily available P as well as P uptake by trees.

CRediT authorship contribution statement

J.R. Marius Tuyishime: Conceptualization, Methodology, Software, Formal analysis, Investigation, Writing – original draft, Writing – review & editing, Visualization. **Gbotemi A. Adediran:** Software, Investigation, Writing – review & editing, Visualization. **Bengt A. Olsson:** Conceptualization, Methodology, Validation, Resources, Formal analysis, Writing – review & editing, Supervision. **Therese Sahlén Zetterberg:** Validation, Writing – review & editing, Supervision. **Lars Högbom:** Validation, Resources, Writing – review & editing. **Marie Spohn:** Validation, Writing – review & editing, Supervision. **Hyungwoo Lim:** Validation, Formal analysis, Writing – review & editing. **Wantana Klysubun:** Resources, Writing – review & editing. **Camelia N. Borca:** Resources, Writing – review & editing. **Thomas Huthwelker:** Resources, Writing – review & editing. **Jon Petter Gustafsson:** Conceptualization, Methodology, Software, Validation, Resources, Writing – review & editing, Supervision, Project administration, Funding acquisition.

Declaration of Competing Interest

The authors declare that they have no known competing financial interests or personal relationships that could have appeared to influence the work reported in this paper.

Data availability

We are committed to allowing an open access publishing option.

Appendix A. Supplementary data

Supplementary data to this article can be found online at https://doi.org/10.1016/j.foreco.2022.120432.

References

Adediran, G., Lundberg, D., Almkvist, G., Pradas del Real, A.E., Klysubun, W., Hillier, S., Gustafsson, J.P., Simonsson, M., 2021. Micro and nano sized particles in leachates from agricultural soils: Phosphorus and sulfur speciation by X-ray microspectroscopy. Wat. Res. 189, 116585 https://doi.org/10.1016/j.watres.2020.116585.

Adediran, G.A., Tuyishime, J.M., Vantelon, D., Klysubun, W., Gustafsson, J.P., 2020. Phosphorus in 2D: spatially resolved P speciation in two Swedish forest soils as influenced by apatite weathering and podzolization. Geoderma 376, 114550. https://doi.org/10.1016/j.geoderma.2020.114550.

Akselsson, C., Westling, O., Alveteg, M., Thelin, G., Fransson, A.-M., Hellsten, S., 2008. The influence of N load and harvest intensity on the risk of P limitation in Swedish

forest soils. Sci. Total Environ. 404, 284–289. https://doi.org/10.1016/j.scitotenv.2007.11.017.

Alotaibi, K.D., Schoenau, J.J., Kar, G., Peak, D., Fonstad, T., 2018. Phosphorus speciation in a prairie soil amended with MBM and DDG ash: Sequential chemical extraction and synchrotron-based XANES spectroscopy investigations. Sci. Rep. 8, 1–9. https://doi.org/10.1038/s41598-018-21935-4.

Amadou, I., Faucon, M.-P., Houben, D., 2022. New insights into sorption and desorption of organic phosphorus on goethite, gibbsite, kaolinite and montmorillonite. Appl. Geochem. 143, 105378 https://doi.org/10.1016/j.apgeochem.2022.105378.

An, J.Y., Park, B.B., 2021. Effects of wood ash and N fertilization on soil chemical properties and growth of Zelkova serrata across soil types. Sci. Rep. 11, 14489. https://doi.org/10.1038/s41598-021-93805-5.

Arvidsson, H., Lundkvist, H., 2002. Needle chemistry in young Norway spruce stands after application of crushed wood ash. Plant Soil 238, 159–174.

Augusto, L., Bakker, M.R., Meredieu, C., 2008. Wood ash applications to temperate forest ecosystems—potential benefits and drawbacks. Plant Soil 306, 181–198. https://doi.org/10.1007/s11104-008-9570-z.

Beauchemin, S., Hesterberg, D., Chou, J., Beauchemin, M., Simard, R.R., Sayers, D.E., 2003. Speciation of phosphorus in phosphorus-enriched agricultural soils using X-ray absorption near-edge structure spectroscopy and chemical fractionation. J. Environ. Qual. 32, 1809–1819. https://doi.org/10.2134/jeq2003.1809.

Binkley, D., Högberg, P., 2016. Tamm Review: Revisiting the influence of nitrogen deposition on Swedish forests. For. Ecol. Manage. 368, 222–239. https://doi.org/10.1016/j.foreco.2016.02.035.

Bjurström, H., Ilskog, E., Berg, M. 2003. Askor från biobränslen och blandbränslen – mängder och kvalitet (in Swedish). Report ER10, Swedish Energy Agency, Eskilstuna, Sweden.

Blakemore, L., Searle, P.L., Daly, B.K. 1987. Soil Bureau Laboratory Methods. A. Methods for chemical analysis of soils. NZ Soil Bureau Scientific Report 80, Lower Hutt, New Zealand, pp. 44-45.

Brais, S., Bélanger, N., Guillemette, T., 2015. Wood ash and N fertilization in the Canadian boreal forest: soil properties and the response of jack pine and black spruce. For. Ecol. Manage. 348, 1–14. https://doi.org/10.1016/j.foreco.2015.03.021.

Braun, S., Thomas, V.F., Quiring, R., Flückiger, W., 2010. Does nitrogen deposition increase forest production? The role of phosphorus. Environ. Poll. 158, 2043–2052. https://doi.org/10.1016/j.envpol.2009.11.030.

Camia, A., Giuntoli, J., Jonsson, R., Robert, N., Cazzaniga, N.E., Jasinevičius, G., Grassi, G., Barredo, J.I., Mubareka, S., 2021. The use of woody biomass for energy production in the EU. Publications Office of the European Union. https://doi.org/10.2760/831621.

Clarholm, M., 1994. Granulated wood ash and a 'N-free' fertilizer to a forest soil – effects on P availability. For. Ecol. Manage. 66, 127–136. https://doi.org/10.1016/0378-1127(94)90152-X.

Cruz-Paredes, C., Frøslev, T.G., Michelsen, A., Bang-Andreasen, T., Hansen, M., Ingerslev, M., Skov, S., Wallander, H., Kjøller, R., 2019. Wood ash application in a managed Norway spruce plantation did not affect ectomycorrhizal diversity or N retention capacity. Fungal Ecol. 39, 1–11. https://doi.org/10.1016/j.funeco.2018.11.002.

De Jong, J., Akselsson, C., Egnell, G., Löfgren, S., Olsson, B.A., 2017. Realizing the energy potential of forest biomass in Sweden-How much is environmentally sustainable? For. Ecol. Manage. 383, 3–16. https://doi.org/10.1016/j.foreco.2016.06.028.

Eriksson, J., 1996. Dissolution of hardened wood ashes in forest soils: studies in a column experiment. Scand. J. For. Res. 13 (Suppl 2), 23–32.

Eriksson, A.K., Hesterberg, D., Klysubun, W., Gustafsson, J.P., 2016. Phosphorus dynamics in Swedish agricultural soils as influenced by fertilization and mineralogical development: Insights gained from batch experiments and XANES spectroscopy. Sci. Total Environ. 566, 1410–1419. https://doi.org/10.1016/j.scitotenv.2016.05.225.

Flückiger, W., Braun, S., 1998. Nitrogen deposition in Swiss forests and its possible relevance for leaf nutrient status, parasite attacks and soil acidification. Environ. Poll. 102, 69–76. https://doi.org/10.1016/S0269-7491(98)80017-1.

Forsmark, B., Wallander, H., Nordin, A., Gundale, M.J., Stevens, C., 2021. Long-term nitrogen enrichment does not increase microbial phosphorus mobilization in a northern coniferous forest. Funct. Ecol. 35 (1), 277–287.

Fransson, A.M., Bergkvist, B., Tyler, G., 1999. Phosphorus solubility in an acid forest soil as influenced by form of applied phosphorus and liming. Scand. J. For. Res. 14, 538–544. https://doi.org/10.1080/02827589908540818.

Gomez, K.A., Gomez, A.A., 1984. Statistical procedures for agricultural research, 2nd edition. John Wiley & Sons, New York.

Gustafsson, J.P., Braun, S., Tuyishime, J., Adediran, G.A., Warrinnier, R., Hesterberg, D., 2020. A probabilistic approach to phosphorus speciation of soils using P K-edge XANES spectroscopy with linear combination fitting. Soil Syst. 4, 26. https://doi.org/10.3390/soilsystems4020026.

Hannam, K., Venier, L., Allen, D., Deschamps, C., Hope, E., Jull, M., Kwiaton, M., Mckenney, D., Rutherford, P., Hazlett, P., 2018. Wood ash as a soil amendment in Canadian forests: what are the barriers to utilization? Can. J. For. Res. 48, 442–450. https://doi.org/10.1139/cjfr-2017-0351.

Hedwall, P.-O., Bergh, J., Brunet, J., 2017. Phosphorus and nitrogen co-limitation of forest ground vegetation under elevated anthropogenic nitrogen deposition. Oecologia 185, 317–326. https://doi.org/10.1007/s00442-017-3945-x.

Hesterberg, D., McNulty, I., Thieme, J., 2017. Speciation of soil phosphorus assessed by XANES spectroscopy at different spatial scales. J. Environ. Qual. 46, 1190–1197. https://doi.org/10.2134/jeq2016.11.0431.

Hesterberg, D. 2010. Chapter 11. Macroscale chemical properties and X-ray absorption spectroscopy of soil phosphorus. Dev. Soil Sci. 34, 313-356, https://doi.org/10.1016/S0166-2481(10)34011-6.

Heuck, C., Smolka, G., Whalen, E.D., Frey, S., Gundersen, P., Moldan, F., Fernandez, I.J., Spohn, M., 2018. Effects of long-term nitrogen addition on phosphorus cycling in organic soil horizons of temperate forests. Biogeochem. 141, 167–181. https://doi.org/10.1007/s10533-018-0511-5.

Huotari, N., Tillman-sutela, E., Moilanen, M., Laiho, R., 2015. Recycling of ash–For the good of the environment? For. Ecol. Manage. 348, 226–240. https://doi.org/10.1016/j.foreco.2015.03.008.

ISO, International Organization for Standardization. 1995. Soil Quality - Extraction of trace elements soluble in aqua regia. ISO 11466, Geneva, Switzerland.

ISO, International Organization for Standardization. 1998. Soil Quality - Determination of total nitrogen content by dry combustion ("elemental analysis"). ISO 13878, Geneva, Switzerland.

IUSS Working Group 2014. World reference base for soil resources. International soil classification system for naming soils and creating legends for soil maps. World Soil Resources Reports No. 106. FAO, Rome, Italy.

Jacobson, S., 2003. Addition of stabilized wood ashes to Swedish coniferous stands on mineral soils-effects on stem growth and needle nutrient concentrations. Silva Fenn. 37, 437–450. https://doi.org/10.14214/sf.483.

Jacobson, S., Högbom, L., Ring, E., Nohrstedt, H.-Ö., 2004. Effects of wood ash dose and formulation on soil chemistry at two coniferous forest sites. Water Air Soil Pollut. 158, 113–125. https://doi.org/10.1023/B:WATE.0000044834.18338.a0.

Jacobson, S., Lundström, H., Nordlund, S., Sikström, U., Pettersson, F., 2014. Is tree growth in boreal coniferous stands on mineral soils affected by the addition of wood ash? Scand. J. For. Res. 29, 675–685. https://doi.org/10.1080/02827581.2014.959995.

Karltun, E., Saarsalmi, A., Ingerslev, M., Mandre, M., Andersson, S., Gaitneks, T., Ozolinčius, R., Varnagiryte-Kabasinskiene, I. 2008. Wood ash recycling – possibilities and risks. In: Sustainable Use of Forest Biomass for Energy (eds. D. Röser et al.). Springer, pp. 79-108.

Klysubun, W., Tarawarakarn, P., Thamsanong, N., Amonpattaratkit, P., Cholsuk, C., Lapboonrueng, S., Chaichuay, S., Wongtepa, W., 2020. Upgrade of SLRI BL8 beamline for XAFS spectroscopy in a photon energy range of 1–13 keV. Radiat. Phys. Chem. 175, 108145 https://doi.org/10.1016/j.radphyschem.2019.02.004.

Knecht, M.F., Göransson, A., 2004. Terrestrial plants require nutrients in similar proportions. Tree Physiol. 24, 447–460.

Ladanai, S., Ågren, G.I., Olsson, B.A., 2010. Relationships between tree and soil properties in Picea abies and Pinus sylvestris forests in Sweden. Ecosystems 13, 302–316. https://doi.org/10.1007/s10021-010-9319-4.

Lagerström, A., Esberg, C., Wardle, D.A., Giesler, R., 2009. Soil phosphorus and microbial response to a long-term wildfire chronosequence in northern Sweden. Biogeochem. 95, 199–213. https://doi.org/10.1007/s10533-009-9331-y.

Larsson, P.-E., Westling, O., 1998. Leaching of wood ash and lime products: laboratory study. Scand. J. For. Res. 13 (Suppl. 2), 17–22.

Lim, H., Olsson, B.A., Lundmark, T., Dahl, J., Nordin, A., 2020. Effects of whole-tree harvesting at thinning and subsequent compensatory nutrient additions on carbon sequestration and soil acidification in a boreal forest. GCB Bioenergy 12, 992–1001. https://doi.org/10.1111/gcbb.12737.

Lundström, U., Bain, D., Taylor, A., van Hees, P., 2003. Effects of acidification and its mitigation with lime and wood ash on forest soil processes: a review. Water Air Soil Pollut. Focus 3, 5–28. https://doi.org/10.1023/A:1024115111377.

Lundström, U.S., van Breemen, N., Bain, D.C., van Hees, P.A.W., Giesler, R., Gustafsson, J.P., Ilvesniemi, H., Karltun, E., Melkerud, P.-A., Olsson, M., Riise, G., Wahlberg, O., Bergelin, A., Bishop, K., Finlay, R., Jongmans, A.G., Magnusson, T., Mannerkoski, H., Nordgren, A., Nyberg, L., Starr, M., Tau Strand, L., 2000. Advances in understanding the podzolization process resulting from a multidisciplinary study of three coniferous forest soils in the Nordic Countries. Geoderma 94 (2-4), 335–353.

Mahmood, S., Finlay, R.D., Fransson, A.M., Wallander, H., 2003. Effects of hardened wood ash on microbial activity, plant growth and nutrient uptake by ectomycorrhizal spruce seedlings. FEMS Microbiol. Ecol. 43, 121–131. https://doi.org/10.1111/j.1574-6941.2003.tb01051.x.

Mellbo, P., Sarenbo, S., Stålnacke, O., Claesson, T., 2008. Leaching of wood ash products aimed for spreading in forest floors–Influence of method and L/S ratio. Waste Manage. 28, 2235–2244. https://doi.org/10.1016/j.wasman.2007.09.037.

Nieminen, J.K., 2009. Combined effects of loose wood ash and carbon on inorganic N and P, key organisms, and the growth of Norway spruce seedlings and grasses in a pot experiment. Plant Soil 317, 155–165. https://doi.org/10.1007/s11104-008-9797-8.

Ohno, T., 1992. Neutralization of soil acidity and release of phosphorus and potassium by wood ash. J. Environ. Qual. 21, 433–438. https://doi.org/10.2134/jeq1992.00472425002100030022x.

Olsen, S.R., 1954. Estimation of available phosphorus in soils by extraction with sodium bicarbonate, US Department of Agriculture.

Olsson, B. & Westling, O. 2006. Skogsbränslecykelns näringsbalans, IVL Svenska Miljöinstitutet.

Olsson, B.A., Staaf, H., Lundkvist, H., Bengtsson, J., Rosén, K., 1996. Carbon and nitrogen in coniferous forest soils after clear-felling and harvests of different intensity. For. Ecol. Manage. 82, 19–32. https://doi.org/10.1016/0378-1127(95)03697-0.

Palmqvist, K., Nordin, A., Giesler, R., 2020. Contrasting effects of long-term nitrogen deposition on plant phosphorus in a northern Boreal Forest. Front. For. Glob. Change 3, 65. https://doi.org/10.3389/ffgc.2020.00065.

Persson, T., Rudebeck, A., Wirén, A., 1995. Pools and fluxes of carbon and nitrogen in 40-year-old forest liming experiments in southern Sweden. Water Air Soil Pollut. 85, 901–906. https://doi.org/10.1007/BF00476944.

Persson, T., Andersson, S., Bergholm, J., Grönqvist, T., Högbom, L., Vegerfors, B., Wirén, A., 2021. Long-term impact of liming on soil C and N in a fertile spruce forest ecosystem. Ecosystems 24, 968–987. https://doi.org/10.1007/s10021-020-00563-y.

Pistocchi, C., Mészáros, É., Tamburini, F., Frossard, E., Bünemann, E.K., 2018. Biological processes dominate phosphorus dynamics under low phosphorus availability in organic horizons of temperate forest soils. Soil Biol. Biochem. 126, 64–75. https://doi.org/10.1016/j.soilbio.2018.08.013.

Pitman, R.M., 2006. Wood ash use in forestry – a review of the environmental impacts. Forestry 79, 563–588. https://doi.org/10.1093/forestry/cpl041.

Ponge, J.-F., 2003. Humus forms in terrestrial ecosystems: a framework to biodiversity. Soil Biol. Biochem. 35, 935–945. https://doi.org/10.1016/S0038-0717(03)00149-4.

Prietzel, J., Kögel-Knabner, I., Thieme, J., Paterson, D., McNulty, I., 2011. Microheterogeneity of element distribution and sulfur speciation in an organic surface horizon of a forested Histosol as revealed by synchrotron-based X-ray spectromicroscopy. Org Geochem. 42, 1308–1314. https://doi.org/10.1016/j.orggeochem.2011.09.006.

Prietzel, J., Klysubun, W., Werner, F., 2016. Speciation of phosphorus in temperate zone forest soils as assessed by combined wet-chemical fractionation and XANES spectroscopy. J. Plant Nutr. Soil Sci. 179, 168–185. https://doi.org/10.1002/jpln.201500472.

Ravel, B., 2009. Athena user's guide. Athena IFFEFIT.

Reid, C., Watmough, S.A., 2014. Evaluating the effects of liming and wood-ash treatment on forest ecosystems through systematic meta-analysis. Can. J. For. Res. 44, 867–885. https://doi.org/10.1139/cjfr-2013-0488.

Ring, E., Jacobson, S., Nohrstedt, H.-Ö., 2006. Soil-solution chemistry in a coniferous stand after adding wood ash and nitrogen. Can. J. For. Res. 36, 153–163. https://doi.org/10.1139/x05-242.

Rosenberg, O., Persson, T., Högbom, L., Jacobson, S., 2010. Effects of wood-ash application on potential carbon and nitrogen mineralisation at two forest sites with different tree species, climate and N status. For. Ecol. Manage. 260, 511–518. https://doi.org/10.1016/j.foreco.2010.05.006.

Saarsalmi, A., Mälkönen, E., Kukkola, M., 2004. Effect of wood ash fertilization on soil chemical properties and stand nutrient status and growth in some coniferous stands in Finland. Scand. J. For. Res. 19, 217–233. https://doi.org/10.1080/02827580410024124.

Saarsalmi, A., Smolander, A., Kukkola, M., Arola, M., 2010. Effect of wood ash and nitrogen fertilization on soil chemical properties, soil microbial processes, and stand growth in two coniferious forest stands in Finland. Plant Soil 331, 329–340. https://doi.org/10.1007/s11104-009-0256-y.

Solé, V.A., Papillon, E., Cotte, M., Walter, P.H., Susini, J., 2007. PyMCA: a multiplatform code for the analysis of energy-dispersive X-ray spectra. Spectrochim. Acta B 62, 63–68. https://doi.org/10.1016/j.sab.2006.12.002.

Steenari, B.-M., Lindqvist, O., 1997. Stabilisation of biofuel ashes for recycling to forest soil. Biomass Bioenergy 13, 39–50. https://doi.org/10.1016/S0961-9534(97)00024-X.

Steenari, B.-M., Karlsson, L.-G., Lindqvist, O., 1999a. Evaluation of the leaching characteristics of wood ash and the influence of ash agglomeration. Biomass Bioenerg. 16, 119–136. https://doi.org/10.1016/S0961-9534(98)00070-1.

Steenari, B.-M., Schelander, S., Lindqvist, O., 1999b. Chemical and leaching characteristics of ash from combustion of coal, peat and wood in a 12 MW CFB–a comparative study. Fuel 78, 249–258. https://doi.org/10.1016/S0016-2361(98)00137-9.

Swedish Forest Agency 2019. Regler och rekommendationer för skogsbränsleuttag och kompensationsåtgärder (in Swedish). Report 2009/14, Jönköping, Sweden.

Talkner, U., Meiwes, K.J., Potočić, N., Seletković, I., Cools, N., De Vos, B., Rautio, P., 2015. Phosphorus nutrition of beech (Fagus sylvatica L.) is decreasing in Europe. Ann. Forest Sci. 72, 919–928. https://doi.org/10.1007/s13595-015-0459-8.

Tamm, C. O., Aronsson, A., Popovic, B., Flower-Ellis, J. 1999. Optimum nutrition and nitrogen saturation in Scots pine stands. Studia Forestalia Suecica no. 206, Swedish University of Agricultural Sciences, Uppsala, Sweden.

Tuyishime, J.M.R., Adediran, G.A., Olsson, B.A., Spohn, M., Hillier, S., Klysubun, W., Gustafsson, J.P., 2022. Phosphorus abundance and speciation in acid forest Podzols-Effect of postglacial weathering. Geoderma 406, 115500. https://doi.org/10.1016/j.geoderma.2021.115500.

Vairavamurthy, A., 1998. Using X-ray absorption to probe sulfur oxidation states in complex molecules. Spectrochim. Acta A 54, 2009–2017. https://doi.org/10.1016/S1386-1425(98)00153-X.

van Reeuwijk, L.P., 1995. Procedures for soil analysis. International Soil Reference and Information Centre, Wageningen, Netherlands.

Veronesi, G., Koudouna, E., Cotte, M., Martin, F.L., Quantock, A.J., 2013. X-ray absorption near-edge structure (XANES) spectroscopy identifies differential sulfur speciation in corneal tissue. Anal. Bioanal. Chem. 405, 6613–6620. https://doi.org/10.1007/s00216-013-7120-x.

Vogel, C., Helfenstein, J., Massey, M.S., Sekine, R., Kretzschmar, R., Beiping, L., Peter, T., Chadwick, O.A., Tamburini, F., Rivard, C., Herzel, H., Adam, C., Pradas del Real, A. E., Castillo-Michel, H., Zuin, L., Wang, D., Félix, R., Lassalle-Kaiser, B., Frossard, E., 2021. Microspectroscopy reveals dust-derived apatite grains in acidic, highly-weathered Hawaiian soils. Geoderma 381, 114681.

Weand, M.P., Arthur, M.A., Lovett, G.M., Sikora, F., Weathers, K.C., 2010. The phosphorus status of northern hardwoods differs by species but is unaffected by nitrogen fertilization. Biogeochem. 97, 159–181. https://doi.org/10.1007/s10533-009-9364-2.

Werner, F., de la Haye, T.R., Spielvogel, S., Prietzel, J., 2017. Small scale spatial distribution of phosphorus fractions in soils from silicate parent material with different degree of podzolisation. Geoderma 302, 52–65. https://doi.org/10.1016/j.geoderma.2017.04.026.

Westling, O., Zetterberg, T., 2007. Recovery of acidified streams in forests treated by total catchment liming. Water Air Soil Pollut. Focus 7 (1-3), 347–356.

Wood, T., Bormann, F., Voigt, G., 1984. Phosphorus cycling in a northern hardwood forest: biological and chemical control. Science 223, 391–393. https://doi.org/10.1126/science.223.4634.391.

Yanai, R.D., 1998. The effect of whole-tree harvest on phosphorus cycling in a northern hardwood forest. For. Ecol. Manage. 104, 281–295. https://doi.org/10.1016/S0378-1127(97)00256-9.

Yu, L., Zanchi, G., Akselsson, C., Wallander, H., Belyazid, S., 2018. Modeling the forest phosphorus nutrition in a southwestern Swedish forest site. Ecol. Model. 369, 88–100. https://doi.org/10.1016/j.ecolmodel.2017.12.018.

Phosphorus speciation in the organic layer of two Swedish forest soils 13-24 years after wood ash and nitrogen application

J.R. Marius Tuyishime[a*], Gbotemi A. Adediran[a,b], Bengt A. Olsson[c], Therese Sahlén Zetterberg[a], Lars Högbom[d,e] , Marie Spohn[a], Hyungwoo Lim[e,h], Wantana Klysubun[f], Camelia N. Borca[g], Thomas Huthwelker[g], Jon Petter Gustafsson[a]

[a]*Department of Soil and Environment, Swedish University of Agricultural Sciences, P.O. Box 7014, SE-75007 Uppsala, Sweden*

[b]*UK Centre for Ecology and Hydrology, Wallingford OX10 8BB, United Kingdom.*

[c]*Department of Ecology, Swedish University of Agricultural Sciences, P.O. Box 7044, 750 07 Uppsala, Sweden*

[d]*The Forestry Research Institute of Sweden – Skogforsk, 751 83 Uppsala, Sweden*

[e]*Department of Forest Ecology and Management, Swedish University of Agricultural Sciences, 901 83 Umeå, Sweden*

[f]*Synchrotron Light Research Institute, University Avenue 111, Nakhon Ratchasima, 30000, Thailand*

[g]*Paul Scherrer Institut, Swiss Light Source, 5232 Villigen PSI, Switzerland*

[h]*Institute of Ecology and Earth Sciences, University of Tartu, 50409 Tartu, Estonia*

Contents

1. Supplementary figures
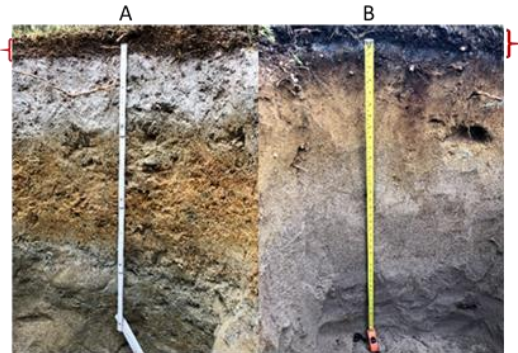
Figure S1: Soil pits excavated from Rödålund (A) and Riddarhyttan (B). Red brackets indicate the part of the organic layer sampled.
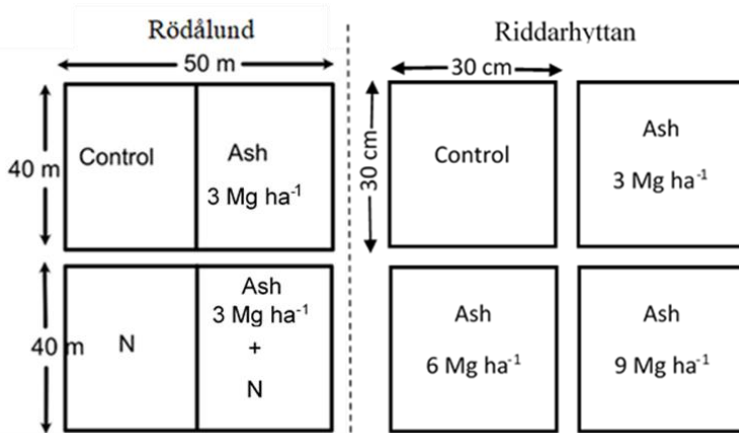
Figure S2*: Schematic representation of the net size of experimental plots from two study sites*
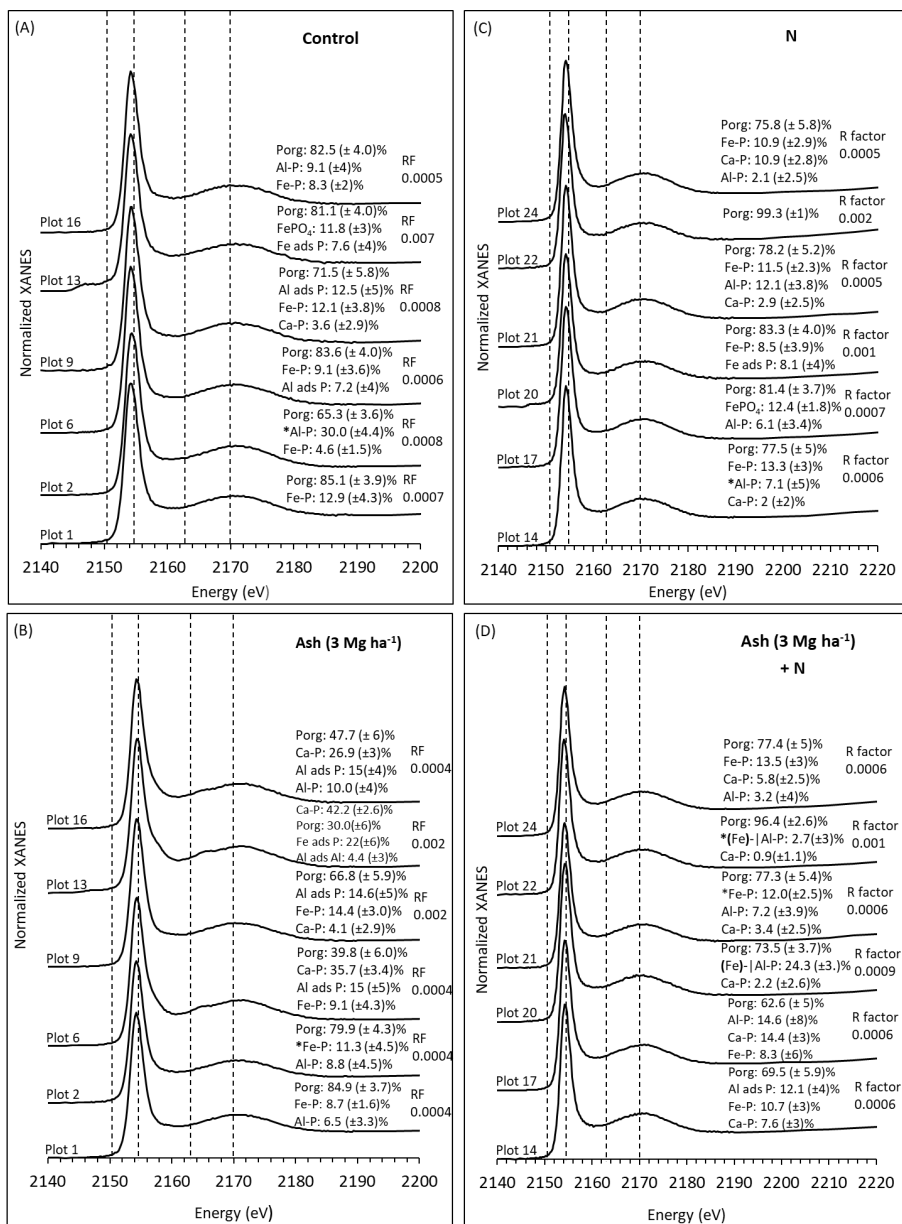
Figure S3: Normalized P *K*-edge XANES data with the relative fractional weights of different P species from unfertilized (A), ash-treated (B), N-treated (C), and ash + N-treated (D) organic layers from Rödålund. Porg: organic P, Al ads P: Al-adsorbed P, Fe ads P: Fe-adsorbed P, Ca-P: Ca-bound P, Al-P and Fe-P represent cases when the probabilistic LCF could not distinguish the P adsorbed to Al from AlPO$_4$, as well as P adsorbed to Fe from FePO$_4$. Fe-|Al-P: represent cases when the probabilistic LCF could not distinguish between all Fe-and Al-bound P. * indicates FePO4 or AlPO4 most likely represents the cases when probabilistic LCF showed that unseparated Fe-P or Al-P species groups. Otherwise, Al-adsorbed P or Fe-adsorbed P was the most likely P forms represented by Al or Fe-P.
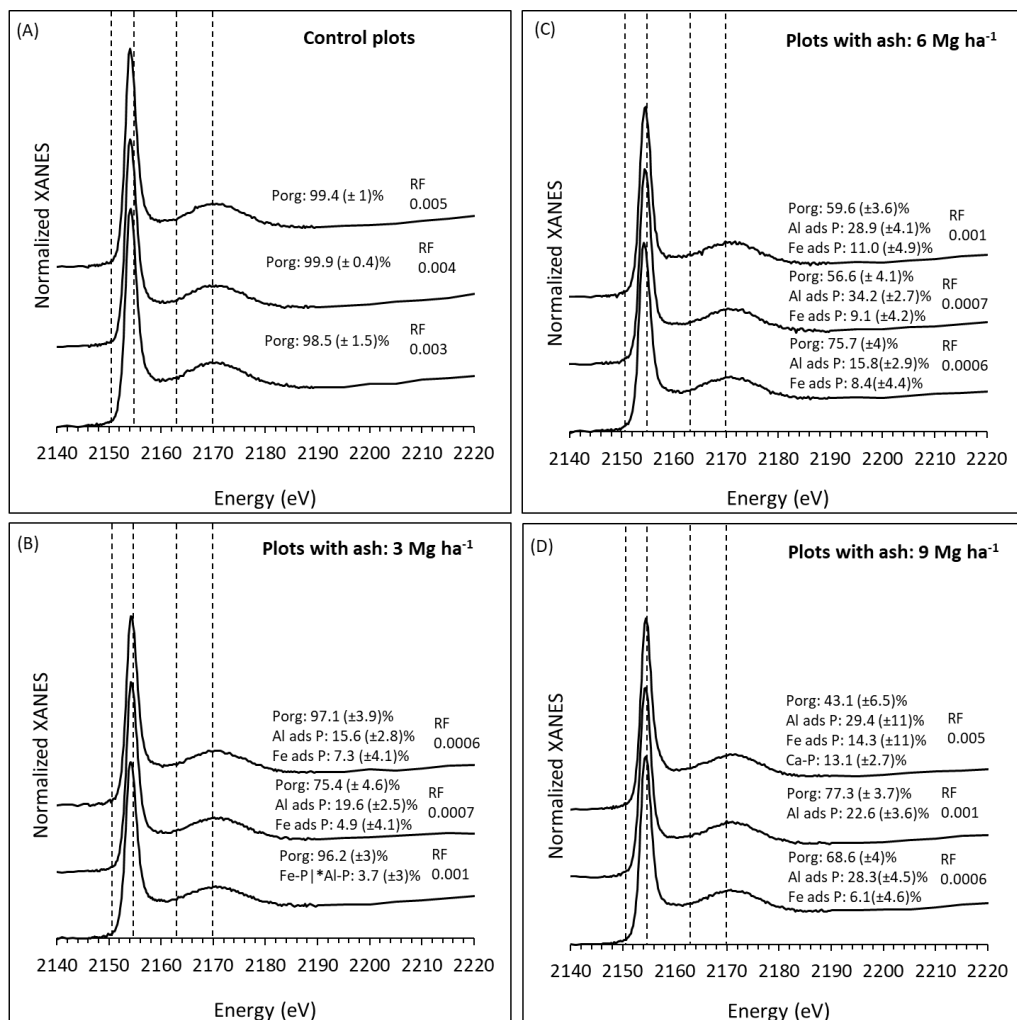
Figure S4: Normalized P K-edge XANES data with the relative fractional weights of different P species from unfertilized (A), ash (3 Mg ha^{-1})-treated (B), ash-treated (6 Mg ha^{-1}) (C), and ash -treated (9 Mg ha^{-1}) (D) organic layers from Rödålund. Porg: organic P, Al ads P: Al-adsorbed P, Fe ads P: Fe-adsorbed P, Ca-P: Ca-bound P, Al-P and Fe-P represent cases when the probabilistic LCF could not distinguish the P adsorbed to Al from AlPO$_4$, as well as P adsorbed to Fe from FePO$_4$. Fe-|Al-P: represent cases when the probabilistic LCF could not distinguish between all Fe-, and Al-bound P. * indicates FePO4 or AlPO4 most likely represents the cases when probabilistic LCF showed that unseparated Fe-P or Al-P species groups. Otherwise, Al-adsorbed P or Fe-adsorbed P was the most likely P forms represented by Al or Fe-P.
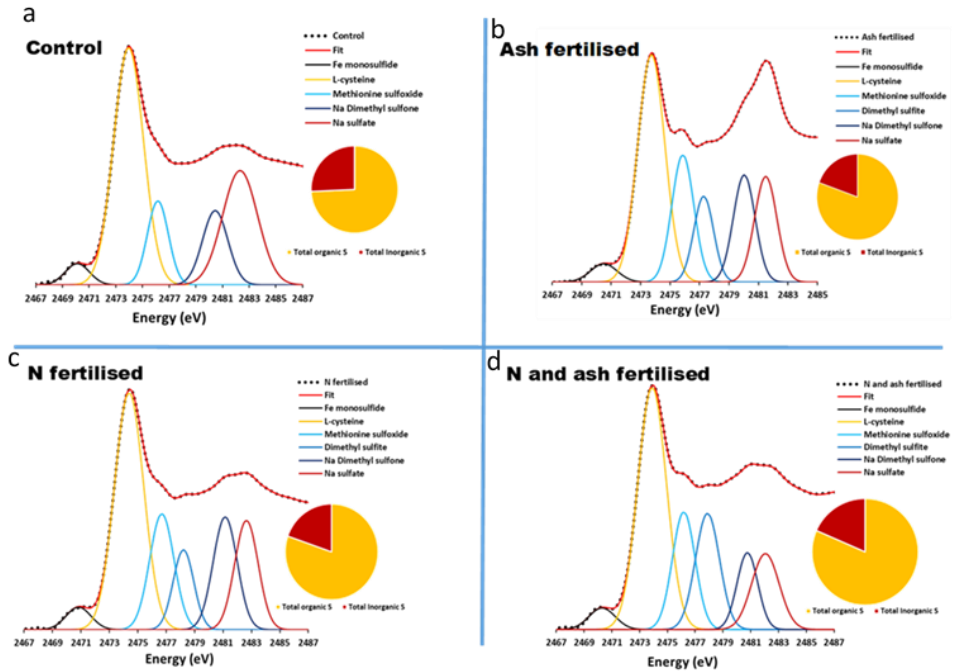
Figure S5: Molecular speciation of S as deduced by Gaussian curve fittings of S K-edge µ_XANES in selected experimental plots at Rödålund.

2. Supplementary tables

Table S1: Stocks of general chemical properties of studied O horizons

Study site	Treatment	Alox	Feox	Siox	TOC	TN
		kg ha⁻¹				
Rödålund	Control	20.2±7.1	13.9±3.1	0.48±0.1	6520±2342	189±31.6
	Ash	19.0±4.4	17.9±4.4	3.6±1.8	7069±1165	194±57.5
	N	21.0±5.6	14.8±3.2	0.5±0.1	7368±619.7	264±15.5
	Ash+N	28.2±9.9	19.0±5.5	0.95±0.3	8253±259	301±8.5
Riddarhyttan	0 Ash	55.8±4.2	50.2±3.5	0.70±0.4	21616±3818	548±82
	3 Ash	69.2±32.2	77.9±43.8	2.3±2.1	17596±3179	490±96
	6 Ash	57.5±15.1	56.8±16.3	1.5±1.2	16609±1497	467±26
	9 Ash	83.8±18.4	77.8±10.3	12.98±11	13559±880	395±22

Table S2: Phosphorus solubility and speciation of investigated O horizons

Study site	Treatment	TP	Olsen-P	Pox	Porg*	P ads Al*	P ads Fe*	AlPO$_4$*	FePO$_4$*	CaP*
						mmol kg^{-1}				
Rödålund	Control	29.0±2.1	3.18±0.4	11.2±2	22.6±1.8	1.16±0.5	2.6±0.4	1.7±1.7	0.56±0.6	0.15±0.15
	Ash	37.8±5.4	3.78±0.3	16.6±3	21.7±4.3	4.37±1.2	3.9±0.9	0.00±0.0	0.82±0.8	7.1±3.5
	N	25.5±0.8	1.72±0.2	5.6±0.4	21.1±1.3	0.71±0.4	2.4±0.5	0.3±0.3	0.35±0.3	0.7±0.44
	Ash+N	28.0±2.6	1.81±1.2	7.7±2	21.1±1.95	1.90±0.9	2.6±0.9	0.00±0.0	0.60±0.5	1.8±0.8
Riddarhyttan	Control	19.8±1.1	1.48±0.1	7.08±2.2	19.7±1.2	0.00±0.0	0.00±0.0	n.d	n.d	0±0.0
	3 Ash	25.5±0.4	1.69±0.1	7.42±2.3	21.1±1.4	3.33±1.2	1.07±0.6	n.d	n.d	0.0±0.0
	6 Ash	28.7±1.5	2.29±0.3	7.85±2.7	18.2±0.8	7.7±1.9	2.77±0.3	n.d	n.d	0.0±0.0
	9 Ash	39.1±6.1	3.21±0.8	15.9±6.7	23.4±2.4	10.3±2.6	3.10±2.3	n.d	n.d	2.3±2.3

*indicates P species as evidenced by the P K-edge XANES in the bulk soil samples

Table S3: The mass of O horizons studied from Rödålund

Ash treatment (Mg ha^{-1}) in plots	O horizon mass (sieved)
	kg m^{-2}
Control (0)	1.36
Control (0)	1.32
Control (0)	1.30
Control (0)	2.07
Control (0)	2.19
Control (0)	3.45
Ash (3 Mg ha^{-1})	1.52
Ash (3 Mg ha^{-1})	1.30
Ash (3 Mg ha^{-1})	1.51
Ash (3 Mg ha^{-1})	1.72
Ash (3 Mg ha^{-1})	4.36
Ash (3 Mg ha^{-1})	1.34
N	1.46
N	1.68
N	2.25
N	1.66
N	1.76
N	2.10
Ash + N	2.54
Ash + N	2.02
Ash + N	2.14
Ash + N	1.96
Ash + N	2.02
Ash + N	1.81

Lim et al. (2020). N represent repeated 150 kg ha^{-1} fertilization of nitrogen every three years.

Table S4: The mass of O horizons studied from 250 Riddarhyttan

Ash treatment (Mg ha^{-1}) in plots	organic Layer mass (sieved)
Mg ha-1	kg m^{-2}
Control (0)	6.55
Control (0)	4.08
Control (0)	4.35
3	3.19
3	4.45
3	6.00
6	3.68
6	5.09
6	4.65
9	4.79
9	4.17
9	5.36

Acta Universitatis Agriculturae Sueciae

Doctoral Thesis No. 2022:75

Effects of weathering and wood ash application on bulk and microscale P speciation were investigated in eight Swedish forest soils. Most of the apatite in the topsoils has been dissolved. In the soil profiles, P bound to Al surface minerals was the largest pool. The dissolution of Ca-bound P in the ash was almost complete, contributing to increased P availability.

J.R. Marius Tuyishime received his graduate education at the department of Soil and Environment, Swedish University of Agricultural Sciences, Uppsala. He holds a Master of Science in Soil and Water Management with a major in Soil Science from the same university.

Acta Universitatis Agriculturae Sueciae presents doctoral theses from the Swedish University of Agricultural Sciences (SLU).

SLU generates knowledge for the sustainable use of biological natural resources. Research, education, extension, as well as environmental monitoring and assessment are used to achieve this goal.